PRACTICAL ASPECTS OF KALMAN FILTERING IMPLEMENTATION

ADVISORY GROUP FOR AEROSPACE RESEARCH
AND DEVELOPMENT

PREPARED FOR
NORTH ATLANTIC TREATY ORGANIZATION

MARCH 1976

AGARD-LS-82

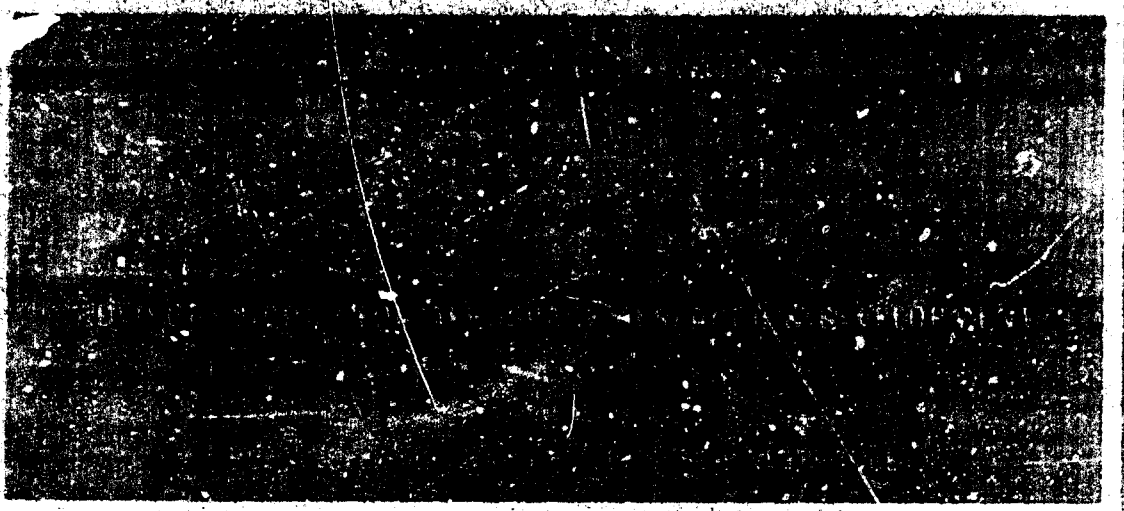

AGARD LECTURE SERIES No. 82

on

Practical Aspects of Kalman Filtering Implementation

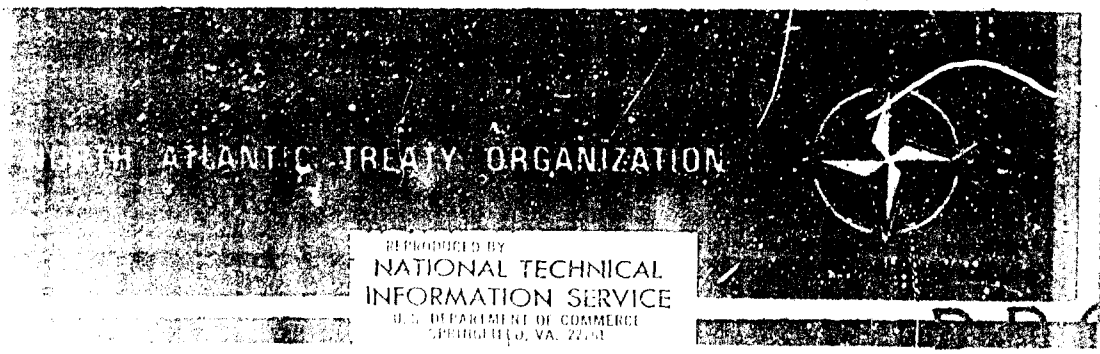

REPORT DOCUMENTATION PAGE

1. Recipient's Reference	2. Originator's Reference	3. Further Reference	4. Security Classification of Document
	AGARD-LS-82	ISBN 92-835-0160-8	UNCLASSIFIED

5. Originator	Advisory Group for Aerospace Research and Development North Atlantic Treaty Organization 7 rue Ancelle, 92200 Neuilly sur Seine, France
6. Title	PRACTICAL ASPECTS OF KALMAN FILTERING IMPLEMENTATION
7. Presented at	Norway (10--11 May 1976), The Netherlands (13--14 May 1976), and Italy (17--18 May 1976), sponsored by the Guidance and Control Panel and organised by the Consultant and Exchange Panel of AGARD.

8. Author(s)	9. Date
Various	March 1976
10. Author's Address	**11. Pages**
Various	190

12. Distribution Statement	This document is distributed in accordance with AGARD policies and regulations, which are outlined on the Outside Back Covers of all AGARD publications.

13. Keywords/Descriptors		14. UDC
Kalman filter theory	Electric filters	621.372.45:629.7.051
Airborne equipment	Air navigation	
Avionics	Design	

15. Abstract

This Lecture Series No.82, on the subject of Practical Aspects of Kalman Filtering Implementation was intended to emphasise the practical aspects of the use of optimal filters in guidance, navigation and control systems. All of the Lecturers for this Series have many years of experience in the field, and they relate their experiences on various projects involving implementation techniques and problems with optimal filters. Lecture Series No.82, aims to provide an account of how optimal filters are actually designed and implemented in practice. The techniques should be applicable to a wide variety of situations.

NORTH ATLANTIC TREATY ORGANIZATION

ADVISORY GROUP FOR AEROSPACE RESEARCH AND DEVELOPMENT

(ORGANISATION DU TRAITE DE L'ATLANTIQUE NORD)

AGARD Lecture Series No.82

PRACTICAL ASPECTS OF KALMAN FILTERING IMPLEMENTATION

The material in this book has been assembled in support of a Lecture Series presented in Norway (10–11 May 1976), The Netherlands (13–14 May 1976) and Italy (17–18 May 1976), sponsored by the Guidance and Control Panel and organised by the Consultant and Exchange Panel of AGARD.

THE MISSION OF AGARD

The mission of AGARD is to bring together the leading personalities of the NATO nations in the fields of science and technology relating to aerospace for the following purposes:

- Exchanging of scientific and technical information;
- Continuously stimulating advances in the aerospace sciences relevant to strengthening the common defence posture;
- Improving the co-operation among member nations in aerospace research and development;
- Providing scientific and technical advice and assistance to the North Atlantic Military Committee in the field of aerospace research and development;
- Rendering scientific and technical assistance, as requested, to other NATO bodies and to member nations in connection with research and development problems in the aerospace field;
- Providing assistance to member nations for the purpose of increasing their scientific and technical potential;
- Recommending effective ways for the member nations to use their research and development capabilities for the common benefit of the NATO community.

The highest authority within AGARD is the National Delegates Board consisting of officially appointed senior representatives from each member nation. The mission of AGARD is carried out through the Panels which are composed of experts appointed by the National Delegates, the Consultant and Exchange Program and the Aerospace Applications Studies Program. The results of AGARD work are reported to the member nations and the NATO Authorities through the AGARD series of publications of which this is one.

Participation in AGARD activities is by invitation only and is normally limited to citizens of the NATO nations.

Published March 1976

ISBN 92-835-0160-8

621.372.45:629.7.051

Printed by Technical Editing and Reproduction Ltd
Harford House, 7–9 Charlotte St, London, W1P 1HD

FOREWORD

This Lecture Series, No 82, on the Practical Aspects of Kalman Filtering Implementation is sponsored by the Guidance and Control Panel of AGARD and organized by the Consultant and Exchange Program.

The development of the Kalman filter in the early 1960's removed from the Wiener filter approach the assumptions of stationarity and the availability of an infinite time interval of data. The solution, in the form of a recursive computer algorithm, made study and analysis of its application to guidance and control a relatively straightforward matter Early hardware implementations at the Charles Stark Draper Laboratory, Autonetics, and elsewhere validated the conceptual framework and practicality of the filter implementation for a variety of problems.

In actual practice, however, considerable experience is needed when the questions of modeling, design, and implementation are considered. Each of the lecturers brings to this series a depth of experience that was gained by "hands on" development of filters that work with hardware.

The emphasis throughout the Lecture Series is on developing practical approaches to the development of filters which lead to satisfactory system performance, where "satisfactory" is defined by the design engineer. "Satisfactory" is used instead of "optimal" because, as each of the lecturers points out, the optimization of a particular filter mechanization generally includes many factors that are difficult or impossible to describe mathematically, such as the tradeoff between computer requirements and performance of the filter. The techniques and approaches described should be applicable to a variety of guidance and control problems.

Dr. George T.SCHMIDT
The Charles Stark Draper Laboratory, Inc.
Cambridge, Massachusetts.

LIST OF SPEAKERS

Lecture Series Director: Dr.G.T.Schmidt
The Charles Stark Draper Laboratory
Cambridge, Massachusetts, USA.

Dr S.F.Schmidt
Analytical Mechanics Associates Inc.
Mountain View, California, USA.

Dr J.C.Wauer
Autonetics, Rockwell International Corp.
Anaheim, California, USA

Dr J.E.Bergeson
The Boeing Company
Seattle, Washington, 98124, USA

Dr H.Winter
DFVLR, Institut für Flugführung
33 Braunschweig, Germany

Dr P.L.Faurre
SAGEM, 6 Avenue d'Iéna
Paris 75116, France

Prof. C.A.Darmon
Le Petit Monthélon
Acigné 35690
France

Dr W.Kortüm
DFVLR
8031 Oberpfaffenhofen, Germany

CONTENTS

EXPERIENCES IN THE DEVELOPMENT OF AIDED INS FOR AIRCRAFT

by
Dr. Stanley F. Schmidt
Analytical Mechanics Associates, Inc.
80 W. El Camino Real
Mt. View, California 94045

Summary

Experiences in the development and test evaluation of Kalman filters in aided navigation systems for aircraft are presented. Designs for two operational systems for enroute-navigation uses and two experimental systems for terminal area and landing uses are described. The primary emphasis is on the developmental approach used with examples from the actual designs. Practical considerations are stressed rather than the mathematical formulations and theory. Details are presented on the square-root implementation of the Kalman filter which is used in three of the actual systems. Problems encountered in actual designs and the solutions selected for these problems are discussed. A brief overview of the possible future trends in aircraft navigation systems is also given.

1. Introduction

This lecture presents the author's experiences in the development of Kalman filters for combining external (navaid) measurements with an inertial navigation system to form an "aided" INS for aircraft-navigation purposes. This experience includes designs for two operational systems for enroute-navigation uses and designs for several experimental systems for terminal-area and landing uses. These designs have been made over the past 10 years, during which airborne-computer technology has advanced tremendously. These advances in computational capabilities, along with advances in theory, have provided for the design improvements which are discussed. The inertial sensing devices used in the designs have covered ranges from high-accuracy platform-type inertial measurement units (IMU) to very simple low-accuracy strapped-down sensors.

The lecture begins with a brief overview of aided inertial navigation systems. Characteristics are discussed which are relevant to the subsequent material, and this is followed by the main topic covering the development approach used with examples from the actual designs. Some problems which have been experienced in actual systems are also described. The lecture concludes with a brief overview of the possible future trends in aircraft navigation systems.

2. Overview of Aided Inertial Navigators

Figure 1 is a highly simplified block diagram illustrating the fundamental operation of one type of inertial navigation system. The principal components, the inertial measurement unit (IMU) and the computer, are shown.

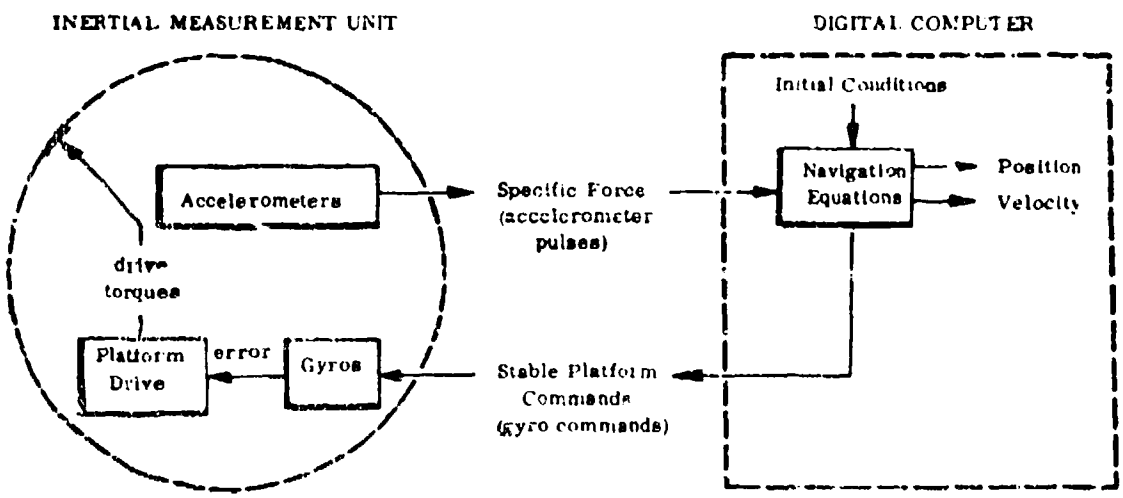

Figure 1. Simplified Block Diagram of an Inertial Navigation System.

The IMU contains a stable platform on which three gyros and three linear accelerometers are orthogonally mounted. As implied by its name, the stable platform maintains an orientation commanded by the computer, which is independent of the orientation of the case. This is accomplished as indicated in Figure 1 by sensing error signals from the gyro-output-axis pickoffs and through feedback providing the appropriate platform-drive-nulling torques. This inner-loop feedback-control system must have sufficient gain and dynamic response to keep the pickoff errors small, regardless of IMU-case attitude motions.

If the inner loop functions properly, then the platform maintains the orientation commanded by the computer. Each gyro, however, is an imperfect device and tends to exhibit a small drift rate. That is, even though the gyro output axis is nulled, the gyro case (fixed to the platform) has a rotation rate about the input-axis direction, which differs slightly from the command rate. These drift rates arise because of internal rotational imbalances in the gyro, torquer-scale-factor errors, and from several other more subtle mechanisms. Estimates of these drift rates can be used to minimize their effect on platform orientation by applying appropriate compensating signals to the gyro torquers.

As indicated in Figure 1, the accelerometer outputs are the measured specific forces which are sent to the computer in the form of a pulse train or the sum of pulses over a specific time interval. The specific force vector, f, is given as

$$f = \ddot{a} - g$$

where

a = the inertial acceleration vector

g = the gravitational attraction per unit mass

If the position is known, then g can be calculated to a high degree of accuracy. The navigation equations calculate the acceleration from the measured specific force and the calculated gravity, and doubly integrate these accelerations for position. These calculations are executed at a sufficiently high rate that the position and velocity are continuously available (for all practical purposes).

To initialize operations, the system must be aligned so that the coordinate frame of the computer and the platform are coincident, and the initial position and velocity must be inserted into the appropriate cells of the computer.

The stable platforms for most aircraft navigation systems are commanded to stay level with respect to the local vertical. This means that two of the axes lie in the locally level plane and the third axis lies along the vertical plane. The navigation equations solve for the velocity with respect to the earth (rather than inertial velocity) in the moving coordinate frame, which stays in the locally level orientation. A frequently used set of navigation equations are referred to a wander-azimuth geodetic-vertical mechanization. Wander azimuth means that no attempt is made to keep the azimuth of a level axis in any preferred direction such as north. The azimuth gyro is torqued with the computed vertical component of earth rate in such a manner that the level frame remains fixed with respect to the earth when the aircraft is stationary.

The stable platform is initially aligned by first driving it (with the torquers) until the two level-accelerometer outputs are zero. Once it has been leveled, its azimuth with respect to north is determined by monitoring the level-gyro command rates which are necessary to keep the platform level in the presence of the rotation rate of the earth.

Platform-type inertial navigation systems are in widespread use today for both military and commercial aircraft. The commercially available systems have error characteristics which grow from alignment at about 1 nautical mile per hour. This error growth is primarily caused by gyro drift rates that are not properly compensated for in the computer. The vertical channel in these systems is either clamped (that is, not used) or a barometric altimeter is used as an altitude reference for stabilizing the vertical channel.

Figure 2 shows a sample run of a free inertial navigation system in the laboratory. The system was aligned for about 15 minutes prior to starting the system in the navigation mode. The error growth with time is evident in these results.

Figure 3 shows the inertial path as computed by the free inertial system versus the position computed from the multiple-station DME measurements. In this instance, the navigation system was aligned at point 1 on Figure 3 while the aircraft was stationary. The aircraft then took off and flew the path close to that indicated by the DME-derived position. The aircraft flew over the starting point at the end of the run, which at least is a one-point check of the DME position accuracy. As may be noted, the deviation between the two paths grows with time from initialization.

Error growths of 1 nautical mile per hour are certainly tolerable for many enroute-navigation purposes. They are, however, completely unacceptable for terminal-area and landing purposes. The traditional approach to solving problems like this is to have a separate navigation system for each phase of flight; for example, we could use a multiple-DME solution for the position reference during enroute and terminal-area phases. On final approach we could use the ILS for the reference. With such a mechanization there is no need for the INS, as long as the aircraft flies in areas where the multiple-DME measurements are possible.

In recent years, military uses have required accurate navigation during periods when no external navaids are available, as well as accurate navigation for long periods of flight. The free inertial navigation systems could not

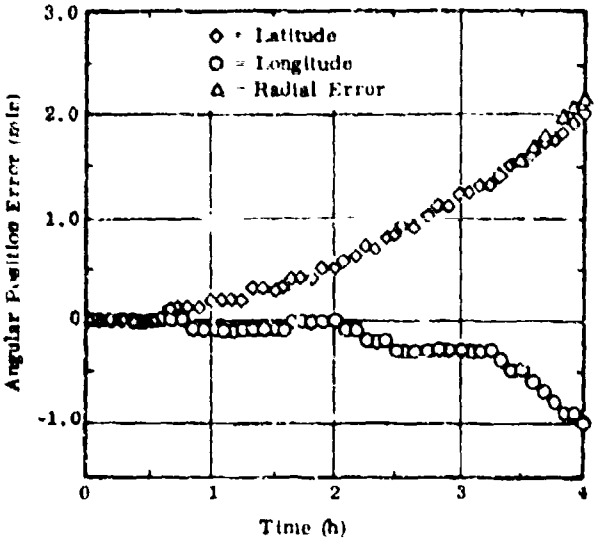

Figure 2. Laboratory System Free Inertial Navigation Performance Following Fine Ground Alignment

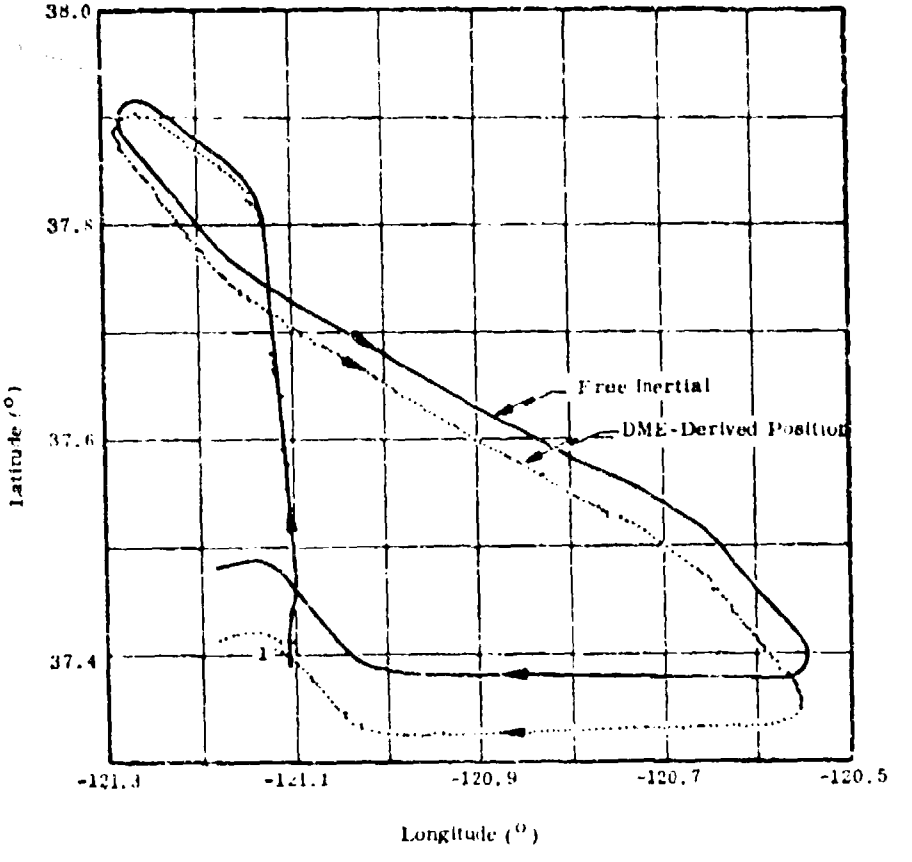

Figure 3. Flight Characteristics of an Experimental Navigation System

satisfy the requirements, so aided navigation systems came into existence. For example, the first systems were:

(1) Doppler-inertial,
(2) loran-inertial,
(3) stellar-inertial.

Generally, these first systems had simple algorithms for combining the inertial data with the navaid measurements, since the airborne computational capabilities were quite limited. Kalman filtering was introduced, and airborne digital computational capabilities improved substantially in the early 1960's. These two events have led to far greater sophistication of the algorithms in aided inertial navigation systems.

Figure 4 is a simplified block diagram of an aided inertial navigation system for a platform-type IMU. The system is mechanized such that the estimated state is calculated (i.e., updated) at a moderately high frequency (10 to 40 Hz). The Kalman filter uses the navaid measurements, along with the estimated state, to estimate the error state. The error state is, in turn, used to correct the estimated state. This process of estimation and correction is done at a considerably lower frequency (from 0.017 Hz to 1 Hz in the designs the author has implemented).

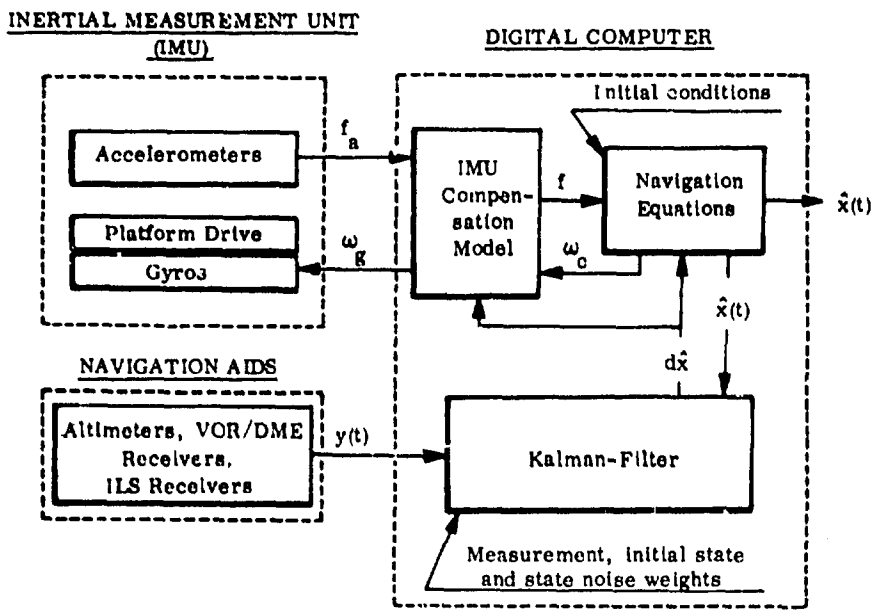

f_a = digitized accelerometer data

f = compensated accelerometer data in computer frame

ω_c = desired platform rate

ω_g = compensated platform command rate

$\hat{x}(t)$ = estimated state

$d\hat{x}$ = incremental state estimated by the filter

y(t) = vector of measurements from the navigation aids

Figure 4. Block Diagram of an Aided Inertial Navigation System

The primary objective of this lecture is to show experiences with design and tests of such aided inertial navigation systems. Before doing this, it is pertinent to consider what the error characteristics of a properly designed aided system should be. First, in the presence of navigation-aid measurements the error in the estimated state should never be worse than that of the measuring device. For example, if we were using DME to aid the inertial navigation system and the DME error were around 500 feet, then the system errors should be of the order of 500 feet or less. In the absence of navaid measurements, the error in the estimated state will grow in accordance with the free inertial characteristics. The rate of error growth depends on the filter design and the error characteristics of the IMU. The more sophisticated filters estimate the parameters such as steady gyro drifts, tilt errors, and so forth. With such systems the inertial system enters the free inertial mode in a well-calibrated condition. If the real error sources are deterministic, then the rate of error growth during the free inertial mode can be very small.

3. Experiences in Filter Design and Validation

This section presents material in the general chronological order of filter development that has been experienced by the writer. Examples from several systems and suggestions based on experience are included. An attempt is made to describe the highlights, the problem areas, and the solutions which have been used in these systems. The principles and practical considerations are emphasized rather than the mathematical formulations and theory.

3.1 Overview of the design problem. One of the most important factors in the design of Kalman filters is in obtaining a complete understanding of the overall problem. One invariably starts with a knowledge of:

(1) The performance objectives or requirements.

(2) The constraints on the equipment. For example,

- (a) The IMU may be specified.
- (b) The computer may be specified.
- (c) The navaid references (measurement devices) may be specified.

(3) The desired modes of operation. For example,

- (a) Ground alignment.
- (b) Air alignment (air start).
- (c) Barometric altitude-inertial.
- (d) Tacan-inertial.
- (e) Stellar-inertial.
- (f) ILS-inertial (for landing).

(4) Whether the system is to be automatic or a navigator is to be involved in the operations.

(5) The development schedule.

In the development of the C5A aircraft navigation system we had relevant information on each of the items shown in Figure 5 [1]. Generally speaking, one starts with a simple functional diagram as shown in Figure 5, along with all of the available information on each of the devices and the design objectives, and one performs a preliminary design. This preliminary design focuses a good deal of attention on the constraints imposed by the digital computer.

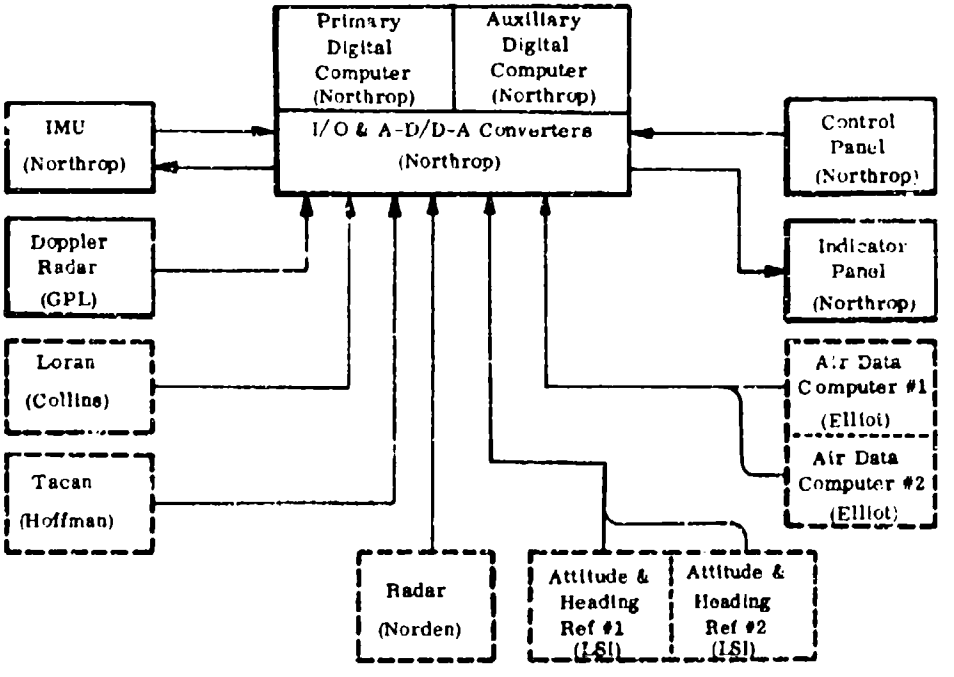

Figure 5. Block Diagram of C-5 Navigation System Equipments.

For example, the navigation functions associated with

(1) Bringing all data into the computer.

(2) Servicing the display panel.

(3) Solving the navigation equations.

(4) Servicing the platform.

may require a significant amount of the available memory and real time of the computer. If the computer must also execute guidance and control logic, then even more memory and real time is used for necessary functions other than filtering. The preliminary design allocates memory and real time to each of the functions to be executed in the airborne computer. Quite obviously, the percentage of real time and memory allocated to the Kalman filter can have a strong influence on the filter design.

In developing the preliminary design for the filter one must select:

(1) The number of state variables.

(2) The number of measurements.

(3) Which measurements at any time period (or mode) are to be used.

(4) The filter cycle times, and so forth.

This selection must satisfy the memory and real-time constraints of the airborne computer and satisfy the accuracy requirements of the specifications.

To the author's knowledge, there is no straightforward design procedure; rather, one uses a cut-and-try approach based on past experience and ensemble error analysis (if available) to give a tentative design.

In relating machine time to number of measurements, cycle times, and number of state variables, the equations in Reference [2] are useful for preliminary design purposes. For the square-root covariance I filter, the reference gives:

(1) Number of multiplies $= \frac{10n^3}{6} + n^2 (3r + m + 1) + n (4r + m + \frac{8}{6}) + 2r$

(2) Number of adds $= \frac{10n^3}{6} + n^2 (3r + m - \frac{1}{2}) + n (r + \frac{5}{6}) + r$

(3) Number of square roots $= n + r$

(4) Number of divides $= n + 2r$

where

n = number of state variables
m = number of random forcing functions
r = number of measurements

We take as an example a platform system with a three-axis Kalman filter and measurements consisting of TACAN range and bearing plus barometric altitude. We assume the following state variables are estimated by the filter:

(1) Three components of position.

(2) Three components of velocity.

(3) Three components of platform/computer misalignment (tilts).

(4) Three components of gyro drifts.

(5) One component of vertical acceleration bias.

(6) Three components of measurement calibration.

The last seven state variables are assumed to be treated as exponentially correlated noise in the filter.

For the example $n = 16$, $m = 7$, and $r = 3$. We also assume that this particular computer has the following times for the operations in microseconds.

(1) Multiply = 24

(2) Add = 8

(3) Square root = 200

(4) Divide = 24

The equations, along with the computer assumptions, give:

	Number	Execution time (milliseconds)
multiplies	11,510	276,240
adds	10,659	85,154
square roots	19	3,8
divides	22	0,528
overhead (for indexing, etc.)		85,154
TOTAL		410,876

The overhead used depends on the computer instruction capabilities. A time equal to the add time has been reasonable for the computers used by the author.

The total time (410.876 milliseconds) is the estimate of the execution time if all calculations are executed sequentially. Other calculations take priority over the filter. If the filter were allocated 20 percent real time for this problem, then the filter could be cycled every 2.0544 seconds. If the measurements are to be accepted at a higher rate (e.g., 10 Hz), then we must introduce data averaging (preprocessing logic) or simplify the filter substantially.

This type of information, along with the available frequency of the navaid data, which is frequently high (e.g., 40 Hz for elevation data from the microwave landing system (MLS)), illustrates the practical problems of:

(1) What data should be accepted?

(2) Should preprocessing (e.g., simple averaging) be used so that all data can be accepted?

(3) What minimum frequency of filter cycling is required?

These type of problems have to be resolved in the design.

3.1 Navigation Equations. The navigation equations accept raw accelerometer data and calculate position, velocity, and platform-control torques. In the aided systems discussed, the navigation equations are used to keep the best estimate of the state current. This means that the form of the navigation equations has to allow the estimated error state to be introduced and correct the estimate. The error-state vector for a three-axis implementation will have at least 10 components:

(1) Three position errors.

(2) Three velocity errors.

(3) Three platform/computer misalignment angles (tilts).

(4) One vertical acceleration bias.

The position, velocity, and acceleration-bias estimates are carried in registers in the computer so that there is never a problem in adding estimated errors to the state. The tilts are not immediately changed, unless the navigation equations are mechanized in a manner which permits this change. Figure 6 is a block diagram of the type of mechanization which provides for compensation of the dominant error sources of a platform IMU, including tilts. The accelerometer outputs are compensated for bias, scale factor, and misalignments before compensation for tilts. The output of the compensation is the specific-force vector used by the navigation equations. The computed platform rate required to keep the platform level is compensated for tilts followed by scale factor and misalignments, steady drifts, and drifts due to mass unbalance (g-dependent drifts). The mechanization shown permits a leveling rate to drive the estimate of tilts to zero without having any influence on the navigation or estimation results. This type of mechanization has the following advantages:

(1) The linearization assumptions embodied in the filter algorithm are less prone to cause problems.

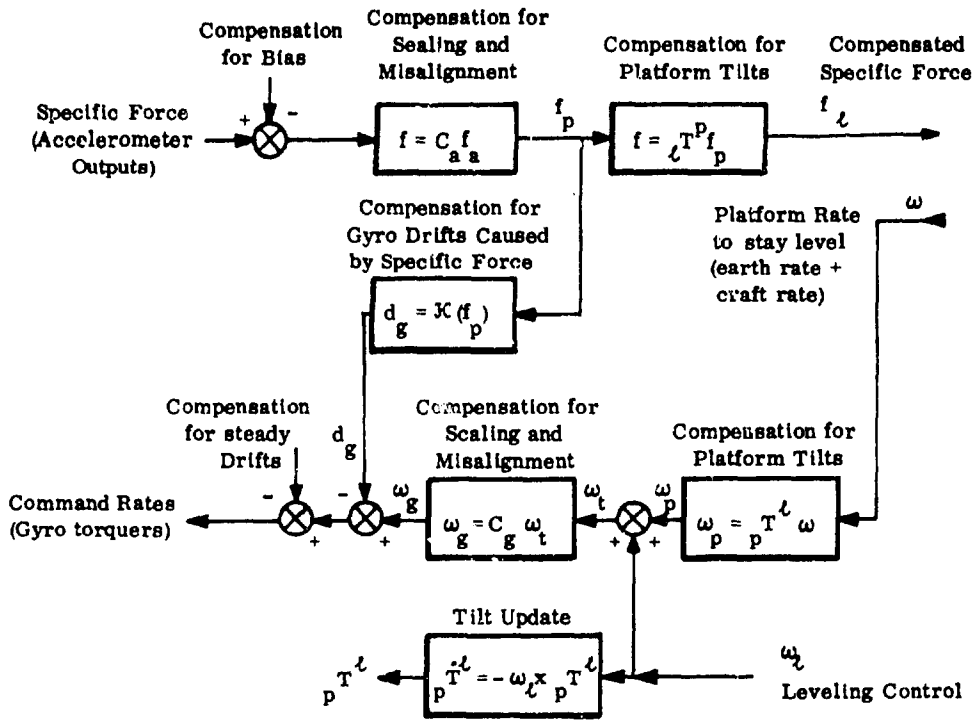

Figure 6. Block Diagram of Software Compensation for IMU Anomalies

(2) Control for platform leveling is completely independent of the estimation problem. Estimates of state changes due to the leveling control need not be carried by the filter while the platform is being leveled.

(3) The conceptual "errorless navigator" is a perfectly compensated real platform rather than an ideal errorless platform. This modeling simplifies (at least conceptually) the development of error models for the Kalman filter.

This mechanization has been implemented in two of the systems the author has developed. Its only disadvantage is a small increase in the memory and real time required by the navigation equations in the airborne computer.

3.3 Systems Modes. An aided INS for airborne uses must generally have the following modes:

(1) Warm-up and coarse alignment.

(2) Fine ground alignment (platform is leveled, heading estimated, and gyro drifts calibrated).

(3) Aided navigation using the available navigation measurements in accordance with some predetermined schedule or priority assignment.

(4) Airstart (for a restart in the air in case of power dropout or other causes).

In the systems the author has worked on, Modes 2 and 3 are very similar in the filter implementation. The prime difference is in the type of measurement used for the mode. For ground alignment a pseudo-measurement is used, which gives the information to the filter that the aircraft is stationary on the ground. For example, changes in position (from the input reference value) as the accelerometer data is integrated are attributed to tilts, gyro drifts, and so forth, in accordance with the dynamic error model used in the Kalman filter. With such a mechanization, ground alignment can be terminated at any time by simply removing the pseudo-measurements from the filter. The filter covariance will be properly initialized for subsequent aided uses with this type of system.

The airstart mode has been implemented so that:

(1) The initial state is set from available measurements or inputs. For example,

(a) The platform is coarsely aligned in level flight.
(b) Platform heading is set from magnetic compass plus input.
(c) Velocity registers are computed from airspeed and heading information.
(d) The position registers are set from TACAN and barometric altitude data.

(2) The initial covariance matrix is set in accordance with a reasonable error model of the state initialization used in item 1.

This system is then started in the aided mode (Mode 3) and, if navaid measurements continue, the system converges to a reasonably accurate navigation reference. If the system were to enter a period of free inertial operation (no navaids) right after such a start, the performance would be very poor.

3.4 Error-state Variables. The error states for four systems the author has worked on are listed in Table 1. System 1 is the C5 navigation system described in Reference [1]. This system uses 16 error states for a three-axis implementation of the aided navigator. Of these, 13 are used for the inertial navigation errors and three are used for navaid calibration.

Table 1. Error States for Four Example Designs

	SYSTEM 1	SYSTEM 2	SYSTEM 3	SYSTEM 4
position error	3	2	3	3
velocity error	3	2	3	3
tilt error	3	3	3	0
gyro drifts	3	3	0	0
acceleration bias	1	2	1	3
Doppler	2	NA	NA	NA
star tracker	NA	1	NA	NA
airspeed (winds estimated)	NA	3	NA	2
barometric altitude	1	NA*	1	1
TACAN (range and bearing)	0	0	NA	2
	16	16	11	14**

*The vertical channel was stabilized by a constant-gain filter using barometric altitude as the reference. This filter was external to the Kalman filter.

**This system uses two Kalman filters in parallel. The level channel has 10 error states and the vertical channel has four error states.

System 2 uses a star tracker as the primary navaid. The vertical channel of this mechanization is stabilized with barometric altitude data by a constant-gain filter external to the Kalman filter. Here there are 12 states for the level-channel errors of the inertial navigator, one state for calibration of the primary navaid, and three states for incorporating airspeed information into the Kalman filter. Winds are estimated by the Kalman filter in this application.

System 3 was an experimental system [3, 4, 5] for potential use in automatic landing. The primary navaid reference was a precision ranging system using three transponders which were located at selected positions with respect to the runway. This mechanization used 10 error states for the three-axis inertial navigator and one error state for navaid calibration (bias in the baromtric altimeter).

System 4 is an experimental system for potential use in aircraft landing operations where the microwave landing system (MLS) is the primary reference. In this instance, real-time constraints of the airborne computer caused the filter to be configured as 10 error states for the level channel, and a separate (run-in-parallel) four-error-state filter for the vertical channel. It has nine error states for describing error of the inertial reference, and five error states for navaid calibration. Airspeed data is used in the level-channel filter, so two of the error states are for estimating winds.

The first three systems all incorporate a high-accuracy platform-type IMU. System 4 uses a low-cost strapdown reference IMU consisting of directional and vertical gyros for aircraft attitude and a triad of body-mounted accelerometers. The gyro and accelerometer outputs are digitized by a 12-bit A/D converter. The accuracy of this inertial reference is very low; however, the MLS measurements are of high accuracy and almost continuous, so the overall system accuracy is adequate for automatic landing.

The design of all of the systems was limited in the number of state variables by the real-time or memory constraints of the airborne computer. The particular error states used were selected as the best compromise for the particular application of the system. Some other relevant information on these systems is given in Table 2.

3.5 Filter Algorithms. The first aided INS for aircraft navigation uses experienced by the author was begun in 1966. The extended Kalman filter with the covariance matrix calculated in the computer was implemented in this system. The potential scaling problems with fixed-point arithmetic led to the selection of 14-bit floating-point software for the filter. Several numerical problems were experienced and "fixes" were added to provide a satisfactory algorithm. The square-root algorithm (without forcing functions) was developed by MIT for the Apollo system in the early 1960's. A fairly efficient square-root algorithm, including random forcing functions, was developed by the author in 1968 [6]; however, it was not until 1970 that the algorithm could be applied. By this time, a more efficient algorithm was available [2] and was therefore selected for System 3 of Tables 1 and 2.

Table 2. Characteristic of Example Systems

	SYSTEM 1	SYSTEM 2	SYSTEM 3	SYSTEM 4
Filter algorithm	Extended Kalman normal variance	Extended Kalman square-root cov.	Extended Kalman square-root cov.	Extended Kalman square-root cov.
Computer arithmetic	13 bit + sign floating point software	31 bit + sign fixed point	23 bit + sign fixed point	17 bit + sign fixed point
Cycle time	(Ref. 1)	60 (sec)	2 (sec)	1 (sec)
Measurement averaging	on some meas.	on some meas.	no	on all meas.
Multiply speed	software (slow)	12-24 μs	32 μs	24 μs
% real time	?	10-20	30-40	23-27
Storage	2-3 k 26-bit words	5.8 k 16-bit words	3 k 24-bit words	3 k 18-bit words
Development period	1966-1968	1972-1974	1970-1972	1974-1976

The algorithms used in Systems 2, 3, and 4 are, for all practical purposes, identical except for minor modifications for the specific application and the instruction repertoire of the airborne computer. The square-root algorithm used for these systems is summarized in this section.

The timing and order of calculations carried out in the filter is described with reference to Figure 7. The filter reference time is updated at a relatively low frequency compared to the other operations shown.

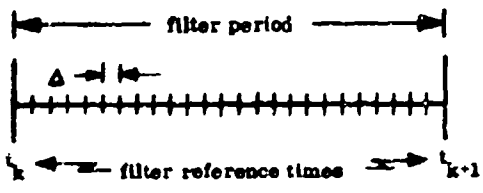

Δ = period of accepting measurements

Δ/m = period of navigation update

Figure 7. Timing for Filter Calculations.

The navigation-equation update occurs at the highest frequency. Logic for processing measurements is entered every m^{th} cycle of the navigation equations. This logic computes residual sums for measurements which are handled in this manner, or residuals for the measurements which are handled discretely.

The filter reference time is always behind real time. The maximum lag (before logic will fail to operate properly) is two filter periods. Assume that real time, t, lies in the region $t_k < t < t_{k+1}$. The quantities necessary for defining the transition matrix, $\Phi(t; t_k)$, are calculated at the frequency of accepting measurements.

As previously mentioned, two types of measurement preprocessing have been implemented:

(1) Residual sums where the sum is carried over a filter cycle (from t_k to t_{k+1} in Figure 7). If the measuring device provides nearly continuous measurements, as can be the case for airspeed and barometric altitude, then the preprocessing logic accumulates residual sums and partial sums for referencing the residual sums to the filter time, t_k. At time $t_{k+1} - \Delta$, the preprocessing logic loads the residual sums and partials for processing by the Kalman filter. The arrays used for accumulation are cleared for use in the next filter cycle.

(2) Discrete measurements which occur at some time in the time interval t_k to t_{k+1} as, for example, a position fix or a star fix. The preprocessing logic forms the residual and partial (for referencing the residual to time t_k) and loads the data for processing by the Kalman filter.

The Kalman-filter logic is arranged so that once keyed to process measurements, it will take care of all the measurements and then reference the incremental (error) state to current time. In this manner, errors in the estimated state are corrected as soon as possible. After the filter has completed all the measurements in the time interval t_k to t_{k+1}, the logic performs a time update to establish a new filter reference time at t_{k+1}.

The filter equations for the incremental state, $d\hat{x}$, and the square-root covariance, W^T, are:

(1) Time Update

$$d\hat{x}(t) = \Phi(t; t_k)\, d\hat{x}(t_k) \tag{1}$$

Let

$$W(t_k)\, W(t_k)^T = P(t_k) \tag{2}$$

where

$P(t_k)$ = the $n \times n$ covariance matrix, and

$W(t_k)^T$ = the $n \times n$ square-root covariance matrix updated in the filter

Then, $W(t_{k+1})^T$ is formed by the two-step computational order:

(a) Step 1

$$A^T = \begin{matrix} \\ n \\ m \end{matrix} \overbrace{\begin{bmatrix} W(t_k)^T\, \Phi(t_{k+1}\, t_k) \\ U^T(t_k) \end{bmatrix}}^{n}$$

(b) Step 2 $W(t_{k+1})^T = A^T$ reduced to upper triangular form with the Householder algorithm [2].

In Step 1 we note that $AA^T = \Phi(t_{k+1}; t_k)\, P(t_k)\, \Phi^T(t_{k+1}; t_k) + U(t_k)\, U(t_k)^T$.

This shows that $U(t_k)$ represents the square root of noise contribution to the growth of the covariance matrix in a time update.

(2) Measurement Update

$$d\hat{x}^+ = d\hat{x}^- + K(k)\, (\Delta y(k) - H(k)\, d\hat{x}^-) \tag{4}$$

where

$\Delta y(k)$ = the residual or residual sum for the k^{th} measurement,

and

$H(k)$ = the partial (referenced to time t_k) for the $\Delta y(k)$ residual.

Define

$$\zeta = (W(k)^{-})^{T} H(k)^{T}$$

$$\eta = W(k)^{-}\zeta \tag{5}$$

$$\alpha = (\zeta^{T}\zeta + R(k))\sqrt{R(k)/(\zeta^{T}\zeta + R(k))}$$

Then, K(k) of Eq. (4) is given by

$$K(k) = \eta/(\zeta^{T}\zeta + R(k)) \tag{6}$$

and the square-root covariance is updated by

$$W(k)^{T+} = W(k)^{T-} - \zeta\eta^{T}/\alpha \tag{7}$$

(3) Transition Matrix

Let

$$\Phi(t; t_k) = e^{\int_{t_k}^{t} F(\tau)\, d\tau} \tag{8}$$

The integral in Eq. (8) is approximated by

$$\int_{t_k}^{t} F(\tau)\, d\tau = \sum_{l=1}^{n} F_l(t_l)\,\Delta \tag{9}$$

where

$$n\Delta = t - t_k \tag{10}$$

Only the non-zero terms in $F(t_l)$ are stored and updated.

When the transition matrix is needed, the non-zero terms of

$$B = \sum_{l=1}^{n} F(t_l)\,\Delta + \left(\sum_{l=1}^{n} F(t_l)\,\Delta\right)^{2}/2 \tag{11}$$

are formed. To implement Eq. (1) the logic below is executed.

$$d\hat{x}(t) = d\hat{x}(t_k) + B\, d\hat{x}(t_k) \tag{12}$$

The matrix B of Eq. (11) is kept as a vector of the non-zero elements. Arrays containing indices (or addresses) are appropriately set up to execute a matrix multiply as in Eq. (12) without any multiplications by zeroes.

3.5 Design Validation. The aided INS is sufficiently complex that a design validation by means of digital simulation is almost mandatory. In the simulation all the known factors affecting the system are simulated and the overall system performance is evaluated. A simulation consists of the digital implementation of the elements shown on Figure 8. The flight-profile generator shown in Figure 8 produces the specific-force vector acting on the simulated IMU and a vector of true position and velocity, and other items necessary in the measurement simulation. The flight-profile generator must be capable of producing time histories of the indicated variables for "typical" flight plans the real aircraft will fly.

The IMU simulation generates the simulated accelerometer measurements and the simulated platform response to torque inputs. This simulation includes the relevant IMU error sources:

(1) Accelerometer scale factor, misalignments, null bias, noise, and quantization.

(2) Gyro scale factor, misalignments, steady and random drifts, mass unbalance drifts, anisoelastic drifts, and quantization.

The airborne-computer simulation simulates the relevant factors affecting performance:

(1) Approximations used in the navigation equations (gravity model, earth-curvature model, and so forth).

(2) Airborne-computer compensation for the IMU (see Figure 6).

(3) Scaling, word size, and other numerical characteristics.

(4) Kalman-filter approximations in areas such as the transition matrix, measurement partials, and so forth.

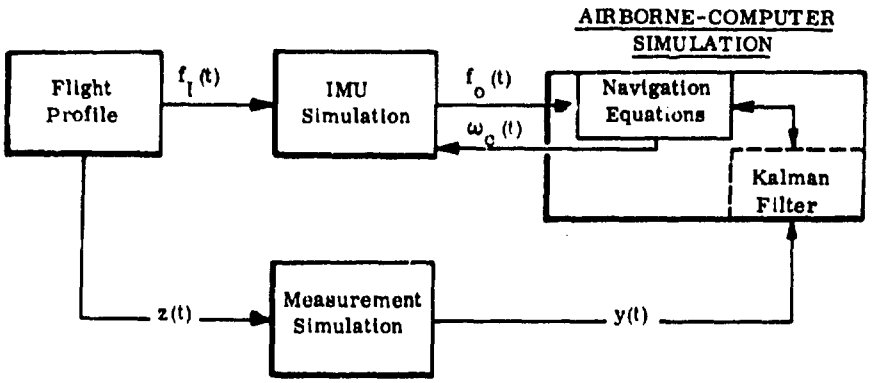

$f_I(t)$ = specific-force vector acting on IMU

$f_o(t)$ = measured specific-force vector (by accelerometers)

$\omega_c(t)$ = vector of commanded-gyro-torque rates

$z(t)$ = vector of true position - velocity, etc.

$y(t)$ = vector of simulated measurements

Figure 8. Functional Block Diagram on an Aided-Navigation-System Simulation

The measurement simulation produces a time history of the simulated measurements which are consistent with the flight path and contain realistic modeling of the measurement error sources:

(1) Random error sources.

(2) Error sources caused by timing.

(3) Bias error sources.

(4) Dropouts.

(5) Bad measurements (outliers).

The digital simulation can uncover many problems in the initial design for an aided INS. Examples of problems found by simulation include:

(1) A singularity in the covariance matrix which under certain conditions caused unsatisfactory performance.

(2) A poor selection of the order of data processing in the initial design which gave unsatisfactory performance in certain modes of operation.

(3) Mistakes which were made in the mathematical formulation of navigation equations, transition matrix, and measurement partials in the initial design.

(4) Nonlinear effects in the initial design which caused unsatisfactory performance with large initial errors.

(5) Approximations developed in the initial design which were not adequate for the full range of operations.

(6) The compensation for unmodeled error sources developed in the initial design which was not adequate.

During the validation phases these types of problems (if discovered) can be readily corrected. In the flight-test phase their isolation and correction can be very difficult and costly.

3.7 Onboard Computer Program Development and Checkout. A considerable amount of detailed programming and checkout was performed in the last three systems the author has helped to design. This experience has demonstrated several important details which are:

(1) It is important to have a good (preferably one-to-one) correspondence between routines in the airborne-computer program and routines in the digital simulation. If the digital simulation has been properly modularized, this correspondence is very useful. For example, check outputs for sample inputs are easily obtained; also, the logical flow governed by flags in the simulation program can be copied in the airborne-computer programming.

(2) A detailed knowledge of the instructions executed in the airborne computer is desirable. For example, suppose that the multiplication of two 32-bit words give a rounded 32-bit answer. Then, one must take care in forming the magnitude of an inner product of two vectors in order to retain significance in the answer.

(3) Knowledge of the interrupt structure and how the filter will be time shared with the other (higher priority) logic is desirable. One must set up the onboard software such that all calculations are completed in the allotted time. Steps should be inserted to provide indication if the time order of calculations is not proper. Also, the timing of when the measurements are made and when they are processed can be important in obtaining the required accuracy.

(4) Advanced planning and extra software is desirable in the checkout of the onboard-computer program. A simulated platform and profile generator, and simulated measurements in onboard software is very helpful in checking out the navigation equations and Kalman filter.

(5) Proper scaling of variables is very important in fixed-point computers. If the filter designer programs the logic, the details of scaling in every operation are very evident, so one can ensure proper significance on all the operations. If the programming is to be given to a programmer, then very detailed flow charts and scaling must be provided to ensure proper significance.

(6) Digital output of many variables on a printer is almost a requirement in Kalman-filter checkout. Such output must come in an on-line manner without affecting system operation. This type of data may require special software in the airborne computer as well as special hardware.

3.5 System Validation. One of the more interesting and challenging phases of the aided INS development is the final validation. The system hardware and software must play together to give the desired overall response. Isolation of the causes of undesired characteristics can be very difficult. In the author's experience the first tests are in the laboratory where the ground alignment and free inertial modes are exercised, and subtle problems in both hardware and software are discovered and corrected. The Kalman filter, which is used in flight, also performs the ground alignment in the designs the author has implemented. As a result, a good series of laboratory tests can validate all the flight software except that associated with the actual navaid measurements.

The importance of recording appropriate data for system validation in the laboratory and in the flight tests cannot be overly stressed. The most desirable recordings are such that post-flight operations permit:

(1) The use of filter-smoothing techniques to estimate the time-varying system errors. This can be accomplished in a general-purpose computer program using the recorded flight data if proper data is taken.

(2) Playback of the recorded flight data into the airborne computer. An option in the I/O of the airborne computer can be designed so that recorded flight data is used in place of the actual measurements.

Item (1), if available, permits one to get at better models of system errors for:

(1) Correcting hardware deficiencies.

(2) Correcting filter approximations for the real error sources.

(3) Correcting the errors by improving the software calibration model.

Item (2), if available, permits one to use the recorded raw data with the modified software to validate improvements before later flight tests.

As an illustration of the type of problems one can encounter in the system-validation phases, an experience in the RAINPAL system development is described [3, 4, 7]. A block diagram of the experimental system is shown in Figure 9. The Litton LTN-51 INS was used for three-axis accelerometer data for this system and the Ames/Cubic Precision Ranging System (PRS) was the primary navaid.

The radar altimeter and the barometric altimeter were also used as navigation aids. The navigation equations and Kalman filter were executed in an SPC 320 computer. During the design phase of this system, all the available information on the PRS indicated that it was a very accurate ranging system. Measurement errors were believed to be less than about 5 feet. Simulation studies indicated that a very high-accuracy navigation reference was obtainable (sufficient for aircraft landing) if the three transponders of the PRS were properly located with respect to the runway. The PRS measurements were the ranges to each of these transponders. These range measurements were available at a very high frequency, but they were only used with a 0.5 Hz filter.

The system was flight tested at the White Sands Missile Range (WSMR) where cine theodolite tracking could give an excellent reference trajectory for accuracy checks. Figure 10 shows the flight pattern for one of the flight tests at WSMR, and Figure 11 shows the range-time histories for this flight. Note that there is a significant amount of bad data in these measurements; however, software was designed to reject these points and the bad data was not a

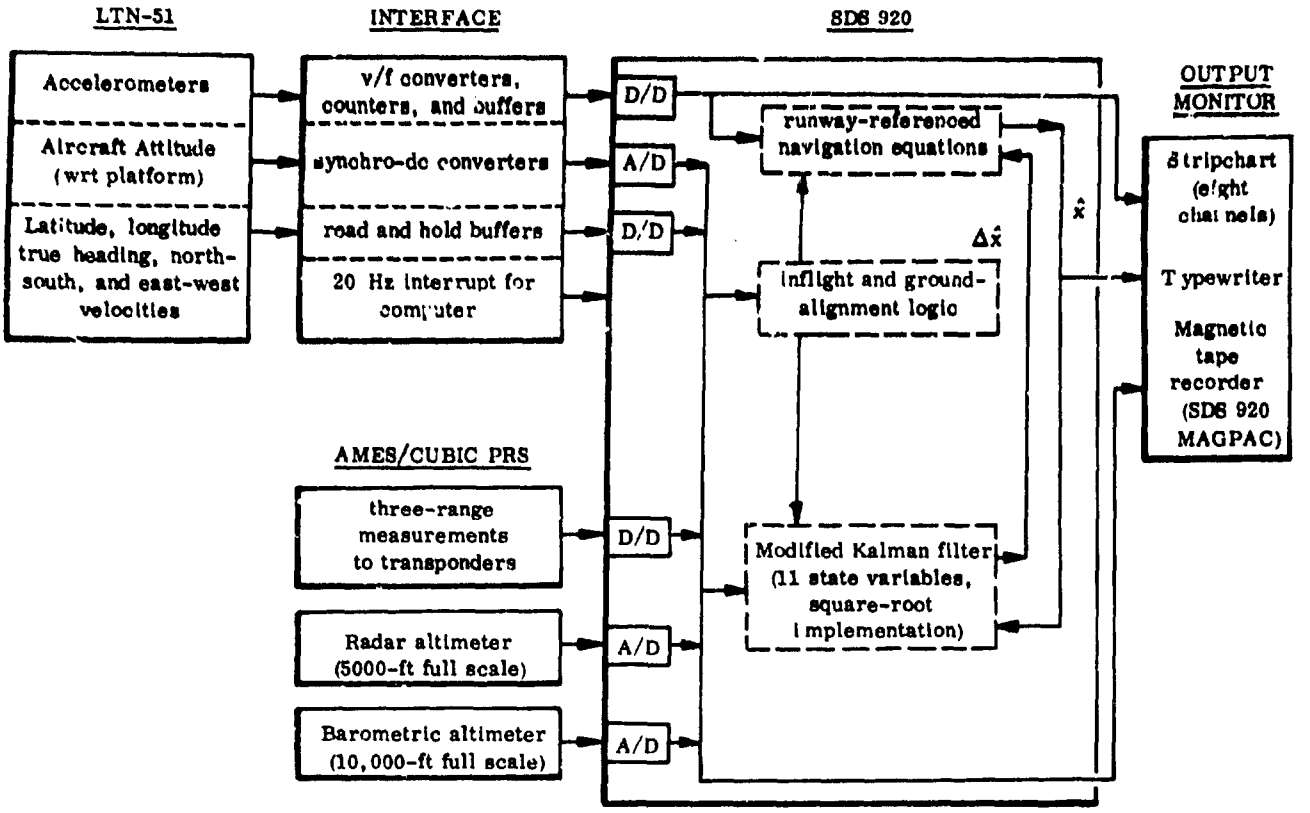

Figure 9. Block Diagram of Experimental Navigation System.

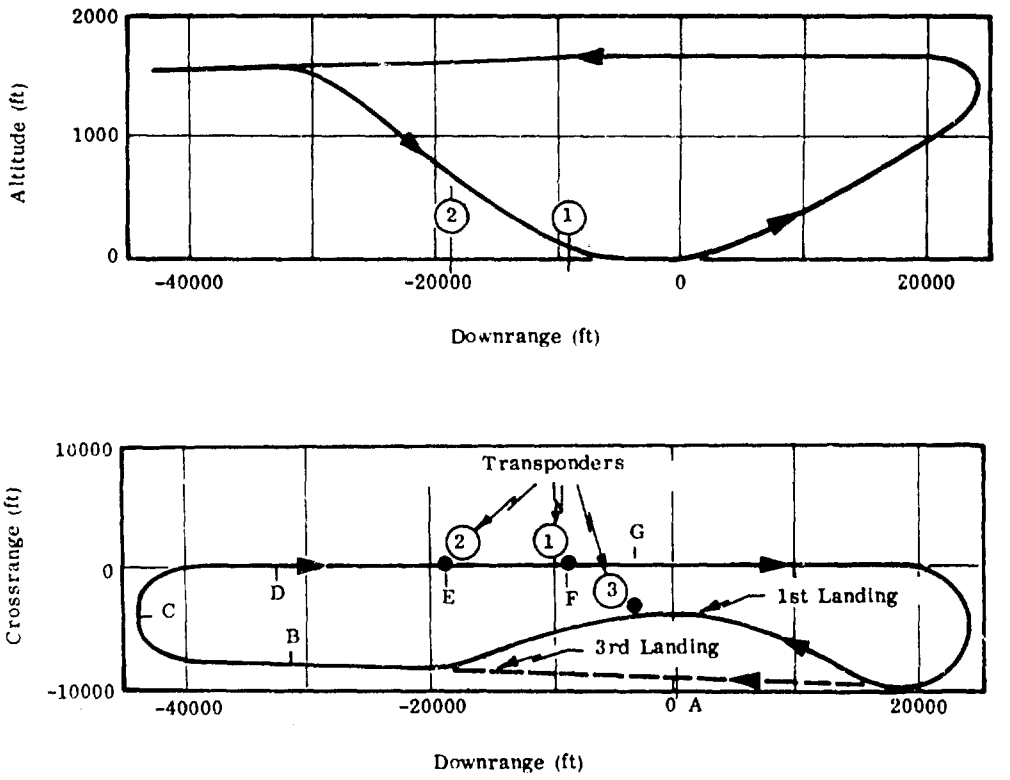

Figure 10. Flight Pattern for WSMR Flight tests of 26 January 1972

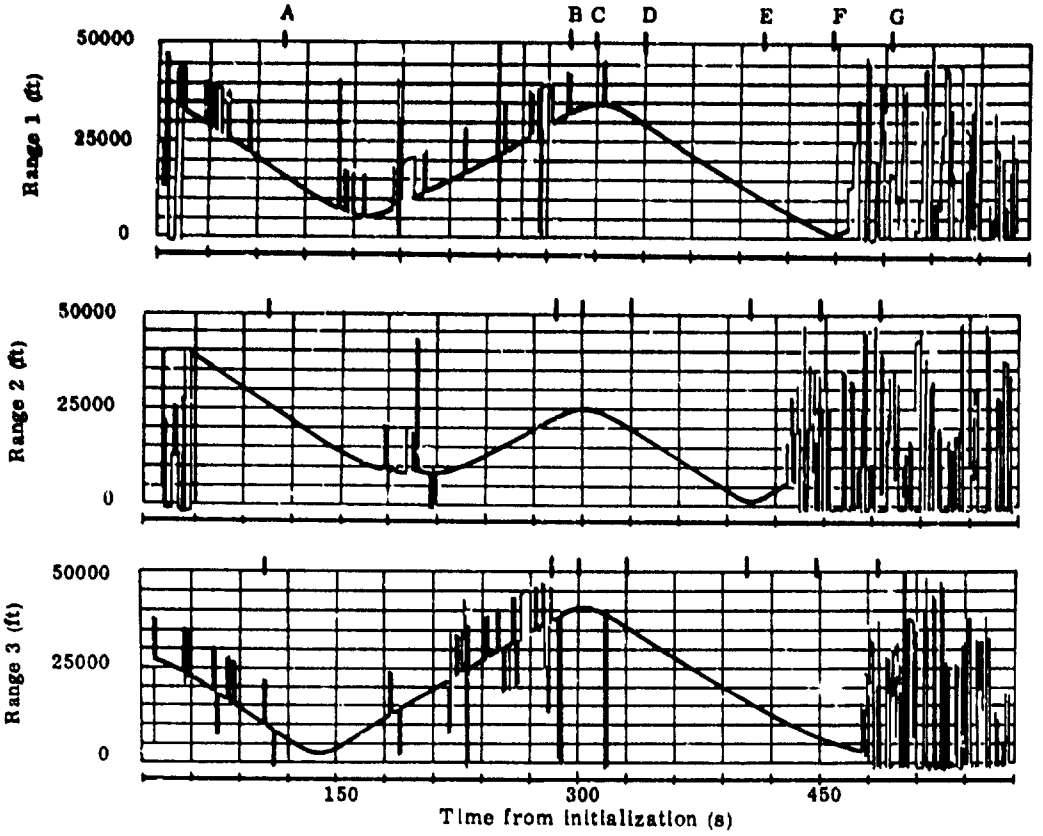

Figure 11. Range-Time Histories for First Landing at WSMR on 26 January 1972

serious problem in the tests. All the raw data was recorded in the tests so that experiments could be run after the fact (post-flight) in the SDS-920 software to access accuracy and study anomalous behavior.

Post-flight processing revealed that we could not achieve the desired accuracy. After considerable effort the problem was traced to the PRS system whose errors were considerably larger than previous tests had indicated. Residuals (differences between the PRS ranges and ranges computed from the WSMR cine theodelite tracking data) along with the computed range-rate histories are shown in Figure 12. There is an obvious strong correlation between the range error and the range rate. The error source was traced to a design deficiency in the automatic gain and frequency control of the PRS. Although the design should have been improved and the tests conducted again, this was not done for this experimental system. Instead, a software compensation was installed to effectively remove the error from the raw data.

Figure 13 presents time histories of the WSMR estimate computed from the cine theodolite data and three Kalman-filter estimates computed by the onboard software using the software-corrected PRS data. The onboard software uses every 20^{th} sample of the recorded navaid data, so each Kalman-filter estimate shown has a different starting time and different samples of the recorded navaid data. This data shows an excellent comparison between all of the estimates, which indicates the potential performance of such an aided INS; however, the real system was never reflown to give an absolute validation of this potential.

4. Future Trends in Aided INS for Aircraft

The applications-type problems and their solutions which have been experienced by the author over the past decade have followed the philosophy of designing the navigation system for some phase of aircraft operati . Two of the system which were discussed could be classified as "enroute" systems and two could be classified as erminal area and landing" systems. The emphasis has not been directed at a single navigation system for all phases of flight from takeoff to landing. Future systems should have this integrated design approach, since it gives a means of checking each new class of measurement (as the flight proceeds) against all previous measurements. This should improve the safety of operations (bad measurements can be rejected and warnings of failed devices provided).

A related area which has been barely considered in these designs is overall reliability of the navigation system. The designs have generally been of a "single thread" type, in that many hardware failures would require the pilot to switch to a less accurate system for a navigation reference. If the aided navigation system is to provide the capability for all-weather operations including landing, then there is an obvious need for very high reliability in all of the systems destined for aircraft use.

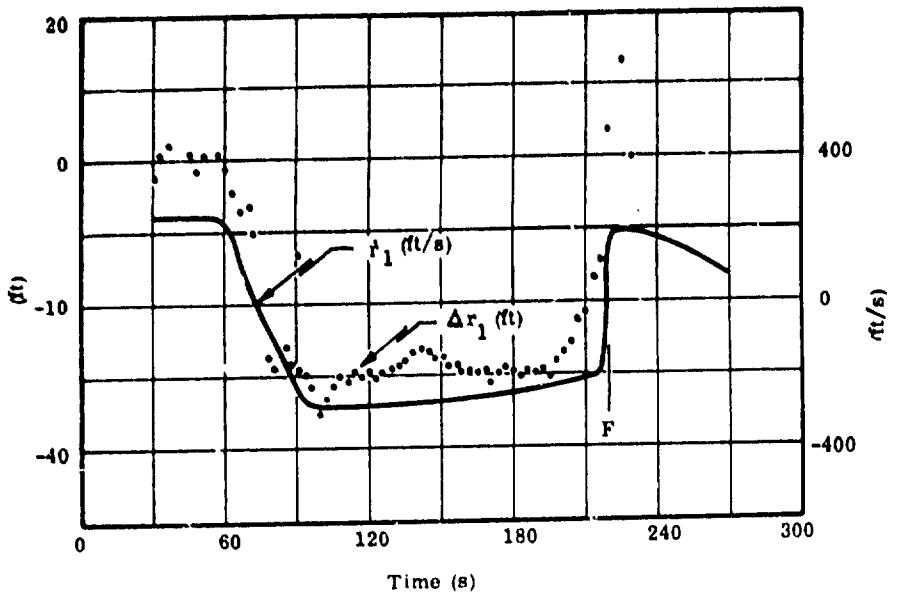

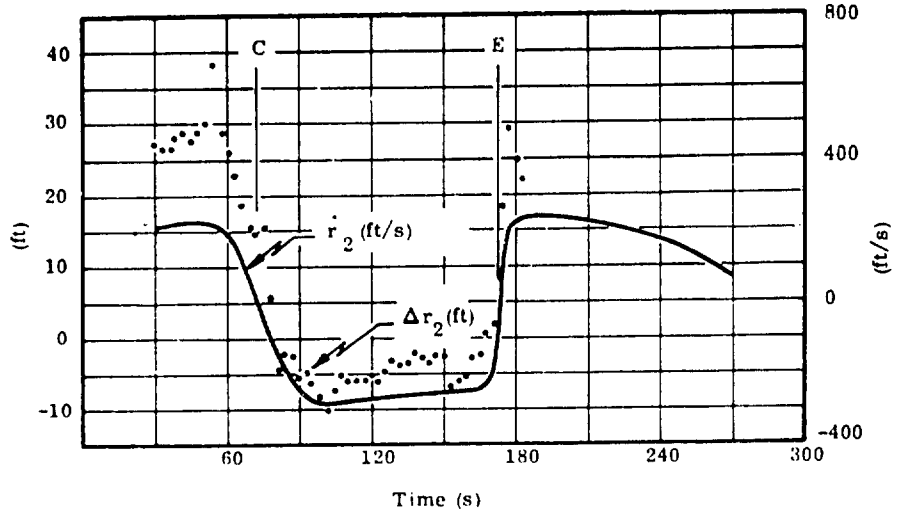

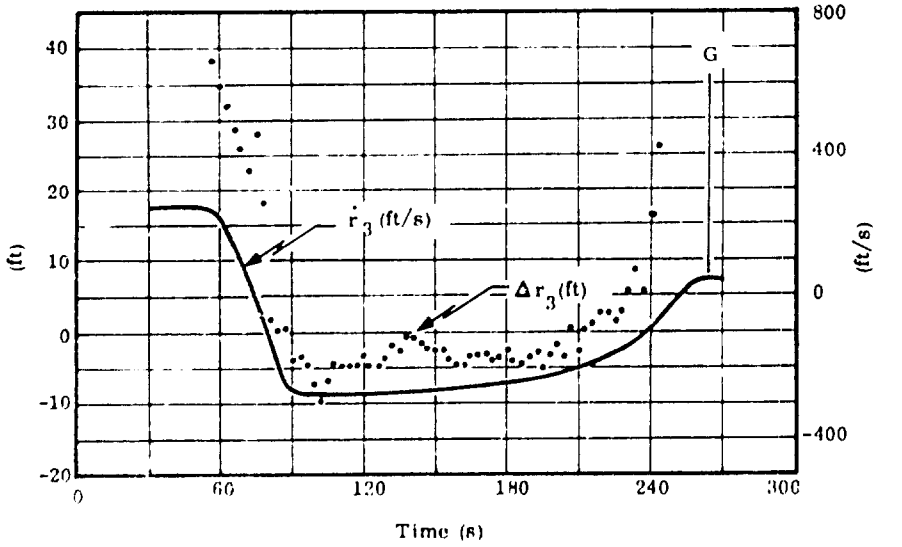

Figure 12. Residuals and Range rates for First Landing

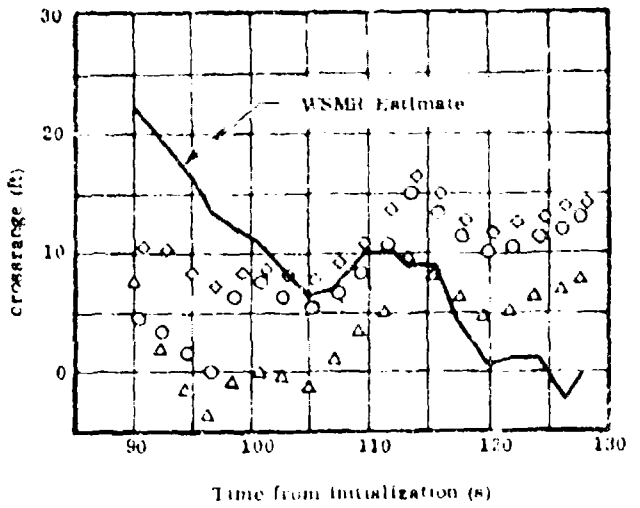

(a) Crossrange vs. Time

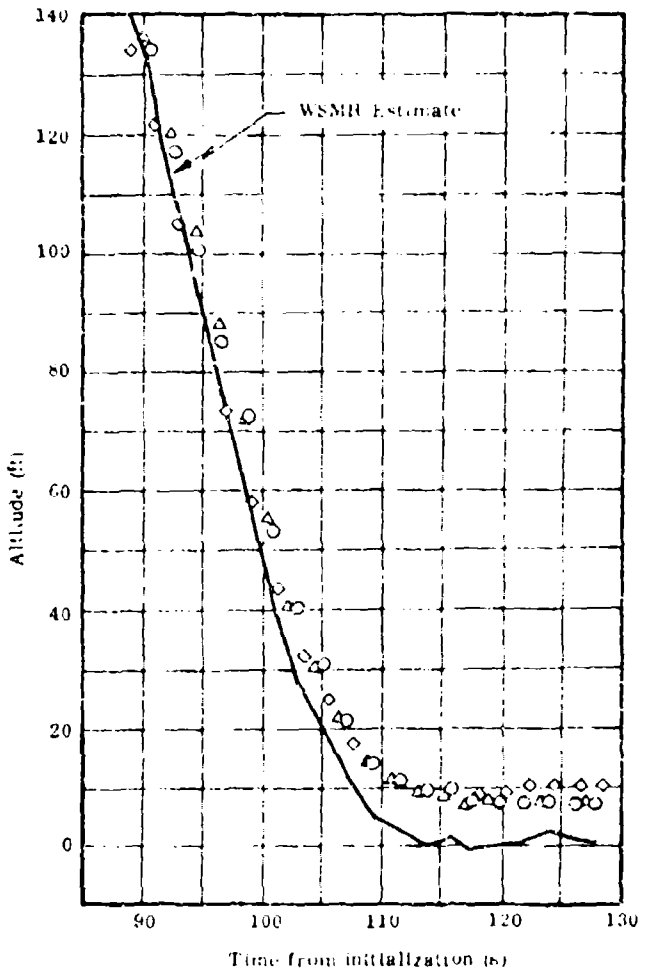

(b) Altitude vs. Time

Figure 13. Comparison of WSMR and Kalman-Filter Results for First Landing

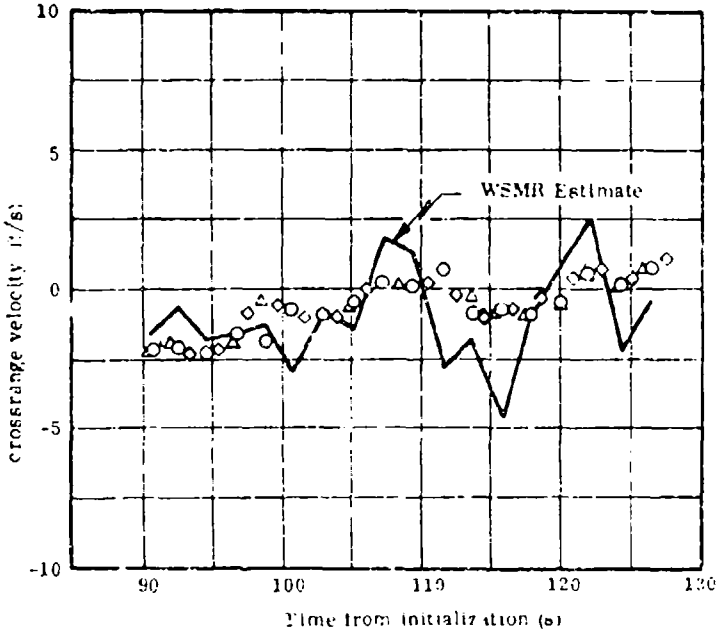

(c) Crossrange Velocity vs. Time

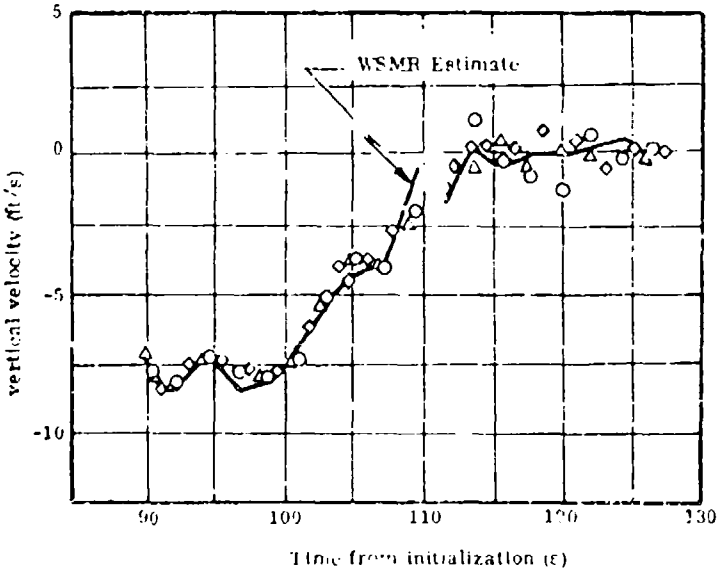

(d) Vertical Velocity vs. Time

Figure 13 (continued)

A promising technique for gaining high reliability in the inertial sensing devices used for navigation and control has been implemented by The Charles Stark Draper Laboratory, Inc. [8, 9, 10]. The techniques uses redundant skewed accelerometers and gyros in a strapped-down configuration (no stable platform is required). Logic in the airborne computers (dual computers are used in the implementation) checks the raw sensor data and removes failed sensors from affecting the system. The IMU consists of six accelerometers and six gyros. Since only three of each type are required for three-axis information, there are three spares of each type (redundant sensors). The software in the computers is designed to detect and isolate failures of up to two sensors of each type. In addition, the software can detect a third failure in either sensor type, but cannot isolate which instrument has failed. Such a mechanization provides fail-operational fail-safe performance for one, two, or three failures, respectively, of either sensor type.

In order to obtain a reliable navigation system for all phases of flight it is necessary to use redundant navigation aids as well as redundant inertial sensors. Let us examine the merits of the aided INS depicted in Figure 14. In this system we have redundant skewed sensors feeding the failure detection and isolation (FDI) software in the computer. The FDI software removes effects of failed sensors so the inputs to the navigation equations are reliable signals. Barring computer failures, the estimated state computed by the navigation equations is therefore reliable.

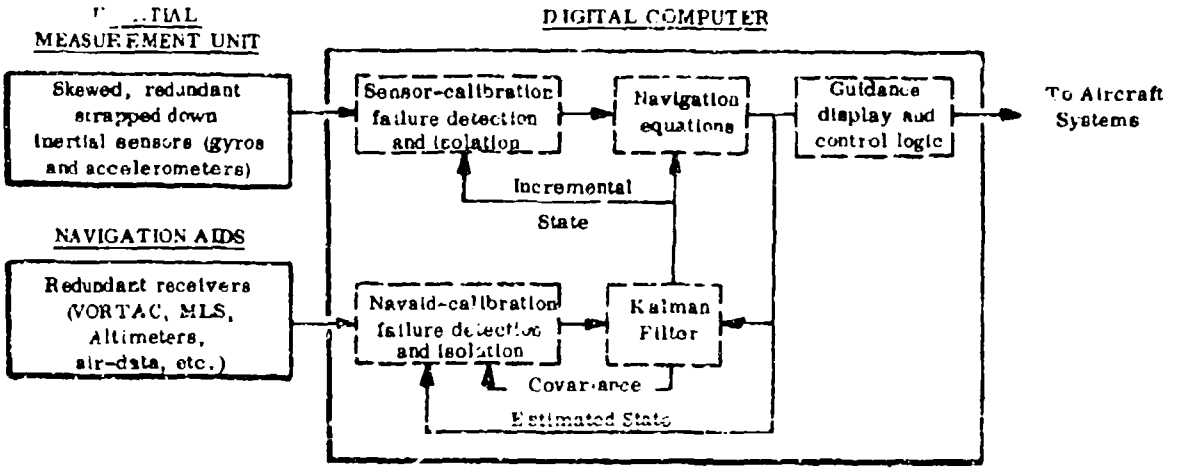

Figure 14. Block Diagram of a Redundant Avionics Navigation System

That is, failures in sensors up to some maximum number are tolerable and do not have a large effect on the state estimate. The accuracy of the state estimate will depend on the past history of operation (from alignment). The covariance matrix calculated by the Kalman filter can be a reliable indication of this accuracy, provided we are able to detect and isolate (remove) bad navaid measurements.

The covariance matrix and the estimated state are used in the failure detection and isolation logic of the measurements from the redundant navigation aids. Residuals calculated in this logic can be accepted or rejected based on comparison of the magnitude of the residual to calculated statistical boundaries which are consistent with the accuracy of the measurement device and the accuracy of the estimated state. If such logic is used on two redundant receiver outputs, then fail-operational fail-safe operation is possible. If one receiver fails, the logic will automatically reject the measurement. If both fail, then both will be rejected and the necessary warning for pilot action will be provided. This warning need not take place instantaneously, since the overall accuracy will degrade slowly rather than abruptly. Hence, if the failure is of an intermittent type the system can continue in many situations. Even with a 100 percent failure in the navaids, the flight may be able to proceed (as, for example, in critical landing problems) without catastrophic results.

This type of system has the desired inherent reliability for advanced automatic landing aircraft. By having a single integrated system for all phases of flight, the desired automatic testing and failure-removal operations are applicable to all of the navaids.

One obvious disadvantage in the approach lies in achieving reliability in the computer. Dual-computer strategy has been implemented in the SIRU system of References [8], [9], and [10]. Since there is also a good deal of applied research directed towards developing reliable computers, this problem should be resolved in the near future.

It is believed that this type of integrated avionic system will eventually supersede the "add-on black box" approach of current avionic systems. A lot of applied research and development and experimental testing is required before such sophisticated designs are practical and cost effective for use in commercial aviation.

6. Conclusions

This paper has presented practical considerations, problem areas and solutions experienced by the author in the development of Kalman filters for aircraft navigation systems. The problem areas experienced have been in three categories as follows:

(1) Numerical problems in carrying out the Kalman filter covariance calculations.

(2) Problems in satisfying the constraints imposed by the specific airborne computer's capabilities used in the design.

(3) Problems in developing an appropriate mathematical model of the overall system which is sufficiently accurate and simple enough for implementation.

The square-root implementation of the Kalman filter described in the paper has eliminated problem area (1) in the designs experienced by the author. Advances made in airborne computational capabilities have reduced the difficulties of problem area (2) to the point where it no longer poses a serious design constraint. Problem area (3) is and will likely continue to be the most difficult problem in applying Kalman-filter theory to practical designs. Problem area (3) will persist because we continue to look for improvements in system performance without necessarily improving the system hardware. Improved performance results from improved modeling and compensation for error sources and consequently requires ever-increasing complexity in the system software.

The designs discussed in the paper were of a single thread nature with respect to reliability considerations. Future avionic systems are likely to require fail-operational fail-safe performance, which is obtained through redundant components and redundancy management software. The conceptual design (as described in the paper) for such a system makes use of Kalman filter quantities in the redundancy management strategy. This appears to offer a promising method for gaining the reliability improvements needed in avionic systems, although practical designs which use such strategy have yet to be demonstrated.

REFERENCES

[1] Schmidt, Stanley F., John D. Weinberg, and John S. Lukesh, "Application of Kalman Filtering to the C-5 Guidance and Control System," Theory and Applications of Kalman Filtering, NATO AGARDograph 139, 1970.

[2] Kaminski, P.G., A.E. Bryson, Jr., and S. F. Schmidt, "Discrete Square Root Filtering: A Survey of Current Techniques," IEEE Transactions on Automatic Control, December 1971.

[3] McGee, L.A., et al., Flight Results from a Study of Aided Inertial Navigation Applied to Landing Operations, NASA TN D-7302, 1973.

[4] Schmidt, S.F., "Precision Navigation for Approach and Landing Operations," Proceedings of the Joint Automatic and Control Conference, Stanford University, 1972.

[5] Schmidt, Stanley F., William S. Bjorkman, and Bjorn Conrad, New Mechanization Equations for Aided Inertial Navigation Systems, NASA CR-2352, December 1973.

[6] Schmidt, S.F., "Computational Techniques in Kalman Filtering," Theory and Applications of Kalman Filtering, NATO AGARDograph 139, 1970.

[7] Schmidt, Stanley F., Analysis and Modelling of Measurement Errors in the Ames-Cubic Precision Ranging System, Report No. 72-30, AMA, Inc., July 1972.

[8] Gilmore, J.P., A Non-Orthogonal Gyro Configuration, MIT Department of Aeronautics and Astronautics, MIT SM Thesis. Charles Stark Draper Laboratory, Report T-472, January 1967.

[9] Musoff, Howard, SIRU Utilization, Volume I Theory Development and Test Evaluations, Charles Stark Draper Laboratory, Report R-747, March 1974.

[10] Gilmore, J.P. and R. J. Cooper, SIRU Development Final Report, System Development, Vol. I, Charles Stark Draper Laboratory Report R-746, July 1973.

PRACTICAL CONSIDERATIONS IN IMPLEMENTING KALMAN FILTERS

John C. Wauer
Autonetics Group, Rockwell International Corporation
Anaheim, California

SUMMARY

Techniques that have been used to implement the Kalman filter for aircraft inertial navigation applications are presented. The applications include AMSA advanced development task flight test, FB-111 and F-111D aircraft avionics, at-sea alignment aboard aircraft carriers, and stationary alignment of electrostatic gyro-strapdown navigation system. Techniques used to simplify the filter model are discussed. The use of random walk and white noise error sources is described. State vector transformations are performed to simplify the filter model. Detection of failures is accomplished by testing the measurements for reasonableness. Computational techniques used in computers with fixed-point arithmetic are discussed. A flexible covariance matrix scaling technique is essential to maintain adequate resolution in a fixed-point computer. Efficient algorithms for covariance matrix and state vector extrapolation and reset are described.

1. INTRODUCTION

This lecture discusses some of the practical considerations that have been found to be useful in implementing Kalman filters. Specifically discussed is the application to aircraft inertial navigation; however, the techniques should prove useful in many other applications.

This lecture is based on experience in Kalman filter applications to aircraft navigation that dates from 1964. The Kalman filter has been implemented in real-time digital computers for flight test of Doppler-inertial-checkpoint navigation and transfer alignment on the AMSA advanced development task (1966-1968), FB-111 and F-111D aircraft navigation systems (1968-1970), at-sea alignment aboard aircraft carriers (1968-1974), and stationary alignment of electrostatic gyro-strapdown navigation systems (1973-1974).

The AMSA mechanization was the first real-time implementation of the Kalman filter to aircraft navigation at Autonetics, although a relatively simple filter was used for submarine navigation at an earlier date. The AMSA mechanization is programmed in a 24-bit MARDAN computer with a disk memory having a 10 millisecond access time. The Doppler-inertial-checkpoint mechanization has a 14-element state vector and a filter cycle time of 24 seconds. The transfer alignment mechanization has an 11-element state vector. The MARDAN computer has a digital differential analyzer (DDA) section that does the navigation function, which leaves the general-purpose section free to do the filter computations.

The FB-111 mechanization is programmed in a 16-bit IBM 4- computer. The mechanization has a 13-element state vector and a filter cycle time of 8 seconds. Maximum execution time for one filter cycle is 180 milliseconds. It requires 2200 16-bit words. The F-111D mechanization is similar, but somewhat simpler because it has fewer sensors. The FB-111 filter cycle operates in either the inertial navigation mode or the dead-reckoning mode. The dead-reckoning mode navigates with a magnetic compass, and either Doppler radar or true airspeed velocity sensors. The measurements that can be processed by the filter are position (visual or radar), Doppler, true airspeed, astrocompass azimuth and elevation, velocity fix, hand-entered wind, and hand-entered magnetic variation. The velocity fix consists of two successive position fixes on an unknown landmark. The hand-entered wind and magnetic variation measurements are techniques to allow the pilot to initialize those elements of the state vector while in flight. A priori uncertainty in the pilot's information is used as the measurement noise to provide an optimal estimation of wind or magnetic variation when the error terms are included in the state vector.

The mechanization is divided into estimation and control sections. The estimation section implements a Kalman filter algorithm for discrete measurements. The measurements are, in general, a nonlinear function of attitude (sine and cosine of heading). However, the estimated state vector, $\hat{x}$, is extrapolated with the linearized state equation

$$\dot{\hat{x}}(t) = F(t)\,\hat{x}(t) \tag{1}$$

since it only contains small error terms. The estimated state vector is carried primarily to correct timing errors in control applications. The estimated state vector $\hat{x}(t_k)$ is applied as the control to correct plant errors at time t_{k+1}. This is because the digital computation must lag real time. The sequence of events is shown in Figure 1. The computations associated with the control vector are

$$x_c(t_{k+1}) = \hat{x}(t_k) \tag{2}$$

$$\tilde{x}(t_{k+1}) = \Phi(t_{k+1}, t_k)\,\hat{x}^{+}(t_k) - x_c(t_{k+1}) \tag{3}$$

where x_c is the control vector and Φ is the transition matrix.

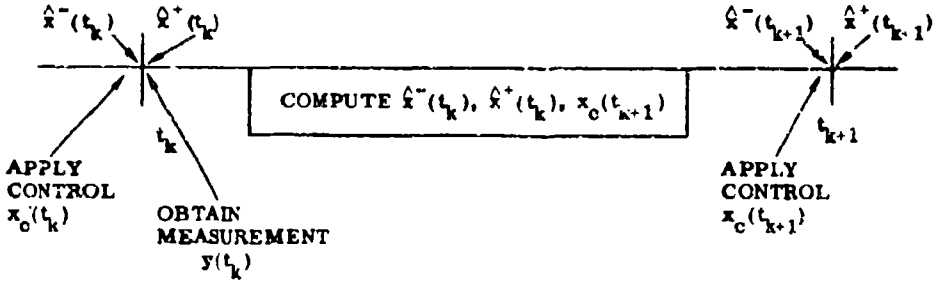

Figure 1. Time Sequence of Estimation and Control Computations

Control is applied impulsively to all plant states. All inertial navigation states are directly accessable except platform tilt, since only a finite gyro torquing rate can be applied. A nonlinear platform controller is built into the navigation mechanization that mathematically transforms the accelerometer data through the estimated but uncorrected platform tilt. The inverse transformation is used to rotate the angular rate vector of the navigation frame back to the tilted platform coordinates for use in gyro torquing. This allows effective impulsive tilt control and still uses small gyro torquing rates.

The following discussion is applicable to all of these applications. Successive applications represent refinements of the basic ideas. Most of the examples are taken from FB-111.

The techniques discussed generally fall into two categories, modeling considerations and computational techniques. The importance of developing an adequate model for the suboptimal Kalman filter is well known. Several techniques for further simplifying the mathematical model are discussed in Section 2. Algorithms have been developed to allow efficient computation of the Kalman filter equations. The algorithms are implemented in computers with fixed-point arithmetic and are discussed in Section 3.

2. MODELING CONSIDERATIONS

The mathematical filter model of the plant used in the Kalman filter is defined by the state equation

$$\dot{x}(t) = F(t)\,x(t) + G(t)\,u(t) \tag{4}$$

and the measurement equation

$$y(t_k) = H(t_k)\,x(t_k) + v(t_k) \tag{5}$$

where

- x = state vector
- F = coefficient matrix
- G = process noise distribution matrix
- u = white process noise vector
- y = measurement vector
- H = measurement matrix
- v = Gaussian sequence of measurement noise

The filter model is suboptimal in that it does not exactly describe the plant. However, it must effectively describe the major error mechanisms. The filter model is evaluated by means of computer error analysis. A covariance analysis program is used which runs on an IBM 370 computer. The program uses the filter coefficients from the suboptimal filter to compute the covariance of navigation errors (position, velocity, and attitude) due to one or a group of error sources. Time history of total system performance is obtained by summing the covariances computed from the individual error sources. The Kalman filter model is chosen by analyzing several models with the program and choosing the one that gives the best performance without unduly complicating the mechanization. The choice of a filter model is an heuristic judgment and no attempt has been made to quantize it. The filter evaluation must be made on several flight profiles and multisensor mixes based on expected missions. Several design concepts have evolved based on a large number of analyses which were performed over the last decade. Some of the major concepts are described in the following sections.

2.1 ERROR SOURCE DESCRIPTION

The error budget for gyro drift rate error usually consists of bias error, long-correlation-time exponentially correlated error, and short-correlation-time exponentially correlated noise.

An exponentially correlated error is described by the state equation

$$\dot{\epsilon} = -\frac{1}{\tau}\epsilon + u_\epsilon \tag{6}$$

where τ is the correlation time and u_ϵ is white noise with power spectral density amplitude

$$Q_\epsilon = 2\sigma^2/\tau \tag{7}$$

and ϵ has variance σ^2. The steady state process has autocorrelation function

$$\phi(t) = \sigma^2 e^{-|t|/\tau} \tag{8}$$

and power spectral density (PSD)

$$PSD(\omega) = \frac{2\sigma^2/\tau}{1/\tau^2 + \omega^2} \tag{9}$$

The short-correlation-time random gyro drift rate is approximated by white noise. The white noise power spectral density amplitude is chosen equal to the zero frequency PSD amplitude of the correlated error

$$Q_u = 2\sigma_s^2\tau_s \tag{10}$$

where Q_u white noise PSD amplitude and σ_s^2 and τ_s are variance and correlation time of the short-correlation-time error, respectively. The approximation is valid if

$$\tau_s < 1/\omega_s = 800 \text{ seconds} \tag{11}$$

where ω_s is Schuler frequency, since the transfer function from gyro drift rate error to velocity error has a pass band between zero frequency and Schuler frequency. The effects of error signals significantly above Schuler frequency are highly attenuated.

The bias and long-correlation-time error sources are approximated in the suboptimal filter by a random walk model. The equivalence between the statistics of an exponentially correlated random process and a random walk process is strictly empirical. The suboptimal filter using a random walk model tends to result in slightly pessimistic filter error statistics. Some pessimism is desirable in a suboptimal filter to account for unmodeled errors.

The differential equation for the random walk model, ϵ_r, is

$$\dot{\epsilon}_r = u_r \tag{12}$$

where u_r is white noise with PSD amplitude Q_r. The variance of an uncontrolled random walk model grows linearly with time. The intent is to describe an error source that changes value in some fixed time, T, in a manner similar to the long-correlation-time error, ϵ_L, or

$$\Delta\epsilon_L^2(T) = E\left|\epsilon_L(0) - \epsilon_L(T)\right|^2 \tag{13}$$

$$= 2\sigma_L^2(1-e^{-T/\tau_L})$$

where $\Delta\epsilon_L^2$ is the variance of the change and σ_L^2 and τ_L are variance and correlation time of the long-correlation-time error, ϵ_L. It has been empirically found through error analysis that the best filter performance is obtained when the change in variance of the random walk model is near σ_L^2 in time τ_L or in other words the PSD amplitude of u_r is

$$Q_r = \sigma_L^2/\tau_L \tag{14}$$

The random walk model has several practical advantages that make it attractive. A single state variable can be used to model the sum of bias plus several exponentially correlated errors. The control law is a bias. If models for bias and exponentially correlated processes are used instead of the random walk model, separate state variables must be used for each model. Separate control laws must also be used for bias and exponentially correlated models, since the control applied from the exponentially correlated model must be decayed to zero.

Doppler radar presents a similar modeling problem. The error budget for over-land operations usually contains high-frequency fluctuation noise and scale factor and boresight errors. The scale factor and boresight errors are described as bias and long-correlation-time exponentially correlated errors. The fluctuation noise is modeled as white noise at the velocity level. It has a PSD amplitude proportional to aircraft velocity. The bias and long-correlation-time errors are modeled as random walk in scale factor and boresight as described above.

Doppler radar performance operating over water is corrupted by the velocity of the water surface, called sea-drift. Sea-drift is modeled as random walk in two horizontal components. This error replaces the Doppler scale factor and boresight random walk states in the state vector during over-water operation. State variable replacement is commonly used to maintain a small state vector. This results in a suboptimal filter since scale factor and boresight errors are still present over water. However, the sea-drift effect is the largest, so acceptable filter performance is obtained without the scale factor and boresight models while over water.

If Doppler radar is not available, true airspeed reference velocity is used and two components of wind velocity uncertainty are modeled as random walk in the two reference velocity state variables.

High-frequency accelerometer errors are modeled as white noise. Accelerometer bias errors are generally unobservable unless a platform-mounted star tracker is used and so are not modeled. Long-correlation-time accelerometer errors should be modeled if they are significant. However, the white noise gyro drift rate model is approximately equivalent to random walk accelerometer errors since the difference between tilt and accelerometer errors is unobservable. It should be recognized that gyro drift rate and tilt are both observable so the approximation yields a suboptimal model. Long-correlation-time accelerometer errors are not explicitly modeled in the applications discussed.

Gravitational anomaly deflection of the vertical is modeled as white acceleration noise. The effective correlation time of the white noise, τ_g, is

$$\tau_g = 50 \text{ nmi}/V \tag{15}$$

where V is aircraft speed and the correlation distance of the gravitational anomaly is assumed to be 50 nmi.

The state vector chosen for FB-111 navigation system has 13 elements which are

x, y position error

x, y velocity error

x, y, z ψ-angle

x, y, z drift rate error

2 reference velocity errors

astrocompass boresight error.

where x, y, z define a locally-level, azimuth wander coordinate frame with z axis up.

The same state vector is used for dead-reckoning mode with the ψ-angle states identical to the position error states and the drift rate error states not used.

Notice that vertical channel is not included in the state vector. The vertical channel only weakly couples the two horizontal channels through Coriolis terms. If vertical velocity error is kept small through conventional baro-altitude damping, horizontal velocity error is not significantly affected.

2.2 CHOICE OF COORDINATE FRAME

The importance of choosing the proper state variables to simplify the problem is well known. Two examples are given in Sections 2.2.1 and 2.2.2 of state variable transformations that simplify the filter calculations.

2.2.1 Elimination of Acceleration Terms

The inertial navigation system linearized error equations [1] can be written as

$$\Delta\dot{V}_c = A x \psi - (\omega_c + \Omega) x \Delta V_c - \omega_s^2 \Delta R - 2\omega_s (\Delta\omega_s) R + \nabla \tag{16}$$

$$\Delta\dot{R} = \Delta V_c - \rho x \Delta R \tag{17}$$

$$\dot{\psi} = -\omega_c x \psi + \epsilon \tag{18}$$

where

ΔR = geocentric position error vector

ΔV_c = velocity error vector in computer coordinates

ψ = vector angle rotation from computer to platform axes

A = specific force acceleration vector

V = vehicle velocity vector

Ω = earth rate vector

ω_c = spatial rate vector of locally level frame with respect to inertial frame

ω_s = Schuler frequency

ρ = vehicle rate vector of locally-level frame with respect to Earth fixed frame

∇ = accelerometer error vector

ϵ = gyro drift rate error vector

$\Delta\omega_s = \frac{\partial \omega_s}{\partial R} \Delta R$

R = geocentric position vector

These state equations are time varying. The solution to the equations is complicated by the fact that the acceleration vector can vary quite rapidly. It is possible to choose a linear combination of these state variables that eliminate acceleration terms from the state equation. The transformation is

$$\Delta V_p = \Delta V_c + \psi \times V \tag{19}$$

Physically this can be interpreted as treating the three components of velocity contained in the computer memory as being along the platform axes instead of the computer axes when computing velocity error. ΔV_p is called the velocity error vector in platform coordinates.

The derivative of Eq (19) is

$$\Delta \dot{V}_p = \Delta \dot{V}_c + \dot{\psi} \times V + \psi \times [A - (\omega_c + \Omega) \times V + g] \tag{20}$$

where g is gravity vector. Using Eq (19) and (20) to eliminate ΔV_c in Eq (16) and (17) gives the state equations

$$\Delta \dot{V}_p = -(\omega_c + \Omega) \times \Delta V_p - \omega_s^2 \Delta R - g \times \psi - V \times (\Omega \times \psi + \epsilon) - 2\omega_s (\Delta \omega_s) R + \nabla \tag{21}$$

$$\Delta \dot{R} = \Delta V_p - \rho \times \Delta R + V \times \psi \tag{22}$$

$$\dot{\psi} = \psi \times \omega_c + \epsilon \tag{23}$$

Figure 2 shows the state equations (Eq (21) through (23)) in matrix form for two horizontal channels with an azimuth wander coordinate frame and neglecting vertical velocity. These equations do not contain acceleration and so are much easier to accurately integrate numerically.

$$\begin{bmatrix} \Delta\dot{R}_x \\ \Delta\dot{R}_y \\ \Delta\dot{V}_{px} \\ \Delta\dot{V}_{py} \\ \dot{\psi}_x \\ \dot{\psi}_y \\ \dot{\psi}_z \end{bmatrix} = \begin{bmatrix} 0 & 0 & 1 & 0 & 0 & 0 & V_y \\ 0 & 0 & 0 & 1 & 0 & 0 & -V_x \\ -\omega_s^2 & 0 & 0 & 2\Omega_z & V_y\Omega_y & (-g-V_y\Omega_x) & 0 \\ 0 & -\omega_s^2 & -2\Omega_z & 0 & (g-V_x\Omega_y) & V_x\Omega_x & 0 \\ 0 & 0 & 0 & 0 & 0 & \omega_z & -\omega_y \\ 0 & 0 & 0 & 0 & -\omega_z & 0 & \omega_x \\ 0 & 0 & 0 & 0 & \omega_y & -\omega_x & 0 \end{bmatrix} \begin{bmatrix} \Delta R_x \\ \Delta R_y \\ \Delta V_{px} \\ \Delta V_{py} \\ \psi_x \\ \psi_y \\ \psi_z \end{bmatrix}$$

$$+ \begin{bmatrix} 0 & 0 & 0 & 0 & 0 \\ 0 & 0 & 0 & 0 & 0 \\ 1 & 0 & 0 & 0 & -V_y \\ 0 & 1 & 0 & 0 & V_x \\ 0 & 0 & 1 & 0 & 0 \\ 0 & 0 & 0 & 1 & 0 \\ 0 & 0 & 0 & 0 & 1 \end{bmatrix} \begin{bmatrix} \nabla_x \\ \nabla_y \\ \epsilon_x \\ \epsilon_y \\ \epsilon_z \end{bmatrix}$$

Figure 2. Inertial Navigation Error Equations in the Platform Frame

2.2.2 Stationary Alignment

The stationary alignment filter is a special case because of the many simplifications that can be made. Of course, stationary alignment can be performed with the general navigation filter but many applications only require a stationary alignment such as F-111 autonomous navigation or any application that has no airborne navigation aids.

After initial tilt errors have been removed, the cross coupling between the two horizontal navigation channels is very small. A three-state filter is used which contains

$$x = \begin{bmatrix} \Delta V, \text{ velocity error} \\ \theta, \text{ tilt error} \\ \epsilon, \text{ drift rate error} \end{bmatrix} \tag{24}$$

One set of filter coefficients is computed for both x and y channels. The correspondence is

$$x = \begin{bmatrix} \Delta V_x \\ -\theta_y \\ -\epsilon_y \end{bmatrix}, \text{ x channel} \tag{25}$$

$$x = \begin{bmatrix} \Delta V_y \\ \theta_x \\ \epsilon_x \end{bmatrix}, \text{ y channel} \tag{26}$$

Azimuth is initialized by computing the angle from north to the x-axis (positive counter clockwise), α, as

$$\alpha = -\tan^{-1}\left(\frac{\Omega_y^- + \epsilon_y}{\Omega_x^- + \epsilon_x}\right) \tag{27}$$

which defines north as the direction of the sensed horizontal angular rate vector. Estimated north gyro drift rate vector is

$$\hat{\Omega}_N = \Omega^- + \begin{bmatrix} \epsilon_x \\ \epsilon_y \\ 0 \end{bmatrix} - \Omega^+ \tag{28}$$

where

Ω^- = earth rate vector before azimuth control

Ω^+ = earth rate vector after azimuth control.

The simplest way to eliminate the cross coupling due to initial tilts is to restart the filter after the first few seconds when the large tilts have been removed.

The stationary alignment mechanization is not Schuler tuned. The gyros are only torqued at earth rate plus estimated gyro precession rates. Coriolis compensation is not mechanized. This simplifies the model, eliminates unnecessary cross coupling, and reduces the numerical errors in computation of the average velocity measurement. The state equations are

$$\dot{x} = \begin{bmatrix} 0 & g & 0 \\ 0 & 0 & 1 \\ 0 & 0 & 0 \end{bmatrix} x + u \tag{29}$$

where u is a white noise vector. The average velocity measurement matrix is

$$H = [1 \quad -gT/2 \quad gT^2/6] \tag{30}$$

and the transition matrix is

$$\Phi = \begin{bmatrix} 1 & gT & gT^2/2 \\ 0 & 1 & T \\ 0 & 0 & 1 \end{bmatrix} \tag{31}$$

where T is the filter cycle time. An additional simplification can be realized by linear transformation of the state vector to x' as

$$x' = \begin{bmatrix} 1 & -gT/2 & gT^2/6 \\ 0 & 1 & 0 \\ 0 & 0 & 1 \end{bmatrix} x \tag{32}$$

which gives an average velocity state variable. The measurement and transition matrices become

$$H' = \begin{bmatrix} 1 & 0 & 0 \end{bmatrix} \tag{33}$$

$$\Phi' = \begin{bmatrix} 1 & gT & 0 \\ 0 & 1 & T \\ 0 & 0 & 1 \end{bmatrix} \tag{34}$$

The initial covariance matrix, P_o, is also transformed from

$$P_o = \begin{bmatrix} q_v & 0 & 0 \\ 0 & q_\theta & 0 \\ 0 & 0 & q_\epsilon \end{bmatrix} \tag{35}$$

to

$$P'_o = \begin{bmatrix} [q_v + (gT/2)^2 q_\theta + (gT^2/6)^2 q_\epsilon] & [-(gT/2)q_\theta] & [(gT^2/6)q_\epsilon] \\ [-(gT/2)q_\theta] & q_\theta & 0 \\ [(gT^2/6)q_\epsilon] & 0 & q_\epsilon \end{bmatrix} \tag{36}$$

The initial covariance matrix is precomputed so the addition of the non-zero off-diagonal terms is not a significant complication. However, the zeros introduced in the H' and Φ' matrices do significantly reduce the amount of computation done each filter cycle. Filter coefficients are computed in the conventional manner. Scaling is combined with the filter coefficient computation as described in Section 3.1.

2.3 MEASUREMENTS

Measurements are obtained from sensors that supply continuous data such as Doppler radar or discrete data such as a position checkpoint. Continuous data measurements are prefiltered by means of integration to obtain a discrete measurement. For example the Doppler measurement is

$$y(t_k) = \int_{t_{k-1}}^{t_k} (V_I(\tau) - V_D(\tau))\, d\tau \tag{37}$$

where V_I and V_D are inertial and Doppler sensed horizontal velocities, respectively. There is no significant information loss relative to a continuous Kalman filter as long as the integration time is very short relative to system dynamics, i.e., aircraft maneuvers. Error analysis studies have demonstrated that filter performance is not sensitive to filter cycle time, $(t_k - t_{k-1})$. The basic Doppler radar information is position change pulses. The prefilter mechanization alleviates the need to generate Doppler velocity. The measurement matrix, $H(t_k, t_{k-1})$, must model the prefilter integration.

A discrete measurement, such as position checkpoint, can occur at any time during the filter cycle. The measurement, $y(t_m)$, is computed at the time the measurement occurs, t_m. However, it is used as if it occurred at the end of the filter cycle, t_k, $(t_{k-1} \le t_m \le t_k)$. This simplifying approximation is made because a constant time interval filter cycle requires less computation. The approximation can be made because the estimated measurement, $H\hat{x}$, is small since control is applied regularly. Also the filter coefficients will not change significantly with a small change in the position checkpoint time of occurrence.

The approximation of a constant time interval filter cycle cannot always be made. For example, if the velocity difference integral, Eq (37), was only available over irregular intervals, the filter cycle would have to be variable to fit the integration time.

2.4 FAILURE DETECTION

The measurement-error variances computed in the Kalman filter can be used to check for failure or degraded performance. The technique has been used to detect incorrect position checkpoint designations on the AMSA flight tests. A failure is said to occur when the measurement magnitude exceeds its 3- value where measurement magnitude squared is

$$|\bar{y}|^2 = (y - H\hat{x})^T (y - H\hat{x}) \tag{38}$$

and its variance is

$$\sigma^2_{|\bar{y}|} = \text{Trace}\left\{ HPH^T + R \right\}. \tag{39}$$

A failure occurs if

$$|\bar{y}|^2 > 9\,\sigma^2_{|\bar{y}|} \tag{40}$$

and the checkpoint is rejected. The pilot has a few seconds to override the rejection and force the checkpoint to be accepted. If the checkpoint rejection is overridden, the measurement, $\bar{y}$, is applied to the current filter cycle without further compensation for the delayed application. This does place an additional burden on the pilot to evaluate rejected checkpoints and make a go/no-go decision. The mechanization was only used for flight test and not in an operational system.

A similar mechanization has been proposed, but not mechanized to detect bad data or failure in reference velocity information. Reference velocity measurements are tested at each filter cycle and a pass/fail decision is made. Continuous failure of Doppler information could indicate over-water operation with a large sea-drift error. In this case the filter model is switched to the over-water mode which models sea-drift velocity error.

Failure detection allows the computer to override the navigation mode selection made by the pilot. This approach admittedly has its pitfalls. Good data can be rejected due to a misaligned system relative to its covariance matrix. For this reason, there is reluctance to place failure detection capability into an operational system.

3. MECHANIZATION FOR FIXED POINT ARITHMETIC

The basic equations associated with the discrete Kalman filter are

$$P^-(k) = \Phi(k, k-1)\, P^+(k-1)\, \Phi^T(k, k-1) + Q(k, k-1) \tag{41}$$

$$\hat{x}^-(k) = \Phi(k, k-1)\, \hat{x}^+(k-1) \tag{42}$$

$$K(k) = P^-(k)\, H^T(k)\, [H(k)\, P^-(k)\, H^T(k) + R(k)]^{-1} \tag{43}$$

$$P^+(k) = [1 - K(k)\, H(k)]\, P^-(k) \tag{44}$$

$$\hat{x}^+(k) = \hat{x}^-(k) + K(k)\, [y(k) - H(k)\, \hat{x}^-(k)] \tag{45}$$

where

- P = covariance matrix
- $\hat{x}$ = state vector
- y = measurement vector
- H = measurement matrix
- Φ = transition matrix
- Q = process noise covariance matrix
- K = filter coefficient matrix
- R = measurement noise covariance matrix

This section is devoted to methods of solving these equations, or equivalent equations, in a computationally efficient manner for a real-time computer using fixed-point arithmetic.

A Fortran computer program that simulates fixed-point arithmetic with a specified word length was used to develop the algorithms. The fixed-point results were compared with identical computations performed with double-precision floating-point arithmetic. The simulation program doubled as a source of check problems for the assembly language real-time program

3.1 SCALING

If the filter equations (Eq (41) through (45)) are to be solved in a fixed-point digital computer, all variables in these equations must be scaled to values less than one. Scaling of the covariance matrix represents the most difficult problem because of the very large range in covariance matrix values. The position error variance can grow unbounded, yet the resolution is required to a few feet. As another example, assume initial tilt or azimuth error variance is $(5 \text{ degrees})^2$ and the desired resolution is $(0.4 \text{ sec})^2$, so that the range is 1.2×10^9 which is barely within the capability of a 32-bit word. However, the Kalman filter has successfully operated with an inertial navigation system using 24-bit words for the covariance matrix. The filter has been successfully simulated with a 21-bit word length. However, the same simulation failed at 18 bits. The FB-111 covariance matrix is held in double precision words with a 16-bit word length.

Notice that all filter equations (Eq (41) through (55)) are unchanged when matrices P, Q, and R are multiplied by a single scalar parameter, E. E is called the shifting-point scale and is chosen to make the largest diagonal element of P equal 1/2. E is recomputed on each filter cycle as

$$M_p = \text{Max}\left\{E, P_{ii};\ i = 1, 2, 3 \cdots N\right\} \tag{46}$$

$$P^{+} = P^{-}/2M_p \tag{47}$$

$$E^{+} = E^{-}/2M_p \tag{48}$$

This algorithm automatically keeps $E \geq 1/2$. Matrices R and Q are multiplied by E before use in each filter cycle.

The shifting-point scale allows the covariance matrix to have a large dynamic range with a relatively small word length. The covariance matrix is effectively held as floating-point numbers but with a common exponent. This is much simpler than performing full floating-point arithmetic. The relative scaling of the covariance matrix is very important in order to maintain an approximately equal scaled covariance diagonal. Relative scaling is equivalent to scaling the transition matrix. Relative scaling was empirically chosen through simulation of a wide variety of flight profiles.

A simplified shifting-point scale is possible for stationary alignment. In this case, the measurement covariance, $(HPH^T + R)$, is scalar and is monotonic nonincreasing. At each filter cycle P, Q, and R are normalized by $(HPH^T + R)$ before computing the filter coefficients. This maintains optimum scaling on the covariance matrix and also simplifies the filter coefficient computation, since the normalized $(HPH^T + R)$ is unity.

3.2 STATE VECTOR AND COVARIANCE EXTRAPOLATION

The state vector and covariance extrapolation can be performed by Eq (41) and (42). This is the transition matrix technique. Covariance extrapolation by direct integration of the matrix Riccati equations was attempted when the mechanization was first developed. It was found that numerical integration errors can cause the covariance matrix to fail to be non-negative-definite. For example the rectangular integration of the matrix Riccati equation does not preserve the non-negative-definite property. However, the transition matrix technique does preserve non-negative definiteness regardless of the approximations in computing the transition matrix (ignoring the truncation errors in the matrix product).

The mechanization that is used does not explicitly compute the transition matrix. Instead, the state equation

$$\dot{x} = F\,x \tag{49}$$

is numerically integrated. Covariance extrapolation is performed by treating each row of the covariance matrix as a state vector and numerically integrating it using Eq (49). The process is then repeated by treating each column of the resulting matrix as a state vector and again numerically integrating. Note that this is equivalent to $\Phi\,P\,\Phi^T$.

Process noise covariance, Q, is a convolution integral defined by state equation, Eq (4),

$$Q(k, k-1) = \int_{t_{k-1}}^{t_k} \Phi(t_k, t)\, G(t)\, S(t)\, G^T(t)\, \Phi^T(t_k, t)\, dt \tag{50}$$

where

$$S(t) = \text{Cov}\,[u(t)]$$

which can be approximated by trapezoidal integration as

$$Q(k, k-1) = \frac{T}{2}\left[\Phi(k, k-1)\, G(k-1)\, Q(k-1)\, G^T(k-1)\, \Phi^T(k, k-1) + G(k)\, S(k)\, G^T(k)\right] \tag{51}$$

where $T = t_k - t_{k-1}$. The total covariance extrapolation is

$$P^{-}(k) = \Phi(k, k-1)\left[P^{+}(k-1) + \frac{T}{2}\, G(k-1)\, S(k-1)\, G^T(k-1)\right]\Phi^T(k, k-1) + \frac{T}{2}\, G(k)\, S(k)\, G^T(k) \tag{52}$$

The matrix products involving Φ are performed by state equation integration as described above. S is a diagonal matrix and, in most cases, is independent of k. G is usually an identity matrix in the inertial navigation application.

Considerable effort has been spent developing an efficient algorithm for the integration of the state equation. Trapezoidal integration with an average coefficient matrix is used. The general solution is

$$x_k^{-} = x_{k-1}^{+} + \frac{1}{2}\bar{F}\,(x_k^{-} + x_{k-1}^{+}) \tag{53}$$

$$\bar{F} = \int_{t_{k-1}}^{t_k} F(t)\, dt \tag{54}$$

The FB-111 state vector is integrated using 29 multiplies and 5 one-bit right shifts. This compares with 70 multiplies in a (13 x 13) transition matrix extrapolation assuming a (7 x 10) submatrix of non-zero, non-unity elements. A truncated algorithm for computing the transition matrix will probably result in some zeros in the (7 x 10) submatrix. The complete covariance matrix and state vector extrapolation require 27 vector extrapolations using either the transition matrix or direct integration.

The efficiency of the integration algorithm relies directly on the sparse coefficient matrix. The FB-111 integration algorithm uses a combination of rectangular and trapezoidal integration to extrapolate the ψ-equations where the error states are slowly time-varying with approximately a 24-hour period. Complete trapezoidal integration is used on the position and velocity equations.

Integration errors for the trapezoidal integration algorithm has been acceptable for cycle times as large as 24 seconds as demonstrated by both computer simulation and actual flight test. The integration error has also been computed analytically. The trapezoidal integration algorithm is defined by Eq (53) and (54) which can be solved for x(t) using a Taylor series expansion of F. The exact solution is

$$x(t) = x(0) + \int_0^t \dot{x}(\tau)\, d\tau \tag{55}$$

which is also solved for x(t) using Taylor series expansions of $\dot{x}(\tau)$ and $F(\tau)$. The trapezoidal integration error, $\delta x(t)$, is

$$\delta x(t) = \left[\frac{1}{12}\left(F(0)^3 + F(0)\,\dot{F}(0) - \dot{F}(0)\,F(0)\right) t^3 + \cdots\right] x(0) \tag{56}$$

For comparison the state vector error, using the matrix exponential expansion of $\bar{F}$, is computed. The transition matrix is

$$\Phi(t, 0) = I + \bar{F} + \frac{1}{2}\bar{F}^2 + \frac{1}{6}\bar{F}^3 + \frac{1}{24}\bar{F}^4 + \cdots \tag{57}$$

and the state vector error at time t, using $\Phi(t, 0)$ instead of Eq (55), is

$$\delta x(t) = \left[\frac{1}{12}\left(F(0)\,F(0) - \dot{F}(0)\,F(0)\right) t^3 + \cdots\right] x(0) \tag{58}$$

Truncating the matrix exponential expansion at the second order term yields an additional third order error term $(1/6)\,F(0)^3\,t^3\,x(0)$ which is larger than the trapezoidal error.

In addition trapezoidal integration using endpoint values for coefficient matrix F(t) rather than the integrated value $\bar{F}$ has a state vector error

$$\delta x(t) = \left[\frac{1}{12}\left(F(0)^3 + F(0)\,\dot{F}(0) + 2\dot{F}(0)\,F(0) + \dot{F}(0)\right) t^3 + \cdots\right] x(0) \tag{59}$$

This algorithm is not attractive because it has a third order error term proportional to $\dot{F}$ which may cause difficulty in a highly maneuvering aircraft.

3.3 STATE VECTOR AND COVARIANCE RESET

The reset equations can be performed by

$$K = P^- H^T \left(H P^- H^T + R\right)^{-1} \tag{60}$$

$$\hat{x}^+ = \hat{x}^- - K\,\dot{y} \tag{61}$$

$$P^+ = P^- - KHP^- \tag{62}$$

The first problem encountered when implementing the equations in a computer with fixed-point arithmetic is scaling the filter coefficient matrix, K. The values of the filter coefficient matrix vary greatly with flight profile. Since the matrix is found by ratios of covariance elements, the maximum values are difficult to predict. The mechanization used avoids the scaling problem by not explicitly computing the filter coefficient matrix. Instead, the state vector and covariance matrix are reset directly. The mechanization that has been implemented is restricted to two measurements at a time.

A more convenient computational form is obtained by defining some auxiliary matrices

$$f \triangleq P^- H^T \tag{63}$$

$$d \triangleq H f + R \tag{64}$$

so the coefficient matrix is

$$K = f\,d^{-1} \tag{65}$$

To avoid numerical problems in the matrix inverse, the measurement vector, $\dot{y}$, is transformed onto axes in which the measurements are uncorrelated, y^*,

$$y^* = D\,\dot{y} \tag{66}$$

where B is the transformation matrix. It follows that d is transformed into a diagonal matrix, d^*,

$$d^* = B\,d\,B^T \tag{67}$$

A simple choice for the transformation matrix B is

$$B = \begin{pmatrix} 1 & 0 \\ \frac{-d_{21}}{d_{11}} & 1 \end{pmatrix} \quad \text{or} \quad \begin{pmatrix} 1 & \frac{-d_{12}}{d_{22}} \\ 0 & 1 \end{pmatrix} \tag{68}$$

where d_{11}, d_{12}, d_{21}, d_{22} are the elements of d. f and K are also transformed

$$f^* = f\,B^T \tag{69}$$

$$K^* = f^*\,d^{*-1} \tag{70}$$

The state vector and covariance reset equations can then be expressed

$$\hat{x}^+ = \hat{x}^- - f^*\,d^{*-1}\,y^* \tag{71}$$

$$P^+ = P^- - f^*\,d^{*-1}\,f^{*T} \tag{72}$$

The computational detail can be more clearly seen when expressed in scalar form

$$\hat{x}_i^+ = \hat{x}_i^- - \frac{f^*_{i1}\,y^*_1}{d_{11}} - \frac{f^*_{i2}\,y^*_2}{d_{22}} \tag{73}$$

$$P^+_{ij} = P^-_{ij} - \frac{f^*_{i1}\,f^*_{j1}}{d^*_{11}} - \frac{f^*_{i2}\,f^*_{j2}}{d^*_{22}} \tag{74}$$

$i, j = 1, 2, 3 \cdots N$

By performing the multiplication first to generate a double-length product and then dividing with the double-length dividend to give a single-length quotinent, truncation errors are minimized and overflow problems are avoided. If the filter coefficients were explicitly computed, the divide would be performed before the multiply. This requires twice as many truncation operations.

The computational load of this mechanization is greater than the conventional one because of the additional divides. This is felt to be justified by the ease of scaling and the greater numerical precision. Assuming a 13-element state vector and 2 measurements, and starting with the matrices f and d, this mechanization requires 379 multiplies and 379 divides. By comparison, the conventional mechanization, which explicitly computes the filter coefficient matrix, requires 438 multiplies and 4 divides for the same computation. The computation, in either case, can be reduced by only computing a triangle of the covariance matrix.

Covariance matrix symmetry is forced by storing the lower triangle into the upper triangle. This is sufficient to avoid numerical problems and is somewhat simpler than the averaging technique

$$P^+ = \frac{1}{2}(P^- + P^{-T}) \tag{75}$$

4. CONCLUSIONS

A number of techniques used in the practical implementation of the Kalman filter are presented. Techniques to minimize the computer requirements are emphasized including simplifying the filter model and using algorithms suitable for fixed-point arithmetic. All of these techniques have been proven by many flight tests on several applications at Autonetics.

REFERENCES

[1] Leondes, C. T., Guidance and Control of Aerospace Vehicles, McGraw-Hill Book Company, Inc., New York, 1963.

ACKNOWLEDGEMENTS

The development of the Kalman filter mechanization described here was a team effort involving many engineers from the Autonetics Group of Rockwell International. Major contributions were made by Dr. T. W. DeVries and Mr. R. G. Schmidt. Dr. DeVries made significant contributions to error modeling and overall refinement of the mechanization. Mr. Schmidt developed many of the basic computational algorithms.

EXPERIENCES WITH THE B-1 NAVIGATION FILTER

Dr. John E. Bergeson
The Boeing Company
Seattle, Washington 98124, USA

SUMMARY

This lecture discusses some practical aspects of Kalman filter design. Topics presented include error model definition, software-implementation considerations and flight test verification. Although B-1 navigation filter experiences are emphasized, the discussion is applicable to Kalman filter design for any long-range, high-speed cruise vehicle with similar navigation sensors. From a practical standpoint, the principal contribution of this lecture is perceived to be a discussion of inertial-platform slew-induced phenomena and their implication for filter design.

LIST OF SYMBOLS

KALMAN FILTER SYMBOLS

X	state vector
Y	observation vector
P	filter covariance matrix
S	truth-model covariance matrix
F	dynamics matrix
H	measurement matrix
Q	process noise matrix
R	measurement noise matrix
K	Kalman gain matrix
Φ	transition matrix
G	control vector

SUBSCRIPTS/SUPERSCRIPTS

X,Y,Z	local-level wander-azimuth axes
T	true axes
C	computer axes or filter model
P	platform axes
E	earth-fixed axes
A,B	after/before system correction

ERROR SYMBOLS

δ	component difference
Δ	vector difference

NAVIGATION SYMBOLS

λ	latitude
L	longitude
α	platform wander angle
$\omega_x, \omega_y, \omega_z$	platform inertial-angular-rate components
$\Omega_x, \Omega_y, \Omega_z$	earth-rate components
$\omega_x, \omega_y, \omega_z$	platform earth-relative angular-rate components
A_x, A_y, A_z	measured acceleration components
V_x, V_y, V_z	earth-relative velocity components
C	navigation direction cosine matrix
g	plumb-bob gravity
R	aircraft position vector
ψ_x, ψ_y, ψ_z	angular misalignment of computer axes with respect to platform axes
ϕ_x, ϕ_y, ϕ_z	angular misalignment of platform axes with respect to true axes
$\delta\theta_x, \delta\theta_y, \delta\theta_z$	angular misalignments of computer axes with respect to true axes
b_x, b_y, b_z	accelerometer bias
h_b	altimeter bias
$\epsilon_x, \epsilon_y, \epsilon_z$	gyro fixed drift
κ	Doppler scale-factor error
ℓ	Doppler drift-angle error
V_g	groundspeed
η_x, η_y	gyro non-orthogonalities
θ_s	yaw-synchro angle
$\Delta\theta_s$	yaw-synchro angle-readout error

OTHER SYMBOLS

σ	standard deviation
τ	correlation time
ϕ_0	Doppler error autocorrelation function
ξ	autocorrelation function frequency parameter
U	white noise

1. Introduction

The B-1 is an intercontinential weapon system which is capable of delivering both air-to-ground missiles and gravity weapons. Rockwell International is building the airframe. The Boeing Aerospace Company is the Avionics System Integration Contractor (ASIC). The offensive avionics system contains the aircraft's navigation and weapon delivery hardware and software.

This lecture discusses the Kalman filter which the ASIC has designed, implemented, and flight tested for B-1 navigation-sensor data integration. Section 2 is an overview of the B-1 navigation system configuration and Kalman filter design. Section 3 summarizes the ASIC's analytical approach to filter design, while Section 4 discusses some practical aspects of filter implementation. Section 5 presents some Holloman Air Force Base flight test data and compares design assumptions with real-system behavior. Although the specific analyses and examples cited in these sections are drawn from the collective experiences of the ASIC's B-1 Navigation and Weapon Delivery Group, the general discussion is applicable to Kalman filter design and implementation for any long-range, high-speed cruise vehicle with similar navigation sensors.

This lecture does not discuss B-1 performance capability.

2. B-1 Navigation System Overview

2.1 System Description

The B-1's integrated, multisensor navigation system is shown schematically in Fig. 1. The computer(s) and interface elements in this figure represent the Avionics Control Unit Complex (ACUC), which provides data processing, interfacing and real-time control functions for the avionics hardware. The software, supplied by Boeing, is written in Jovial J3B language. There are two Singer Kearfott SKC-2070 computers in the complex. One of the computers is dedicated to navigation-related functions; the other to weapon-delivery functions. However, each computer can perform all of the navigation and weapon-delivery functions if the other one fails.

2.1.1 Navigation Sensor Hardware

Inertial Measurement Unit

The inertial measurement unit (IMU) is the Litton AN/AJN-17 (LN-15), a three-gimbal platform with two 2-degree-of-freedom gas-bearing gyros and three floated-pendulum accelerometers. For the B-1 application, the inertial platform is stabilized in a local-level wander-azimuth orientation through full inertial-rate level-axis torquing and vertical earth-rate azimuth-axis torquing. There are two LN-15's on the B-1.

Doppler Radar

The Doppler radar unit is either the stabilized-antenna (gimbaled) Singer APN-185 or the fixed-antenna Ryan APN-200. For the B-1 application, both Dopplers output groundspeed and drift angle (the angle between the groundspeed vector and the projection of the aircraft centerline on a local-level plane). The APN-185 provides these outputs directly, whereas the APN-200 employs a digital interface adapter unit (mini-computer) for equivalent groundspeed and drift-angle determination.

Position-Fixing Devices

The forward-looking radar (FLR) is the General Electric AN/APQ-144. The electro-optical viewing system (EVS), supplied by Boeing, contains an infrared sensor.

Central Air-Data Computer and Gyro Stabilization Subsystem

The Central Air-Data Computer (CADC) supplies altitude and airspeed information to the ACUC for vertical channel damping and deadreckoning navigation. The gyro stabilization subsystem (GSS) supplies heading and attitude reference data for in-air IMU-alignment initialization and deadreckoning navigation. The CADC and GSS are part of the B-1 aircraft's air-vehicle equipment. Other offensive avionics sensors on board the B-1, but not shown in Fig. 1, are the Honeywell AN/APN-194 radar altimeter and the Texas Instrument AN/APQ-146 Terrain-Following Radar.

2.1.2 Navigation Mode Heirarchy

The B-1's primary navigation mode is Doppler-inertial. Doppler and airspeed deadreckoning are backup modes. Figure 2 displays the navigation mode heirarchy which is implemented in the B-1. Kalman filters are used for navigation-data processing in the inertial modes and for inertial platform ground alignment and auto-calibration. There are two navigation filters on the B-1, one for each inertial measurement unit. The filters operate independently of each other. There is no mutual aiding.

2.2 Filter Structure

In approaching the task of designing a navigation filter for the B-1, the ASIC first looked at the critical performance requirements of the navigation system during a typical mission. The mission in Fig. 3 is a constant-velocity great-circle flight path with an initial in-air alignment segment over land, a subsequent cruise-out portion over water, and extended penetration over land. Position error is a critical performance parameter at landfall for an intercontinental bomber since the probability of landfall position-fix acquisition is inversely proportional to landfall position error. Both position and velocity errors are critical performance parameters for weapon delivery, since accurate initialization at launch is vital to achieving acceptable impact CEP (circular error probability). This is particularly true for air-launched, inertially-guided missiles such as SRAM (Short Range Attack Missile).

The performance requirements and mission scenario essentially dictated the structure and dimensionality of

the B-1 navigation filter. (The filter equations are shown in Fig. 4.) For example, acceptable position accuracy at landfall, after many hours of over-water flight, requires good gyro performance - performance which is only obtainable through precise and periodic ground and in-air calibration. Hence, three gyro fixed-drift elements are included in the state vector. Likewise, acceptable velocity accuracy during penetration requires good Doppler performance, and Doppler scale-factor and drift-angle errors are modeled in the filter. Consequently, the state error vector in Fig. 5 was selected almost at the outset of the filter design process. The state error vector contains 13 level-channel error elements and 4 vertical-channel elements. The vertical-channel elements are included on the basis of B-1 altitude and vertical-velocity accuracy requirements during penetration.

Figure 6 displays the control vector, as it is currently implemented in the B-1 navigation filter. This vector represents a set of corrections which are applied mathematically to the navigation-system position and velocity equations and electro-mechanically (through gyro torquing corrections) to the inertial platform. The control vector also contains Doppler scale-factor and drift-angle error estimates, as well as a vertical-accelerometer bias-error estimate, which are accumulated and used to correct the Doppler inputs to each navigation filter and the vertical accelerometer outputs from each inertial measurement unit to the vertical-channel mechanization equations. The CADC altitude output is not corrected via feedback of the estimated baro-altimeter bias error and this error element does not appear in the control vector. Instead, the estimate of this error is used in forming the residual at an altitude update.

3. Analytical Aspects of Filter Design

The critical design phase of the B-1 filter design process involved the development of a complete error model, the synthesis of specialized computer program sensitivity analysis and performance verification tools, and the refinement of the preliminary suboptimal filter design. When the B-1 Avionics contract was awarded in April 1972, elements of a basic suboptimal filter design methodology had emerged in the literature. For example, the C-5 filter design experience, as recorded in [1], was helpful in developing a basic approach to the design task. Later on, the error propagation and update equations of [2] were useful in checking out a suboptimal filter covariance analysis program. But there is a vast difference between devising equations and constructing computer programs for suboptimal filter analysis or system simulation and evolving confidence that these equations and computer programs adequately represent real-system behavior. This section, therefore, emphasizes some analytical aspects of the filter design process that proved to be of particular practical significance.

3.1 System Error Models

The term "error model" in this lecture denotes, in general, a mathematical representation of navigation-sensor imperfections and environmental errors. The term also denotes a set of linear differential equations which govern the transformation - or mapping - of these errors (as well as navigation system initial-condition errors) into carrier position, velocity, and heading errors as a function of time. Gyro drift and accelerometer bias fall under the category of sensor imperfections; gravity-vector deflections from the local vertical and ocean-surface motion are examples of environmental effects which adversely impact navigation system performance. The error-propagation equations, on the other hand, are derived from the kinematic relationships between vehicle inertial acceleration components and rotating reference axes. Since the essence of Kalman filtering for applications such as the B-1 is a statistical weighting of inertial-navigator and Doppler-velocity or position-fixing errors, the formulation of realistic error models is central to filter design.

3.1.1 Navigation-Parameter Error Definition

Dynamics (F) Matrix

The usual approach to deriving inertial-system error-propagation equations is to take first-order variations of the mechanization equations. This technique leads to the "psi-angle" error model in Fig. 7 for a local-level wander-azimuth mechanization, where the errors are defined as vector differences between computed and true values resolved along the true (or ideal) navigation axes. The vector difference error may be represented mathematically by

$$\delta V^T = V_C^T - V_T^T , \tag{1}$$

where V is a vector and "T" and "C" denote true and computer coordinates, respectively. An alternate approach defines the basic error quantities as vector component differences

$$\Delta V = V_C^C - V_T^T , \tag{2}$$

where ΔV has no superscript since it does not represent a set of vector components. With this approach, for example, the three components of vehicle velocity error are defined as

$$\begin{aligned} \delta V_x &= V_{C_x}^C - V_{T_x}^T \\ \delta V_y &= V_{C_y}^C - V_{T_y}^T \\ \delta V_z &= V_{C_z}^C - V_{T_z}^T \end{aligned} \tag{3}$$

The component difference definition leads to the "phi-angle" error model in Fig. 8 for a local-level wander-azimuth mechanization. The velocity errors in Figs. 7 and 8 are related by the expression

$$\delta V_C^C = \delta V_T^T - \delta\theta \times V_T^I \tag{4}$$

where V_T^T is the true velocity and $\delta\theta$ denotes the set of computer-to-true-axis misalignment angles.

Reference [3] derives a generalized version of the error model in Fig. 8, which is applicable to space-stable platforms. Reference [4] provides a formal comparison of both approaches. The latter reference shows that the "psi-angle" error model evolves from the assumption that the navigation equations are solved in the computer frame, whereas the "phi-angle" model evolves from the assumption that the navigation equations are solved in an ideal frame. The error model in Fig. 8 has one more error element than the one in Fig. 7; this element is $\delta\theta_z$, which represents a computer-axis-to-true-axis azimuth misalignment.

Measurement (H) Matrix

The vector-difference and component-difference approaches to error dynamics derivation also lead to different measurement matrix formulations for a Doppler-aided inertial navigation system. The velocity measurement matrix derived from the component-difference definition is shown in the upper half of Fig. 9 for measurement processing in navigation axes. In deriving this matrix, the velocity component-difference definition may be used in conjunction with the velocity divergence components

$$V_{C_x}^C - V_{D_x}^P \quad \text{and} \quad V_{C_y}^C - V_{D_y}^P \tag{5}$$

where the $V_{C_i}^C$'s are computer or inertial system velocities in computer coordinates and the $V_{D_i}^P$'s represent Doppler-$_i$ velocity components in platform coordinates. The measurement matrix follows from the relationships

$$V_D^P = V_T^P + \delta V_D^P \tag{6}$$

where δV_D^P represents Doppler scale-factor and drift-angle errors, and

$$V_T^P = V_T^T - \phi \times V_T^T \tag{7}$$

where ϕ_z is the significant component of ϕ. An expression for velocity divergence equivalent to the formulations in Fig. 9 is given in [4].

The Doppler measurements may also be processed in local-level axes which are parallel and perpendicular to the groundspeed vector. The measurement matrix in the lower half of Fig. 9 utilizes groundspeed and drift-angle directly as observables. In this matrix, the symbol V_g represents groundspeed and it has been assumed that ϕ_z is positive about Z up and δ is positive about Z down.

The "phi-angle" error dynamics matrix in Fig. 7 and the Yv_x/Yv_y form of the measurement matrix have been implemented in the B-1 navigation filter. The practical basis for this implementation is discussed in Sections 4.1.1 and 4.4.3.

3.1.2 Navigation-Sensor Error Sources

The state vector in Fig. 5, the error-dynamics matrix in Fig. 8, and the measurement matrices in Fig. 9 are subsets of a real-world error model or "truth model" which was used for B-1 suboptimal filter design. Figure 10 summarizes the complete set of navigation-sensor error sources. In addition to the instrument errors displayed in the figure, such as gyro g-sensitive drift, deflections of the vertical and random sea-surface effects were modeled as accelerometer and Doppler noise, respectively. Both of these errors, as well as inherent gyro and accelerometer noise, were modeled in the real world as exponentially-correlated random variables. Of the error sources shown, Doppler noise and accelerometer bias errors turned out to be the most interesting from a design verification standpoint.

3.2 Suboptimal Filter Design Tools

A family of computer program analysis tools was used in designing the B-1 navigation filter. An optimal filter covariance analysis program is the progenitor of this family and contains subroutines which are common to all.

3.2.1 Suboptimal Covariance Analysis Program

The basic suboptimal filter covariance analysis equations are:

Filter Model

$$\dot{P} = F_C P + P F_C^T + Q_C \qquad \text{Extrapolation}$$

$$P^+ = P^- H_C^T (H_C P H_C^T + R_C)^{-1} H_C P^- \qquad \text{Update} \tag{8}$$

Truth Model

$$\dot{D} = F D + D F^T + Q \qquad \text{Extrapolation}$$

$$D^{+} = \begin{bmatrix} (I-K_cH_1) - K_cH_2 \\ 0 \qquad\qquad I \end{bmatrix} D^{-} \begin{bmatrix} (I-K_cH_1) - K_cH_2 \\ 0 \qquad\qquad I \end{bmatrix}^{T} + \begin{bmatrix} K_cR\,K_c^{T} & 0 \\ 0 & 0 \end{bmatrix} \text{ Update} \qquad (9)$$

The covariance matrix P is a measure of filter performance since its diagonal elements are the mean-square errors in the state-vector estimate. The covariance matrix D represents the mean-square errors of the actual states, including those not modeled in the filter. The F_c, H_c, Q_c and R_c are filter design models for the error dynamics, measurement, process noise, and measurement noise matrices, whereas F and Q are truth-model matrices. The suboptimal Kalman gain matrix is K_c. The symbols H_1 and H_2 are true measurement matrices for modeled and unmodeled states, respectively. The set of real-world equations above is applicable to the design situation where all states are reset or corrected instantaneously after estimation. The equations are considerably more complex for non-instantaneous reset.

The difference between the truth-model and filter-model performance associated with a critical design parameter such as landfall position error may be minimized by adjusting the process noise (Q_c matrix) in the filter equations. The determination of process noise compensation is an important practical aspect of filter design; it is, to a large extent, an iterative, time-consuming process. The approach used to evolve compensation for the B-1 navigation filter was to optimize system free-inertial performance by adding process noise at the velocity, tilt and gyro error levels in the Q_c matrix and then to optimize system Doppler-inertial performance independently by adjusting Q_c values at the Doppler-error level.

3.2.2 Navigation Simulation Program

A navigation-system simulation program is functionally displayed in Fig. 11. This program simulates the operation of an integrated multisensor navigation system. The filter module of this program is similar to the filter side of the suboptimal filter covariance analysis program except that:

(1) Error propagation is accomplished via a transition matrix (as in the airborne computer) rather than by solving the Riccati equation.

(2) The simulation contains state-vector propagation and system-correction equations.

Also, in the simulation program, the actual navigation-system mechanization equations replace the truth model covariance propagation equations. For a given set of (signed) error inputs to these equations, the program will simulate system performance for a given filter design.

Although both the covariance analysis and the simulation programs were indispensable to the B-1 filter design process, the practical value of the simulation in verifying mechanization integrity and in identifying the cause of flight-test anomalies cannot be over-emphasized.

3.3 Pseudostates and the Ground-Alignment Filter

Inspection of the differential equations which comprise the navigation-system error model shows that only linear combinations of certain error states are observable [5]. These linear combinations are sometimes called pseudostates. For example, from the error equations*

$$\begin{aligned} \dot{\delta v}_x &= -g\,\phi_y + b_x \\ \dot{\delta v}_y &= g\,\phi_x + b_y \\ \dot{\phi}_x &= \omega_z\,\phi_y + \epsilon_x \\ \dot{\phi}_y &= -\omega_z\,\phi_x + \epsilon_y \\ \dot{\phi}_z &= \omega_y\,\phi_x - \omega_x\,\phi_y + \epsilon_z \end{aligned} \qquad (10)$$

one can define the following set of pseudostates:

Tilt Pseudostates

$$\begin{aligned} \tilde{\phi}_x &= \phi_x + \frac{b_y}{g} \\ \tilde{\phi}_y &= \phi_y - \frac{b_x}{g} \end{aligned} \qquad (11)$$

where b_x and b_y are level-accelerometer biases, ϕ_x and ϕ_y are the original platform tilt variables, and g is the magnitude of the effective gravity vector.

* Some terms in the standard error equations have been omitted.

Drift Pseudostates

$$\bar{\epsilon}_x = \epsilon_x + \frac{\omega_z b_x}{g}$$

$$\bar{\epsilon}_y = \epsilon_y + \frac{\omega_z b_y}{g} \qquad (12)$$

$$\bar{\epsilon}_z = \epsilon_z - \frac{\omega_y b_y + \omega_x b_x}{g}$$

where ω_x, ω_y, and ω_z are inertial-angular-rate components and ϵ_x, ϵ_y, and ϵ_z are gyro drifts.

The pseudostate constructions show that accelerometer bias errors may be deleted from the filter for operation in the airborne-alignment and navigation mode, where the vertical platform torquing rate, ω_z, is essentially the vertical component of earth rate. For this condition the terms containing accelerometer biases in the drift pseudostates are much less than the inherent gyro drifts. Conversely, however, the pseudostates also imply that level-accelerometer bias errors become observable when the platform vertical-axis torquing rate is very large, as it is during platform slew (about 100 times earth rate).

During the preliminary design phase, a decision was made to implement a Kalman filter for B-1 gyrocompass or ground alignment in order to maximize unaided inertial system performance. Initial covariance analysis studies in this area with implicit platform slew were highly encourgaging. Subsequent covariance analyses with actual slew-rate modeling were disastrous -- unless accelerometer biases were modeled explicitly in the filter. Simulation studies confirmed the pseudostate implication that accelerometer biases are observable during slew. Figure 12 is simulation data which illustrates this estimation. In practice, the apparent accelerometer biases are themselves linear combinations of inherent bias, input-axis misalignment and vertical-gyro torquer-axis/platform level-axis non-orthogonality. The subject of real-system slew-induced phenomena is discussed in Section 5.2.

4. Practical Aspects of Filter Implementation

There are many important practical considerations in designing and implementing a Kalman filter for cruise navigation. Airborne computer capability is usually the most critical practical limitation. However, other factors such as operational flexibility, error-model sensitivity and software commonality shape the final form of the filter and its associated update and correction mechanization. This section discusses some of these considerations as they apply to the B-1 navigation filter.

4.1 Position Updates

4.1.1 Two Azimuth-Error Variable Utilization

In its present configuration the B-1 navigation filter models 13 level-channel error states: two position, two velocity, four attitude, three gyro, and two Doppler. Other operational navigation filters for Doppler-aided inertial cruise systems use 12 level-channel error states. The difference is that the B-1 filter models two azimuth-error states: $\delta\theta_z$, the computer-to-ideal axes azimuth misalignment; and ϕ_z, the platform-to-ideal axes azimuth misalignment.[2] The practical reasons for implementing two azimuth-error states are discussed in the following.

The B-1 inertial navigation system mechanization employs a set of direction cosine matrix elements as the basic navigation parameters. The direction cosine elements which define the orientation of local-level wander-azimuth navigation axes with respect to earth-fixed, rotating reference axes (Fig. 13), are functions of latitude, longitude and wander angle (Fig. 14). The errors in the direction-cosine elements or equivalently in latitude, longitude, and wander angle, are functions of the angular position errors, $\delta\theta_x$ and $\delta\theta_y$, and the azimuthal misalignment error, $\delta\theta_z$. The error equations have the form

$$\delta C_{1j} = \delta\theta_z C_{2j} - \delta\theta_y C_{3j}$$

$$\delta C_{2j} = \delta\theta_x C_{3j} - \delta\theta_z C_{1j} \qquad (13)$$

$$\delta C_{3j} = \delta\theta_y C_{1j} - \delta\theta_x C_{2j}$$

where the C_{ij} $(i,j = 1, 2, 3)$ are navigation direction cosine elements and

$$\delta\lambda = \delta\theta_x \sin\alpha + \delta\theta_y \cos\alpha$$

$$\delta\phi = (\delta\theta_x \cos\alpha - \delta\theta_y \sin\alpha)/\cos\lambda \qquad (14)$$

$$\delta\alpha = \delta\theta_z - \delta L \sin\lambda,$$

where λ, L, and α are latitude, longitude, and wander angle. The δ's denote differences between computed and true values.

Equations (13) and (14) show that it is convenient to retain $\delta\theta_z$ in the navigation-error state vector and to utilize estimates of this variable in correcting system position errors. The fact is, however, that this variable is omitted from many navigation filter designs. Both published (Ref. [4] for example) and unpublished analyses show that the decision to retain or not to retain $\delta\theta_z$ should be influenced by the following considerations:

(1) Observability

In the air, $\delta\theta_z$ appears at the position-error-rate level and is multiplicative with level-velocity components, whereas ϕ_z appears at the velocity-error-rate level and is multiplicative with lateral acceleration components. The two variables are, therefore, distinguishable when the vehicle is airborne. The two variables are not distinguishable when the vehicle is stationary on the ground.

(2) Velocity Error Definition

The natural definition of velocity error in building simulation programs or in analyzing flight-test data is velocity register contents minus reference-velocity components, i.e., component differences. If the vector-difference definition is employed, then the velocity transformation in Eq. (4) must be either incorporated into the error model directly, or separately applied when making position and velocity updates and flight-test data comparisons.

On the basis of these considerations, and in view of the fact that the B-1 is a long-range, high-speed cruise vehicle, the error model in Fig. 8 was used in the B-1 navigation filter.*

4.1.2 Update Algorithms

Equations (13) and (14) have been implemented in the B-1 Offensive Flight Software (OFS) for correcting navigation direction cosines when filter estimates of δx, δy and $\delta\theta_z$ are available. (The computer-axis misalignment angles, $\delta\theta_x$ and $\delta\theta_y$, are related to the filter's linear position-error variables, δx and δy, by the relationships $\delta\theta_x = -\frac{\delta y}{R}$ and $\delta\theta_y = \frac{\delta x}{R}$.) Equations (13) are used when position-error estimates are based on Doppler measurements, since position-error estimates derived from velocity updates are usually quite small. The direction-cosine update algorithm for Doppler-derived updates is therefore

$$C^{TE} = M\,C^{CE} \tag{15}$$

where C^{TE} is the direction-cosine transformation from earth-fixed axes to true-platform axes, C^{CE} is the direction-cosine transformation from earth-fixed axes to computer axes, and M is the correction matrix

$$\begin{bmatrix} 1 & -\delta\theta_z & \delta\theta_y \\ \delta\theta_z & 1 & -\delta\theta_x \\ -\delta\theta_y & \delta\theta_x & 1 \end{bmatrix}.$$

When position fixes are available, however, the filter's position-error estimates can be relatively large, and the application of Eq. (15) may result in unacceptable direction cosine matrix non-orthogonality. To circumvent this problem, Eqs. (14) are used in the OFS to correct latitude, longitude, and wander angle directly at position-fix updates. The correction equations are

$$\begin{aligned} \lambda^{+} &= \lambda^{-} - \delta\hat{\lambda} \\ L^{+} &= L^{-} - \delta\hat{L} \\ \alpha^{+} &= \alpha^{-} - \delta\hat{\alpha} \end{aligned} \tag{16}$$

and the updated latitude, longitude and wander angle are used to re-initialize or re-compute the elements of the direction cosine matrix. This technique guarantees direction cosine matrix orthogonality.

An alternate direction-cosine update algorithm, which works well in the simulation program for both Doppler-derived and fix-derived position updates, is

$$C^{TE} = NC^{CE} \tag{17}$$

where N is the correction matrix

$$\begin{bmatrix} 1 - \frac{\delta\theta_y^2 + \delta\theta_z^2}{2} & -\delta\theta_z & \delta\theta_y \\ \delta\theta_z & 1 - \frac{\delta\theta_x^2 + \delta\theta_z^2}{2} & -\delta\theta_x \\ -\delta\theta_y & \delta\theta_x & 1 - \frac{\delta\theta_x^2 + \delta\theta_y^2}{2} \end{bmatrix}.$$

*Another error model, which might be suitable for an application such as the B-1, retains ϕ_x, ϕ_y, and ϕ_z for the platform attitude error variables but eliminates $\delta\theta_z$ by driving the true axes into coincidence with the computer axes through additional azimuth axis torquing. This error model, which incorporates the velocity transformation in Eq. (4), utilizes only one azimuth-angle variable.

The reason why this algorithm is suitable for position-fix updates is that N satisfies the orthogonality condition

$$\sum_i c_{ij} c_{ik} = \delta_{jk} = 1 \ (j = k) \text{ or } 0 \ (j \neq k) \tag{18}$$

more accurately than does M for $j = k$. The reason why this algorithm was not implemented in the B-1 navigation filter is that (17) does not improve the orthogonality of the direction cosine matrix at a position update, whereas direction cosine matrix re-initialization satisfies the orthogonality condition for both $j = k$ and $j \neq k$. If an accurate direction-cosine update algorithm is not employed at position-fix updates, simulation runs show that the errors in the filter's gyro drift estimates become large due to erroneous earth-rate resolution.

4.1.3 Position-Fix Quality Weighting

From both the theoretical and practical standpoints, the accuracy with which the B-1 Offensive System Operator actually makes a position fix is dependent on aircraft altitude, reference-point quality, operator skill, and other factors. Consequently, the B-1 mechanization incorporates a quality weighting scheme for processing position-fix information in the Kalman filter. The scheme is simple: The position-fix measurement noise variance, σ_R^2, in the filter's measurement noise (R) matrix may be manually set to one of three preprogrammed values:

Quality 1 - σ_R^2 = 1/4 times Quality 2

2 - σ_R^2 = Reference Value

3 - σ_R^2 = 9 times Quality 2

The operator, therefore, has the option of weighting a position fix in accordance with his subjective feeling concerning its accuracy.

4.2 Doppler Error Model

4.2.1 First-Order Markov-Process Assumption

The Doppler scale-factor and drift-angle bias-like errors in Fig. 10 consist of exponentially-correlated and random constant or time-independent components. The corresponding truth model is

$$\begin{bmatrix} \dot{X}_B \\ \dot{X}_N \end{bmatrix} = \begin{bmatrix} 0 & 0 \\ 0 & -\frac{1}{\tau} \end{bmatrix} \begin{bmatrix} X_B \\ X_N \end{bmatrix} + \begin{bmatrix} 0 \\ 1 \end{bmatrix} U \tag{19}$$

where τ is the correlation time and U is white noise with power spectral density Q. Since only linear combinations of scale-factor or drift-angle error states are observable, these Doppler errors were originally modeled in the airborne navigation filter as the first-order Markov-processes

$$\dot{X}_D = -\frac{1}{\tau} X_D + U \tag{20}$$

with initial (over land) covariance uncertainties of

$$P_{D_o} = P_{B_o} + P_{N_o} \tag{21}$$

and correlation times of 15 minutes. The subscripts "B" and "N" in Eqs. (19), (20), and (21) refer to random-constant and exponentially-correlated error sources, respectively. The subscript "D" refers to composite scale-factor or drift-angle errors as modeled in the filter.

The rationale for implementing a first-order Markov-process Doppler model in the B-1 navigation filter was provided by sensitivity analyses (in the form of error budget histograms) which exhibited the relative contribution of Doppler exponentially-correlated noise and time-independent bias errors to system position error at landfall and velocity error during penetration. The sensitivity analyses, which were generated with the suboptimal covariance analysis program, were based on the assumption that 80% of a specified Doppler scale-factor error or equivalent drift-angle error should be treated as a time-independent bias and that 60% of these errors should be treated as exponentially-correlated noise (root-sum-square to 100%). The error budget histograms showed that system performance was significantly more sensitive to Doppler noise than to Doppler bias.

The 15-minute correlation time was selected partly on the basis of its popularity over the years in the filter-design business and partly on the basis of in-house simulation and sensitivity studies. Figure 15, for example, is data obtained from the covariance analysis program for a candidate suboptimal filter design by varying the real-world Doppler correlation time and fixing the filter-model correlation time. (In this suboptimal design the Doppler scale-factor and drift-angle process noises were not set equal to the equilibrium values $\frac{2P_{D_o}}{\tau}$ implied by Eqs. (20) and (21).) The figure shows that performance sensitivity to real-world correlation time uncertainty is reduced by modeling relatively short correlation times in the

filter. The popularity of the 15 minute correlation time may be traceable to Ref. [6] which states, in effect, that 15 minutes is the least desirable (and therefore most conservative) correlation time for Doppler bias errors in a Doppler-inertial system because of Schuler effects.

4.2.2 Sea State Reset

Throughout the B-1 navigation filter design process, it was assumed that Doppler performance over water is significantly degraded relative to Doppler performance over land. Sea-surface motion was postulated as the basic physical source of this degradation, since Doppler reflection is relative to a moving medium. Although ocean currents (gross motion) are predictable in many parts of the world, a global omnidirectional sea-bias uncertainty of 3.5 knots per axis was used for Doppler over-water error modeling.

The B-1 Offensive Systems display panel contains a land/sea switch for Doppler over-land or over-water operation. From a filter-implementation standpoint, the switch controls Doppler covariance matrix, dynamics matrix (correlation time), process-noise (compensation) matrix, and state vector re-initializations and resets for transition from land to sea and sea to land. The off-diagonal covariance elements in the Doppler scale-factor and drift-angle rows and columns are set to zero at transitions. For flight over water, the Doppler scale-factor and drift-angle variances are reset to values commensurate with the 3.5 knot sea-bias uncertainty, while the accumulated estimates of scale-factor and drift-angle errors are retained. At land-fall the scale-factor and drift-angle variances are reset to their initial (original) over-land values, while the accumulated scale-factor and drift-angle error estimates, which have presumably been corrupted by sea-surface effects, are reset to their (stored) pre-over-water values.

The process-noise (Q) matrix is reset concurrently with the covariance matrix to new Markov-process equilibrium values. Process-noise matrix reset alone will, of course, stimulate the same increase (or decrease) in Doppler-error-estimate uncertainty - but over a longer period of time. Resetting both the covariance matrix and the noise matrix at land/sea or sea/land transition tells the filter immediately that the Doppler information is less trustworthy over water or reliable when the aircraft is again over land. This is particularly important for weapon delivery, since it results in markedly lower post-landfall velocity errors. The measurement-noise (R) matrix is not reset at transitions under the assumption that Doppler fluctuation noise is relatively independent of terrain.

Figure 16 displays relative over-water growth rates for three operational situations (mission scenario similar to the one in Fig. 3):

(1) Doppler off over water
(2) Filter reset over water (sea setting)
(3) No filter reset over water (land setting)

The performance predictions were obtained from the suboptimal covariance analysis program with an initial 3.5 knots per axis sea-bias uncertainty modeled in the real world. The figure shows that the performance degradation is significant when Doppler errors in the filter are not re-initialized for flight over water. The figure also shows that the large Q values in the filter for reset over water inhibit heavy Doppler-velocity damping.

4.3 Gyrocompass/Autocalibration Filter

As discussed in Section 2, long-range over-water cruise navigation with no position fixing places a premium on periodic inertial measurement unit autocalibration and on gyro-calibration stability. To maximize the interval between autocalibrations, a two-position ground alignment - or gyrocompass - mechanization was originally implemented for the B-1. The idea here was that operational ground alignments would then provide level-gyro re-calibrations.

The B-1 ground alignment and autocalibration mechanization is designed around a Kalman filter which uses velocity as an observable. The original mechanization consisted of seven and one-half minutes of fine leveling, azimuth estimation, and north-gyro calibration in the first position; a 90 degree slew; and eight minutes of azimuth refinement and (original) east-gyro calibration in the second position. The filter is "on" during slew. For the sake of software commonality, the gyrocompass filter is structurally identical to the navigation filter, except that (in accordance with the discussion in Section 3.3) there are two level-accelerometer bias-error states. Since Doppler-error states are redundant on the ground, the accelerometer bias errors are modeled in place of the Doppler errors, thereby preserving filter dimensionality. The accelerometer states are replaced by Doppler states at transition from the ground-alignment mode to the navigation mode. Also, for the sake of software commonality, the B-1 gyrocompass filter is a subset of the B-1 autocalibration filter; that is, autocalibration is simply extended gyro-compass. About 2 hours are required for autocalibration in order to achieve acceptable azimuth-gyro calibration accuracy. Figure 17 displays the gyrocompass/autocalibration error-dynamics equations as they are currently implemented. The critical terms in these equations relative to slew-induced accelerometer-bias observability are $\omega_z\phi_y$ and $\omega_z\phi_x$ in the $\dot{\phi}_x$ and $\dot{\phi}_y$ equations, respectively.

During the verification phase of gyrocompass/autocalibration filter development, a single-position gyro-compass was implemented in order to increase gyro-calibration time in the first position during autocal. This decision was also based on an analysis of the anomalies discussed in Section 5.2 and on accumulating evidence to the effect that "in-the-field" LN-15 gyro-calibration stability is much better than had been anticipated.

4.4 Software Considerations

4.4.1 Transition Matrix Generation

First-Order Algorithm

The problem of choosing an algorithm for transition matrix generation arose quite early in the B-1 navigation

filter software-development process. An analysis of algorithm accuracy requirements, similar to that described in [1] resulted in the selection of

$$\Phi(m\,\Delta t) = \prod_{k=1}^{m} (I + F_k\,\Delta t), \tag{22}$$

where Δt is set equal to 1 second and m is 6, the number of seconds in the B-1 Kalman update cycle. Setting Δt equal to 1 second eliminates a multiplication.

Dual Filter Commonality

There are two navigation filters in the B-1, one for each inertial platform. The filters operate independently of each other, except for the fact that they use the same Doppler-velocity and position-fix update information. The coarse-alignment mechanization ensures that the wander angles of the two platforms are approximately equal at the initiation of fine alignment with the Kalman filters. Since both platforms will indicate approximately the same level-axis velocity components for parallel alignment, the two filters use a common transition matrix for error propagation.

4.4.2 Design Simplifications

Airborne computer capacity eventually becomes a limiting design factor on any software development program. The B-1 is no exception and navigation filter design simplifications have been introduced to save software. The resulting performance degradation is negligible for a typical mission.

Vertical-Channel Decoupling

The dynamics-matrix elements in Fig. 8, which couple the level and vertical-channel errors, have been set to zero in the current B-1 filter design, and the level and vertical-channel filters operate independently of each other. Since the vertical-channel error equations are independent of aircraft dynamics, the Kalman gains become constant in time after an initial transient period.

Prefilter Approximations

The Doppler prefilter in the B-1 consists of simple velocity observation averaging. The predicted velocity-measurement errors are not averaged. As a result, the velocity residuals are of the form

$$\bar{y} - H\bar{x}^{-}$$

where $\bar{y} = \frac{1}{n}\sum y_k$ (n = number of measurements)

and $H\bar{x}^{-}$ is evaluated at the end of the measurement interval. The 6-second Kalman update cycle used on the B-1, together with the fact that Doppler updates are inhibited during severe lateral maneuvers (large bank angles), makes this a workable approximation.

4.4.3 Measurement Matrix Implementation

The software code and timing requirements for implementing either measurement matrix in Fig. 9 are similar. However, the matrix which utilizes Y_{V_x} and Y_{V_y}, rather than Y_{V_g} and Y_{Δ}, as velocity observables has been implemented in the B-1 navigation filter in order to avoid a square-root computation for groundspeed and an arc-tangent computation for drift angle. These computations are

$$V_g = [V_x^2 + V_y^2]^{\frac{1}{2}}$$

$$\Delta = \tan^{-1}\left(-\frac{V_y}{V_x}\right) - \theta_s, \tag{23}$$

where V_x and V_y are system velocity components and θ_s is the platform yaw-synchro angle. The disadvantage of using Y_{V_x} and Y_{V_y} as velocity observables in the Kalman filter is that it constrains the designer to model equal groundspeed and drift-angle measurement noises in the filter R matrix when, in fact, these noises are not equal for all Dopplers.

5. Flight-Test Verification

From June 1974 through August 1975, a B-1 navigation system flight-test program was conducted at Holloman Air Force Base (New Mexico) aboard a modified C-141 Starlifter Aircraft. Some of the objectives and goals for this flight test program were [7]:

(1) To verify navigation hardware/software compatibility in a realistic dynamic environment.

(2) To identify navigation hardware, software and mechanization equation problems at an early point in the B-1 development schedule.

The avionics software on board the aircraft contained the B-1 navigation filter. Although the avionics hardware included an inertial platform and Doppler radar, it did not include a forward-looking radar. Instead, aircraft position measurements were performed with the aircraft's optical viewfinder by overflying checkpoints.

The navigation flight-test sequence at Holloman proceeded from ground tests of the gyrocompass/autocalibration

mechanization through free-inertial flight tests with ground-alignment or autocalibration initialization to Doppler-inertial flights with both ground and in-air inertial platform alignment. The primary objective of the final phase of Holloman flight testing was to verify the feasibility of using fixed-antenna Doppler hardware with stabilized-antenna Doppler software. From the standpoint of filter design verification, the Holloman Program:

(1) Provided range-calibrated Doppler performance data for error model refinement.

(2) Exhibited some unexpected inertial platform slew-induced phenomena during the initial phases of ground-alignment checkout.

5.1 Real-World Doppler Errors

The Holloman flight-test program provided a unique opportunity to compare the performance of three Doppler radars under identical operating conditions (same terrain, altitude, and speed) and relative to the same velocity reference. The three Dopplers are the APN-185, the APN-200, and the APN-206. Two of the Dopplers (APN-200 and APN-206) are fixed-antenna designs; the third (APN-185) utilizes an electromechanically stabilized antenna. The APN-185 and APN-200 are made in the United States; the APN-206 is made in Great Britain. The velocity reference was CIRIS (Completely Integrated Reference Instrumentation System).

5.1.1 Second-Order Markov-Process Approximation

Autocorrelation Function

Groundspeed and drift-angle outputs from all three Dopplers, when differenced with the CIRIS data, exhibited similar autocorrelation properties. Figure 18 is a typical groundspeed-error autocorrelation function. The salient characteristics of this autocorrelation function are a very rapid exponential decay (essentially a white-noise component) and the presence of non-decaying oscillations (periodic component). The periodic component, which appears to be a sum of oscillatory random variables, is the critical data component in Fig. 18. However, as of this writing, there is some uncertainty as to precisely how much of the periodicity in this figure is due to inherent Doppler errors and how much is attributable to reference data handling.

Reference [8] (preliminary version) states that a sum of autocorrelation functions of the form

$$\phi_D(\tau) = E\left[x_1(t)\, x_1(t+\tau)\right] = \phi_D(0)\cos\beta|\tau| \tag{24}$$

results in a reasonable analytical approximation to the periodic component in Fig. 18. This reference also suggests that a basic model which represents this type of autocorrelation function is the second-order Markov process

$$\begin{bmatrix}\dot{x}_1\\ \dot{x}_2\end{bmatrix} = \begin{bmatrix}0 & 1\\ -\beta^2 & 0\end{bmatrix}\begin{bmatrix}x_1\\ x_2\end{bmatrix} + \begin{bmatrix}1\\ \beta\end{bmatrix} U \tag{25}$$

where β is a frequency parameter and the damping parameter has been set to zero. The transition matrix for this equation is

$$\Phi(\tau) = \begin{bmatrix}\cos\beta t & \frac{1}{\beta}\sin\beta t\\ -\beta\sin\beta t & \cos\beta t\end{bmatrix}. \tag{26}$$

With $Q = 0$ and $P(0) = \begin{bmatrix}P_{11}(0) & 0\\ 0 & 0\end{bmatrix}$, the covariance P_{11} of x_1 oscillates in time as

$$P_{11}(t) = P_{11}(0)\cos^2\beta t = \frac{P_{11}(0)}{2}\left[1+\cos 2\beta t\right]. \tag{27}$$

It can be shown that the autocorrelation function

$$\phi(t+\tau,t) = \Phi(t+\tau,t)\, P(t)$$

gives:

$$\begin{aligned}\phi_{11}(t+\tau,t) &= P_{11}(0)\left[\cos\beta\tau\cos^2\beta t - \sin\beta\tau\sin\beta t\cos\beta t\right]\\ &= P_{11}(0)\cos\beta t\cos\beta(t+\tau)\end{aligned} \tag{28}$$

The amplitude of $P_{11}(0)$ and the oscillation frequency β can be selected from the flight data. In general, matching the autocorrelation data to an analytical expression like the one above requires additional independent periodic random variables - some with non-zero Q's and non-zero damping coefficients.

Truth Model

The autocorrelation function in Fig. 18 does not exhibit the Doppler (time-independent) bias errors which were measured during the Doppler comparison study. These errors can be significant for Dopplers which

have not been calibrated at the navigation-system level. Hence, the Holloman data seemed to show that the combination of random constant, uncorrelated noise and second-order Markov process errors may be a better truth model (if the periodic component is really inherent to the Doppler) than the one assumed in Fig. 10, which consists of random constant, uncorrelated noise, and first-order Markov-process errors.

The implication of these results for Kalman filter design is that the random walk ($\dot{x}_D = U$) is superior to exponentially-correlated noise for Kalman filter Doppler models. In fact, the Doppler model in the B-1 navigation filter at Holloman was converted from exponentially-correlated noise to the random walk as flight testing progressed. (A practical disadvantage of using the random walk to model Doppler errors in a Kalman filter is that its variance grows without bound in time in the absence of updates. Hence, in implementing this error model, it is desirable to inhibit process-noise addition when the error variance has reached a pre-determined limit.) However, the Holloman results as a whole seemed to indicate that either model is suitable for airborne filter implementations. Figure 19 shows this rather dramatically for a flight where the Doppler model in the filter was exponentially-correlated noise. The heavy line in the figure represents the sum of Doppler scale-factor error estimates provided by the filter as a function of time for one of the Holloman flights. The light line in the background is the true velocity scale factor error obtained by differencing CIRIS-derived groundspeed with Doppler-indicated groundspeed, dividing by groundspeed and averaging over the 6-second update interval. The jagged nature of the averages reflects the relatively noisy output of a typical Doppler. The superposition of the true and estimated scale-factor errors shows that the filter is doing its job.

5.1.2 Over-Water Bias

The assumptions below (see Section 4.2.2) were basic to B-1 navigation filter design for Doppler-inertial flight overwater.

(1) Doppler groundspeed and drift-angle accuracy is degraded due to sea-surface motion.
(2) Doppler measurement (fluctuation) noise is essentially independent of terrain.

The upper part of Fig. 20 shows Doppler groundspeed errors over land and over water; the lower part of the figure shows the associated measurement-noise standard deviation. The data is taken from a Holloman flight which "race-tracked" over the Pacific Ocean off the California Coast. The average groundspeed error was obtained by differencing Doppler-measured groundspeed with CIRIS-derived groundspeed and averaging over 6-second (Kalman update) intervals. The groundspeed standard deviation is the empirical dispersion of the sample groundspeed errors about the average error. The data is displayed in three segments: the segment to the left is representative of groundspeed accuracy over land (calibrated Doppler); the segment in the middle typifies groundspeed accuracy over water; the segment to the right includes a sea/land transition.

The figure clearly shows the effect of sea currents in biasing the groundspeed output. (The flight path is parallel to the current. Note that the sea-bias changes polarity when the aircraft executes a 180-degree turn.) The figure also shows that the Doppler measurement noise is only slightly larger over water than it is over land. Both of these results are consistent with the filter design assumptions.

5.2 Gyrocompass/Autocalibration Anomalies

During the latter stages of B-1 Offensive Software development, the two-position gyrocompass/autocalibration filter was subjected to exhaustive verification with the simulation program. The solid lines in Figs. 21, 22, and 23 are simulation program plots of expected gyro-calibration and wander-angle estimation errors over a 40-minute time interval. The data in these figures represent computed standard deviations for a five-case Monte Carlo random sample of inertial-sensor and initialization errors. In the first position the north gyro is calibrated and the wander angle is estimated to an accuracy commensurate with east-gyro calibration uncertainty. In the second position the (original) east gyro is calibrated and the wander-angle estimate is refined.

The real-world results were not always this pretty. Figure 24 is a real system analog of the simulated results in Figs. 21 and 22 and is typical of many gyrocompass/autocalibration checkout runs at Holloman. (The error curves in Fig. 24 are plotted so that the gyro which is pointed north in the first position has zero calibration error prior to slew and the gyro which is pointed north in the second position has zero calibration error after a 30-minute time interval.) The post-slew gyro-calibration overshoots and offsets were completely unexpected. Moreover, the magnitude of the filter's gyro-calibration estimates varied from run to run and appeared to be a function of the wander angle used to initialize the system. As a final surprise, the accelerometer biases estimated by the filter during real-platform slew differed appreciably from accelerometer biases measured during IMU acceptance test procedures (ATP).

Analytical investigations of these phenomena focused sequentially on the following candidate causes:

(1) Level-gyro scale-factor calibration inaccuracy.
(2) Vertical-gyro torquer-axis misalignment.
(3) Yaw-synchro noise during platform slew.

Analysis of long-term level-gyro scale-factor calibration data revealed stability to within 0.01 percent - less than .0015 degree per hour of equivalent gyro drift at Holloman latitudes. Consequently level-gyro scale-factor calibration inaccuracy did not appear to be the problem.

5.2.1 Vertical-Gyro Torquer-Axis Misalignment

Consider the error equations

$$\dot{\delta v}_x = -g\,\phi_y + b_x$$

$$\begin{aligned} \dot{\delta v}_y &= g\,\phi_x + b_y \\ \dot{\phi}_x &= \omega_z\,(\phi_y + \eta_x) + \varepsilon_x \\ \dot{\phi}_y &= \omega_z\,(-\phi_x + \eta_y) + \varepsilon_y \end{aligned} \tag{29}$$

for a stationary inertial measurement unit. The symbols η_x and η_y in these equations are vertical-gyro torquer-axis misalignment-angle components along the platform level axes. Before platform slew $\omega_z = \Omega_z$ (on the order of 10 degrees per hour) and the filter cannot distinguish between platform tilt and accelerometer bias. During platform slew $\omega_z = \rho_z$ (about 1000 degrees per hour) and the equations show that the platform will be tilted until the z-gyro torquer-axis is vertical. The tilt is accomplished through accelerometer-bias-correction buildup - the filter, in effect, adding vertical-gyro misalignments to accelerometer-bias estimates. Although vertical-gyro torquer-axis misalignment helped explain the difference between ATP-measured and filter-estimated accelerometer biases, simulation studies showed that this error source did not stimulate the post-slew gyro-calibration overshoots and offsets.

5.2.2 Yaw-Synchro Noise during Platform Slew

One advantage (at least for analysts) of a local-level wander-azimuth mechanization which utilizes vertical earth-rate torquing is that inertial platform heading is constant during ground alignment and autocalibration. In the B-1 mechanization the on-board computer's estimate of platform heading or wander angle is used in the equations

$$\begin{aligned} \Omega_{x_i} &= \Omega \cos \alpha_i \cos \lambda_o \\ \Omega_{y_i} &= -\Omega \sin \alpha_i \cos \lambda_o \end{aligned} \tag{30}$$

to resolve earth rate along the platform x and y axes for level-gyro torquing. In Eq. (30) Ω is earth rate, λ_o is input latitude, and α_i is current wander angle. During platform slew the wander angle is updated with the equation

$$\alpha_i = \alpha_{i-1} - \delta\hat{\theta}_{z_i} + \Delta\theta_s \tag{31}$$

where $\delta\hat{\theta}_z$ is the wander-angle error estimate from the filter (zero longitude error in Eqs. (14)) and $\Delta\theta_s$ is an increment in the yaw-synchro-angle readout. A new wander-angle-error estimate is available from the filter every 6 seconds - with or without slew; the $\Delta\theta_s$ increments are available every 1/16 of a second.

The solid lines in Figs. 21, 22, and 23 were taken from a simulation run with an error-free synchro angle. However, when yaw-synchro noise was added to the simulation during slew, the overshoots and offsets appeared. The dotted lines in Figs. 21, 22 and 23 are taken from a simulation run which is identical to the one which generated the solid lines, except that uncorrelated noise was added to the simulated yaw-synchro readout. The reason why the offsets appear is that yaw-synchro noise results in post-slew wander-angle errors of which the filter is unaware, and the filter assigns this error to gyro drift. Laboratory evaluations have confirmed the presence of readout noise in even the best IMU gimbal-angle synchros. Hence, the cumulative effects of yaw-synchro noise (or an equivalent yaw-synchro bias shift during platform slew) turned out to be the cause of the gyro-calibration anomalies observed at Holloman.

A filter modification which eliminates this problem is the addition of process-noise compensation during slew at the wander-angle-error ($\delta\theta_z$) level. The dashed lines in Figs. 21, 22, and 23 are the same simulation run once more with additional process-noise compensation during slew. The anomalies have been removed and the gyro-calibration curves are almost congruent with the original results. The compensation increases the $\delta\theta_z$-estimate uncertainty at the end of slew and permits the filter to re-estimate the wander-angle error prior to resuming gyro calibration. As a result of these investigations, yaw-synchro noise compensation was added to the B-1 gyrocompass/autocalibration filter mechanization.

6. Conclusions

The B-1 navigation filter is a conservative, straight-forward design. Although Holloman flight-test verification produced some hardware/software interaction surprises, design refinements resulted in filter performance which was actually better than had been anticipated. The principal design refinement to the navigation filter was Doppler error model conversion to the random walk.

In retrospect, the Holloman experience associated with leaving the gyrocompass/autocalibration filter on during inertial platform slew at high angular rates suggests that attendant theoretical advantages, such as accelerometer-bias estimation, may be minimized by real-system phenomena, such as vertical-gyro torquer-axis misalignment and yaw-synchro readout inaccuracies. Since the primary purpose of inertial-measurement-unit autocalibration is gyro-drift estimation and since navigation system performance in the Doppler-inertial mode is relatively insensitive to accelerometer bias errors, it would probably suffice, in practice, to turn the filter off during slew (while maintaining software coarse leveling) and to re-initialize the filter for platform re-alignment and gyro-calibration refinement in the second position.

REFERENCES

[1] Schmidt, S. F., J. E. Weinberg and J. S. Lukesh, "Application of Kalman Filtering to the C-5 Guidance and Control System," appearing in Theory and Applications of Kalman Filtering (NATO AGARDograph 139), February 1970, pp 289-334.

[2] Nash, R. A., Jr., J. A. D'Appolito and K. J. Roy, Error Analysis of Hybrid Aircraft Inertial Navigation Systems, AIAA Guidance and Control Conference, Stanford, California, August 14-16, 1972, No. 72-848.

[3] Bergeson, J. E. and J. H. Witte, Performance Comparison of Space Stable and Local Level Inertial Platform Mechanizations for a Strategic Aircraft Application, Proceedings of the IEEE 1975 National Aerospace and Electronics Conference (NAECON 75), pp 617-624.

[4] Benson, D. O., A Comparison of Two Approaches to Pure-Inertial and Doppler-Inertial Error Analysis, IEEE Transactions on Aerospace and Electronic Systems, Vol. AES-11, No. 4, July 1975, pp 447-455.

[5] Bryson, A. E., Jr., Simplified Design of Filters to Estimate Misalignment Angles and Gyro Drifts of a Stationary IMU, Department of Aeronautics and Astronautics, Stanford University, SUDAAR No. 449, December 1972.

[6] Kayton, M., and W. R. Fried (eds.), Avionics Navigation Systems, John Wiley & Sons, Inc. (1969) p. 255.

[7] Preston, R. T. and J. W. Warmuth, B-1 Navigation Mechanization and Development Flight Test Planning and Instrumentation, Seventh Biennial Guidance Test Symposium Proceedings, Vol. 1, AFSWC TR 7526, May 1975.

[8] Molnar, D. and N. Walton, A Doppler Markov Error Model Development Based on Flight Test Data Analysis, to appear in Proceedings of the IEEE 1976 National Aerospace and Electronics Conference (NAECON 76).

ACKNOWLEDGEMENT

The design and flight-test verification of the B-1 Navigation Filter has been a collective effort of the Avionics System Integration Contractor's Navigation and Weapon Delivery Group. In particular, the author acknowledges the technical contributions of the following individuals:

N. Walton - Systems analysis

D. Molnar - Suboptimal covariance analysis program development

J. Witte - Navigation system simulation program development

R. Kuhns - Gyrocompass anomalies investigation

J. Burrows - Autocalibration repeatability analysis

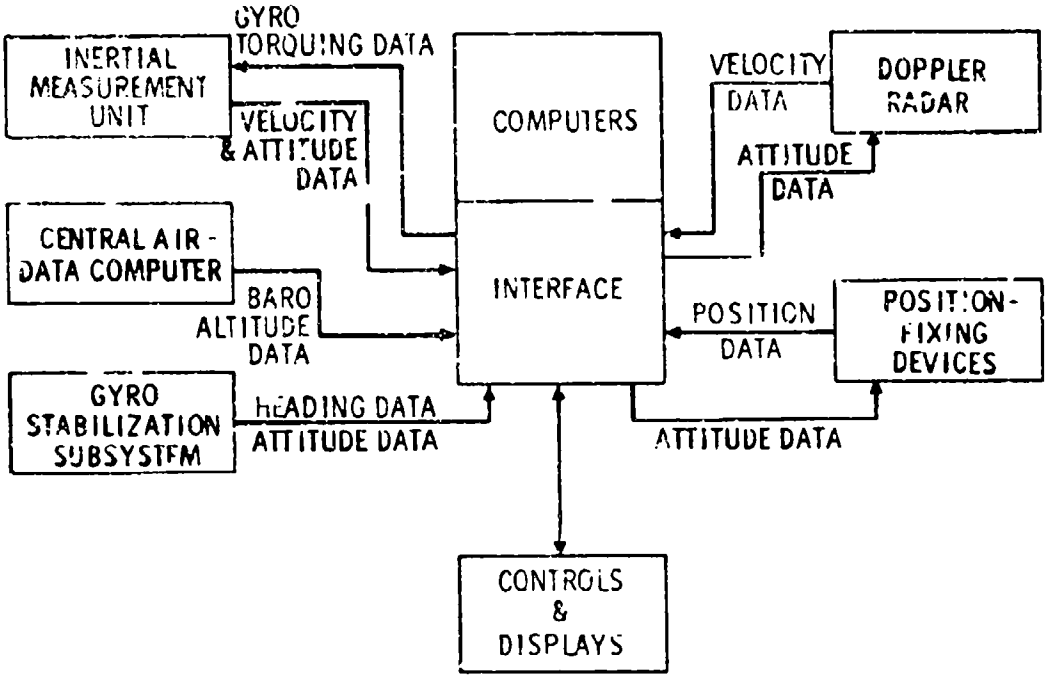

FIG. 1 NAVIGATION SYSTEM SCHEMATIC

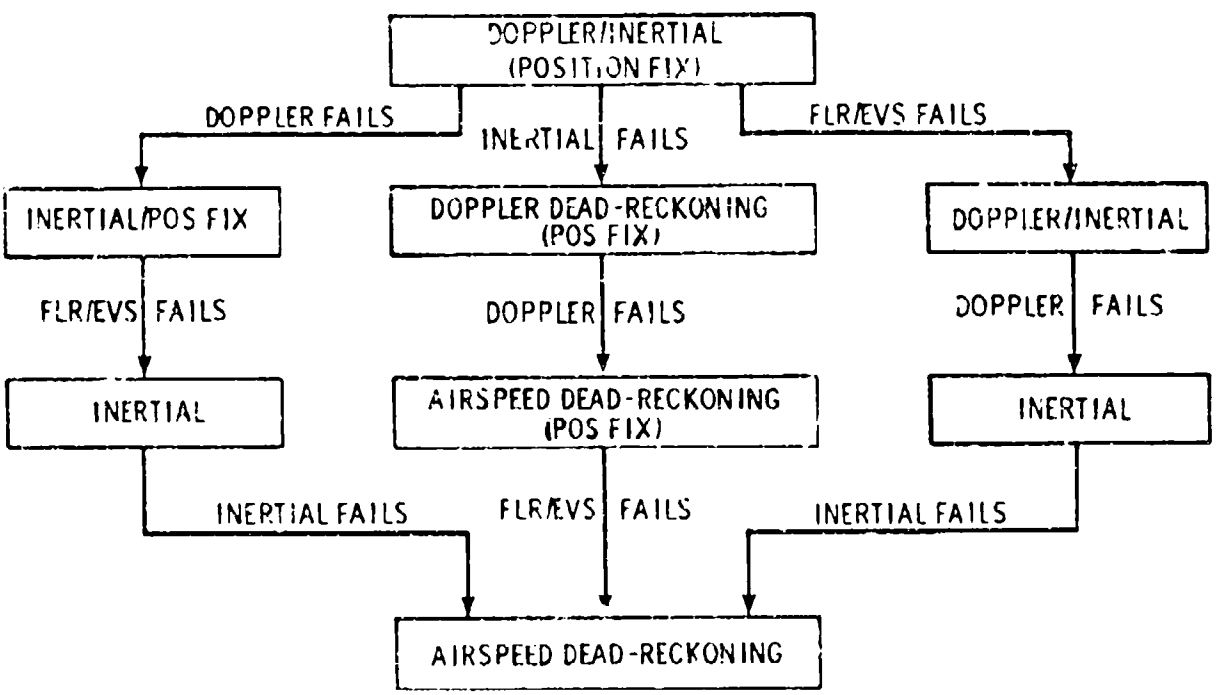

FIG. 2 NAVIGATION MODE HEIRARCHY

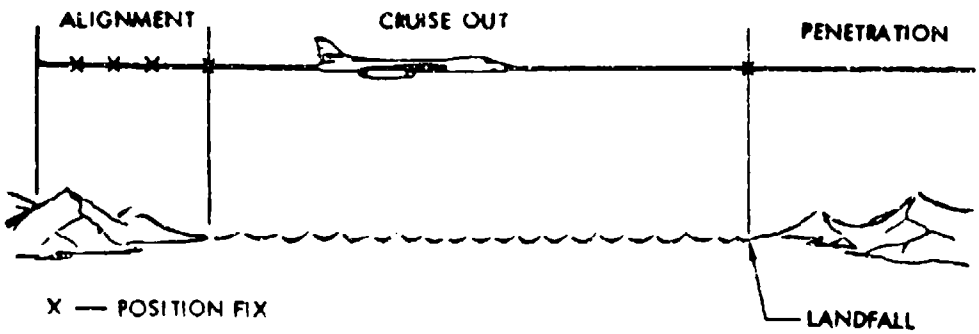

FIG. 3 TYPICAL MISSION SCENARIO

BETWEEN MEASUREMENTS

$$\hat{X}(k)^{-} = \Phi(k, k-1)\,\hat{X}(k-1)^{+A}$$
$$P(k)^{-} = \Phi(k, k-1)\,P(k-1)^{+}\,\Phi(k, k-1)^{T} + Q(k-1)$$

AT A MEASUREMENT

$$\hat{X}(k)^{+B} = \hat{X}(k)^{-} + K(k)\left[Y(k) - H(k)\,\hat{X}(k)^{-}\right]$$
$$K(k) = P(k)^{-}\,H(k)^{T}\left[H(k)P(k)^{-}H(k)^{T} + R(k)\right]^{-1}$$
$$P(k)^{+} = \left[I - K(k)H(k)\right]\,P(k)^{-}$$

AFTER SYSTEM CORRECTION

$$\hat{X}(K)^{+A} = \hat{X}(k)^{+B} + G(k)$$

FIG. 4 KALMAN FILTER EQUATIONS

NAVIGATION ERRORS

δx
δY
δZ } POSITION ERRORS

δV_x
δV_y
δV_z } VELOCITY ERRORS

ϕ_x
ϕ_y
ϕ_z } PLATFORM AXIS MISALIGNMENTS (PLATFORM/TRUE)

$\delta\theta_z$ AZIMUTH MISALIGNMENT (COMPUTER/TRUE)

SENSOR ERRORS

ε_x
ε_y
ε_z } GYRO BIAS ERRORS

K DOPPLER SCALE FACTOR

Δ DOPPLER DRIFT ANGLE

b_z VERTICAL ACCELEROMETER BIAS

b_b ALTIMETER BIAS

FIG. 5 STATE ERROR VECTOR

NAVIGATION ERRORS

$-\delta\hat{x}$
$-\delta\hat{Y}$
$-\delta\hat{Z}$ } POSITION ERRORS

$-\delta\hat{V}_x$
$-\delta\hat{V}_y$
$-\delta\hat{V}_z$ } VELOCITY ERRORS

0
0
0 } PLATFORM AXIS MISALIGNMENTS (PLATFORM/TRUE)

$-\delta\hat{\theta}_z$ AZIMUTH MISALIGNMENT (COMPUTER/TRUE)

SENSOR ERRORS

$-\left(\frac{\hat{\phi}_x}{T} + \hat{\varepsilon}_x\right)$
$-\left(\frac{\hat{\phi}_y}{T} + \hat{\varepsilon}_y\right)$
$-\left(\frac{\hat{\phi}_z}{T} + \hat{\varepsilon}_z\right)$ } GYRO TORQUING CORRECTIONS

$-\hat{K}$ DOPPLER SCALE FACTOR

$-\hat{\Delta}$ DOPPLER DRIFT ANGLE

$-\hat{b}_z$ VERTICAL ACCELEROMETER BIAS

0 ALTIMETER BIAS

FIG. 6 CONTROL VECTOR (AFTER K th UPDATE)

	δx	δY	δZ	δV_x	δV_y	δV_z	Ψ_x	Ψ_y	Ψ_z
$\delta\dot{X}$	0	0	0	1	0	0	0	0	0
$\delta\dot{Y}$	0	0	0	0	1	0	0	0	0
$\delta\dot{Z}$	0	0	0	0	0	1	0	0	0
$\delta\dot{V}_x$	$-g/R$	0	0	0	$2\Omega_z$	$-(\omega_y+\Omega_y)$	0	$-A_z$	A_y
$\delta\dot{V}_y$	0	$-g/R$	0	$-2\Omega_z$	0	$(\omega_x+\Omega_x)$	A_z	0	$-A_x$
$\delta\dot{V}_z$	0	0	$2g/R$	$(\omega_y+\Omega_y)$	$-(\omega_x+\Omega_x)$	0	$-A_y$	A_x	0
$\dot{\Psi}_x$	0	0	0	0	0	0	0	Ω_z	$-\omega_y$
$\dot{\Psi}_y$	0	0	0	0	0	0	$-\Omega_z$	0	ω_x
$\dot{\Psi}_z$	0	0	0	0	0	0	ω_y	$-\omega_x$	0

FIG. 7 "PSI-ANGLE" ERROR MODEL

	δx	δY	δZ	δV_x	δV_y	δV_z	ϕ_x	ϕ_y	ϕ_z	$\delta\theta_z$
$\delta\dot{X}$	0	0	$-V_x/R$	1	0	0	0	0	0	$-v_y$
$\delta\dot{Y}$	0	0	$-V_y/R$	0	1	0	0	0	0	v_x
$\delta\dot{Z}$	0	0	0	0	0	1	0	0	0	0
$\delta\dot{V}_x$	$2V_y\Omega_x/R$	$2V_y\Omega_y/R$	0	0	$2\Omega_z$	$-(\omega_y+\Omega_y)$	0	$-A_z$	A_y	
$\delta\dot{V}_y$	$-2V_x\Omega_x/R$	$-2V_x\Omega_y/R$	0	$-2\Omega_z$	0	$\omega_x+\Omega_x$	A_z	0	$-A_x$	
$\delta\dot{V}_z$	$2V_y\Omega_z/R$	$-2V_x\Omega_z/R$	$2g/R$	$V_x/R+(\omega_y+\Omega_y)$	$V_y/R-(\omega_x+\Omega_x)$	0	$-A_y$	A_x		$2(V_y\Omega_y+V_x\Omega_x)$
$\dot{\phi}_x$	$-\Omega_z/R$	0	V_y/R^2	0	$-1/R$	0	0	Ω_z	$-\omega_y$	Ω_y
$\dot{\phi}_y$	0	$-\Omega_z/R$	$-V_x/R^2$	$1/R$	0	0	$-\Omega_x$	0	ω_x	$-\Omega_x$
$\dot{\phi}_z$	Ω_x/R	Ω_y/R	0	0	0	0	ω_y	$-\omega_x$	0	0
$\delta\ddot{\theta}_z$	V_y/R^2	$-V_x/R^2$	0	0	0	0	0	0	0	0

FIG. 8 "PHI-ANGLE" ERROR MODEL

	δV_x	δV_y	ϕ_z	κ	Δ
Yv_x	1	0	$-V_y$	$-V_x$	$-V_y$
Yv_y	0	1	V_x	$-V_y$	V_x

RESIDUAL FORMATION IN NAVIGATION AXES

	δV_x	δV_y	ϕ_z	κ	Δ
Yv_g	$\frac{V_x}{V_g}$	$\frac{V_y}{V_g}$	0	$-V_g$	0
Y_Δ	$\frac{V_y}{V_g^2}$	$-\frac{V_x}{V_g^2}$	1	0	-1

RESIDUAL FORMATION IN DOPPLER - ORIENTED (LOCAL LEVEL) AXES

FIG. 9 MEASUREMENT MATRICES

INERTIAL MEASUREMENT UNIT

- GYRO
  - G - INSENSITIVE DRIFT
    - RANDOM CONSTANT
    - EXPONENTIALLY CORRELATED
  - G - SENSITIVE DRIFT
  - TORQUER SCALE FACTOR
  - MISALIGNMENTS
- ACCELEROMETER
  - BIAS
    - RANDOM CONSTANT
    - EXPONENTIALLY CORRELATED
  - SCALE FACTOR
  - MISALIGNMENTS

NAVIGATION RADARS

- DOPPLER
  - SCALE FACTOR AND DRIFT ANGLE
    - RANDOM CONSTANT
    - EXPONENTIALLY CORRELATED
    - UNCORRELATED NOISE
- POSITION FIX
  - UNCORRELATED NOISE

ENVIRONMENTAL

- SEA BIAS
- VERTICAL DEFLECTIONS

FIG. 10 NAVIGATION SENSOR ERROR SOURCES

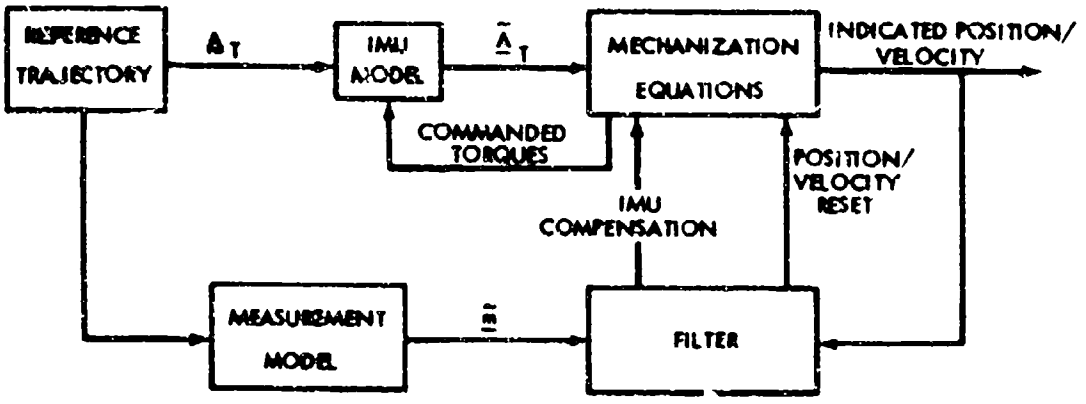

$\underline{A}_T$ - TRUE ACCELERATION

$\tilde{\underline{A}}_T$ - SENSED ACCELERATION

$\tilde{\underline{m}}$ - ACTUAL MEASUREMENT

FIG. 11 SIMULATION FUNCTIONAL BLOCK DIAGRAM

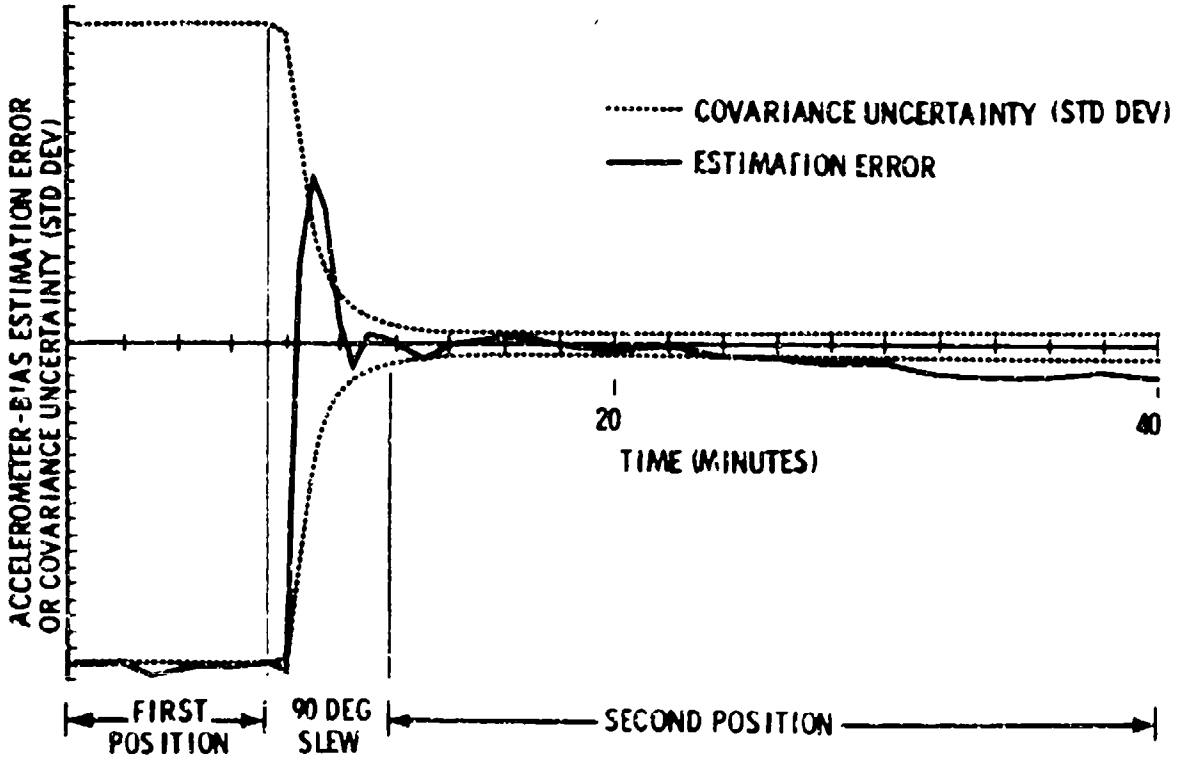

FIG. 12 SIMULATED ACCELEROMETER BIAS ESTIMATION

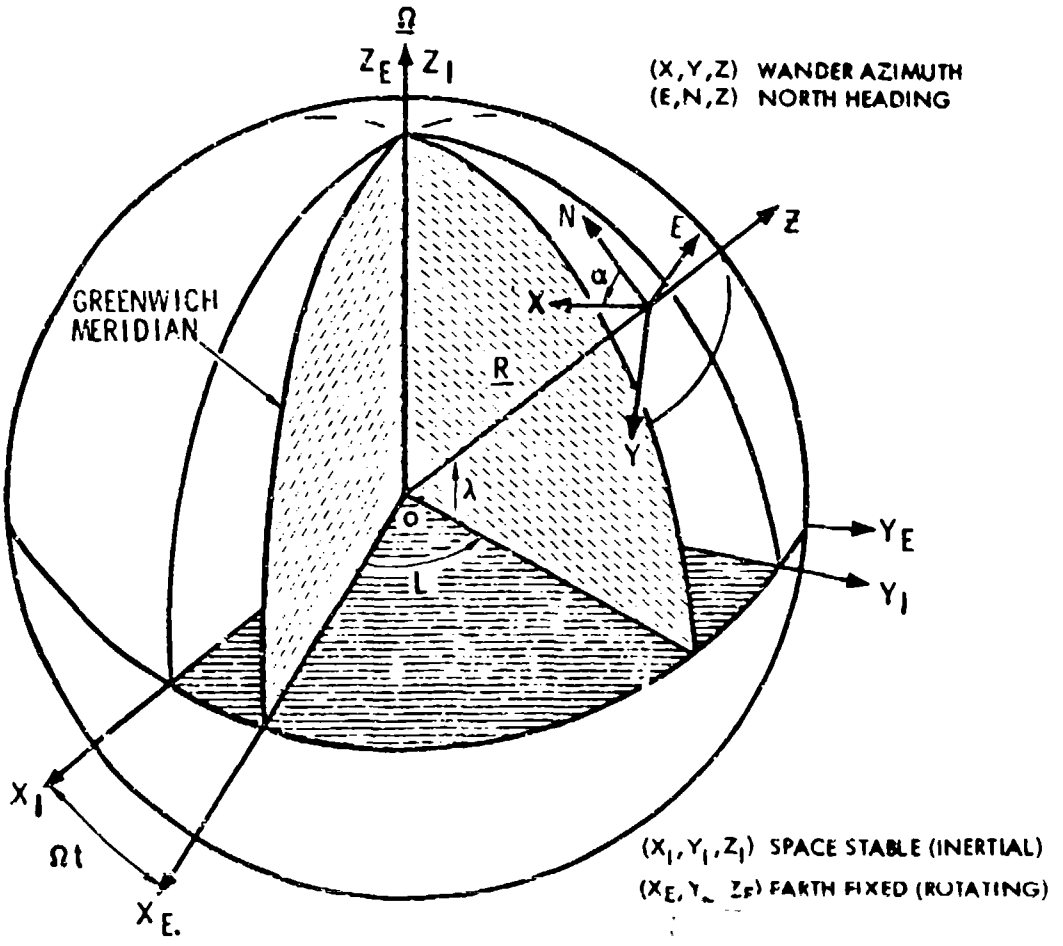

FIG. 13 COORDINATE SYSTEMS

$$C^{CE} = \begin{bmatrix} \sin L \sin\alpha - \sin\lambda \cos L \cos\alpha & -\sin\lambda \sin L \cos\alpha - \cos L \sin\alpha & \cos\lambda \cos\alpha \\ \sin L \cos\alpha + \sin\lambda \cos L \sin\alpha & \sin\lambda \sin L \sin\alpha - \cos L \cos\alpha & -\cos\lambda \sin\alpha \\ \cos\lambda \cos L & \cos\lambda \sin L & \sin\lambda \end{bmatrix}$$

FIG. 14 NAVIGATION DIRECTION COSINE MATRIX

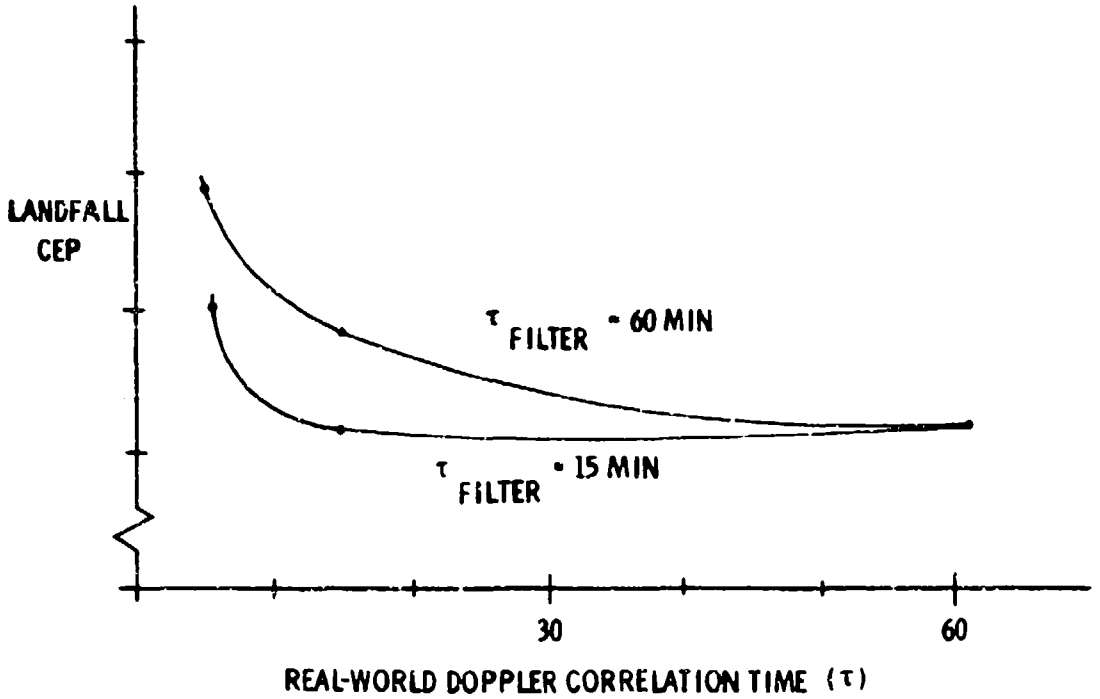

FIG. 15 PERFORMANCE SENSITIVITY TO DOPPLER CORRELATION TIME UNCERTAINTY

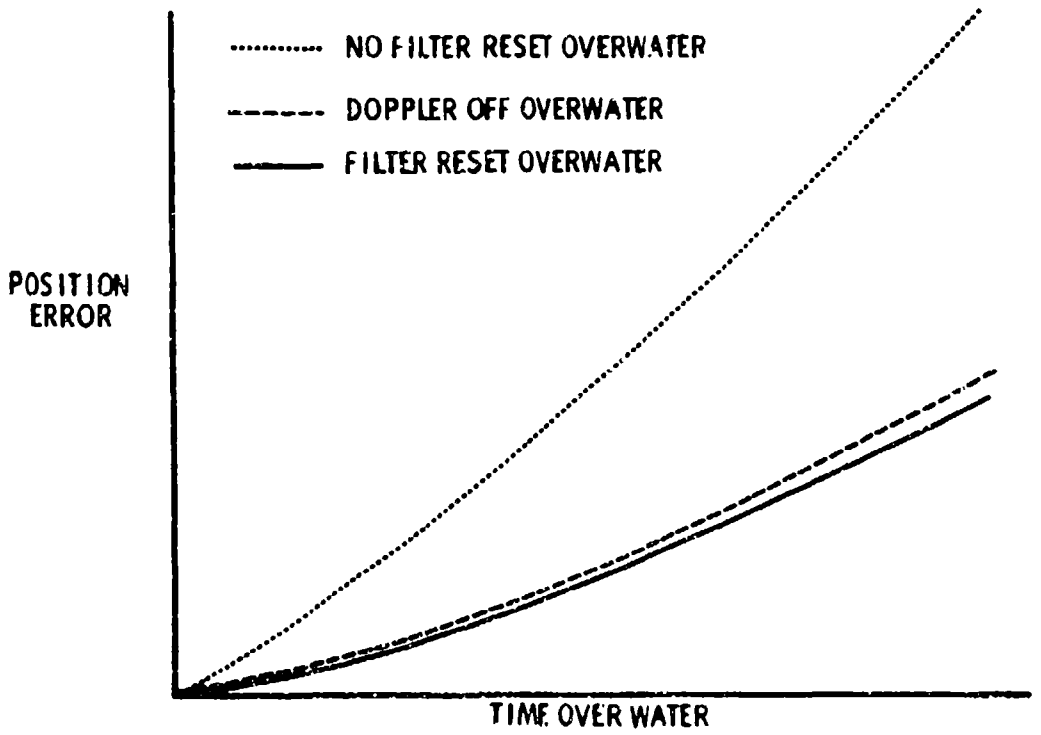

FIG. 16 OVER WATER POSITION ERROR GROWTH

$$
\begin{aligned}
\delta\dot{x} &= \rho_z\,\delta y + \delta v_x \\
\delta\dot{y} &= -\rho_z\,\delta x + \delta v_y \\
\delta\dot{v}_x &= (2\Omega_z + \rho_z)\,\delta v_y - g\,\phi_y + b_x \\
\delta\dot{v}_y &= -(2\Omega_z + \rho_z)\,\delta v_x + g\,\phi_x + b_y \\
\dot{\phi}_x &= -\frac{\Omega_z}{R}\,\delta x - \frac{1}{R}\,\delta v_y + \omega_z\,\phi_y - \Omega_y(\phi_z - \delta\theta_z) + \epsilon_x \\
\dot{\phi}_y &= -\frac{\Omega_z}{R}\,\delta y + \frac{1}{R}\,\delta v_x - \omega_z\,\phi_x + \Omega_x(\phi_z - \delta\theta_z) + \epsilon_y \\
\dot{\phi}_z &= \frac{\Omega_x}{R}\,\delta x + \frac{\Omega_y}{R}\,\delta v + \Omega_y\,\phi_x + \Omega_x\,\phi_y + \epsilon_z \\
\delta\dot{\theta}_z &= 0
\end{aligned}
$$

FIG. 17 ERROR DYNAMICS FOR EQUATIONS FOR GYROCOMPASS/AUTOCALIBRATION

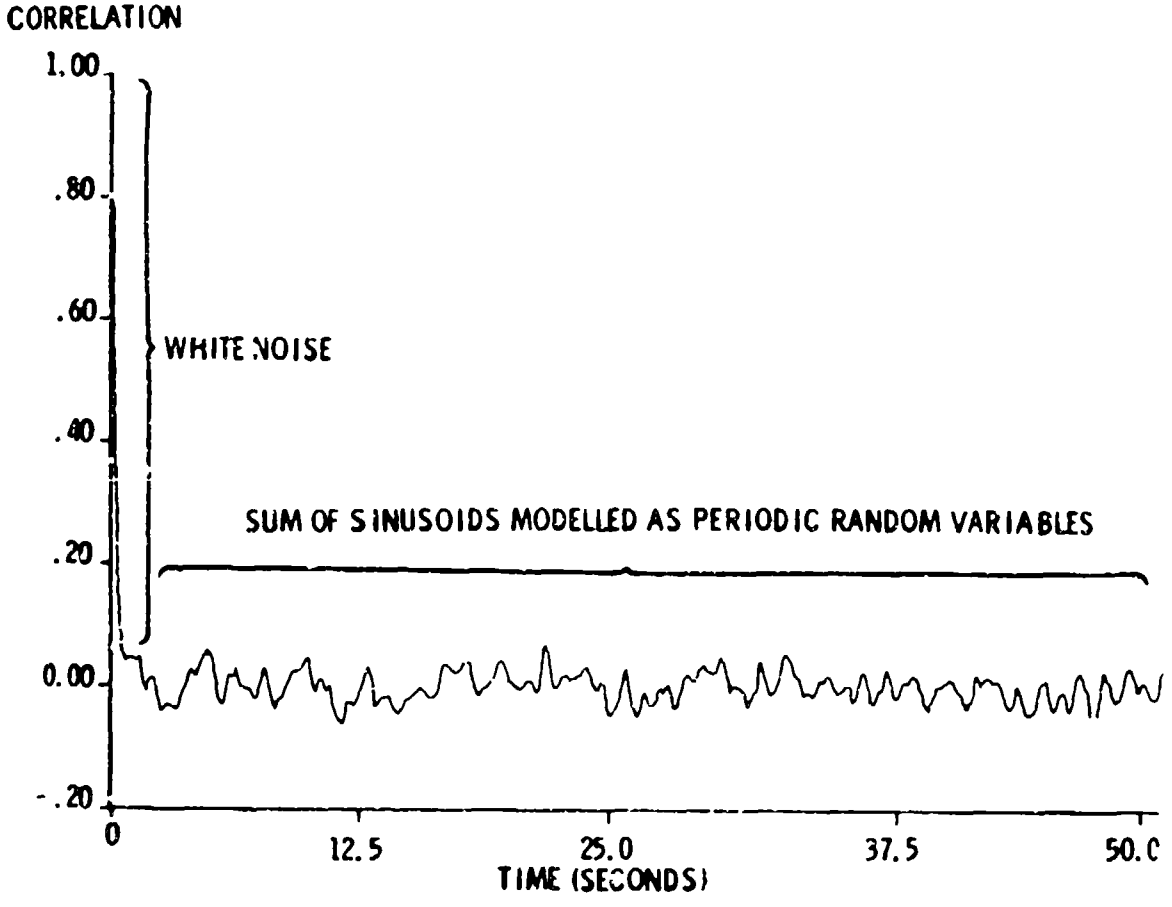

FIG. 18 DOPPLER ERROR AUTOCORRELATION FUNCTION

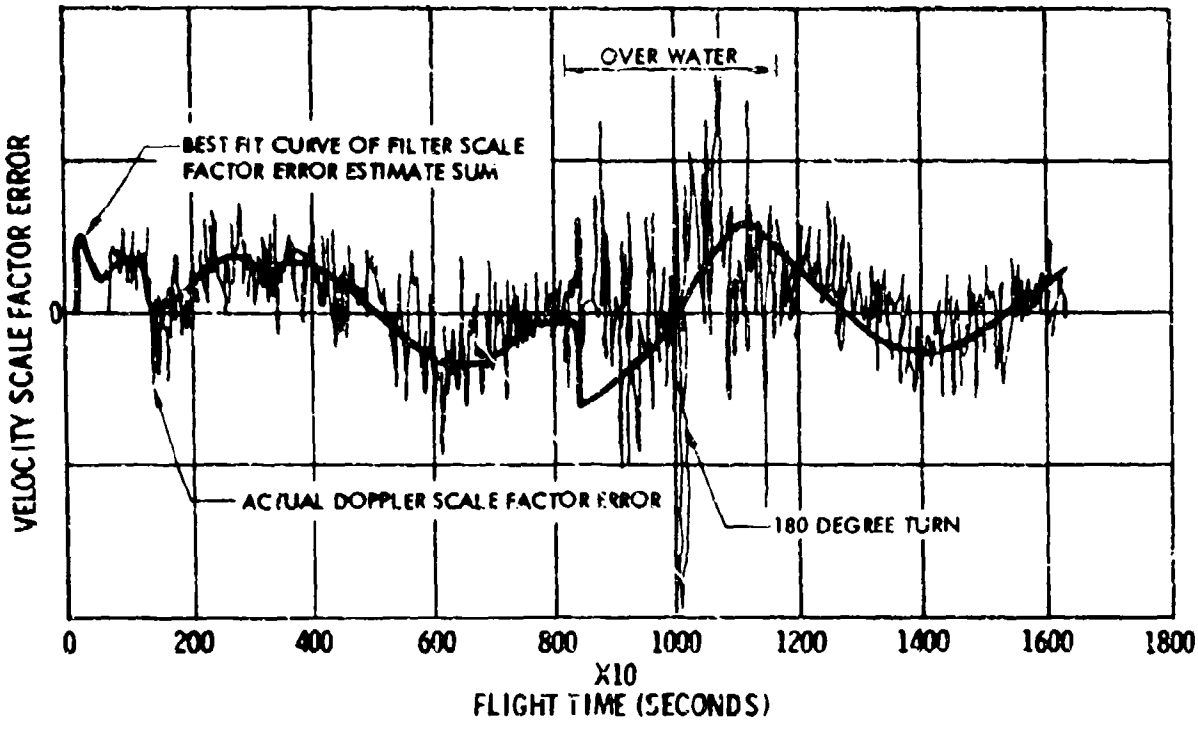

FIG. 19 VELOCITY SCALE FACTOR ERROR

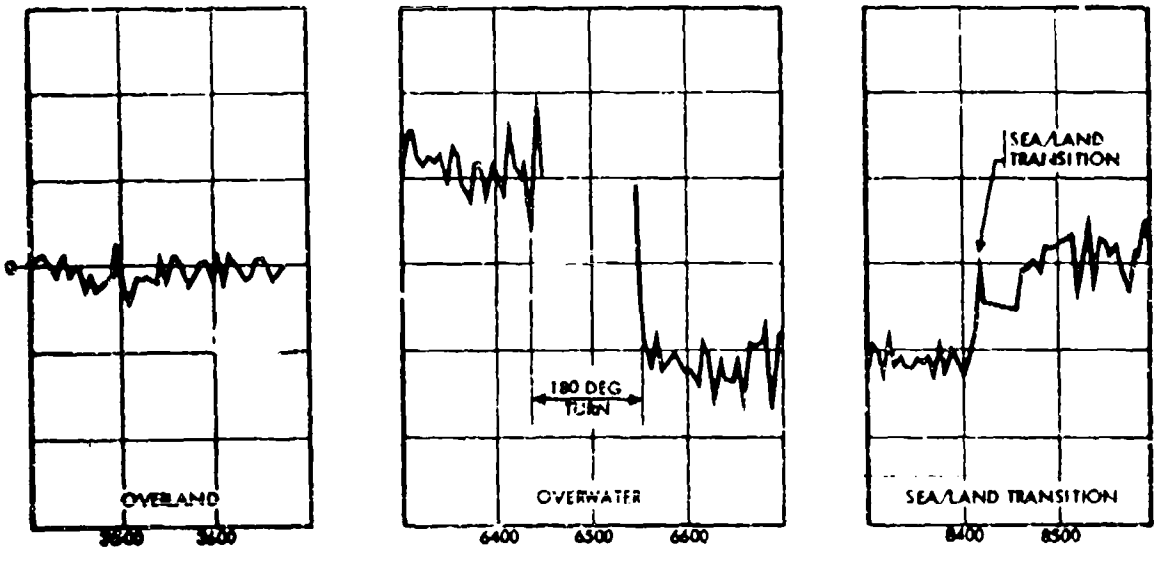

ACTUAL GROUND SPEED EPROR AVERAGED OVER 6 SEC

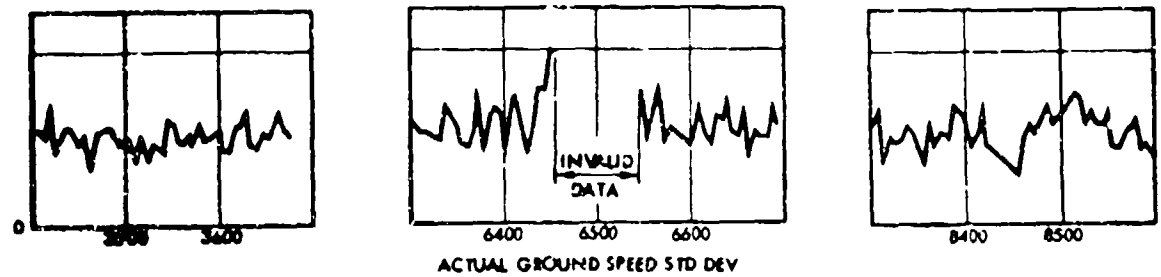

ACTUAL GROUND SPEED STD DEV

FIG. 20 OVER WATER EFFECTS

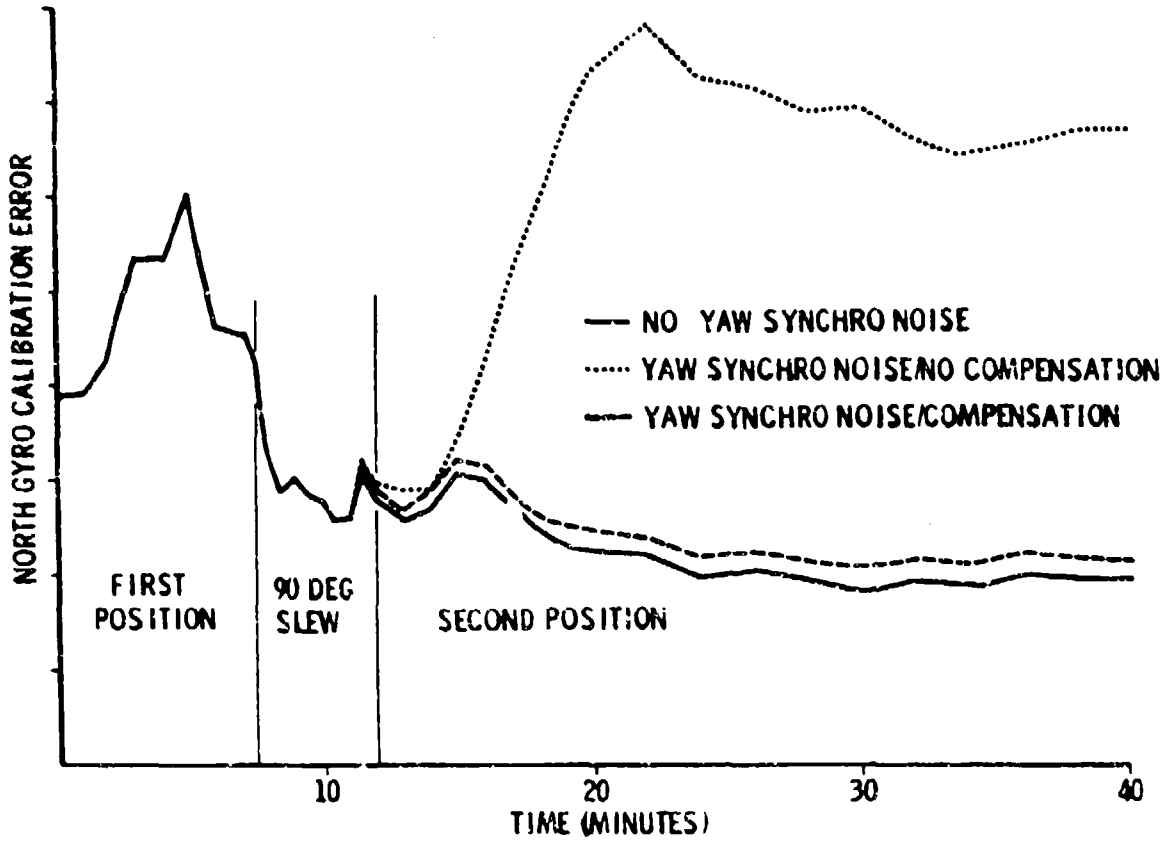

FIG. 21 SIMULATED NORTH GYRO CALIBRATION ERROR

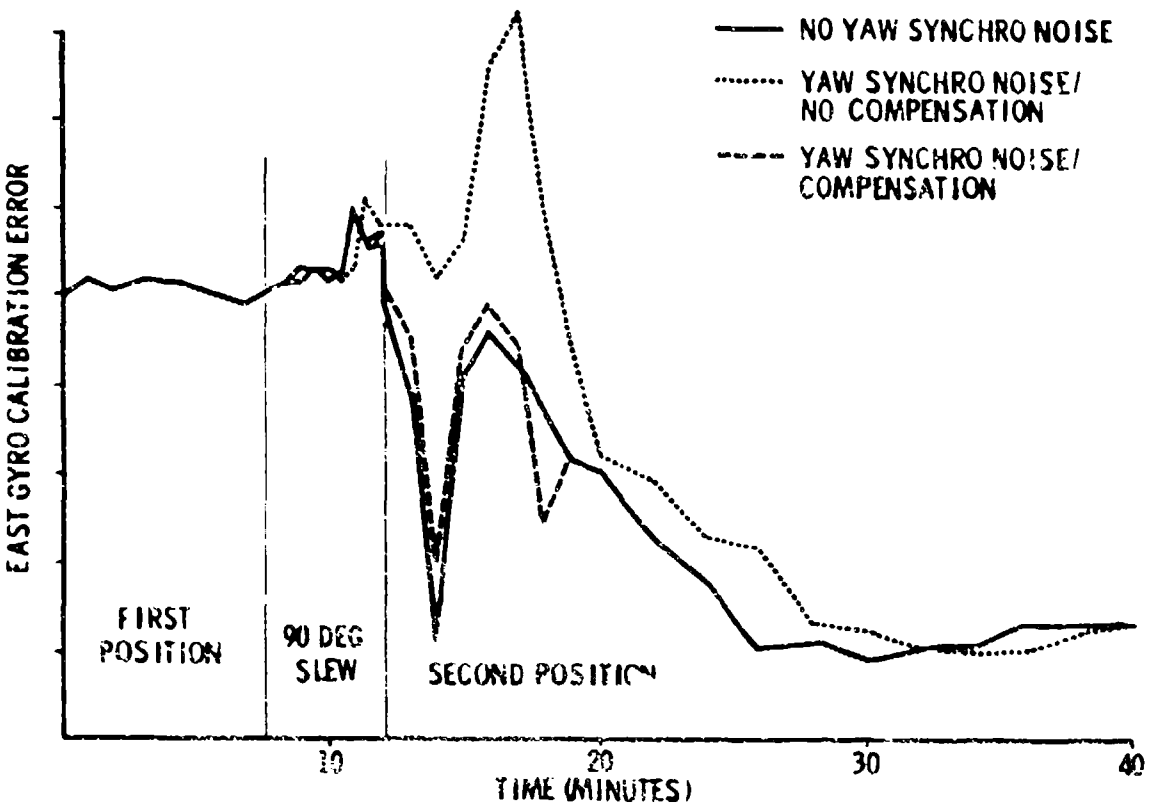

FIG. 22 SIMULATED EAST GYRO CALIBRATION ERROR

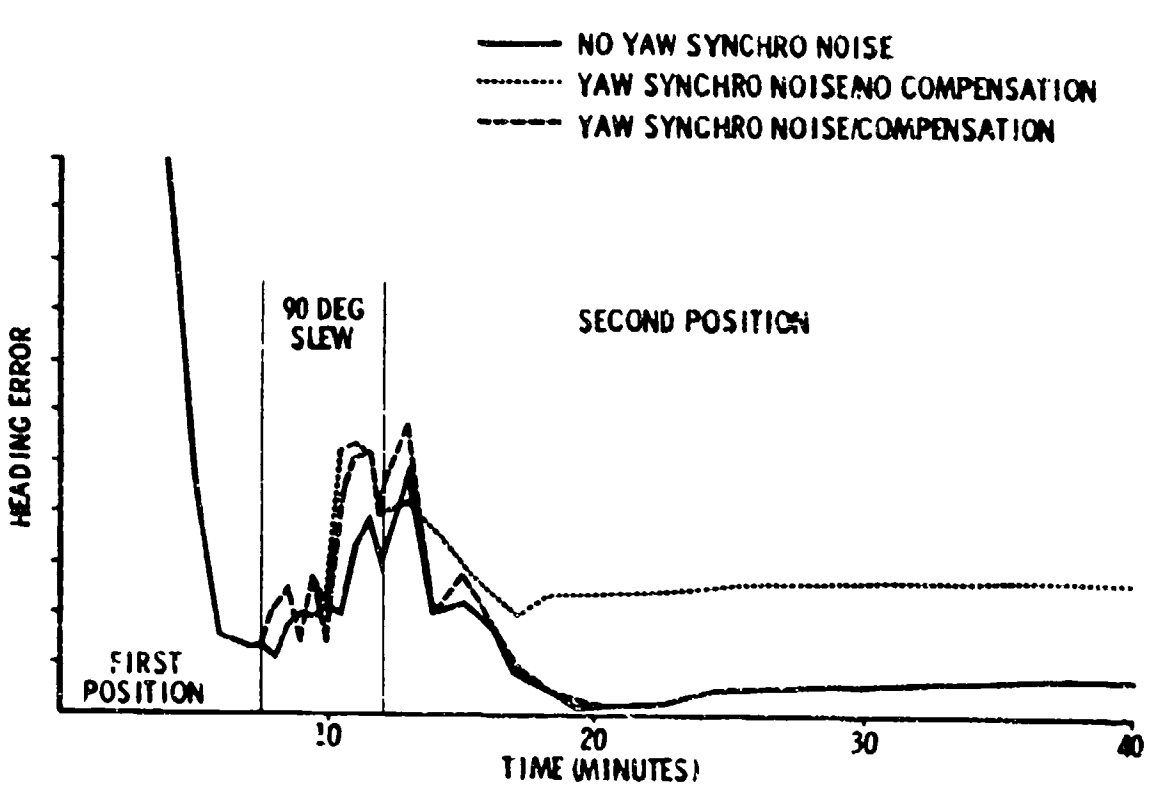

FIG. 23 SIMULATED HEADING ERROR

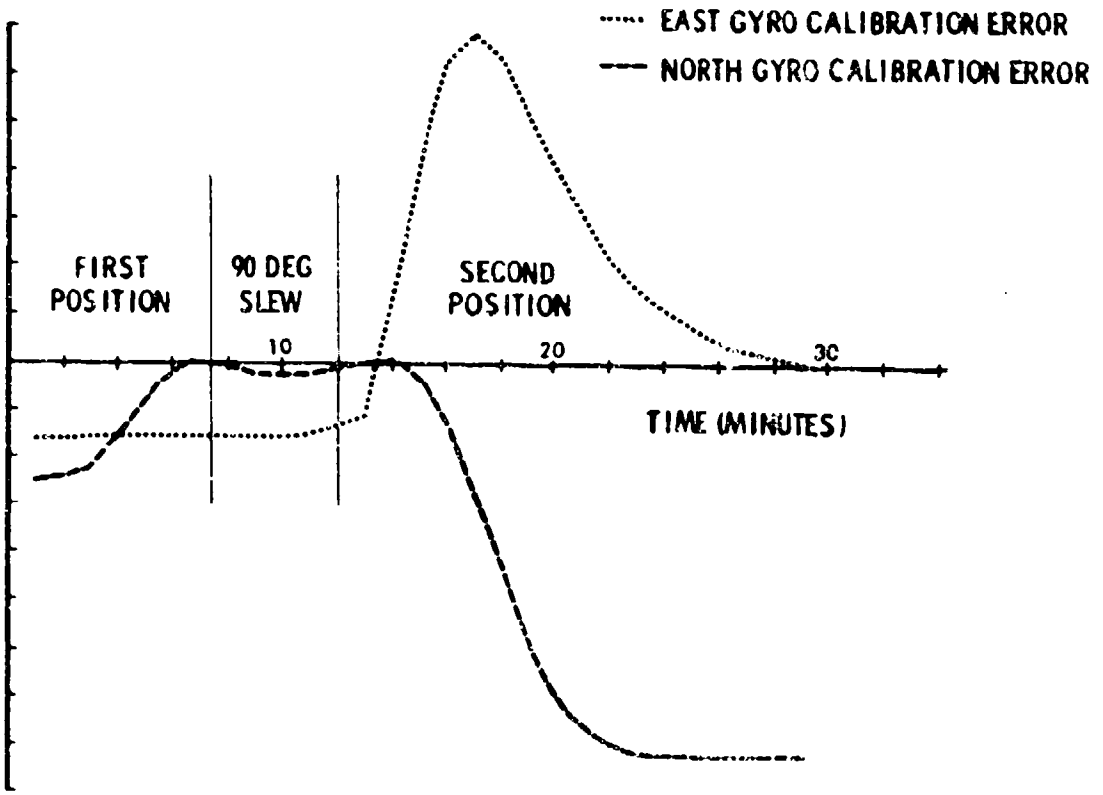

FIG. 24 REAL SYSTEM GYRO CALIBRATION ERRORS

EXPERIENCES IN FLIGHT TESTING HYBRID NAVIGATION SYSTEMS

Dr. Heinz Winter
Deutsche Forschungs- und Versuchsanstalt
für Luft- und Raumfahrt e.V. (DFVLR)
Institut für Flugführung
33 Braunschweig, Germany

SUMMARY

This lecture describes the experiences gained at the DFVLR Braunschweig in

- error modeling for navigation sensors
- designing filters for hybrid navigation systems
- sensitivity analysis of these filters
- building up high precision reference systems for the flight tests
- flight testing hybrid navigation systems and
- evaluating the flight test results.

The navigation accuracies of Doppler-inertial and baro-inertial systems, derived from theoretical analysis and flight tests, are given.

1. INTRODUCTION

Inertial navigation systems (INS) of the present generation attain navigational accuracies with a positional error of less than 1 nautical mile after 1 hour of flight. These errors are, in general, increasing with time, so that in long-duration flights or in missions where very high navigational accuracy is required, the position and velocity accuracy of the INS alone is not sufficient to guarantee mission success. In these cases, the INS is aided with the help of additional navigation sensors such as Doppler radar, pressure altimeter, etc.

In this lecture the experiences gained at the DFVLR Braunschweig in designing and flight testing hybrid navigation systems are described. As examples, the conventional and the optimal aiding of the horizontal channels of an INS with a Doppler radar, and of the vertical channel with a pressure altimeter, are considered in detail.

2. FLIGHT-TEST ARRANGEMENT AND REFERENCE SYSTEM

The test flights are carried out with the HFB 320 aircraft of the DFVLR (see Figure 1), which has an LN3 inertial platform, a Honeywell H316 computer, a magnetic tape for data recording (5 times per second) (see Figure 2), a Doppler radar, a pressure altimeter, and different radio-navigation aids on board.

The test flights are, in general, carried out within the lock-in range of one or several tracking radars, to obtain the high precision required for the position and velocity reference. Figure 3 shows a typical flight path of the HFB 320 and the lock-in range (some 75 kilometers) of the MPS 36 radar equipment, located in Meppen, Germany. The corresponding velocities of the aircraft are shown in Figure 4, and the horizontal accelerations are shown in Figure 5. (The accelerations, velocities, and flight path have been measured by the unaided INS.)

The high-precision velocity and position measurements are obtained by off-line smoothing of the data obtained from the tracking radar with the help of the INS. The most appropriate form of the smoother, for the purpose of evaluating this data, is the optimal-smoothing algorithm developed by Rauch, Tung, and Striebel [1], which consists of a Kalman forward and backward filter.

The time-discrete model equations of the system to be smoothed are

$$x(k) = \Phi(k,k-1)\, x(k-1) + u(k-1)$$
$$y(k) = H(k)\, x(k) + v(k) \qquad (1)$$

where

$\Phi(k,k-1)$, $H(k)$ = transition and measurement matrices
$x(k)$, $y(k)$ = state and measurement vectors
$u(k)$, $v(k)$ = uncorrelated noise vectors with covariance matrices $Q(k)$ and $R(k)$.

The Kalman-forward-filter equations of the Rauch/Tung/Striebel algorithm are

$$\begin{aligned}
\hat{x}(k)^- &= \phi(k,k-1)\hat{x}(k-1)^+ \\
\hat{x}(k)^+ &= \hat{x}(k)^- + K(k)\,(y(k) - H(k)\hat{x}(k)^-) \\
P(k)^- &= \phi(k,k-1)P(k-1)^+\phi(k,k-1)^T + Q(k-1) \\
K(k) &= P(k)^-H(k)^T(H(k)P(k)^-H(k)^T + R(k))^{-1} \\
P(k)^+ &= (I - K(k)H(k))P(k)^{-1}
\end{aligned} \tag{2}$$

where

$P(k)^-$, $P(k)^+$ = covariance matrices of $(\hat{x}(k)^- - x(k))$ and $(\hat{x}(k)^+ - x(k))$

$\hat{x}(k)^-$, $\hat{x}(k)^+$ = filtered estimates of $x(k)$ immediately before and after measurement k

$K(k)$ = optimal gain of forward filter.

The backward-filter equations of the Rauch/Tung/Striebel algorithm are

$$\begin{aligned}
\hat{x}(k,N) &= \hat{x}(k)^+ + C(k)\,(\hat{x}(k+1, N) - \phi(k+1, k)\hat{x}(k)^+) \\
C(k) &= P(k)^+\,\phi(k+1, k)^T\,(P(k+1)^-)^{-1} \\
P(k,N) &= P(k)^+ + C(k)\,(P(k+1, N) - P(k+1)^-)C(k)^T
\end{aligned} \tag{3}$$

and are started with

$$\hat{x}(N,N) = \hat{x}(N)^+$$
$$P(N,N) = P(N)^+$$

where

N = total number of measurements

$\hat{x}(k,N)$ = smoothed estimate

$P(k,N)$ = error-covariance matrix of smoothed estimate

$C(k)$ = optimal gain of backward filter

The error model of the INS, which is described in Section 3.1, was combined with an uncorrelated-noise-type error of the radar measurement to obtain the reference-system error model. The result of a sensitivity analysis (see Section 4.1) of the velocity error of the forward filter is presented in Figure 6, showing a good correspondence between the actual error and the forward filter's self-diagnosis. This means that the filter is rather insensitive to the model simplifications described in Section 3.1. The precision of the reference position is illustrated in Figure 7 (filtered estimate) and Figure 8 (smoothed estimate). These figures show the high accuracy of the reference system, in that position errors are on the order of 10 meters and velocity errors are on the order of less than 0.1 meter per second. This accuracy is also obtained in flight periods where the radar has lost the target for several minutes [2].

3. ERROR MODELS OF THE SENSORS

3.1 Inertial Platform

The test aircraft, HFB 320, has an LN3 inertial platform on board. Figure 9 shows the position errors of the horizontal channels during a laboratory test run of the uncalibrated LN3. Figure 10 shows the corresponding acceleration and velocity errors: large Schuler as well as 24-hours oscillations are excited by the bias errors of the uncalibrated gyros and accelerometers. Theoretical analysis [3] and evaluation of laboratory tests (see Figures 9 and 10) lead to the error model for the LN3 given in equation (4). The elements of the state vector, x, are:

(1) Three misalignment angles, α, β, γ, about the east, north and vertical axes (local-level mechanization of the INS).

(2) Corresponding velocity errors, Δv_O, Δv_N, Δv_Z, in east, north, and vertical directions.

(3) Position errors, ΔL, Δl, Δh (latitude, longitude, and height errors).

In addition,

R = distance of aircraft from earth center

ω_E = earth rate (15 degrees/h)

L = latitude

Equation (1)

$$
\begin{bmatrix} \dot{\varepsilon} \\ \dot{\xi} \\ \dot{\gamma} \\ \Delta\dot{v}_O \\ \Delta\dot{v}_N \\ \Delta\dot{v}_Z \\ \Delta\dot{L} \\ \Delta\dot{l} \\ \Delta\dot{h} \end{bmatrix} =
\begin{bmatrix}
0 & \left(\frac{v_O}{R}\tan L + \omega_E \sin L\right) & -\left(\frac{v_O}{R} + \omega_E \cos L\right) & 0 & -\frac{1}{R} & 0 & 0 & 0 & \frac{v_N}{R^2} \\
-\left(\frac{v_O}{R}\tan L + \omega_E \sin L\right) & 0 & -\frac{v_N}{R} & \frac{1}{R} & 0 & 0 & -\omega_E \sin L & 0 & -\frac{v_O}{R^2} \\
\left(\frac{v_O}{R} + \omega_E \cos L\right) & \frac{v_N}{R} & 0 & \frac{\tan L}{R} & 0 & 0 & \left(\frac{v_O}{R\cos^2 L} + \omega_E \cos L\right) & 0 & -\frac{v_O}{R^2}\tan L \\
0 & -A_Z & A_N & \left(\frac{v_N}{R}\tan L - \frac{v_Z}{R}\right) & \left(2\omega_E \sin L + \frac{v_O}{R}\tan L\right) & \left(-2\omega_E \cos L - \frac{v_O}{R}\right) & \left(2\omega_E (v_N \cos L + v_Z \sin L) + \frac{v_O v_N}{R\cos^2 L}\right) & 0 & \left(\frac{-v_O v_N \tan L + v_O v_Z}{R^2}\right) \\
A_Z & 0 & -A_O & \left(-2\omega_E \sin L - \frac{2v_O}{R}\tan L\right) & -\frac{v_Z}{R} & -\frac{v_N}{R} & \left(-2\omega_E v_O \cos L - \frac{v_O^2}{R\cos^2 L}\right) & 0 & \left(\frac{v_O^2 \tan L + v_Z v_N}{R^2}\right) \\
-A_Y & A_O & 0 & \left(2\omega_E \cos L + \frac{2v_O}{R}\right) & \frac{2v_N}{R} & 0 & -2\omega_E v_O \sin L & 0 & -\left(\frac{v_O^2 + v_N^2}{R^2} - \frac{2g}{R_O}\right) \\
0 & 0 & 0 & 0 & \frac{1}{R} & 0 & 0 & 0 & -\frac{v_N}{R^2} \\
0 & 0 & 0 & \frac{1}{R\cos L} & 0 & 0 & \frac{v_O \sin L}{R\cos^2 L} & 0 & -\frac{v_O}{R^2 \cos L} \\
0 & 0 & 0 & 0 & 0 & 1 & 0 & 0 & 0
\end{bmatrix}
\cdot
\begin{bmatrix} \varepsilon \\ \xi \\ \gamma \\ \Delta v_O \\ \Delta v_N \\ \Delta v_Z \\ \Delta L \\ \Delta l \\ \Delta h \end{bmatrix}
+
\begin{bmatrix} d_x \\ d_y \\ d_z \\ a_x \\ a_y \\ a_z \\ 0 \\ 0 \\ 0 \end{bmatrix}
$$

$R = R_o + h$

h = height

v_O, v_N, v_Z = aircraft velocities

A_O, A_N, A_Z = accelerations measured by the INS

R_o = earth radius

g = 9.81 m/s^2

d_x, d_y, d_z, a_x, a_y, a_z = gyro drift rates and accelerometer errors in the three axes.

Neglecting the Foucault modulation, the coupling of the 24-hour oscillation, and the acceleration coefficients given in equation (4), one obtains the simplified error model of the LN3 shown in Figure 11. With these simplifications, the horizontal channels are nearly decoupled from each other and have a very similar error behaviour. The instability of the vertical channel, which is completely decoupled from the horizontal channels in this simplified model, is clearly visible. Figure 12 shows the position errors of the north/south channel excited by several typical alignment and sensor errors. Figure 13 illustrates the instability of the vertical channel. For most applications, the simplified error model shown in Figure 11 is sufficiently accurate.

3.2 Doppler radar

Figure 14 shows a comparison of the horizontal aircraft velocities measured by the well-calibrated and aligned LN3, and by the Doppler radar of the HFB 320: the correlation time of the Doppler radar errors is on the order of a few seconds, so that the assumption of an uncorrelated Doppler error is justified for the sampling interval of 10 seconds, which has been chosen for the Doppler aiding of the INS.

3.3 Pressure altimeter

Assuming a known distribution of air temperature with height, the barometric height can be calculated directly from the measured static pressure, p. The best known relation between height and pressure is the barometric-height formula

$$HB = -8000 \cdot \ln (p/p_o) \quad [m] \; . \tag{5}$$

p_o is the static pressure at sea level which must be known for the determination of the barometric height. The relation given in Eq. (5) is, however, not sufficiently accurate for practical purposes, as it rests on the assumption of a constant air temperature (0°C). A number of "standard atmospheres" have been used at various times. For our test flight, the formula used to calculate the height from the pressure was

$$HB = (a_3 p^3 + a_2 p^2 + a_1 p + a_o) + D \; . \tag{6}$$

a_o, a_1, a_2 and a_3 are coefficients obtained empirically. The parameter, D, is determined before the start, so that at the measured static pressure, HB is the correct height at the start.

The deviations of the real from the standard atmosphere are due to the weather. As an example, Figure 15 shows the altitude variations with time of three pressure levels measured at Hannover airport. To determine the influence of the weather on the barometric measurement in an analysis of errors, we shall start from the following representation of the atmosphere: the atmosphere does not change during the test flight time (1 to 2 hours). In the range of the test flight (some 100 kilometers around the place of start), the inclination of the isobaric surface planes to the horizontal remains the same. The height error at the place of start is a linear function of the height. These assumptions are certainly not very rigorous, but they present a good first approximation to the reality (the model can easily be made more accurate by assuming second order terms and a time dependence, this however requires more computation). If an aircraft flies with east, north, and vertical velocities, v_O, v_N and v_Z through this static atmosphere, then the barometric height shall be wrongly measured by the amount ΔHB_1.

$$\frac{d}{dt} (\Delta HB_1) = \varepsilon_O v_O + \varepsilon_N v_N + \varepsilon_Z v_Z \; . \tag{7}$$

ε_O and ε_N are the inclinations of the pressure surfaces [m/m], and ε_Z is the proportionality factor [m/m] between the height error at the place of start and the height.

The extreme values for ε_O, ε_N and ε_Z can be obtained from the weather charts

$$\varepsilon_O, \varepsilon_N \leq 10^{-3} \quad [m/m]$$
$$\varepsilon_Z \leq 3 \cdot 10^{-2} \quad [m/m] \; .$$

The accuracy with which the static pressure can be measured in an aircraft depends

on the place in which the sensor is positioned. This error has been measured for the HFB 320 with which we carried out our test flight and is shown in Figure 16. The linear approximation has been used for the consideration of errors.

$$\Delta HB_2 = \epsilon_F v \qquad (8)$$
$$\epsilon_F = -0.67 \quad \text{from Figure 16 .}$$

ϵ_F denotes the proportionality factor between the velocity, v, and the error, ΔHB_2. The remaining errors of the barometric height measurement, which, in comparison to the two previously mentioned errors are small, are neglected in the error analysis.

The complete error model for the pressure altimeter (see Eq. (7) and (8)) is presented in Figure 17. WR_B is an additional uncorrelated error.

4. HYBRID NAVIGATION SYSTEMS

4.1 Kalman filtering and sensitivity analysis

Figure 18 shows a schematic block diagram of a hybrid navigation system as it will be considered in following sections; the navigational information delivered by the INS is compared with an additional sensor, such as a Doppler radar, or a pressure altimeter. The difference of both, the "measurement", is fed into a Kalman filter which estimates the errors of the INS and the additional sensor. These errors can be corrected on-line with the help of a suitable controller. Our experiences have shown that in the case of a time-discrete estimator with 10 second sampling period the controller can simply be a constant-feedback matrix Γ^*, chosen in such a way that the estimated errors of the sensors are driven to zero in the sampling period after the measurement. The reason for this is that the low-frequency error behavior of the INS makes the estimation process slow, so that the non-optimal controller practically does not influence the estimation accuracy and the time required to identify the errors.

A major problem is encountered when one attempts to implement these techniques. The model for an exact description of the hybrid system may either be too complex for a computer of reasonable size, or the model is not yet known exactly to the design engineer. For example, the statistical parameters characterizing the random sensor errors (e.g., gyro drift rates) are rarely known exactly.

The solution to this problem can be to design a suboptimal filter of smaller size, one that represents the most important system aspects and neglects minor effects on the navigation accuracy. The suboptimal filter is often less sensitive to inexact implementation of parameters. However, in any case, navigation accuracy is lost when the optimal filter is replaced by a suboptimal one.

The actual estimation errors for a suboptimal filter cannot be calculated by solving the Riccati equation, because this equation is based on the assumption that there is no difference between the model used in the filter and the real world. A set of equations describing the actual estimation error covariance matrix of filtering algorithms in the case of inexact modeling has been given by R.E. Griffin and A.P. Sage [4].

The N-dimensional error model of the hybrid navigation system, containing all known error sources and all couplings, and representing the design engineer's best knowledge of the system errors, is called "real world" in the following sections, and is described by

$$\begin{aligned} \dot{x} &= F\,x + c + G\,u \quad \text{(N-dimensional system)} \\ y &= H\,x + v \quad . \end{aligned} \qquad (9)$$

F, G and H are constant matrices; and u and v are white-noise vectors, uncorrelated with each other. The vector c represents the error-correction inputs, obtained by multiplying the estimated state vector, $\hat{x}$, with the control matrix, Γ^*.

The measurement vector is fed into the suboptimal Kalman filter of dimension M ($M \leq N$) with the well-known structure described by

$$\begin{aligned} \dot{\hat{x}} &= F^* \hat{x} + c + K^* (y - H^* \hat{x}) \\ K^* &= P^* H^{*T} R^{*-1} \\ \dot{P}^* &= F^* P^* + P^* F^{*T} + G^* Q^* G^{*T} - P^* H^{*T} R^{*-1} H^* P^* \end{aligned} \qquad (10)$$

The starred matrices, F^*, G^*, and H^*, are the system matrices of the M-dimensional representation of the hybrid system errors in the filter. The matrices P^*, Q^* and R^* are defined by

$$P^* = E\,(\tilde{x}^*\,\tilde{x}^{*T})$$
$$R^*\,\delta(t-\tau) = E\,(v^*(t)\,v^{*T}(\tau))$$
$$Q^*\,\delta(t-\tau) = E\,(u^*(t)\,u^{*T}(\tau))$$

where

$E(\ldots)$ = expected value

$\delta(t)$ = delta function

$\tilde{x}^*$ = error in the estimate (calculated under the assumption that no discrepancy between the real world and the model system exists)

v^* and u^* = white-noise inputs of the model system.

The covariance matrix, P^*, of the estimation error, $\tilde{x}^*$, may be regarded as giving the self-diagnosis of the filter.

This situation is illustrated in Figure 19, which shows the closed loop of the hybrid navigation system: the real-world model representing the sensor errors, the Kalman filter, based on the simplified error model of these sensors, and the controller, Γ^*, for the correction of the estimated errors.

If the error model used in the filter is incorrect or incomplete, the actual estimation-error covariance matrix is no longer described by the Riccati equation (see Eq. (10)). A set of matrix equations describing the time propagation of the actual estimation-error covariance matrix, P_a, the covariance matrix, P_x, of the actual state vector, and the cross-covariance matrix, P_c, between the actual state and the error in the estimate has been derived in [4] for discrete filters. These equations had to be modified to include the effect of the feedback matrix, Γ^*. The following continuous set of matrix equations is obtained

$$\begin{aligned}
\dot{P}_a &= (F^* - K^*H^*)\,P_a + P_a\,(F^* - K^*H^*)^T \\
&\quad + (\Delta F - K^*\Delta H)\,P_c + P_c^T\,(\Delta F - K^*\Delta H)^T \\
&\quad + K^*RK^{*T} + GQG^T \\
\dot{P}_c &= \Gamma^*P_a + (F+\Gamma^*)\,P_c + P_c\,(F^* - K^*H^*)^T \\
&\quad + P_x\,(\Delta F - K^*\Delta H)^T - GQG^T \\
\dot{P}_x &= \Gamma^*P_c^T + P_c\,\Gamma^{*T} + (F+\Gamma^*)P_x \\
&\quad + P_x(F+\Gamma^*)^T + GQG^T
\end{aligned} \tag{11}$$

where

$$\begin{aligned}
P_a &= E\,((\hat{x} - x)\,(\hat{x} - x)^T) \\
P_c &= E\,(x\,(\hat{x} - x)^T) \\
P_x &= E\,(xx^T) \\
\Delta F &= F^* - F \\
\Delta H &= H^* - H \qquad (E \text{ is the expected value})
\end{aligned}$$

The starred matrices refer to the model system which is the basis for the filter, and the unstarred matrices refer to the real-world system describing the actual sensor errors. If the model state vector, x^*, contains fewer elements than the real-world state vector, x, a linear relationship must exist between the two state vectors

$$x^* = Sx$$

where S is a nonsquare matrix. The starred matrices in Eq. (11) have to be transformed, to be compatible in terms of their dimension with the unstarred matrices, for example

$$F^* \rightarrow S^TF^*S$$

For a one-dimensional real world and a one-dimensional filter, Eq. (11) can be represented in a block diagram as shown in Figure 20. The block in broken lines describes the estimation error covariance propagation for an estimator with the same structure as the Kalman filter, but with arbitrary (not optimal) gains, K^*.

If there are no modeling errors ($\Delta F = \Delta H = 0$), the three dynamic systems describing the time histories of P_a, P_c and P_x are only coupled by the feedback-matrix, Γ^*, and in open-loop operation they are completely uncoupled. If ΔF or ΔH are different from zero, the covariance of the actual state, P_x, excites the dynamic system which describes the time propagation of P_c, and the cross-covariance, P_c, excites the dynamic system of P_a, via $\Delta F - K^*\Delta H$.

The computations for the design of the navigation filters described in the following sections have been carried out with the time-discrete versions of Eq. (10) and (11) with a sample interval of 10 seconds.

4.2 Horizontal Channels

4.2.1 Conventional Doppler INS

The conventional Doppler aiding of the INS consists of feeding the differences between the INS velocities and the Doppler velocities back into the INS to correct the platform attitude and velocity.

In-flight leveling

Figure 21 shows the error diagram of the conventional second-order leveling loop. The Schuler oscillations are damped and their frequency is augmented: the leveling loop is N-times Schuler tuned and, in general, critically damped. The noise content of the Doppler velocity measurements is also fed back into the INS and causes additional errors, the magnitude of which depends on the gain constants N and k_1.

In-flight gyrocompassing

Figure 22 shows the error diagram of a third-order gyrocompassing loop. In addition to the leveling loop in Figure 21, the difference in the measured north velocity is also fed back to the vertical gyro torquer to correct the azimuth misalignment of the INS. This third order loop has to be laid out in such a way that the errors in the INS, caused by the Doppler noise, can still be tolerated, and that the alignment is time-optimal.

4.2.2 Optimal Doppler INS

A Kalman filter is designed on the basis of the sensor-error models, described in Sections 3.1 and 3.2. For the implementation in the on-board computer, the error model of the LN3 (Eq. (4)) is simplified corresponding to Figure 11. Figure 23 shows the position error computed with the real-world model of the LN3 (Eq. (4)) for a 3-hour flight in the north/south channel as curve ①. The platform is aligned to 20 arcseconds (1σ) in the level axes and to 3 arcminutes (1σ) in the azimuth. The gyro-drift rates are 0.01 degree per hour and the accelerometer biases are 10^{-4} g. The curve ② in Figure 23 shows the position error of the filter model (Figure 11), which also neglects the gyro-drift rates and the accelerometer biases. In this model, it is assumed that the alignment errors are the main error sources.

To make the filter for the Doppler INS less sensitive to the model simplifications, the Doppler noise in the model was assumed to be three times as high as it is in reality: 3 meters per second (1σ). No process noise (gyro or accelerometer noise) was assumed in the filter. Figure 24 shows the actual north/south position error of this hybrid system and compares it with the filter's self-diagnosis. After 1 hour the actual error increases more and more due to the model simplifications. This also becomes obvious in Figure 25, which shows the corresponding velocity errors. The model simplifications also cause an increase in the velocity-estimation error. Curve ④ in Figure 25 shows the steady-state error of a 20-times-Schuler-tuned and critically damped leveling loop. The actual error of the optimal system becomes even greater than the error of the conventional mechanization after 2 hours of flight time with this filter. The effect of decreasing the sensibility of this filter to model errors is illustrated in Figure 26: Curves ①, ②, and ③ of this figure show the high dynamics of the gains of the sensitive filter. The addition of an artificial process noise (gyro and accelerometer noise) makes the dynamics disappear and the filter less sensitive to the model simplifications (Curve ④ of Figure 26). The navigation errors obtained with this insensitive filter are illustrated in Figures 27 and 28. These figures show a good correspondence between the filter's self-diagnosis and the actual errors. The position errors of few hundred meters after 1 or 2 hours of flight time have been well confirmed by comparing the flight-test results to the measurements of the reference system described in Section 2.

4.3 Vertical channel

4.3.1 Conventional baro-INS

The conventional aiding of the vertical channel of the platform is shown in Figure 29. The difference between the inertial height, Hi, and the barometric height, HB, is fed back through the gain factors, K_1 and K_2, for the correction of the vertical velocity and height. The factors K_1 and K_2 are chosen so that the control system (second-order) shows a reasonable transient behavior and that the inertial height follows the barometric height well. For the test flights, K_1 and K_2 were chosen such that $K_1 = 2/T$ and $K_2 = 1/T^2$ with T = 30 seconds; that is, the two poles of the control system were identical. As a result of this soft coupling, the inertial height follows long-term alterations of the barometric height, but smoothes out its short-term fluctuations (see Figure 30).

An accelerometer bias, a_z, in this process produces steady velocity and height errors such as

$$\Delta v_z \approx 2Ta_z$$
$$\Delta Hi \approx T^2 a_z$$

For $a_z = 10^{-4}$ g, the errors for T = 30 seconds show $\Delta Hi \approx 1$ meter and $\Delta v_z \approx 0.06$ meter per second. The mixing process has the drawback that the indicated height (baro-inertial height) still has the same low-frequency errors, especially those dependent upon the weather and sensor position.

4.3.2 Optimal baro-INS

The use of a Kalman filter in aiding the vertical channel of the platform makes it possible to create the optimum combination of inertial and barometric height by considering the errors in each kind of information. The filter can be arranged so that it also corrects, in the optimum manner, the vertical velocity and acceleration (see Figure 31). The basis for the Kalman filter is an eight-dimensional error model for the sensors (platform and barometric height meter). This error model is shown in Figure 32. Part ① of Figure 32 shows the error model for the vertical channel of the platform. The gravity correction is no longer calculated with the inertial height, Hi, but with the barometric height, HB. In this manner, the positive feedback of an inertial height error onto acceleration is avoided. Part ② of Figure 32 shows the error model for the barometric height measurement. In addition an additive uncorrelated error (white noise, WR_B) is assumed. Part ③ of Figure 32 describes the error in the measurement of the aircraft's height by a ground-based target-following radar giving white noise, WR_R (the measured quantities Z_1 or Z_2 are the differences between the inertial, barometric, and radar height of the aircraft).

The following two configurations are considered:

(1) The baro-inertial system that is the optimum combination of the platform with the barometric height meter.

(2) The baro-inertial radar system that is the optimum combination of the platform with the barometric height meter and the ground-based radar(reference system; see Figure 33).

The operation of the Kalman filter in the baro-inertial system is illustrated in Figure 31. The difference between the inertial and barometric height is fed into the Kalman filter. The filter then estimates the errors of the two heights on the basis of the model shown in Figure 32, and computes the correction signals for the vertical acceleration and velocity as well as for the barometric height.

In the analysis of the test flights, a time-discrete filter algorithm is used. Every 10 seconds a Kalman filter iteration takes place, and the vertical acceleration, velocity, and barometric height are corrected. The results are presented in the following.

Part of the test flights of the HFB 320 had been tracked by the target-following radar. The radar installation measures both the distance to the aircraft, and the elevation angle. From these two measurements, after considering the corrections required by the refraction of the radar beam, the height of the aircraft above sea level can be calculated. The optimum mix of inertial, barometric, and radar heights is used as the reference height profile. This combination is made with a Kalman filter based on the full model shown in Figure 32.

An example of this is shown in Figure 34. Curve ① shows the height profile of the flight obtained by the conventional mixing of the vertical channel with the barometric height. Similarly, Curve ② shows the radar measurements. The difference of height is some 150 meters. It is illustrated again on a magnified scale in Figure 35 together with the range of the aircraft from the radar. The uncorrelated noise, which arises from measurements of the elevation angle can be clearly recognized. The measurement of distance is accurate up to a few meters. A bias error in the elevation angle would lead to a height error proportional to the distance; such an error cannot be detected.

The standard deviations (1σ values) of the heigt errors and the errors of the vertical velocity are calculated using the data of a typical test flight and the error model. It is assumed here that the parameters ε_0, ε_N, and ε_F of the model shown in Figure 32 are not known. The Kalman filter estimates them with the help of the sensors.

Figure 36 shows the accuracy of the altitude measurement of the reference system (Curve ①) which consists of the radar, the LN3, and the barometer. Curve ② shows the accuracy obtained by the optimal mixing of LN3 and barometer. Curve ③ is the 1σ error of the pressure altimeter for the flight considered.

The error of the vertical velocity from the baro-inertial system is shown in Figure 37. Accuracy depends on the strength of the acceleration noise of the INS: at 10^{-3} g (1σ) the velocity error is about 0.4 meter per second (1σ); at 10^{-4} g it is about 0.1 meter per second (1σ). The analysis of the baro-inertial radar system has shown that the accuracy of the vertical velocity is not improved by the addition of the ground-based radar system. The velocity error is determined by the quality of the platform (see Figure 37). In Figure 38 the reference altitude profile is plotted, and the altitude

established by mixing the platform with the barometric height meter, and the radar height. It can be seen that the high noise content of the radar height has been filtered out.

The flight tests have shown that with conventional mixing of the inertial height with the barometric height, the high-frequency errors (noise) of the barometric height measurements are smoothed out, but the considerable error caused by the weather, some 100 meters (1σ), and by the wrong measurement of the static pressure, some 70 meters (1σ), remain unchanged. If the two forms of height information (inertial and barometric) are combined by means of a Kalman filter, then the good short-term accuracy of the vertical channel of the platform can also be used to correct, to a great extent, the low-frequency errors. The accuracy with which this is possible depends on the quality of the platform used. In the case of a platform of inertial quality (LN3), while making the most unfavorable assumptions about the weather and pressure-measurement errors, the height error can be reduced to less than 50 meters (1σ). If the weather parameters, ε_O, ε_N, and ε_Z, have been obtained from the weather charts and the parameter, ε_P, from a calibration curve then using the Kalman filter for the correction of these errors, the height error can be reduced to some 10 to 15 meters (1σ).

The reference height generated using a Kalman filter with optimum mixing of the barometric and inertial heights, with the height as measured by ground-based target-following radar, has an error which is less than 10 meters (1σ).

The vertical velocity can be measured by means of optimum mixing of the inertial with the barometric height, with an accuracy of up to 0.1 meter per second (1σ). This accuracy cannot be increased by including the measurements from the target-following radar.

These comments apply naturally only to flight profiles comparable to those considered here, i.e., a range of some 100 kilometers, flight height of some 6000 meters, and a velocity of some 100 meters per second.

5. CONCLUSIONS

Aiding the INS with a Doppler radar and a pressure altimeter is a means to considerably improve the position and velocity accuracy. For the evaluation of flight tests, a high-precision reference system is required, which has been realized at the DFVLR, Braunschweig, by smoothing the data of a tracking radar with the help of the INS. Flight tests have demonstrated the high performance of the optimal hybrid navigation systems, and have shown that this navigational accuracy can be obtained with filters of reasonable size, if their sensitivity to the model simplifications is carefully analyzed and minimized.

6. REFERENCES

[1] Rauch, H.E., F. Tung, and C.T. Striebel, "Maximum Likelihood Estimates of Linear Dynamic Systems", AIAA Journal, Vol. 3, No. 8, S. 1445, 1965.

[2] Hurass, K., "Anwendung von optimaler Glättungstechnik bei der Erprobung von Navigationssystemen", DFVLR-Nachrichten, Heft. 17.

[3] Winter, H., and Fuerstenau, N., "Fehleranalyse für ein raumfestes, ein tangentiales und ein örtlich vertikales Trägheitsnavigationssystem", DFVLR-IB 153-75/15.

[4] Griffin, R.E., and Sage, A.P., "Sensitivity Analysis of Discrete Filtering and Smoothing Algorithms", AIAA Journal, Vol. 7, No. 10, Oct. 1969, pp. 1890-1897.

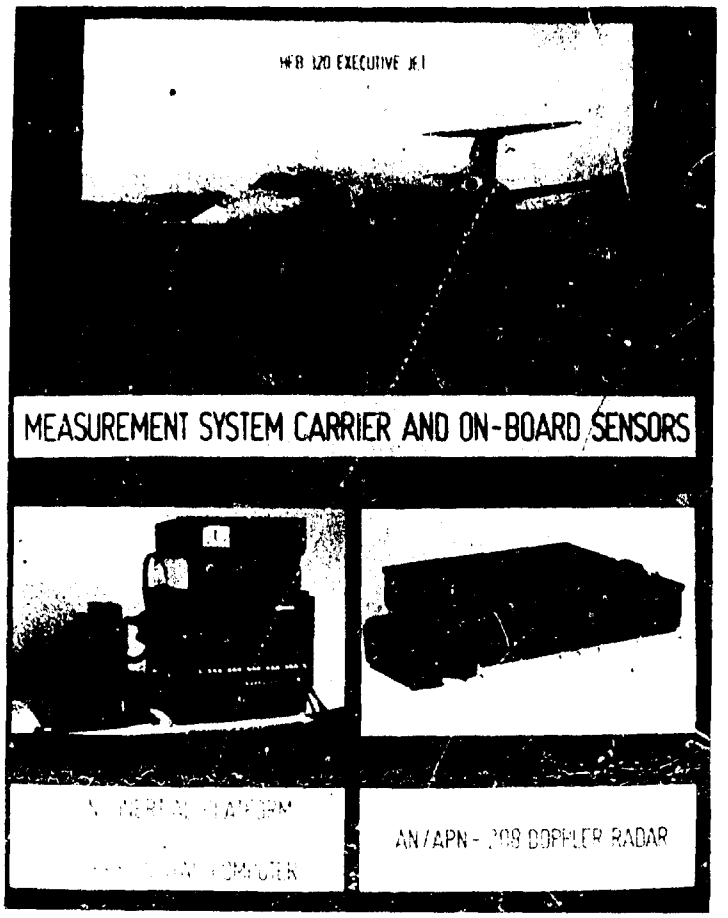

Fig. 1 Test aircraft, computer, inertial platform, and Doppler radar.

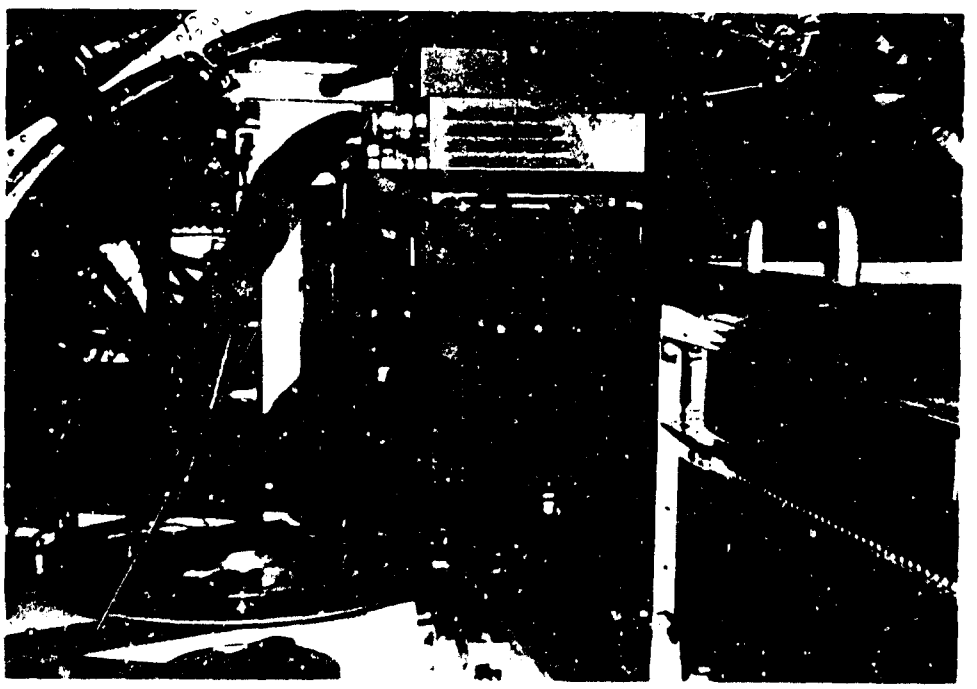

Fig. 2 On-board installation of the INS, the computer, and the magnetic-tape recorder.

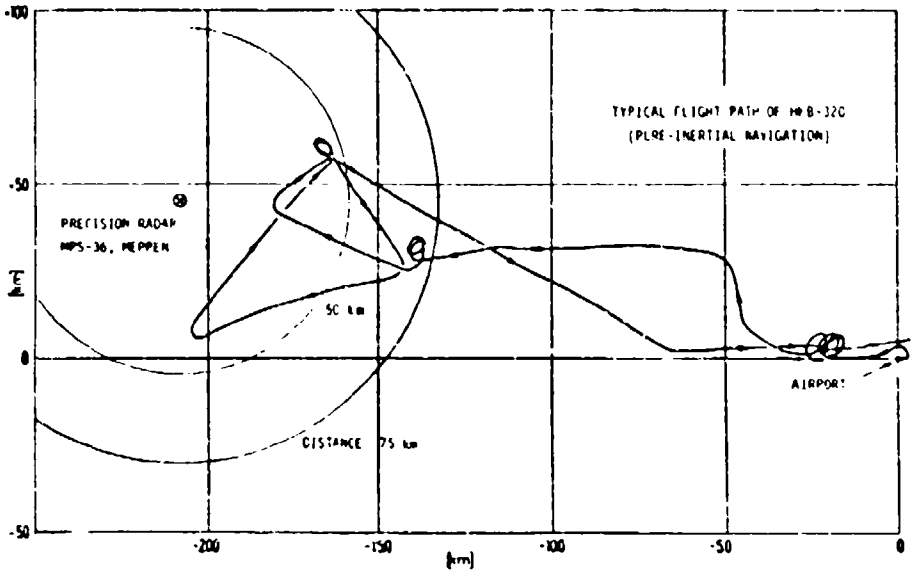

Fig. 3 Flight from Braunschweig airport to the tracking radar at Meppen, Germany.

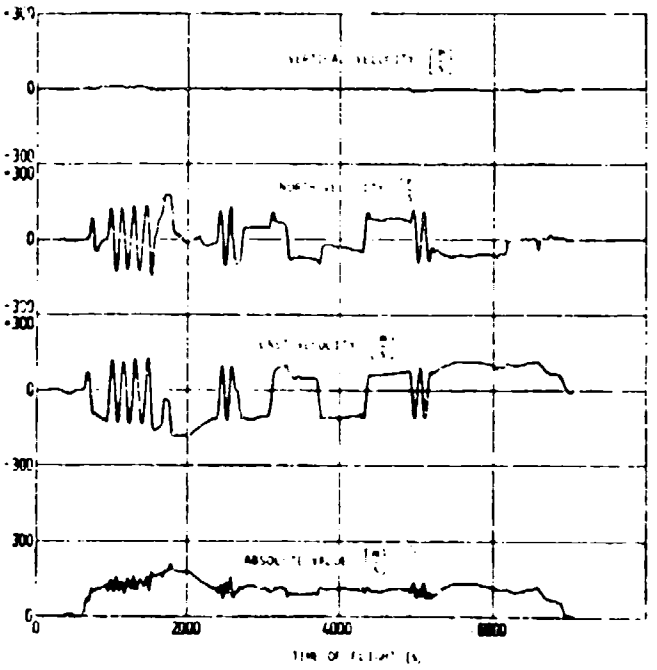

Fig. 4 Velocities measured by the INS during the flight shown in Fig. 3.

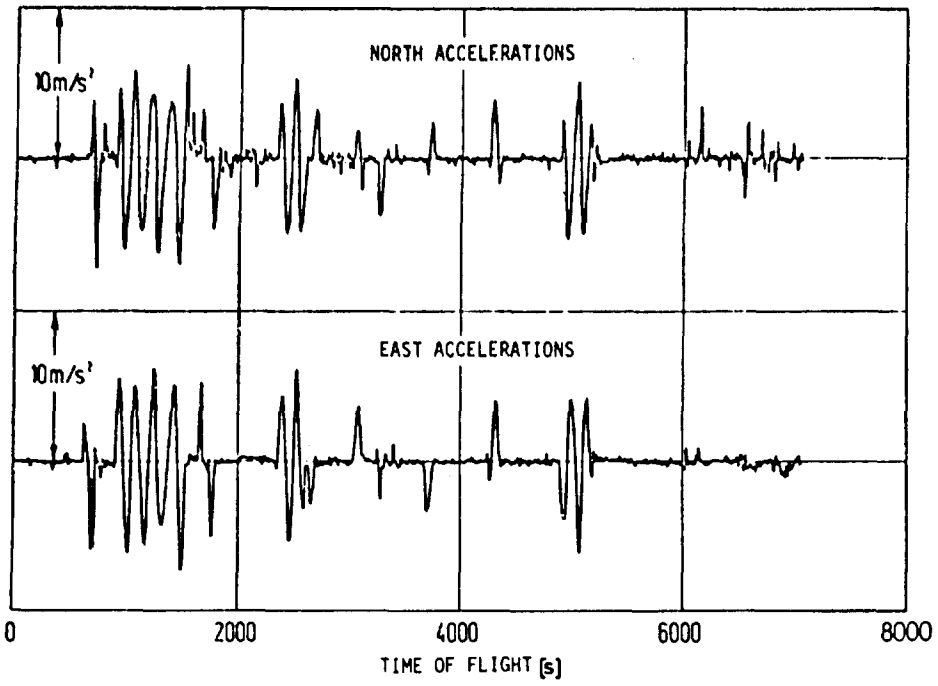

Fig. 5 Horizontal accelerations measured by the INS during the flight shown in Fig. 3.

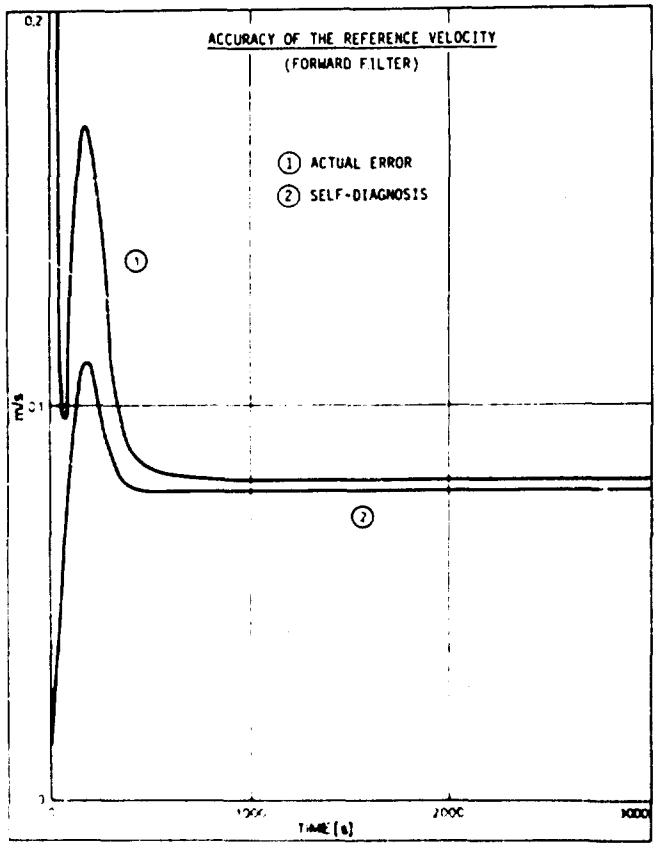

Fig. 6 Sensitivity analysis for the reference system forward filter (Effect of model simplifications on the velocity accuracy).

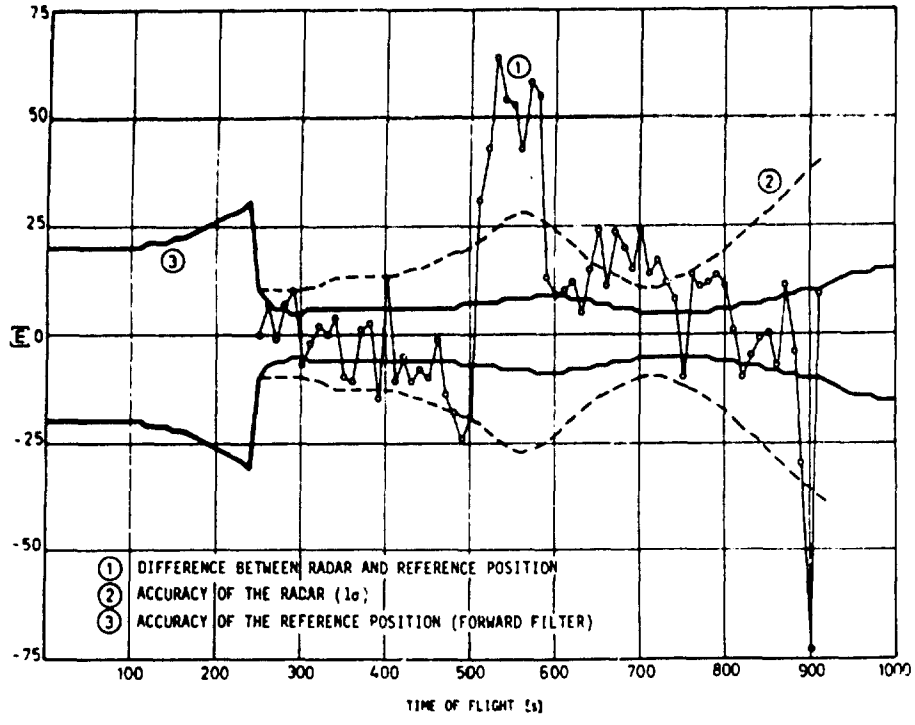

Fig. 7 Position-measuring accuracy of the reference system (forward filter).

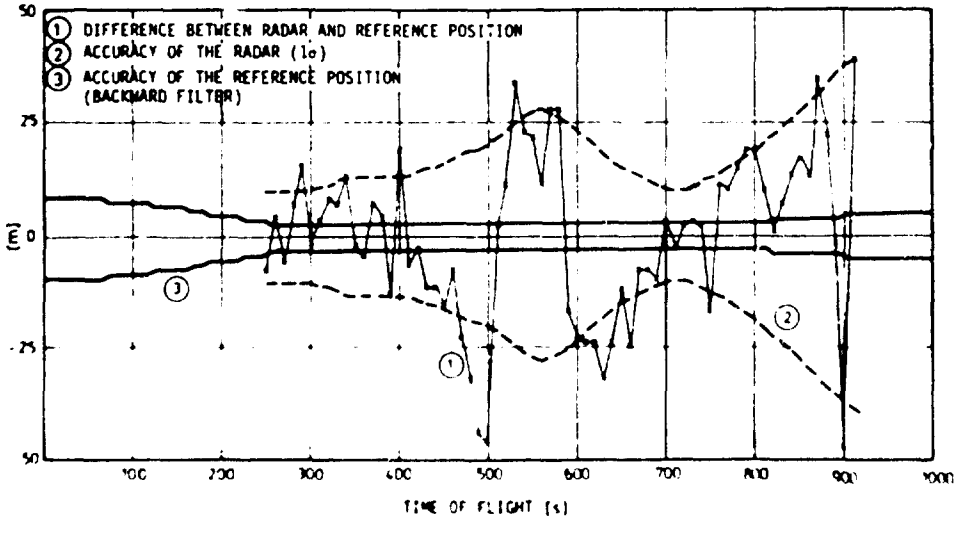

Fig. 8 Position-measuring accuracy of the reference system (smoothed estimate).

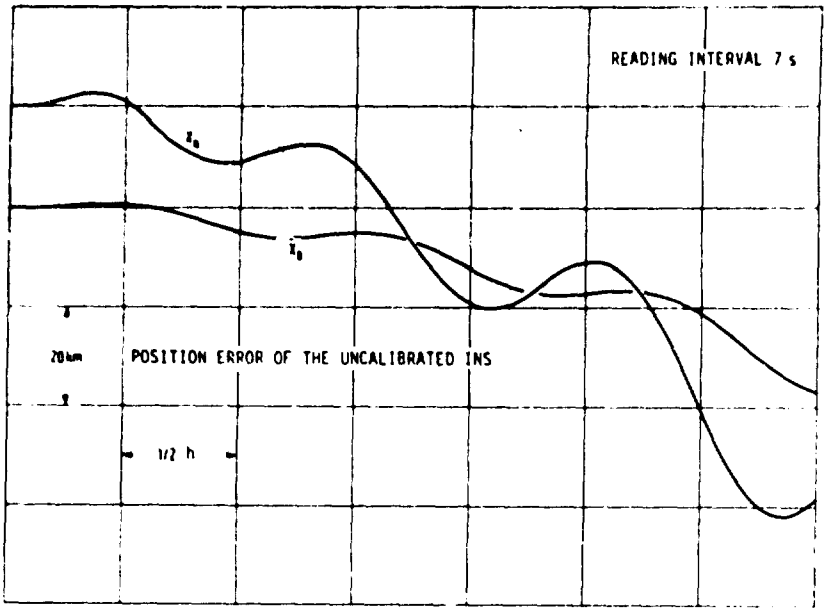

Fig. 9 Position errors in the horizontal channels of the uncalibrated LN3 platform during a laboratory test run.

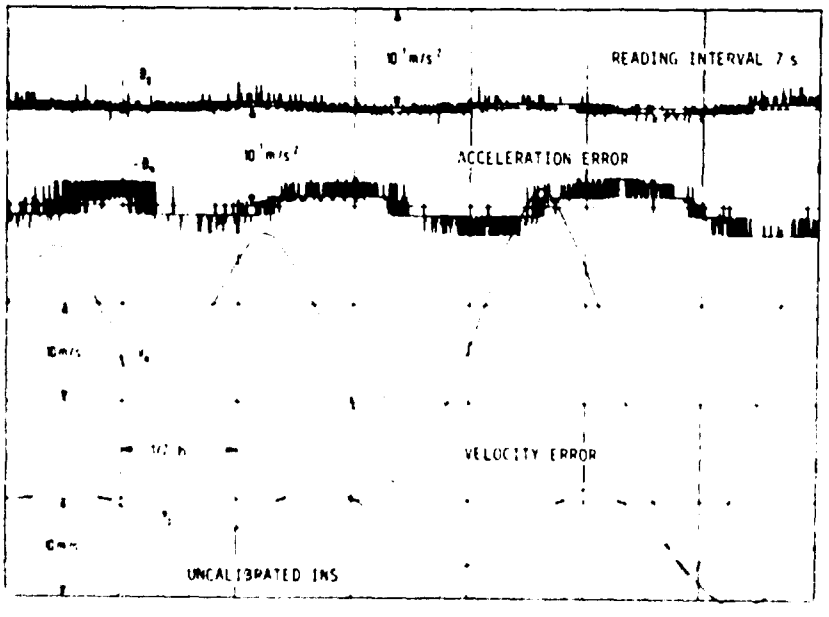

Fig. 10 Acceleration and velocity errors of the uncalibrated LN3 platform, corresponding to Fig. 9.

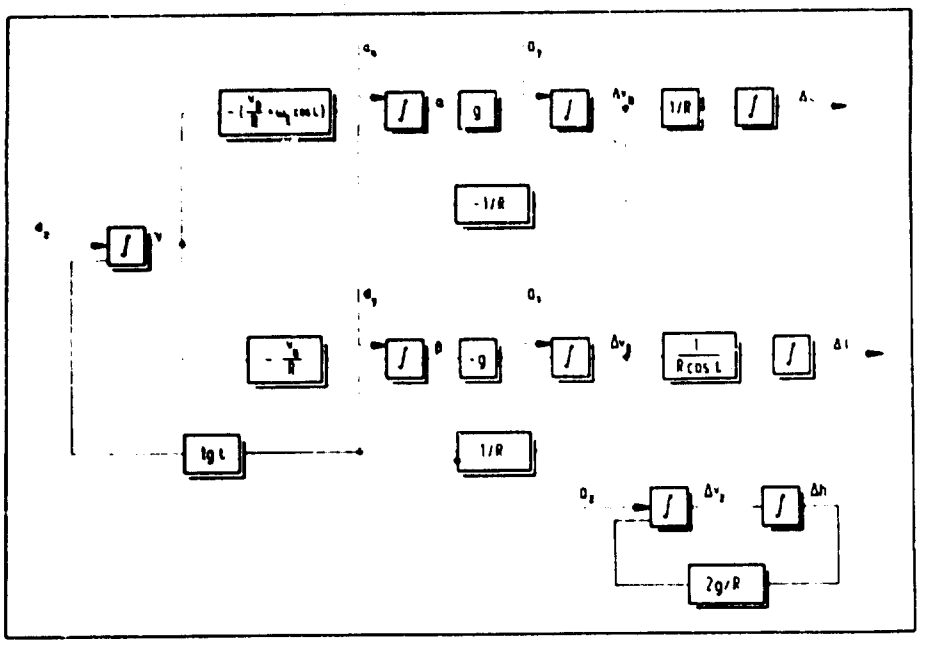

Fig. 11 Simplified error model for the LN3 inertial platform.

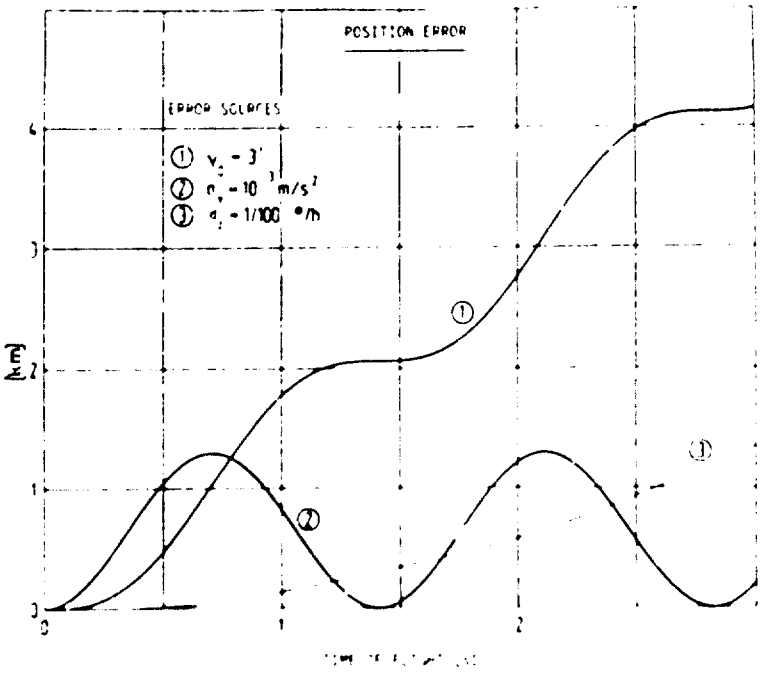

Fig. 12 Position errors in the north/south-channel of the INS, caused by azimuth misalignment, accelerometer bias, and azimuth gyro drift rate, computed with the error model in Fig. 11.

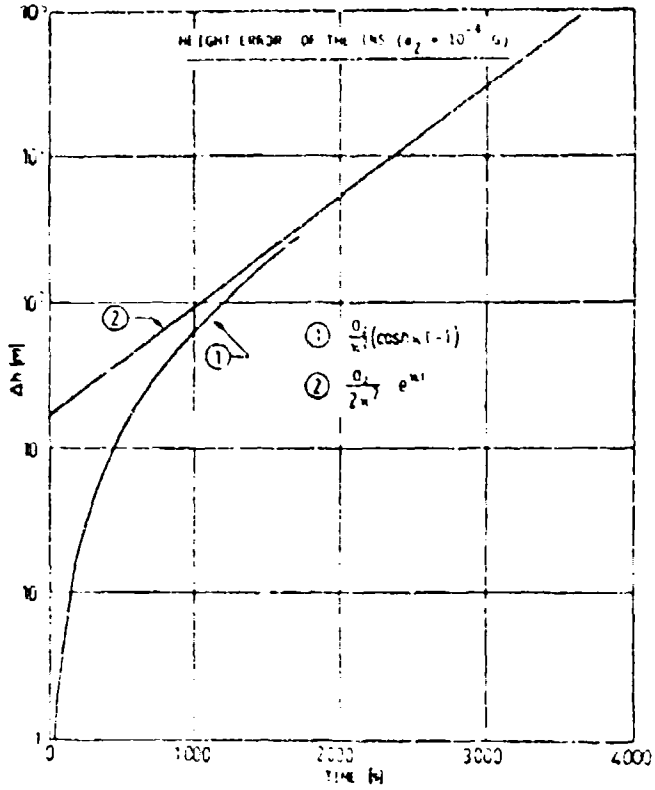

Fig. 13 Instability of the vertical channel of the INS. Time history of the height error and asymptotic exponential function.

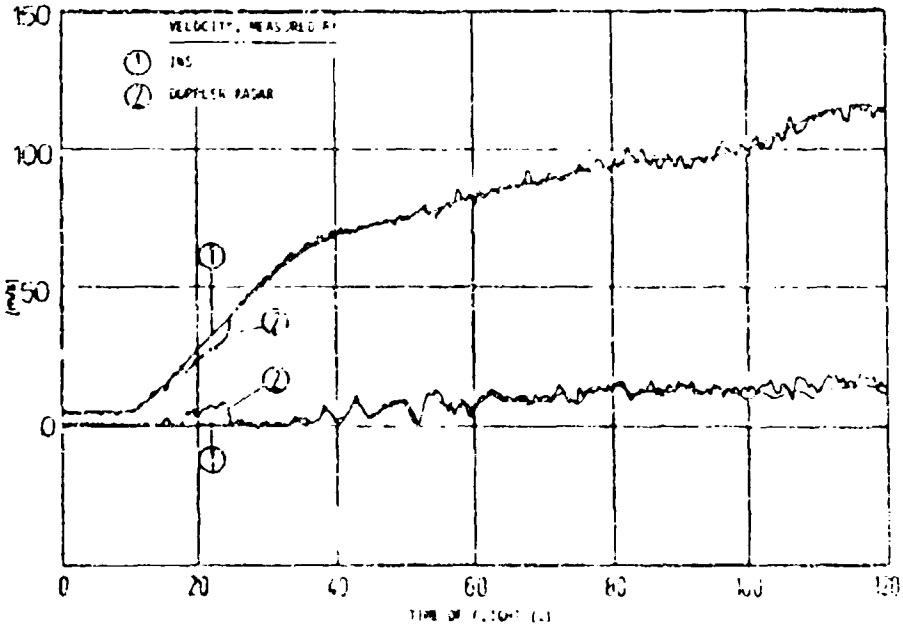

Fig. 14 Comparison of Doppler and INS velocities, showing a noise-type Doppler error.

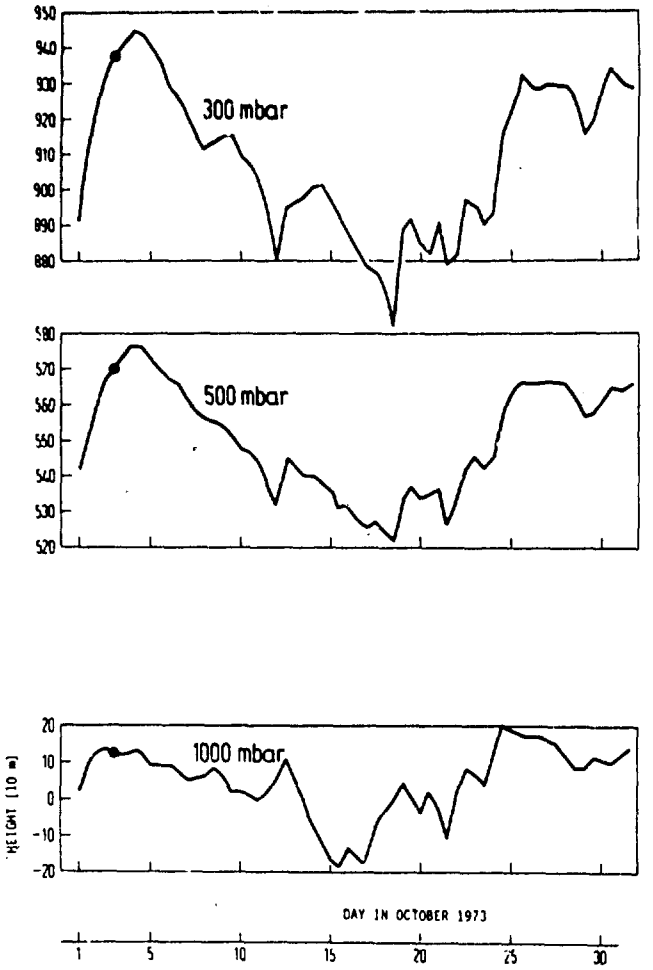

Fig. 15 Altitude variation of three atmospheric pressure levels within 1 month.

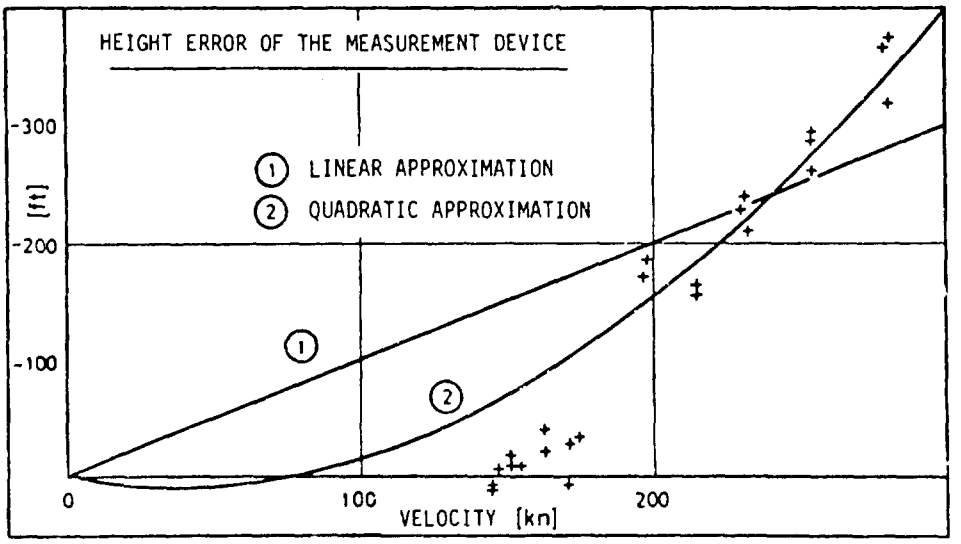

Fig. 16 Pressure altimeter error caused by errors in the static pressure measurement.

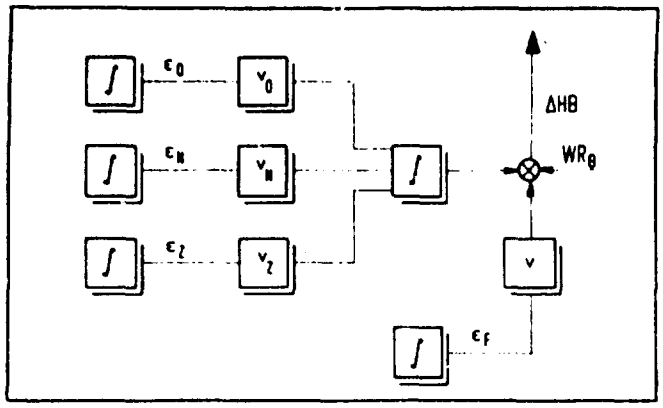

Fig. 17 Error model for the pressure altimeter.

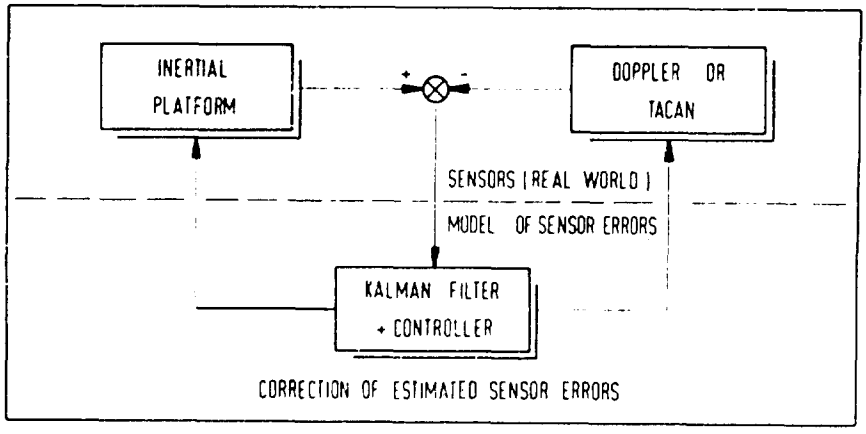

Fig. 18 Schematic diagram of the hybrid navigation system.

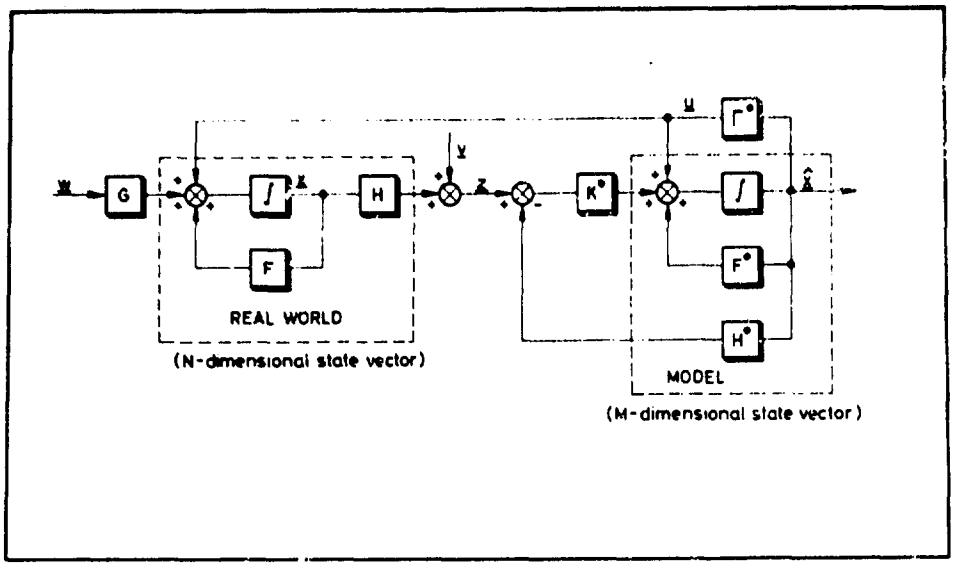

Fig. 19 Closed loop of the hybrid navigation system, with the real-word model describing the actual errors of the sensors and the suboptimal model of these errors in the Kalman filter.

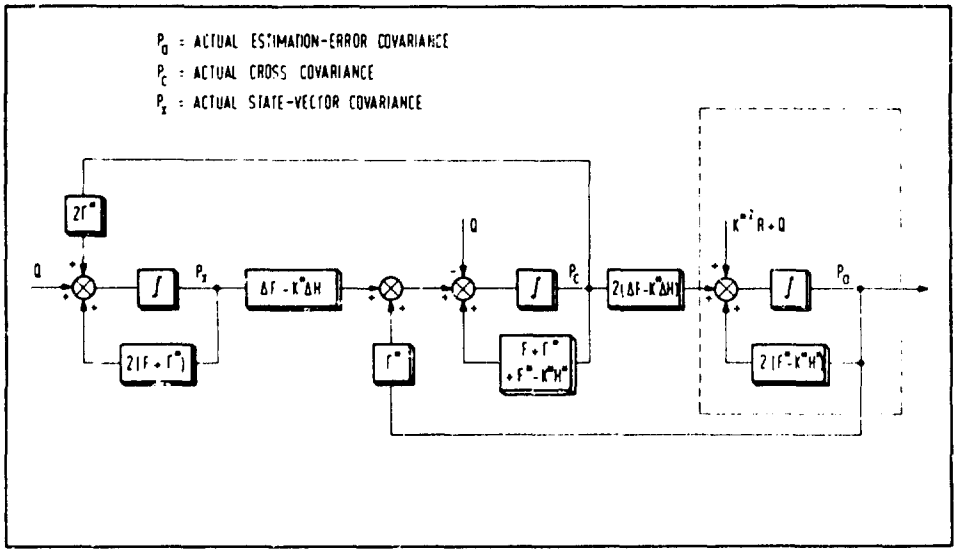

Fig. 20 Block diagram of the sensitivity equations for a one-dimensional system.

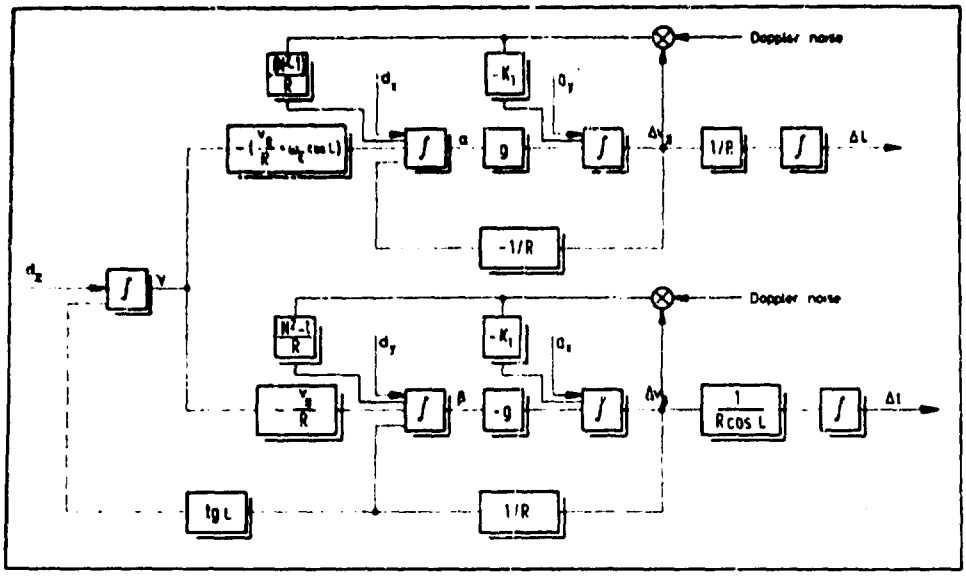

Fig. 21 Error diagram of the second-order leveling loops for the horizontal channels of the INS.

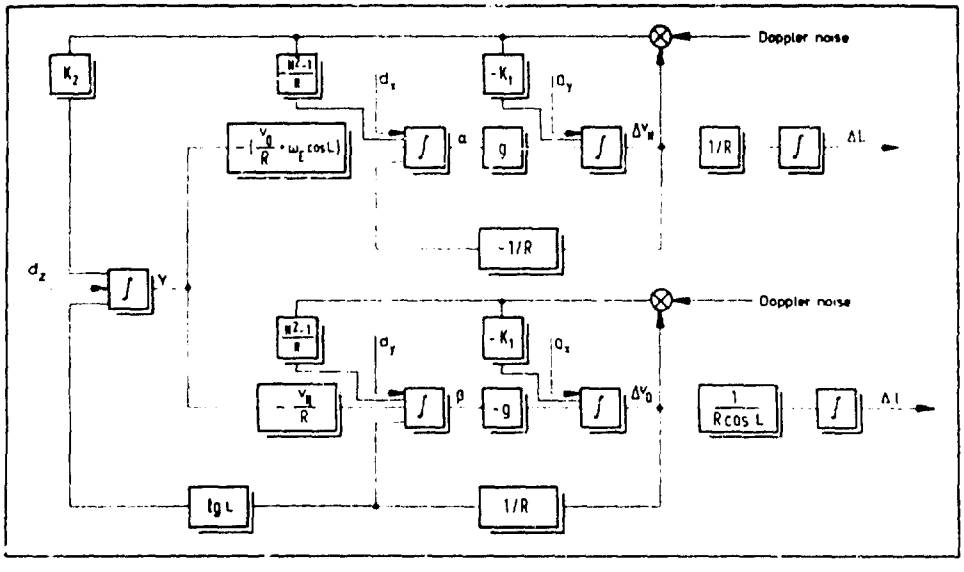

Fig. 22 Error diagram of the third-order gyrocompassing loop.

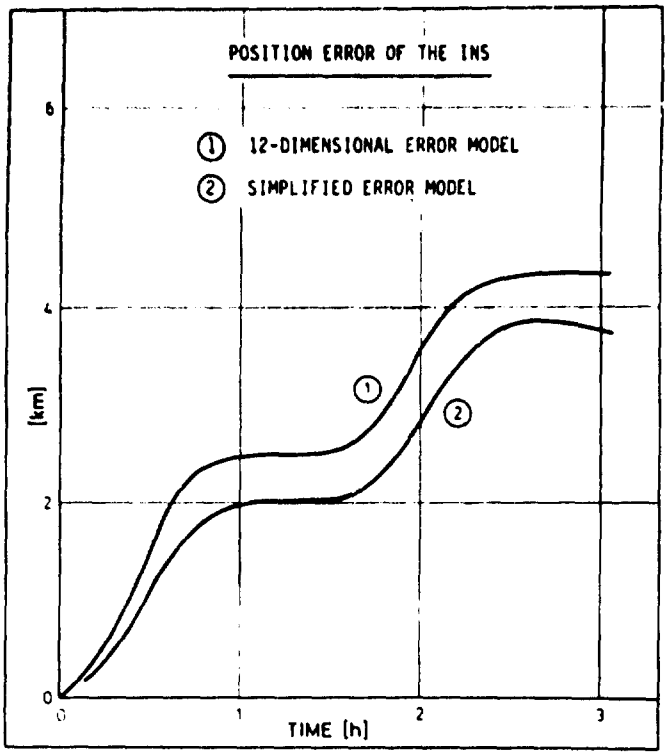

Fig. 23 Position error (1σ) of the north/south-channel of the INS computed with the real-world model and with the simplified model.

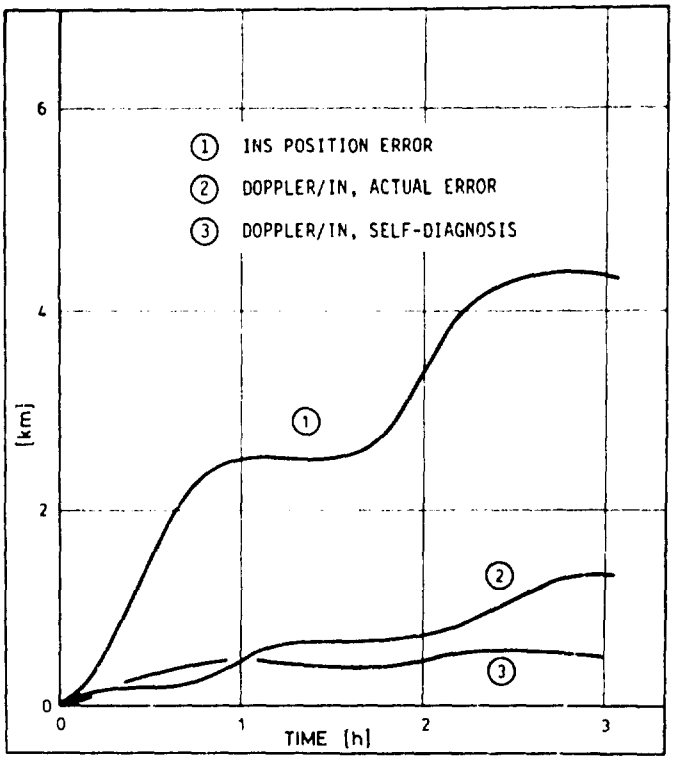

Fig 24 Actual position error of the Doppler INS with the sensitive filter, compared with the filter's self-diagnosis.

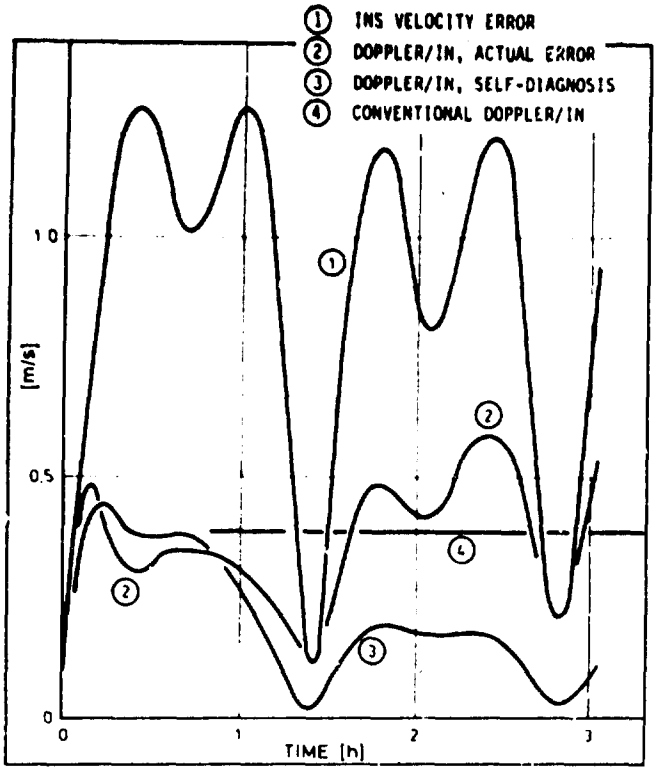

Fig. 25 Actual velocity error of the sensitive filter, compared with the conventional leveling loop.

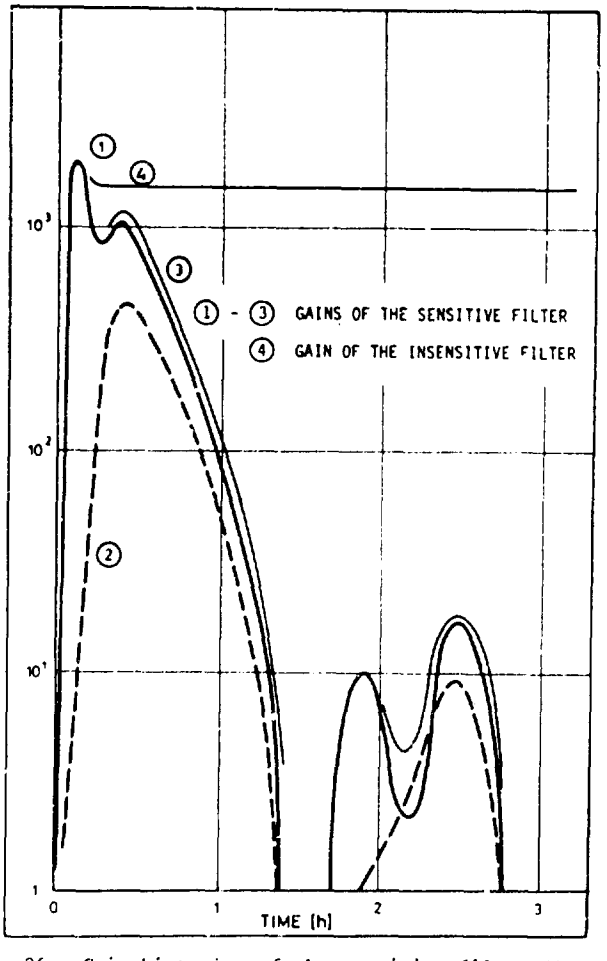

Fig. 26 Gain histories of the sensitive filter (1, 2 and 3) and of the intensitive filter (4).

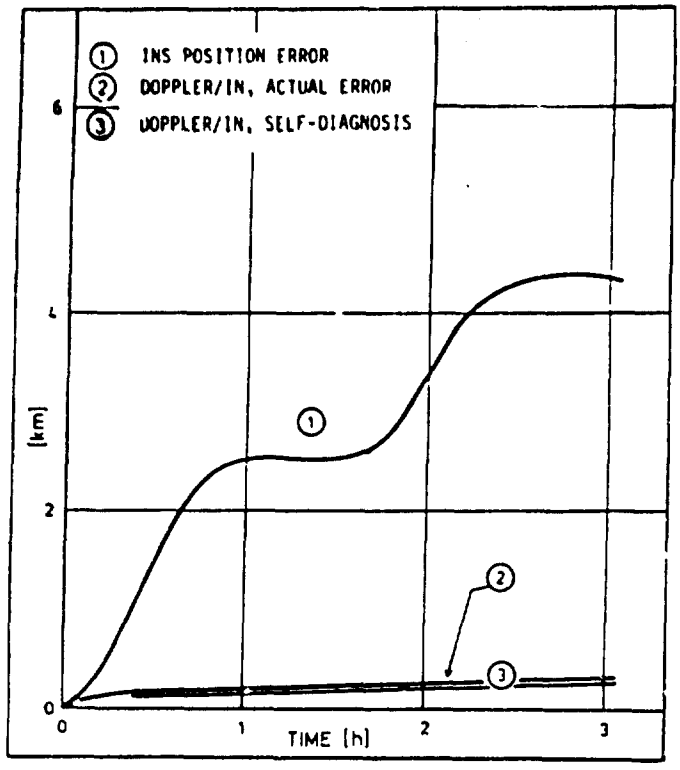

Fig. 27 Position accuracy of the Doppler INS obtained with the insensitive filter.

① INS VELOCITY ERROR
② DOPPLER/IN, ACTUAL ERROR
③ DOPPLER/IN, SELF-DIAGNOSIS
④ CONVENTIONAL DOPPLER/IN

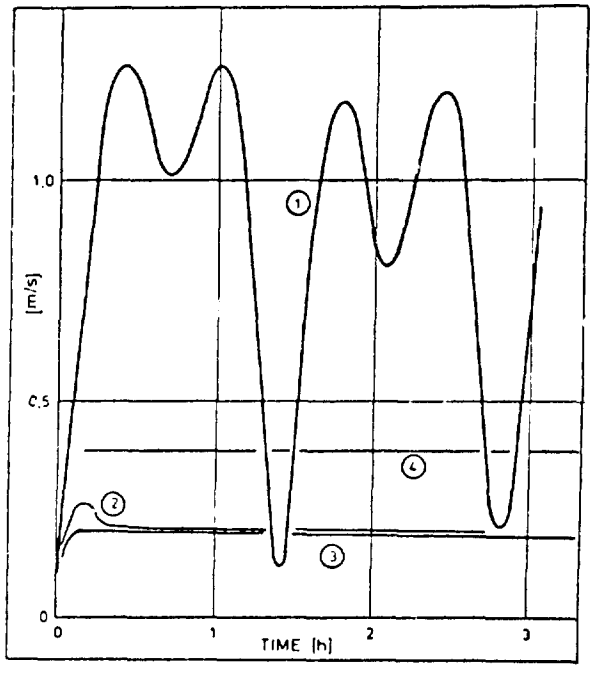

Fig. 28 Velocity accuracy of the insensitive filter, compared with the conventional leveling loop.

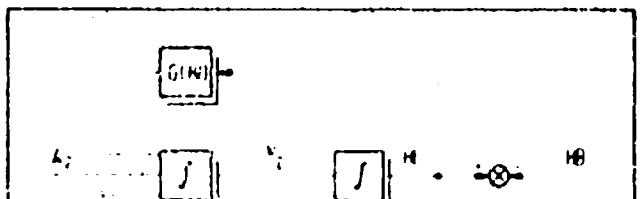

Fig 29 Conventional second-order baro-inertial system.

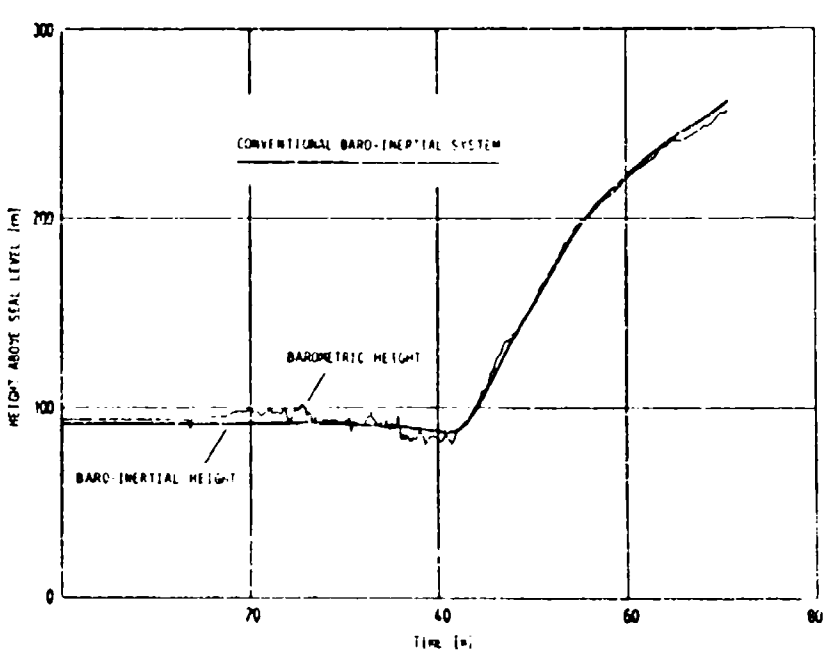

Fig. 30 Baro-inertial hight measured during a HFB 320 take-off.

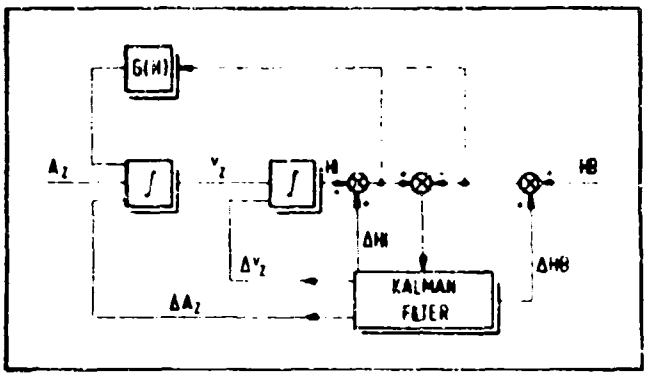

Fig. 31 Schematic diagram of the optimal baro-inertial system.

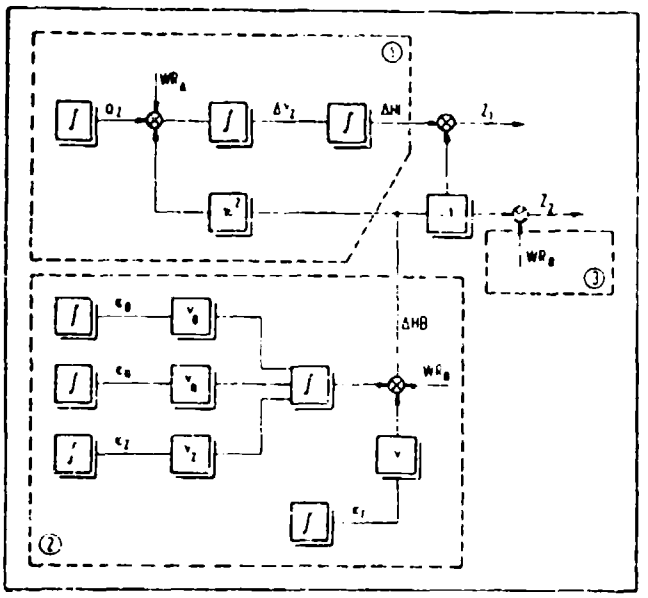

Fig. 32 Error model of the optimal baro-inertial system and radar error model (part 3).

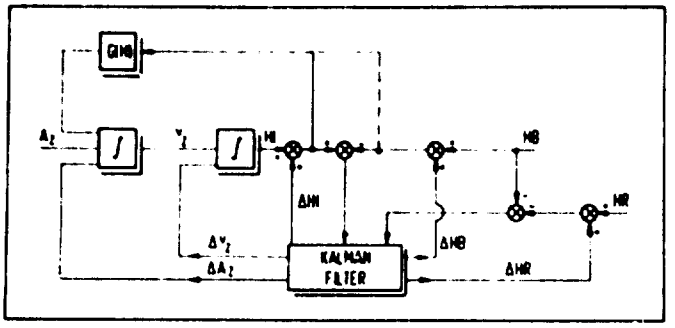

Fig. 33 Schematic diagram of the reference system, consisting of LN3, altimeter, and radar.

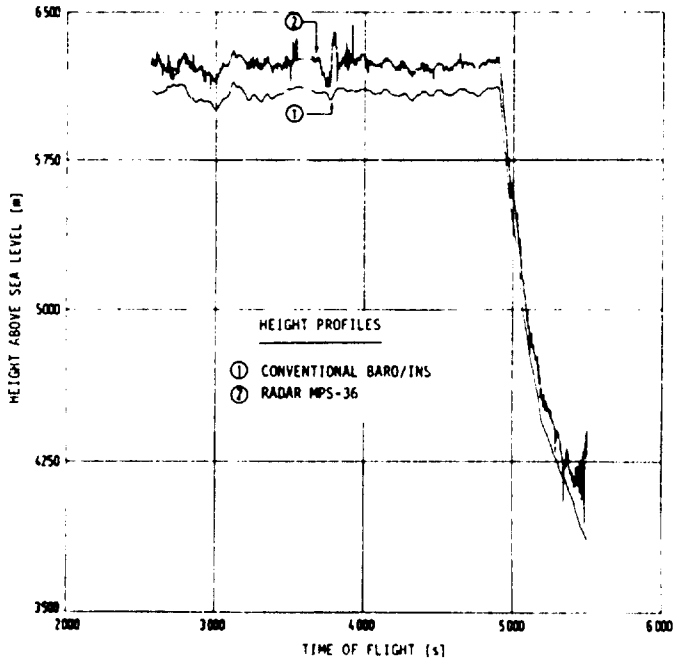

Fig. 34 Altitude profiles measured by the conventional baro-inertial loop and by the tracking radar.

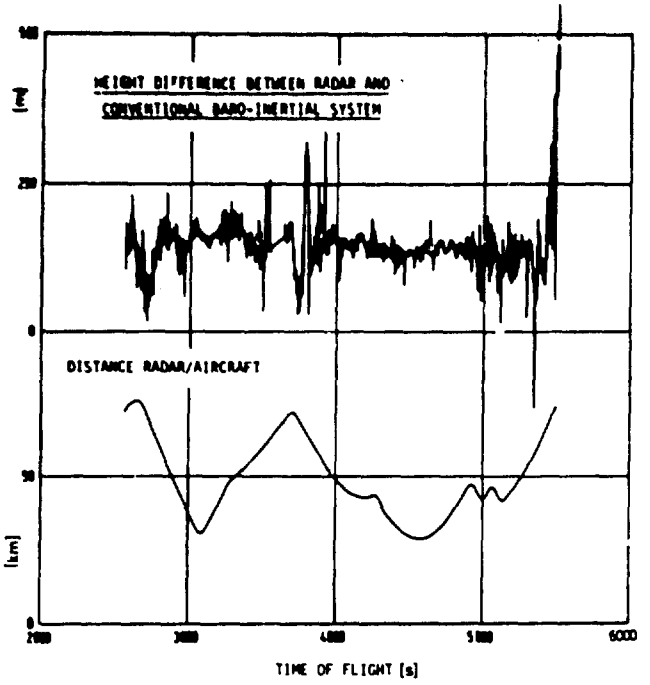

Fig. 35 Difference between the two altitude profiles shown in Fig. 34 and distance between aircraft and tracking radar.

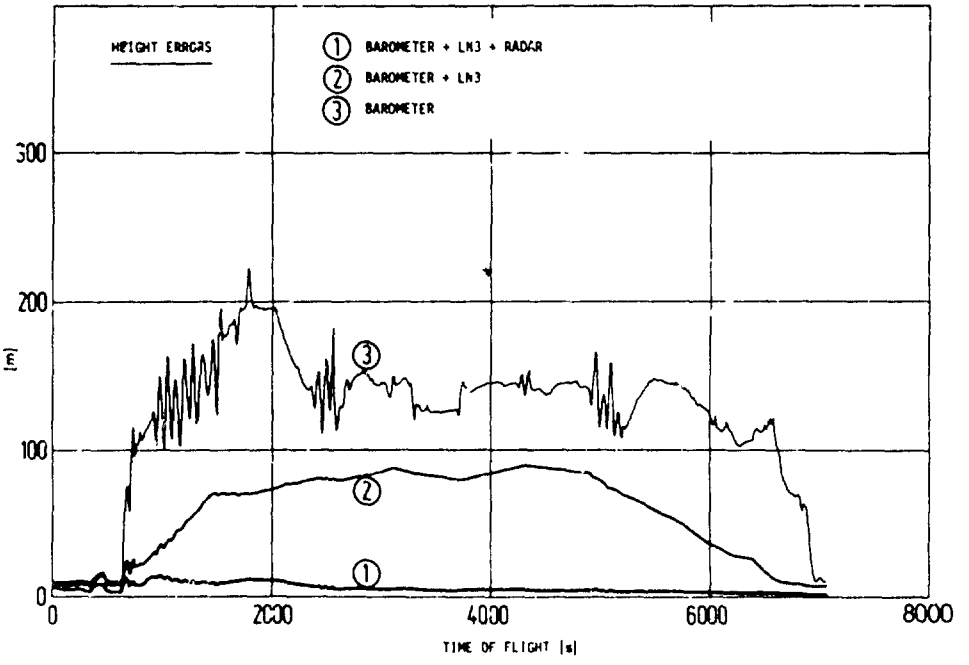

Fig. 36 Altitude measuring accuracies of different optimal combinations of the sensors.

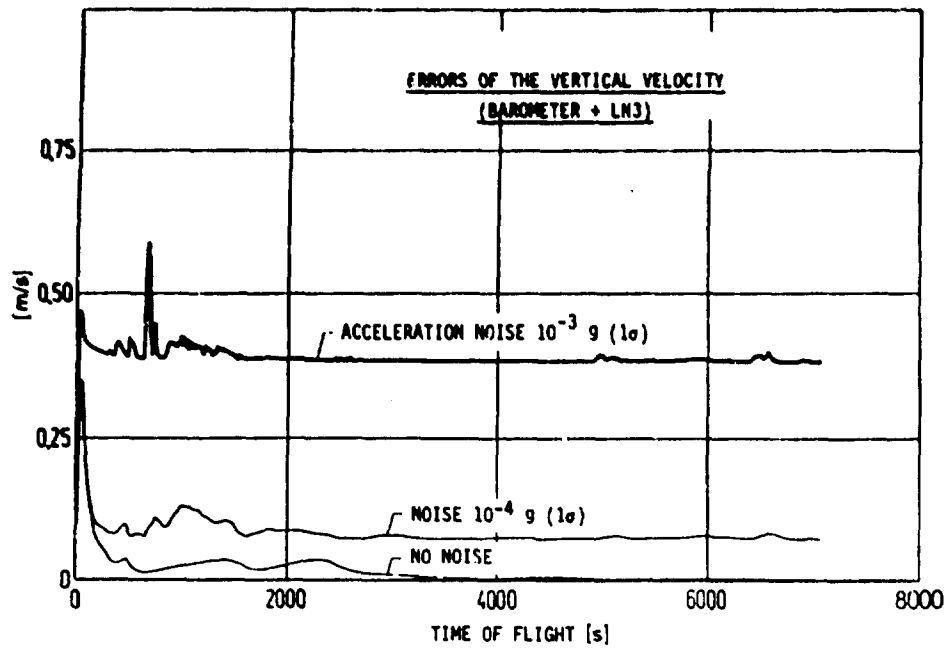

Fig. 37 Measuring accuracy for the vertical velocity of the optimal baro-inertial system (for different accelerometer noise levels of the LN3).

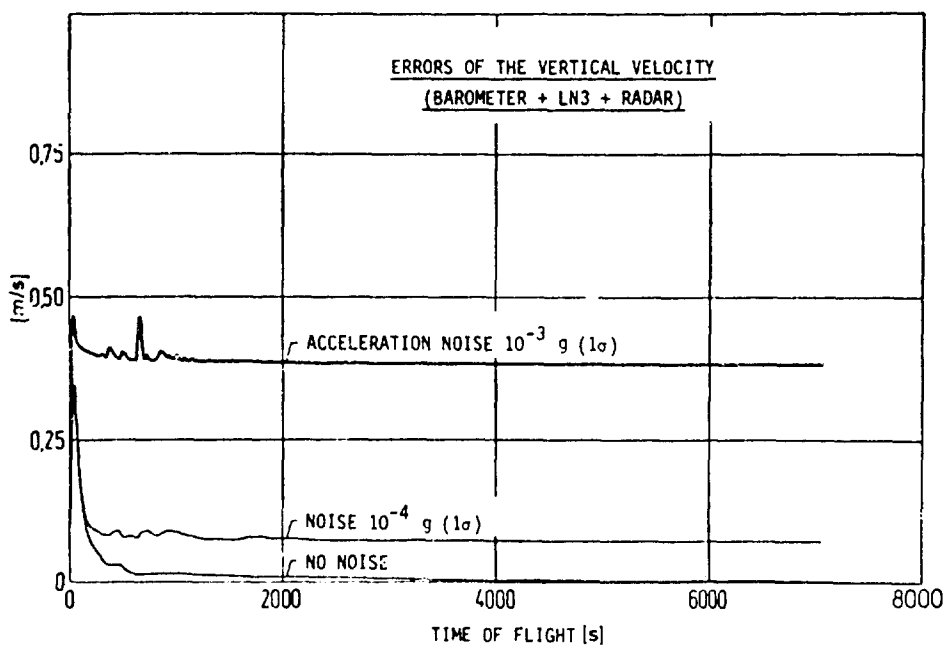

Fig. 38 Measuring accuracy for the vertical velocity of the reference system.

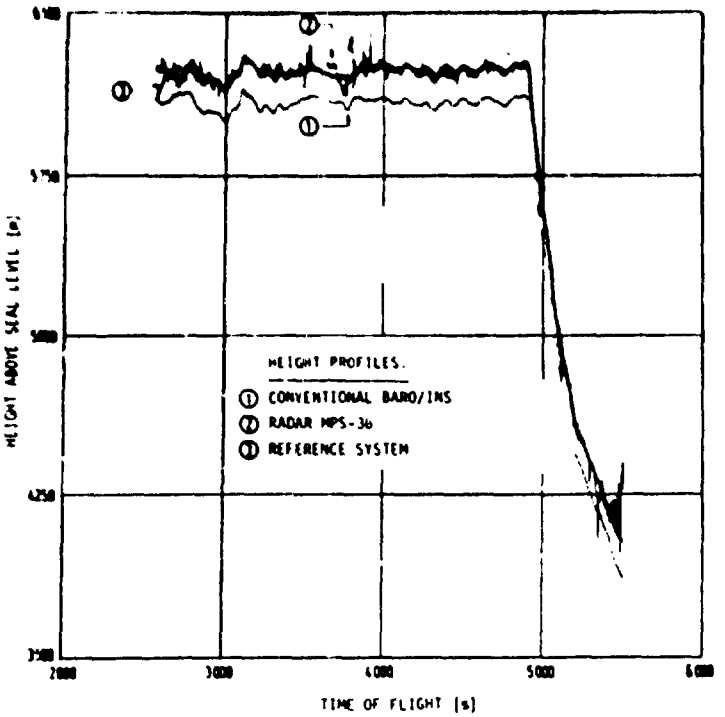

Fig. 39 The reference height profile (Curve ③) as compared with the conventional baro-inertial and the radar profiles.

ETUDE ET REALISATIONS DE FILTRES DE KALMAN POUR SYSTEMES DE NAVIGATION

Pierre FAURRE, Loïc CAMBERLEIN
SAGEM
6, avenue d'Iéna
PARIS
75116
France.

RESUME

Deux études de SAGEM en filtrage optimal, sont présentées dans ce papier avec les expérimentations associées.

(1) Un système de navigation aéronautique inertie-Doppler-recalage de position a été testé avec succès. Le modèle mathématique utilisé, ainsi que la description du programme de 6000 mots répartis en deux calculateurs et les résultats de l'expérimentation, sont donnés.

(2) L'alignement rapide d'une plate-forme à inertie est le deuxième cas présenté. La modélisation retenue est simple et les gains obtenus sont importants : pour des précisions comparables, l'alignement optimal dure 450 secondes à comparer aux 1031 secondes d'un alignement classique. Le programme cependant utilise 1800 mots du calculateur.

Enfin, des considérations générales sur l'engineering des filtres sont données, particulièrement en ce qui concerne la méthodologie générale, et les méthodes d'aide à la programmation : le système DASH (Dispositif d'Aide à la Programmation des Systèmes Hybrides) développé par SAGEM, est présenté rapidement.

SUMMARY

This paper describes in detail two systems using Kalman filtering which were developed and experimented by SAGEM.

(1) A hybrid inertial-Doppler-position reset navigator was studied and experimented from 1967 to 1972.

The technology for both inertial platform and the computer goes back to 1965. The mathematical model uses a 15-state vector. The numerical algorithms were studied and implemented with care, using the ε-technique to avoid sensivity problems.

The complete program was split into two computers, and the subprogram corresponding to the filter represented about 6000 words, over 11000 for the total. Curves are given both for theoretical performances, and for experimental flight results.

(2) Algorithms and software for optimal alignment of an inertial platform were developped and tested from 1972 to 1974.

The inertial system used for the experiment is an MOC 60 of SAGEM. The mathematical model is quite simple, and the complete alignment program uses 1800 words. The improvement in alignment time is quite impressive : 450 seconds for optimal alignment, to be compared to 1031 seconds for classical alignment.

Then the paper gives in its fourth part general considerations on filter engineering :

(1) General methodology used by SAGEM is presented.

(2) From the experience gained during the design and test of system (1), SAGEM has come to the conclusion that one needs a quite involved facility to test and valid real time program of the complexity of an hybrid inertial navigator ; we have designed such a facility we call DASH (System for testing and validating programs for hybrid systems) which is quickly described.

1. INTRODUCTION

Concevoir un système de navigation hybride optimal, c'est essentiellement résoudre un problème d'utilisation optimale d'information, problème posé depuis fort longtemps en sciences et en techniques, et moteur essentiel pour le développement du calcul des probabilités et de la statistique.

Il y eut de nombreux précurseurs illustres dont Gauss, Laplace...; il fallut attendre cependant les années 40 pour que les besoins en systèmes d'armes et systèmes de communication à hautes performances conduisent Shannon [1] et Wiener [2] à effectuer des travaux fondamentaux dans ce domaine. Mais l'on peut considérer que c'est grâce au développement des moyens de calcul numérique d'une part et à l'introduction par Kalman([3] à [5]) de méthodes récursives de filtrage statistique d'autre part que l'on a pu envisager à partir des années 60 la construction des systèmes optimaux fonctionnant en temps réel.

La réalisation de systèmes de navigation a pu être effectuée avec succès par ces méthodes. En effet, la navigation consiste à déterminer les paramètres fondamentaux que sont la position, la vitesse et l'attitude (cap et verticale) d'un véhicule à partir de capteurs ou systèmes donnant des informations le plus souvent redondantes.

Les premières applications ont eu lieu au cours des années 1963 à 1965 (voir [6] à [17]).

SAGEM a mené, dès 1967, plusieurs études et expérimentations de systèmes de navigation en utilisant les techniques de filtrage numérique de Kalman ([18] à [21]).

Nous exposerons en détail aux sections 2 et 3 les réalisations suivantes :

(1) Système de navigation hybride inertie/Doppler/recalage de position pour application aéronautique réalisé et expérimenté de 1967 à 1972.

(2) Alignement rapide optimal d'un système à inertie réalisé et expérimenté de 1972 à 1974.

Les considérations générales qui suivront à la section 4 s'appuient sur l'expérience acquise par SAGEM au cours de la réalisation des systèmes précédents et d'autres systèmes (achevée ou en cours) qui sont :

(1) Filtrage inertie/VOR/DME et filtrage inertie/ILS pour l'aéronautique civile.

(2) Système de navigation de référence et alignement à la mer des systèmes à inertie du Super-Etendard.

(3) Système inertie/Loch/Transit pour la localisation précise pour recherche géophysique marine.

(4) Systèmes performants utilisant plusieurs plateformes.

2. SYSTEME DE NAVIGATION AERONAUTIQUE EXPERIMENTAL

Cette étude et l'expérimentation associée ont été réalisées dans le cadre d'un contrat avec le Service Technique Aéronautique.

Le système de navigation hybride expérimenté intègre les informations redondantes d'un système à inertie, d'un radar Doppler, de recalage de position à partir de moyens divers et d'une centrale barométrique. Les trois premières informations sont traitées par un filtre de Kalman, la dernière est utilisée de façon classique.

Après la description des équipements, on présente le modèle markovien du système hybride -choisi après l'étude de performance et de sensibilité-, les caractéristiques des programmes de filtrage, les difficultés rencontrées dans la réalisation pratique du filtrage, les méthodes de mise au point utilisées et les résultats des essais au sol et des essais en vol.

2.1 Description de l'installation d'essais

2.1.1 Les équipements (Hardware)

La figure 1 décrit le schéma de l'installation expérimentale montée sur la Caravelle du Centre d'Essais en Vol de Brétigny (CEV).

La base de l'installation est un système de navigation à inertie, dont la technologie date de 1965-1966. C'est un système en plusieurs boîtes, dont les performances de navigation sont de la classe 1,5 mille nautique par heure, CEP. Ce système, étudié pour avion d'armes, utilise un calculateur numérique embarqué dont le temps d'addition est de 39 microsecondes et la capacité mémoire d'environ 8 kilo-mots de 24 bits. Les fonctions programmées de façon standard dans ce calculateur sont nombreuses et comprennent la conduite de la plate-forme en alignement et navigation, des couplages classiques accéléromètre de verticale-altitude barométrique et inertie-Doppler, la navigation automatique le long d'une trajectoire définie par points tournants, le recalage simple de position et la conduite des visualisations et des commandes du système.

La puissance de calcul et la mémoire restant disponibles, étant insuffisantes pour les besoins du filtre de Kalman, on a choisi d'ajouter un calculateur identique, en définissant ainsi une structure de calcul parallèle. Le dialogue entre les deux calculateurs se fait par l'intermédiaire d'une mémoire tampon de 600 bits en technologie MOS. Les calculateurs fonctionnent de façon asynchrone sur le principe "maître-esclave". La calculateur 1, celui du système à inertie, est le maître. Il définit le rythme général des calculs et des échanges avec le calculateur 2, l'esclave.

Le radar Doppler, qui fournit l'information redondante de vitesse, est un Doppler moderne à antenne fixe. Il donne les composantes longitudinale et transversale de la vitesse sol sous forme de fréquences d'impulsions. Son domaine d'utilisation est principalement fonction de l'assiette avion, de l'altitude et de la nature de la zone survolée, terre

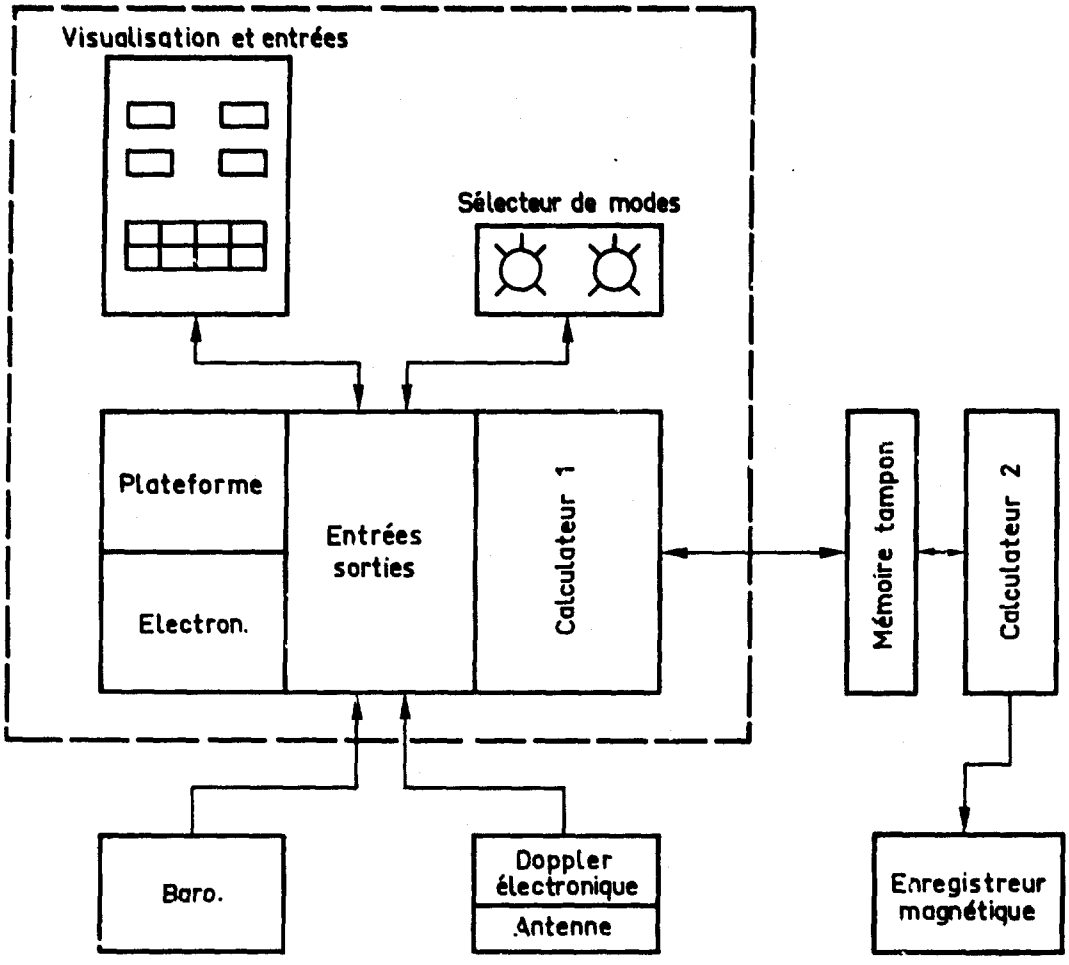

FIGURE 1 - INSTALLATION EN ESSAIS SUR CARAVELLE AU CEV

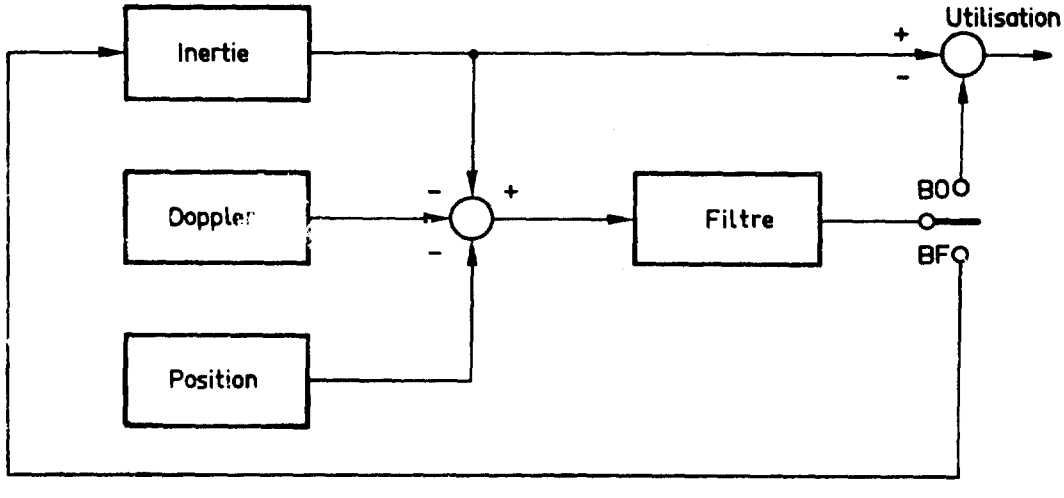

FIGURE 2 - FONCTIONNEMENT EN BOUCLE OUVERTE (B.O) OU FERMEE (B.F)

ou mer.

L'altitude est donnée par la centrale aérodynamique du bord dont le traducteur de pression est du type mécanique classique.

Les recalages de position sont effectués au moyen du boîtier de visualisation et d'entrées numériques du système à inertie. Ils sont faits à partir de moyens divers en particulier un hyposcope. La visualisation permet également l'affichage de la position donnée par l'inertie et de son estimée donnée par le filtre.

Le calculateur 2 est connecté à un enregistreur magnétique embarqué, qui toutes les 50 secondes, emmagasine les 124 paramètres les plus significatifs du fonctionnement du filtre.

Les caractéristiques générales des principaux équipements sont données par les tableaux 1 à 3.

2.1.2 Les modes de fonctionnement

(1) Modes de navigation

La redondance des informations de l'inertie, du Doppler et du recalage de position est utilisée pour définir plusieurs modes de navigation :

(a) inertie pure

(b) inertie-recalage de position optimal

(c) inertie-Doppler optimal

(d) inertie-Doppler-recalage de position optimal

(2) Boucle ouverte et boucle fermée - Alignement en vol

Un sélecteur permet de commander pour les modes b, c et d, un fonctionnement en boucle ouverte (BO) ou en boucle fermée (BF), qui est schématisé par la figure 2.

Dans le fonctionnement en boucle ouverte, les paramètres de navigation et d'attitude sont corrigés à l'extérieur, avant utilisation. Le système à inertie reste autonome.

Dans le fonctionnement en boucle fermée, certaines composantes du vecteur d'état sont corrigées dans le système à inertie. En toute rigueur, cette correction devrait être faite sans retard et instantanément . En pratique, compte tenu de la charge de calcul, la correction est effectuée avec environ un demi pas de retard (26 secondes). Suivant les paramètres, la correction est :

(a) instantanée, pour les grandeurs numériques de position, vitesse, dérives et facteurs d'échelle des gyroscopes.

(b) progressive, pour l'attitude plateforme, par commande des gyroscopes dont la vitesse de précession est limitée.

Le fonctionnement en boucle fermée permet en particulier l'alignement en vol de la plateforme. En outre, dans certains cas le contrôle des erreurs inertielles peut être nécessaire pour satisfaire l'hypothèse de linéarité. Cependant, le fonctionnement en boucle fermée a l'inconvénient de détruire l'autonomie du système à inertie et de dégrader ainsi la fiabilité de ses informations.

(3) Utilisation de l'information barométrique

L'information d'altitude barométrique n'est pas intégrée par le filtre, pour des raisons de simplicité, car l'altitude n'est pas un paramètre critique. Cependant, on réalise un couplage à gain constant avec l'accéléromètre vertical. Ce couplage fournit l'altitude et la vitesse verticale. Un sélecteur permet ou non de les utiliser dans la mécanisation du système à inertie et dans la matrice observation du filtre.

2.2 Modèle markovien des erreurs du système hybride

Cette expérimentation a été précédée d'une étude importante suivant les étapes d'une méthodologie qui sera commentée à la section 4. Les études de performances et de sensibilité ont conduit à adopter le modèle markovien suivant des erreurs du système hybride.

TABLEAU 1 - CALCULATEUR EMBARQUE SAGEM

AE . 51 . A

. Technologie (1965)

- circuit intégré
- mémoire à tambour miniature à palier hydrodynamique

. Capacité mémoire 8709 mots de 24 bits

- programme non modifiable : 7680 mots
- travail : 645 mots
- système : 384 mots

. Structure série parallèle comprenant

- une unité arithmétique universelle
- un analyseur différentiel numérique

. Opération en virgule fixe

. Possibilité de programmer deux opérations simultanées

. Horloge : 640 kHz

. Temps opératoire

- addition : 39 µs
- multiplication : 39 µs
- division (sur 24 bits) : 1000 µs (programmation simultanée d'opérations toutes les 39 µs)

. Entrée/sortie programmée, série

. Poids : 21 Kg

. Volume 3/4 ATR : 18 l.

TABLEAU 2 - SYSTEME A INERTIE SAGEM - S. 111

. Système prototype pour avion d'armes

. Technologie 1966

. Gyroscopes flottants à un degré de liberté

. Plateforme toute attitude à quatre axes de cardan

. Calculateur universel digital AE 51 A

. Mécanisation toute latitude asservie à un pôle arbitraire

. Précision : de la classe 1,5 nm/h, CEP.

TABLEAU 3 - RADAR DOPPPLER EMD . DECCA - 72

. Antenne fixe à trois faisceaux
. Sortie en fréquence
- vitesse longitudinale 35,02 Hz/noeud
- vitesse latérale 17,95 Hz/noeud

TABLEAU 4 - DEFINITION DES SYMBOLES

GRANDEUR	DIMENSION	DEFINITION
x	15 × 1	Vecteur d'état d'erreur du système hybride
$F = \begin{bmatrix} F_{11} & F_{12} \\ 0 & F_{22} \end{bmatrix}$	15 × 15	Matrice dynamique du système hybride.
μ	15 × 1	Bruit excitant, gaussien centré, non corrélé
Q	15 × 15	Covariance de μ, matrice diagonale.
y	4 × 1	Vecteur d'observation.
H	4 × 15	Matrice d'observation.
V	4 × 1	Bruit des observations, gaussien centré, non corrélé.
R	4 × 4	Covariance de v, matrice diagonale.
$\Phi = \begin{bmatrix} \Phi_{11} & \Phi_{12} \\ 0 & \Phi_{22} \end{bmatrix}$	15 × 15	Matrice de transition.
$\hat{x}$	15 × 1	Meilleure estimée de l'erreur du système hybride.
Σ	15 × 15	Covariance des erreurs résiduelles.
K	15 × 4	Gain du filtre.
V	15 × 15	Diagonale de Σ
ε	1 × 1	Coefficient de désensibilisation du filtre, compris entre 0 et 1.
h	1 × 1	Pas numérique du filtre (50 s)
h^*	1 × 1	Pas numérique fractionné (10 s)

EQUATIONS PROGRAMMEES	OBSERVATIONS	CALCULATEUR
CALCULATEUR DE $\Phi_{11}(t+h,t)$ $\Phi_{11}(t+h,t) = \prod_{i=0}^{i=2} \Phi\left[t+(i+1)h^*, t+ih^*\right]$ $\Phi\left[t+(i+1)h^*, t+ih^*\right] = I + \frac{h^*}{4} F_{11}(t+ih^*) + \frac{3}{4}h^* F_{11}\left[t+(i+\frac{2}{3})h^*\right] + \frac{h^{*2}}{2} F_{11}\left[t+(i+\frac{2}{3})h^*\right] F_{11}(t+ih^*)$ CALCULE DE Φ_{12}, Φ_{22} : $\Phi(t+h,t) = I + \frac{h}{4}F(t) + \frac{3}{4}h F(t+\frac{2}{3}h) + \frac{h^2}{2} F(t+\frac{2}{3}h)F(t)$	CALCULATEUR Matrice de transition.	CALCULATEUR 1
$\hat{x}_-(t+h) = \Phi(t+h,t)\,\hat{x}_+(t)$ $\Sigma_-(t+h) = \Phi(t+h,t)\,\Sigma_+(t)\,\Phi'(t+h,t) + hQ + \frac{h^2}{2}\left[F(t)Q+QF'(t)\right]$	Intégration	2
$K = (1-\varepsilon)\,\Sigma_- H'\left[H\Sigma_- H' + R\right]^{-1} + \varepsilon\, VH'(HVH')^{-1}$ $\hat{x}_+ = \hat{x}_- + K(y-H\hat{x}_-)$ $\Sigma_+ = (1-KH)\,\Sigma_-$	Recalage Doppler et position composante par composante.	2

TABLEAU 5 - EQUATIONS DU FILTRE

TABLEAU 6 - UTILISATION DES CALCULATEURS

	VOLUME MEMOIRE	TEMPS DE CALCUL
1	80 %	95 %
2	60 %	55 %

TABLEAU 7 - DETAIL DU VOLUME MEMOIRE

1	Alignement	925
	Navigation	900
	Visualisation	1125
	Kalman	2600
	Divers	1350
	TOTAL	6300
2	Kalman	3700
	Divers	1000
	TOTAL	4700
	TOTAL GENERAL.....	11000 Mots
	TOTAL KALMAN.....	5700 Mots

$$\dot{x} = Fx + u \qquad (1)$$

avec $$x' = [x_1' , x_2' , x_3'] \qquad (2)$$

et où

x_1 = vecteur d'état des erreurs dynamiques du système à inertie,

x_2 = vecteur d'état des erreurs des composants du système à inertie,

x_3 = vecteur d'état des erreurs du Doppler.

2.2.1 Erreurs dynamiques du système à inertie

On a choisi la description classique [21] par deux systèmes d'équations différentielles projetées sur les axes plateforme : les équations en ψ et les équations d'erreurs de position. Cette description conduit à des équations simples. Le vecteur d'état correspondant est :

$$x_1 = [\psi_x, \psi_y, \psi_z, \delta x, \delta y, \dot{\delta x}, \dot{\delta y}]' \qquad (3)$$

où

ψ_x, ψ_y, ψ_z = rotations autour des axes plateforme faisant passer du repère calculateur au repère plateforme.

$\delta x, \delta y$ = erreurs horizontales de position dans les axes plateforme.

$\dot{\delta x}$ $\dot{\delta y}$ = dérivées temporelles de δx et δy.

2.2.2 Erreurs des composants inertiels

A la suite de l'étude de sensibilité les biais des accéléromètres et les balourds des gyroscopes ont été négligés. Les seules erreurs retenues sont les dérives et facteurs d'échelle des gyroscopes. Le modèle pris pour la dérive et suggéré par l'expérience est :

$$\dot{\varepsilon} = -\beta\varepsilon + u \qquad (4)$$

où

ε = dérive aléatoire, variable au cours du vol, dont le modèle choisi est du premier ordre.

u = bruit blanc.

Ce modèle permet de représenter aussi bien un signal à temps d'autocorrélation $T = 1/\beta$ qu'un cheminement aléatoire, si $\beta = 0$.

L'expérience conduit à considérer le facteur d'échelle comme constant au cours du vol et variable d'un jour à l'autre. Le modèle correspondant est donc :

$$\dot{K}_g = 0 \qquad (5)$$

Le vecteur d'état des erreurs de gyroscope s'écrit alors :

$$x_2 = [\varepsilon_x, \varepsilon_y, \varepsilon_z, K_{gy} \quad K_{gz}]' \qquad (6)$$

2.2.3 Erreurs du Doppler

Pour le Doppler utilisé, l'étude de sensibilité conduit à négliger le facteur d'échelle. Les seules erreurs retenues sont des biais sur chaque axe, constants au cours du vol mais aléatoires d'un vol à l'autre, ceci pour des limites d'utilisation précises (voir section 2.3)

$$\dot{b}_d = 0 \qquad (7)$$

Le vecteur d'état des erreurs Doppler est par conséquent :

$$x_3 = [b_{dx}, b_{dy}]' \qquad (8)$$

2.3.4 Erreurs du recalage de position

La position est mesurée à des instants discrets par divers moyens. On considère que les erreurs sont indépendantes d'une mesure à l'autre et qu'elles sont caractérisées par leur CEP.

2.4 Description des programmes (Software)

2.4.1 Equations programmées

Les tableaux 4 et 5 présentent les équations de filtrage programmées ainsi que les notations des vecteurs et matrices utilisés.

Les formules d'intégration et de calcul de la matrice de transition correspondent à un algorithme Runge-Kutta d'ordre deux qui minimise les erreurs. La matrice de transition a été découpée en deux blocs qui sont calculés sur des pas différents, 10 et 50 secondes, pour des raisons de précision développées à la section 2.4.

Les équations classiques du filtre de Kalman ont été modifiées pour inclure la technique de l'"e" de désensibilisation aux erreurs de modèles et aux erreurs numériques.

2.4.2 Répartition des programmes dans les calculateurs

La répartition des programmes a été principalement dictée par les contraintes suivantes :

(1) une bonne partie de la mémoire et de la puissance du calculateur 1 est utilisée par les programmes spécifiques du système à inertie.

(2) un certain nombre de calculs doit être fait en flottant, pour des raisons de précision numérique développées plus loin.

Le partage des programmes et la spécialisation des calculateurs en "fixe" et en "flottant" se sont révélés satisfaisants. Ainsi, le calculateur 1 traite tous les programmes en fixe et le calculateur 2 ceux en flottant (voir figure 3).

Les échanges entre calculateur se font en série, par transfert programmé, vers la mémoire tampon. Le débit de ce mode de transmission est faible mais suffisant pour traiter les 68 paramètres échangés durant chaque pas de calcul (50 secondes).

Le bilan des charges de calcul et des volumes mémoire utilisés est donné par les tableaux 6 et 7. Il est important de noter que l'optimisation du volume mémoire n'a pas été l'objectif principal de l'expérimentation, par contre l'optimisation temps réel a été un souci permanent.

2.4.3 Déroulement des programmes en temps réel

Le déroulement des calculs se fait de façon asynchrone dans les deux calculateurs mais avec un contrôle rigoureux du temps réel par le calculateur 1. C'est ce dernier qui définit la durée du pas d'intégration, lance les programmes du 2 et gère les échanges. Lorsque le 2 a terminé un traitement, il se met en attente d'un nouvel ordre (voir figure 4).

Le début du pas d'intégration coïncide avec l'échantillonnage de l'observation Doppler. L'observation de position peut intervenir à n'importe quel instant.

2.5 Difficultés rencontrées dans la réalisation pratique du filtre

2.5.1 Contrainte temps réel

Le calcul en temps réel ajoute à la programmation un certain nombre de difficultés et de contraintes qui sont liées :

(1) à la vitesse limitée des calculs,

(2) à la nécessité de contrôler le temps de façon rigoureuse, notamment pour les opérations d'intégration, la synchronisation des échantillonnages, des observations, etc...

(3) aux échanges entre les calculateurs.

Ainsi, la meilleure estimée de l'erreur, après recalage Doppler et position, est disponible avec 36 secondes de retard. En raison de la puissance de calcul limitée et de la précision numérique nécessaire, il n'a pas été possible de réaliser un algorithme d'intégration réellement "prédicteur". De plus, le traitement des observations, qui en toute rigueur devrait être instantané, demande environ une dizaine de secondes.

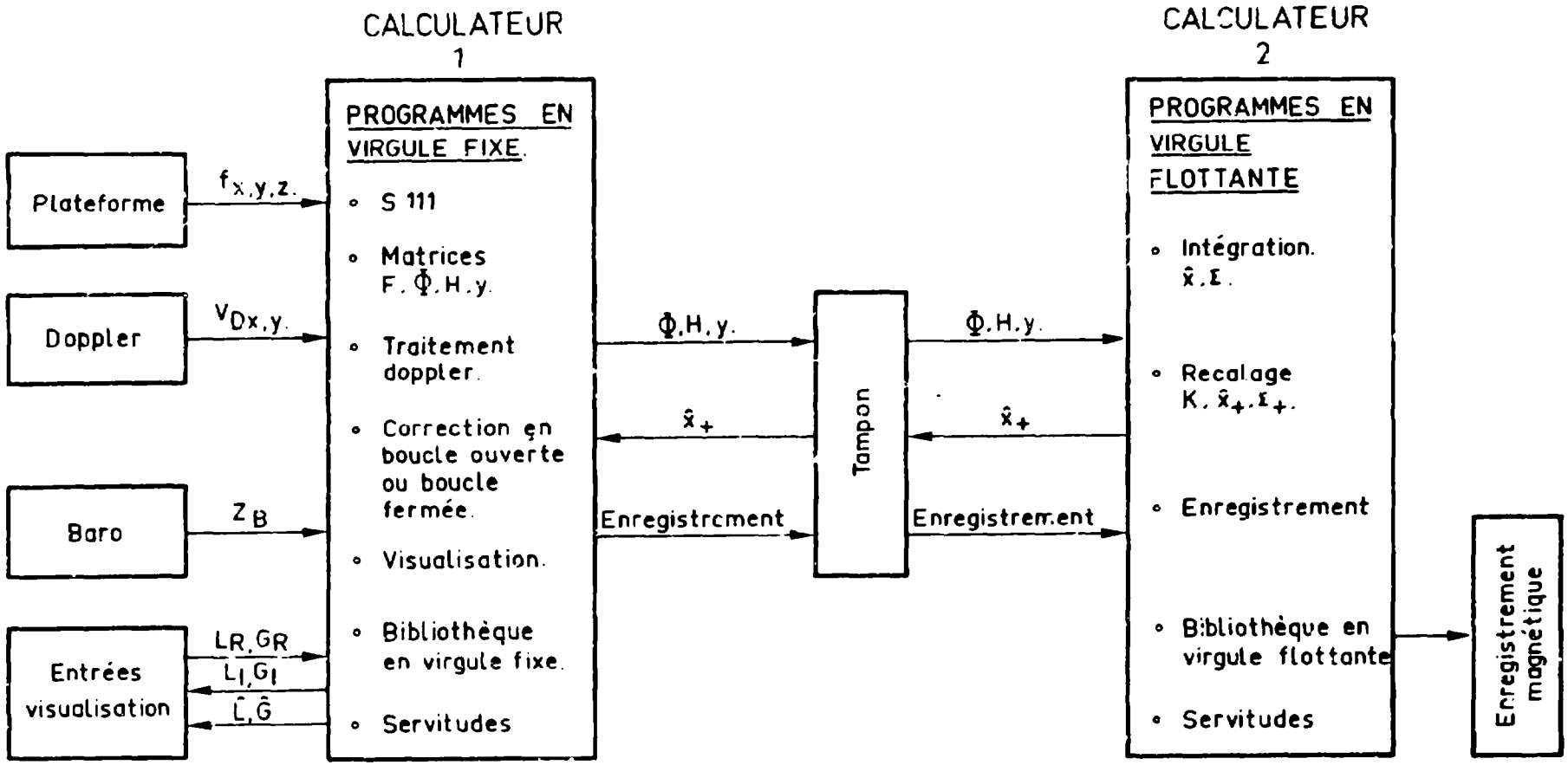

FIGURE 3 - REPARTITION DES PROGRAMMES ET ORGANISATION DES ECHANGES D'INFORMATION

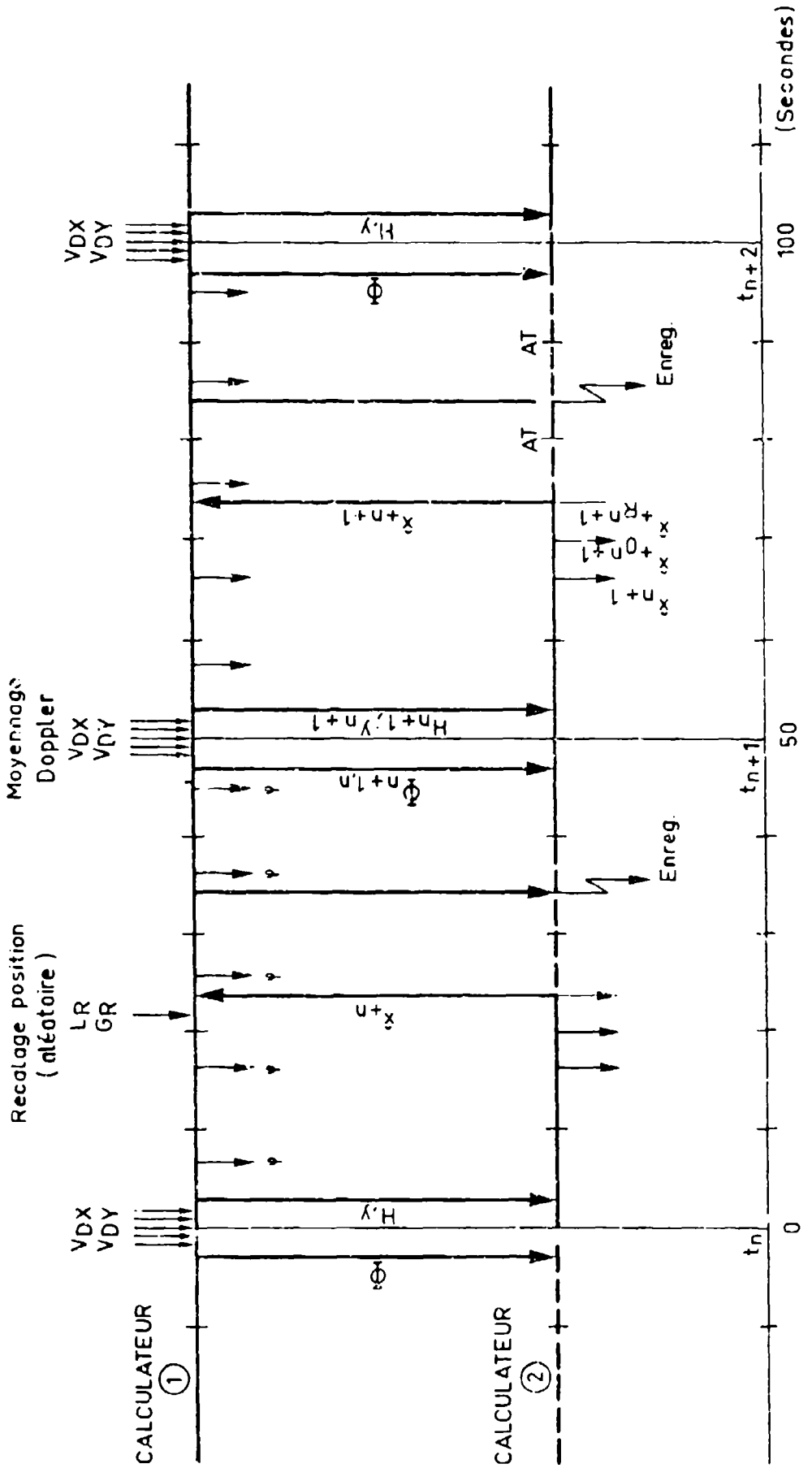
CALCULATEUR ①
CALCULATEUR ②
Recalage position (aléatoire)
LR
GR
Moyennage Doppler
VDX
VDY
H,Y
Φ
AT
Enreg.
x^*_{+n}
$H_{n+1,n}$
$\Phi_{n+1,n}$
$H_{n+1,Y_{n+1}}$
x^*_{+n+1}
x^*_{n+1}
$+R_{n+1}$
$+Q_{n+1}$
t_n
t_{n+1}
t_{n+2}
0
50
100
(Secondes)

En pratique, ce retard n'est pas gênant. En boucle ouverte, il se traduit par un retard de la correction de l'affichage. En boucle fermée il est négligeable devant les constantes de temps dynamiques des erreurs, en particulier la période 84 minutes de l'inertie.

2.4.2 Algorithme d'intégration

La matrice de transition est utilisée pour intégrer (et prédire) la meilleure estimée des erreurs et la matrice de covariance des erreurs résiduelles. Le calcul de la matrice de transition se fait par intégration de la relation.

$$\dot{\Phi} = F\Phi \qquad (9)$$

La précision de cette intégration, qui dépend donc des caractéristiques de la trajectoire, conditionne les performances du filtre. Schématiquement, pour un algorithme et un objectif de précision donnés, plus les évolutions sont sévères, plus le pas d'intégration doit être petit.

Le problème était donc de choisir un algorithme, suffisamment précis pour les trajectoires envisagées, donnant une charge et un volume de calcul minimal.

L'idée exploitée est de considérer que les termes les plus sensibles aux évolutions sont ceux qui dépendent le plus directement des erreurs dynamiques inertielles, c'est à dire le bloc Φ_{11} (dimensions 7 x 7) de Φ. On a donc choisi de calculer les termes correspondants (Φ_{11}) de la matrice de transition avec un pas de 10 secondes et les autres avec un pas de 50 secondes.

La dégradation de performance due à cet algorithme a été calculée. Elle est négligeable (quelques pourcents) pour des vols type Caravelle. Elle serait rédibitoire pour un avion d'armes. La solution pourrait être alors une réduction du pas de calcul en utilisant un calculateur plus puissant ou, si ce n'est pas possible, d'interrompre simplement l'intégration pendant les évolutions trop sévères après avoir vérifié que la dégradation correspondante est tolérable.

2.4.3 Précision numérique - Virgule fixe ou flottante

Le domaine de variation des différents paramètres est important, notamment pour la matrice de covariance des erreurs résiduelles. Pendant l'alignement en vol de la plateforme, l'écart d'horizontal initial est de l'ordre de quelques degrés et l'écart final de l'ordre de la seconde d'arc. La plage de variation correspondante de la covariance est de 10^7. Les impératifs de cadrage et d'arrondi sont de l'ordre de 10^2 ou de 10^3, c'est à dire un total de 10^9 à 10^{10} qui dépasse les possibilités du mot de 24 bits.

Deux solutions ont été envisagées : la double précision en virgule fixe et la virgule flottante. La première a été repoussée car :

(1) le nombre de mémoire inscriptible nécessaire est multiplié par deux,

(2) les problèmes de cadrage en virgule fixe sont considérables dans cette application.

La virgule flottante supprime radicalement la contrainte cadrage. De plus, un seul mot suffit : 1[illegible] bits pour la mantisse plus le signe et 8 bits pour l'exposant. La programmation des opérations en flottant a été très soigneusement optimisée et conduit à des vitesses de calcul suffisantes pour l'expérimentation. Les performances ont été calculées pour un vol type par rapport à une arithmétique flottante en 72 bits. Les résultats montrent une dégradation inférieure à 1 %.

2.4.4 Prétraitement du Doppler

Avant d'utiliser l'observation Doppler, on effectue deux opérations : un moyennage du signal et un test pour définir les limites de validité.

(1) Moyennage du signal

Le Doppler est assez fortement bruité dans les basses fréquences. Pour améliorer le rapport signal sur bruit, on a réalisé un moyennage sur quatre secondes. Le retard de [illegible] est compensé en datant l'observation au milieu de la période de moyennage.

(2) Test de validité

[illegible] l'utilisation du Doppler dépend de l'altitude, de la zone survolée et en [illegible] de l'assiette avion. A la limite le Doppler décroche, cependant la dégra[illegible] est généralement progressive. Pour garantir le modèle utilisé, dont le domaine [illegible] est inférieur au domaine d'utilisation, il est indispensable de doubler [illegible] de [illegible] d'un test d'assiette et d'interdire le Doppler au [illegible] limite.

2.5 Mise au point du software

Les difficultés rencontrées lors de la mise au point d'un programme de 11000 mots sont nombreuses. Les caractéristiques du dispositif de calcul utilisé pour cette expérimentation en ajoutent de nouvelles : mémoire à tambour, fonctionnement asynchrone des calculateurs, dialogue par l'intermédiaire d'un registre tampon de 600 bits et programmation en langage machine.

Une technique de programmation modulaire a été adoptée pour faciliter la mise au point des programmes et leur modification éventuelle.

Les fonctions réalisées par chaque module sont complexes, les entrées et sorties sont multivariables. La mise au point n'est donc pas simple.

La méthode de test utilisée est classique : on compare pour une excitation caractéristique, les réponses du programme du système réel et d'une simulation en langage évolué (voir figure 5). La mise au point a été faite module par module avec des entrées simples (échelon), puis pour l'ensemble des programmes avec des entrées correspondant à la simulation d'un vol type. L'écriture des simulations des modules sur un ordinateur puissant (UNIVAC 1108) a demandé trois mois et la mise au point des programmes réels environ deux mois, ce qui peut être considéré comme rapide pour un système de cette taille et de cette complexité.

2.6 Essais en laboratoire

Les tests précédents permettent de contrôler de façon très fine le software, mais ne vérifient en rien la valeur des modèles choisis ni du filtre utilisé. Cet ultime objectif est le but des essais en vol. Cependant, les essais en vol coûtent cher et sont difficiles à exploiter. Il était donc souhaitable de pouvoir, au sol, vérifier le bon fonctionnement et même évaluer, dans certaines limites, les performances de l'ensemble de l'installation.

La méthode retenue pour les essais en laboratoire (V=0) du système complet a consisté à étudier la réponse du filtre à des échelons d'erreur en position, dérive et facteur d'échelle gyro, et biais Doppler. Les résultats obtenus sont présentés sous forme de courbes, figures 9 à 13.

L'installation a été essayée en fonctionnement "boucle ouverte". De cette façon, il était en effet possible d'apprécier les performances du filtre de Kalman programmé et aussi de les comparer à celles du système à inertie seul.

2.6.1 Recalage optimal de position

Les figures 6 (a) et 7 (a) représentent, en écart de latitude et de longitude, l'erreur de position, en fonction du temps, du système à inertie seul. L'échelle des erreurs n'est pas donnée pour des raisons de classification.

Les figures 6 (e) et 7 (e) montrent les erreurs après des recalages de position simples. On entend par là, une translation de la position de la valeur du vecteur de recalage, au niveau de l'affichage et donc sans influence sur les calculs de mécanisation de la plateforme.

En 6 (c), 6 (d), 7 (c), et 7 (d), on représente les erreurs de position résiduelles après les mêmes recalages de position utilisés de façon optimale par le filtre de Kalman.

2.6.2 Inertie-Doppler optimal

Les figures 8 et 9 montrent les erreurs du système à inertie excité par une dérive de [illegible] d'un des gyroscopes de verticale ainsi que les erreurs résiduelles après filtrage optimal des informations de l'inertie et d'une entrée Doppler nulle, avec pour seul bruit [illegible] celui des calculs numériques.

La figure 10 montre les mêmes paramètres pour une excitation du système à inertie par une dérive des gyroscopes plus faible et pour une observation Doppler bruitée par un [illegible] simulé par une fréquence fixe.

2.7 Essais en vol

[illegible] ont eu lieu sur la Caravelle pour la mise au point définitive [illegible] en performances.

[illegible] figures [illegible] résultats de deux vols [illegible] recalage de position, la position [illegible] de la Caravelle.

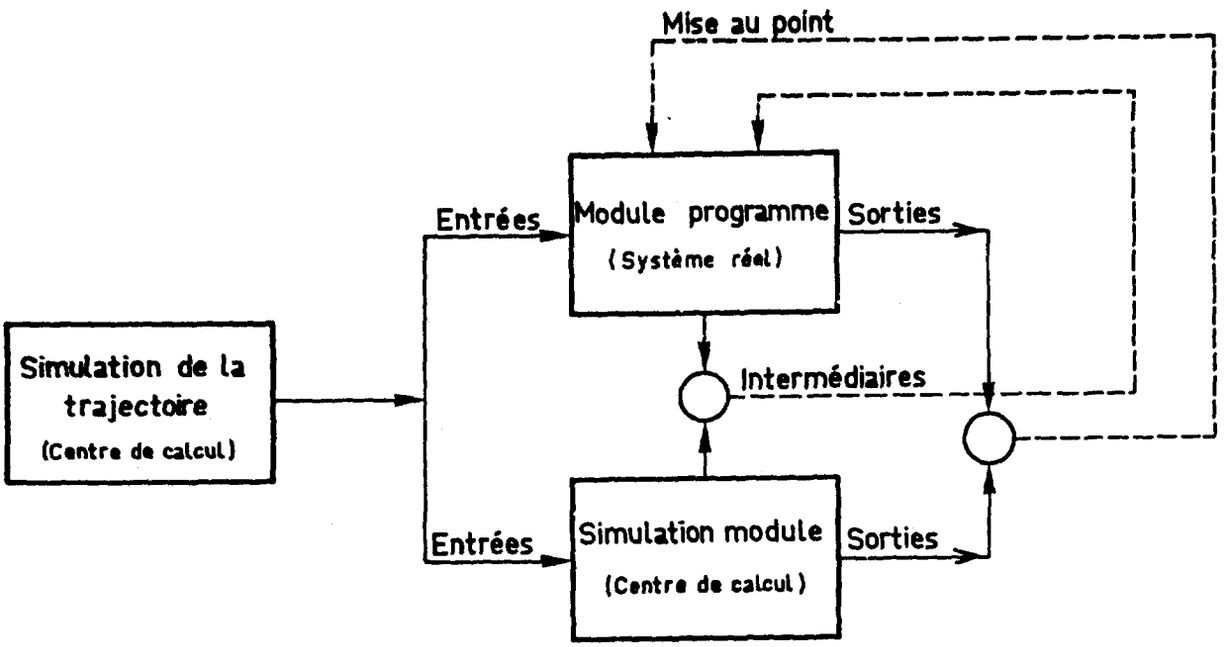

FIGURE 5 - TEST ET MISE AU POINT DES MODULES DE PROGRAMME DU SYSTEME REEL

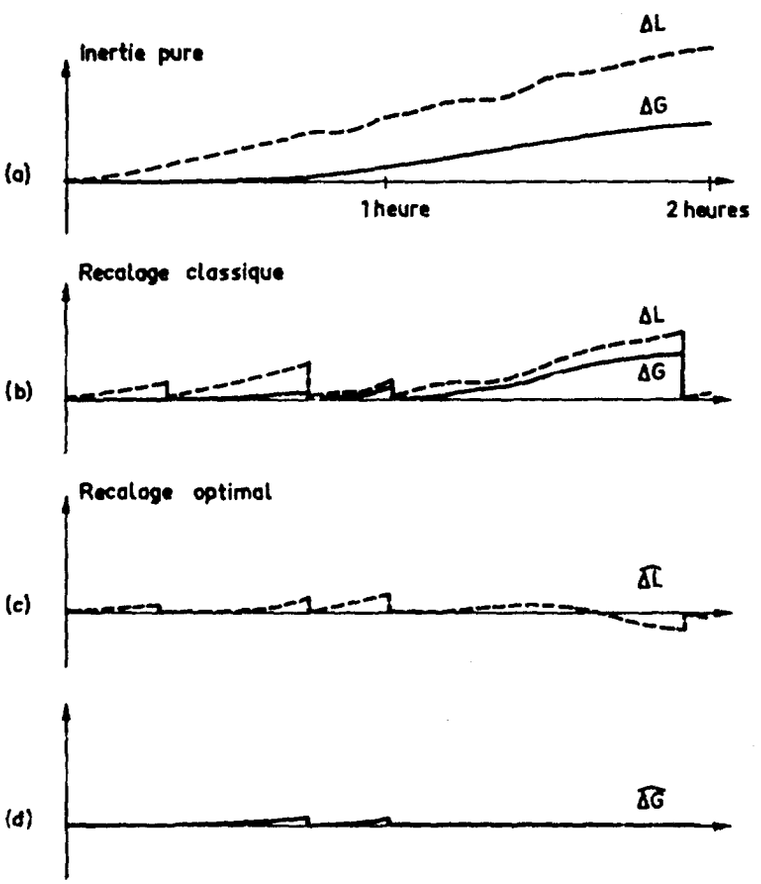

FIGURE 6 - INERTIE RECALAGE DE POSITION

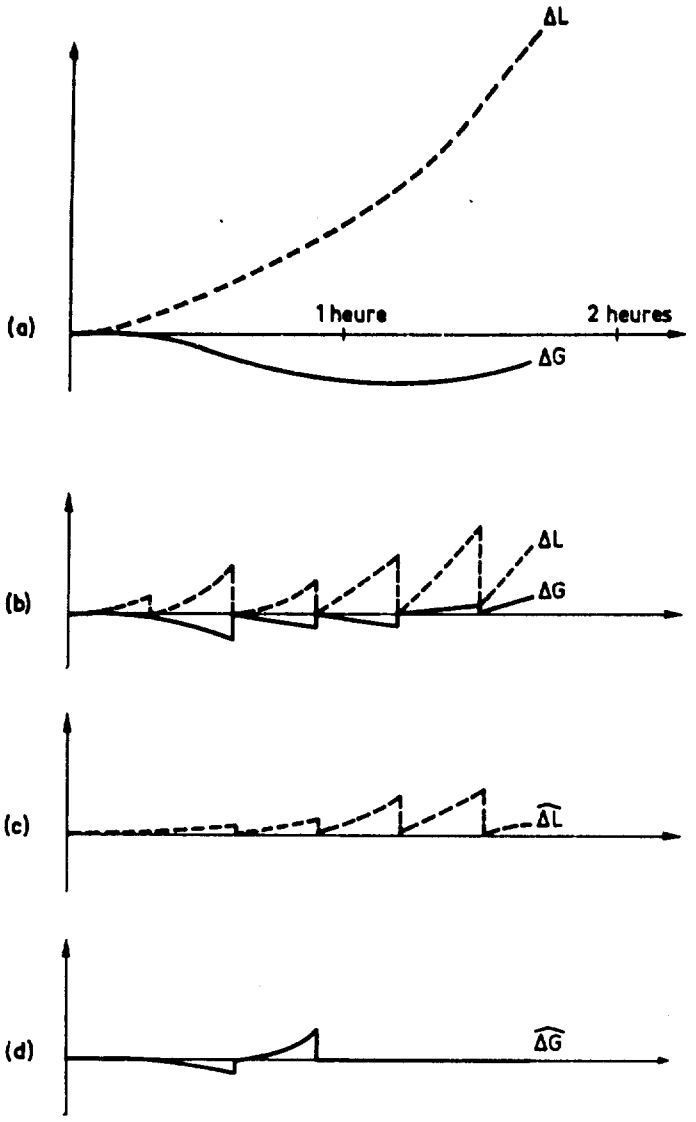

FIGURE 7 - INERTIE RECALAGE DE POSITION

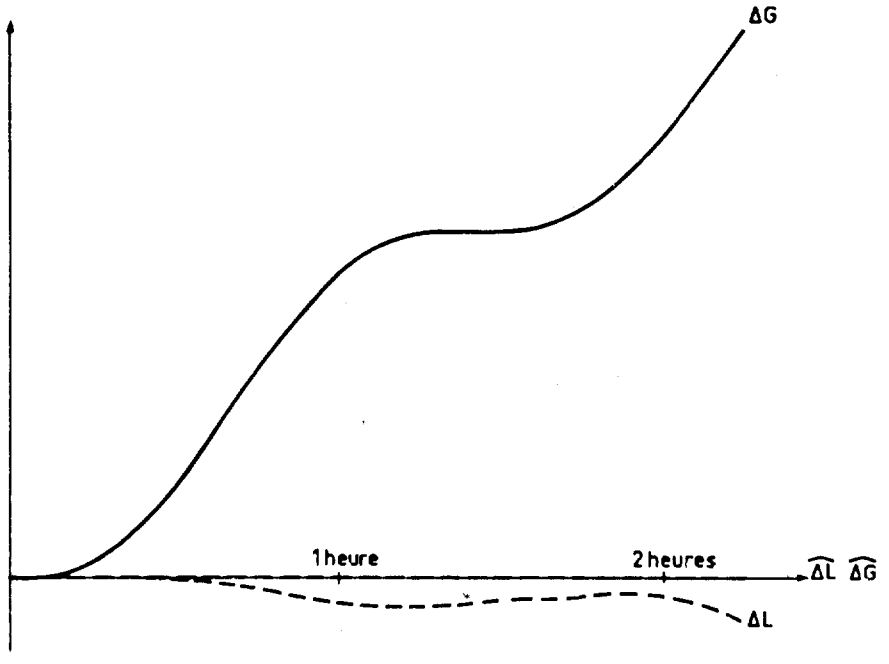

FIGURE 8 - INERTIE RECALAGE DOPPLER

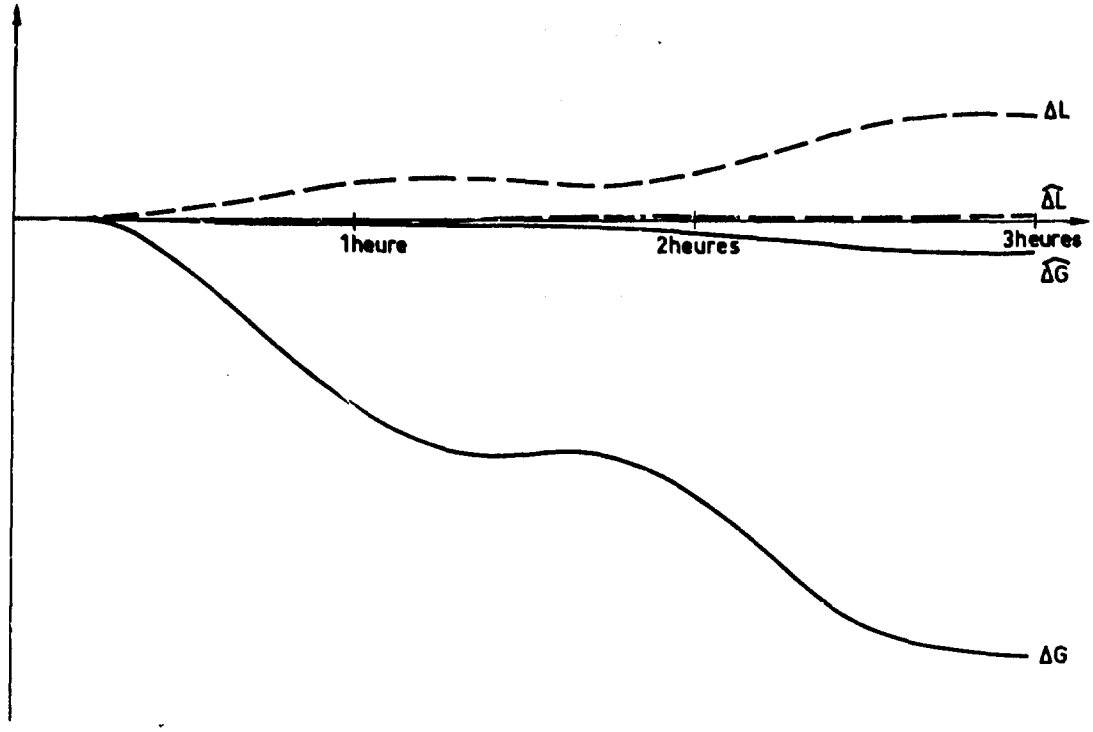

FIGURE 9 - INERTIE RECALAGE DOPPLER

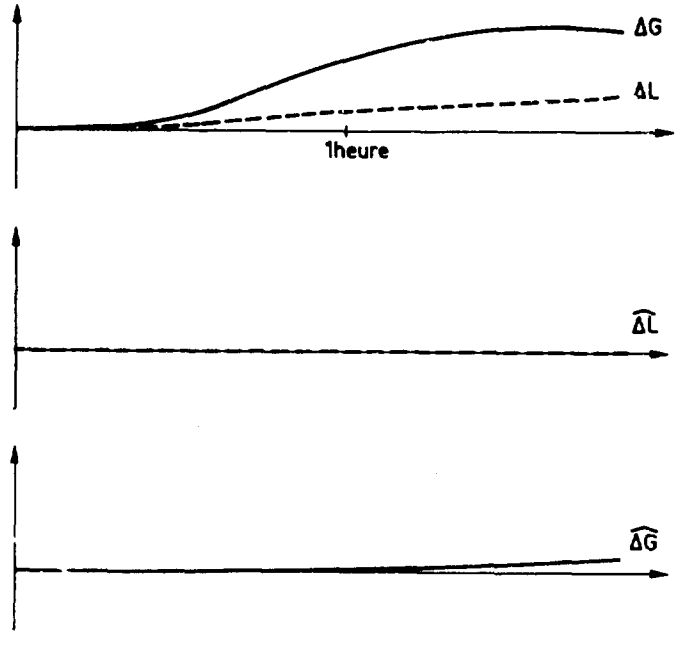

FIGURE 10 - INERTIE RECALAGE DOPPLER

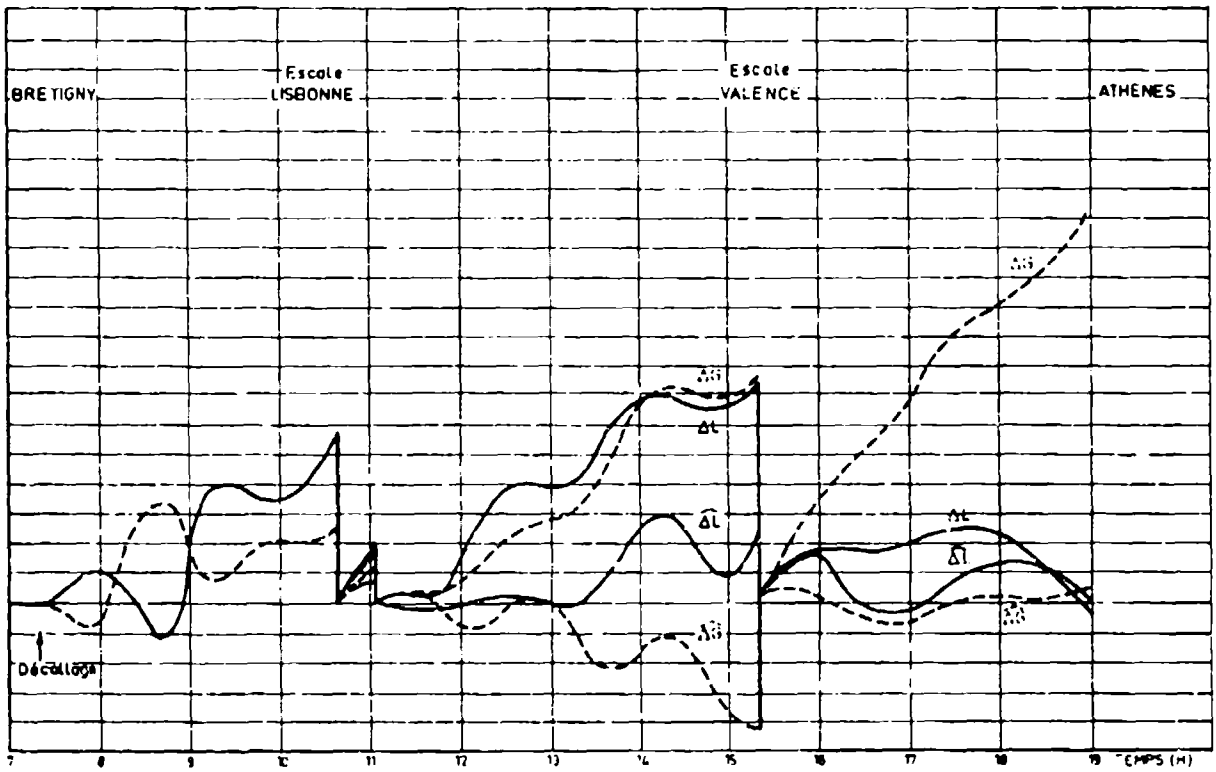

FIGURE 11 - V.I. BRETIGNY-ATHENES

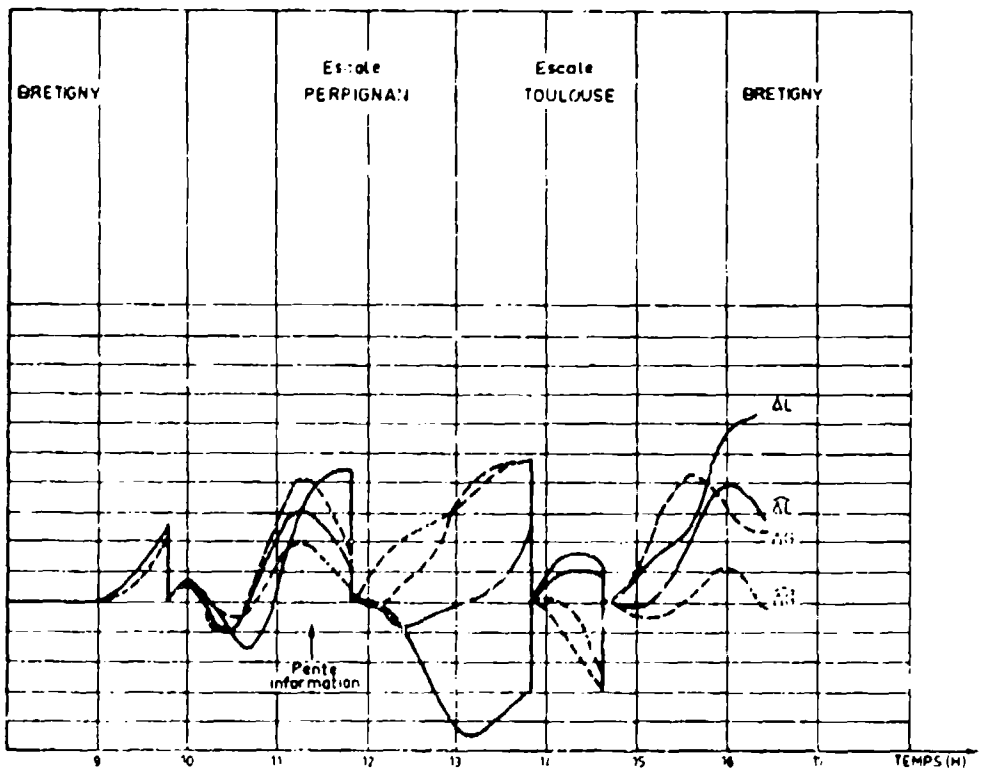

FIGURE 12 - V.I. BRETIGNY-BRETIGNY

On peut comparer sur ces courbes ce que donne l'inertie pure recalée classiquement (simple translation) par opposition au couplage optimal.

Les dérives sont estimées correctement, les oscillations de Schüler sont peu amorties, les recalages n'étant pas assez fréquents.

Cette série de vols a ainsi pu valider le filtre par comparaison des performances obtenues avec les courbes obtenues en simulation au cours de l'étude.

3. ALIGNEMENT RAPIDE D'UNE PLATEFORME A INERTIE

3.1 Généralités

Cette étude a été conduite de 1972 à 1974 sous contrat de la Direction des Pecherches et Moyens d'Essais.

Le but de l'étude était de valider complètement l'optimisation d'un alignement de plateforme sur un système à inertie réel en tenant compte de toutes ses caractéristiques. Le système choisi était une plateforme MGC 30, de la famille MGC des équipements SAGEM.

L'objectif fixé était de réduire de 30 % la durée totale de l'alignement. Les études théoriques ont montré qu'une réduction de 40 % pouvait être obtenue, résultat validé par l'expérimentation réalisée.

On connaît l'importance de l'alignement initial d'un système de navigation par inertie. En effet, toute erreur d'alignement se propage (en s'amplifiant plus ou moins) comme erreur de position, de vitesse et d'attitude au cours de la navigation.

L'alignement initial consiste à effectuer les opérations suivantes :

(1) introduire la position initiale,

(2) introduire la vitesse initiale par ses projections sur les axes calculateurs [c],

(3) aligner les trièdres plateforme [p] et calculateur [c] en faisant subir une rotation convenable à l'un ou à l'autre (éventuellement aux deux à la fois).

L'alignement peut être réalisé de façon externe en transférant à la plateforme une orientation connue par recopie optique et mécanique.

Il peut être réalisé de façon autonome en utilisant les instruments de la plateforme. Il s'agit alors de l'alignement par gyrocompas qui nous intéresse pour la suite.

3.2 Principes d'alignement et modélisation retenue

3.2.1 Principes

On désigne par $\vec{\varphi}$ la rotation faisant passer de l'orientation désirée pour la plateforme (triedre "vrai" [v]) à l'orientation effective de la plateforme (trièdre [p]). (voir figure 13).

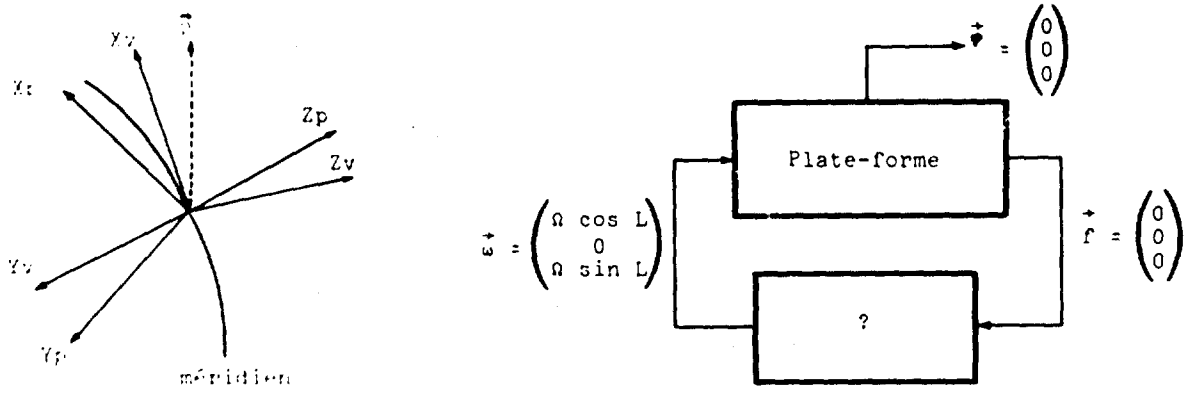

FIGURE 13 - ALIGNEMENT CLASSIQUE

Si la plateforme est parfaitement alignée ($\varphi_1 = \varphi_2 = \varphi_3 = 0$), les signaux accélérométriques sont :

$$f_1 = 0 \qquad (10)$$

$$f_2 = 0 \qquad (11)$$

$$f_3 = g \qquad (12)$$

et les signaux de commande des gyros maintenant la plateforme ainsi alignée sont :

$$\omega_1 = \Omega \cos L \tag{13}$$

$$\omega_2 = 0 \tag{14}$$

$$\omega_3 = \Omega \sin L \tag{15}$$

Deux approches permettent de réaliser l'alignement.

(1) Le point de vue classique est le suivant. L'alignement autonome va consister à faire un bouclage des instruments (voir figure 13) tel que l'état caractérisé par (10) à (15) soit le seul état d'équilibre stable du système ainsi réalisé. On demande en plus que cet état d'équilibre

(a) soit atteint le plus rapidement possible,

(b) ne soit pas affecté par les divers bruits perturbant le système.

Ces deux spécifications sont contradictoires et nécessiteront de faire un compromis rapidité-précision.

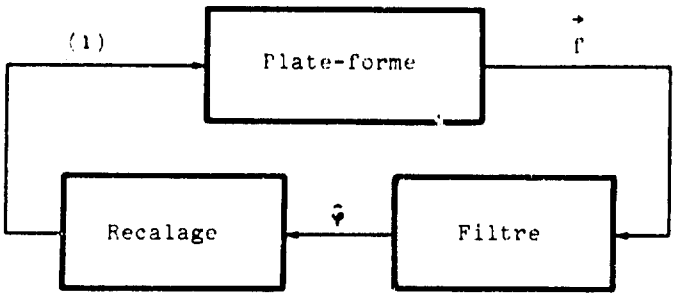

FIGURE 14 - ALIGNEMENT OPTIMAL

(2) Le point de vue optimal, de son côté, consiste à utiliser des modèles statistiques des divers facteurs aléatoires et à suivre le schéma de la figure 14.

Les observations $\vec{f}$ sont filtrées de façon à donner la meilleure estimée possible $\hat{\vec{\varphi}}$ de $\vec{\varphi}$: la plateforme est alors recalée en lui faisant effectuer la rotation $-\hat{\vec{\varphi}}$.

Cet alignement est optimal, car il assure à chaque instant la meilleure précision possible pour la durée écoulée.

3.2.2 Modélisation retenue

(1) Afin de valider au mieux la méthode, on n'a pas cherché à représenter par un modèle le transitoire thermique des gyros, l'alignement fin commençant après chauffage.

En ce qui concerne les dérives des gyroscopes E_1, E_2 et E_3, on suppose donc qu'elles sont constantes pendant l'alignement, mais inconnues ; elles obéissent ainsi au modèle

$$\dot{E}_1 = 0 \tag{16}$$

$$\dot{E}_2 = 0 \tag{17}$$

$$\dot{E}_3 = 0, \tag{18}$$

avec une moyenne nulle et pour écart-types

$$E\,(E_i^2) = \sigma_i^2, \quad i = 1, 2, 3.$$

(2) En ce qui concerne le modèle mathématique représentant les perturbations de l'avion, on a choisi

$$\begin{cases} \dot{\xi}_1 = -\beta \xi_1 + \nu_1 & (20) \\ \dot{\xi}_2 = \frac{1}{M} \xi_1 - \frac{f}{M} \xi_2 - \frac{k}{M} \xi_3 & (21) \\ \dot{\xi}_3 = \xi_2 & (22) \end{cases}$$

où

M = masse de l'avion

f = coefficient d'amortissement visqueux

k = raideur rappelant l'avion à la position d'équilibre (élasticité des pneus et des trains).

ξ_1 = force perturbatrice représentant l'effet du vent.

Cette force est modélisée par une suite d'échelons indépendants, d'amplitude aléatoire gaussienne centrée, de variance σ^2, modifiés à des instants distribués suivant une loi de Poisson de densité moyenne β.

La modélisation et l'estimation des mouvements parasites de l'avion impose une fréquence de calcul élevée compte-tenu de la dynamique de l'avion et entraîne donc une charge de calcul très importante ; de plus, ce modèle dépend du type d'avion sur lequel est installée la plateforme.

C'est ce modèle qui a été retenu pour la simulation des mouvements avion. Par contre, pour le filtre d'alignement, la simplification étant nécessaire, on a choisi un bruit blanc, modèle justifié par la nature aléatoire des sollicitations et par l'utilisation d'une fréquence de calcul en pratique plus faible que la fréquence propre avion.

(3) Si l'on prend comme vecteur d'état :

$$x' = [\varphi_1, \varphi_2, \varphi_3, E_1, E_2, E_3]$$

Il est possible de voir que le système dynamique ainsi constitué n'est pas observable à partir des signaux accélérométriques (voir référence [21] par exemple).

On est ainsi conduit à introduire la variable :

$$\Phi_3 = \varphi_3 + E_2 / \Omega_1 \qquad (23)$$

et les composantes Nord et Verticale E_N et E_Z de la dérive, la composante Est étant inobservable :

$$E_N = E_1 \cos \alpha - E_2 \sin \alpha \qquad (24)$$

$$E_Z = E_3 \qquad (25)$$

Le modèle est alors :

$$\dot{\varphi}_1 = \varphi_2 \Omega \sin L + \Phi_3 \Omega \cos L \sin \alpha + E_N \cos \alpha \qquad (26)$$

$$\dot{\varphi}_2 = -\varphi_1 \Omega \sin L + \Phi_3 \Omega \cos L \cos \alpha - E_N \sin \alpha \qquad (27)$$

$$\dot{\Phi}_3 = -\varphi_1 \Omega \cos L \sin \alpha - \varphi_2 \Omega \cos L \cos \alpha + E_Z \qquad (28)$$

$$\dot{E}_N = 0 \qquad (29)$$

$$\dot{E}_Z = 0 \qquad (30)$$

Les observations - qui sont les signaux accélérométriques - sont alors données par :

$$y_1 = -g \varphi_2 + V_1 \qquad (31)$$

$$y_2 = g \varphi_1 + V_2 \qquad (32)$$

où les V_i sont des bruits blancs et non le modèle (20) - (22) ainsi qu'il a été dit plus haut.

Les signaux accélérométriques arrivent au niveau du filtre, sous forme d'impulsions délivrées par les intégrateurs digitaux d'accélération (IDA). Les registres, qui contiennent ces impulsions, représentent des valeurs homogènes à des vitesses. Deux possibilités sont offertes : dériver les informations pour avoir des observations des variables d'état ou ajouter deux variables d'état et conserver ces informations comme observations. L'arrivée des impulsions en provenance des IDA peut avoir une fréquence du même ordre de grandeur, et même parfois beaucoup plus faible, que la fréquence de calcul (20 secondes d'arc d'inclinaison plateforme sur un axe génère l'arrivée d'une impulsion par seconde), le bruit de quantification est donc important et il faut en tenir compte dans les observations.

Avec le vecteur d'état :

$$x' = [\Psi_1, \Psi_2, \Phi_3, E_N, E_Z] \tag{33}$$

Les équations (23) à (27) s'écrivent :

$$\dot{x} = Fx \tag{34}$$

avec

$$F = \begin{bmatrix} 0 & \Omega \sin L & \Omega \cos L \sin \alpha & \cos \alpha & 0 \\ -\Omega \sin L & 0 & \Omega \cos L \cos \alpha & -\sin \alpha & 0 \\ -\Omega \cos L \sin \alpha & -\Omega \cos L \cos & 0 & 0 & 1 \\ 0 & 0 & 0 & 0 & 0 \\ 0 & 0 & 0 & 0 & 0 \end{bmatrix} \tag{35}$$

La solution, qui consiste à utiliser les sorties accumulées des IDA, étant préférable à celle qui utilise un algorithme de dérivation (à cause du bruit de quantification), les observations s'écrivent :

$$y_1 = z_1 + v_1 \tag{36}$$

$$y_2 = z_2 + v_2 \tag{37}$$

avec

$$z_1 = -g\Psi_2 \tag{38}$$

$$z_2 = g\Psi_1 \tag{39}$$

soit

$$y = h\,z + v \tag{40}$$

$$\dot{z} = Mx \tag{41}$$

avec

$$h = \begin{bmatrix} 1 & 0 \\ 0 & 1 \end{bmatrix} \tag{42}$$

$$M = \begin{bmatrix} 0 & -g & 0 & 0 & 0 \\ g & 0 & 0 & 0 & 0 \end{bmatrix} \tag{43}$$

Prenant le nouveau vecteur d'état

$$X = \begin{bmatrix} x \\ z \end{bmatrix} \tag{44}$$

Il vient

$$\dot{X} = \mathcal{F} X \tag{45}$$

$$y = \mathcal{H} X + v \tag{46}$$

avec

$$\mathcal{F} = \begin{bmatrix} F & 0 \\ M & 0 \end{bmatrix} \tag{47}$$

$$\mathcal{H} = [0 \;\; h] \tag{48}$$

La solution de ce système, obtenue en introduisant la matrice de transition associée à $\mathcal{F}$, s'écrit :

$$X(t) = \Phi(t, t_0)\, X(t_0) = \Phi(t, t_0)\, X_0$$

où la matrice de transition

Φ est telle que, $\mathcal{F}$ étant quasi constant.

$$\Phi(t,0) = e^{t\mathcal{F}} = 1 + t\mathcal{F} + \frac{t^2\mathcal{F}^2}{2} + \ldots$$

$$= \begin{bmatrix} \left(I + t\mathcal{F} + \frac{t^2}{2}\mathcal{F}^2 \right) & 0 \\ \left(tM + \frac{t^2}{2} M\mathcal{F}^2 \right) & I \end{bmatrix} = \begin{bmatrix} \Phi_{11} & 0 \\ \Phi_{21} & I \end{bmatrix} \qquad (50)$$

soit :

$$x(t) = \Phi_{11}\, x_0 \qquad (51)$$

$$z(t) = \Phi_{21}\, x_0 \quad \text{car} \quad z_0 = 0 . \qquad (52)$$

Les observations s'écrivent :

$$y = h\, z + v = h\, \Phi_{21}\, x_0 + v = H\, x_0 + v \qquad (53)$$

avec $$H = h(t)\, \Phi_{21}(t) \qquad (54)$$

Sous cette forme x_0 devient le nouveau vecteur d'état, que l'on va chercher à estimer au temps t ; cette méthode que l'on peut appeler "estimation du vecteur d'état initial", se résume donc à un modèle de la forme

$$x_0(t) = 0 \qquad (55)$$

$$y(t) = H(t)\, x_0 + v \qquad (56)$$

Au cours de la mise au point, il est apparu nécessaire de calculer la matrice d'observation H avec une approximation du troisième ordre pour tenir compte des termes qui deviennent significatifs au bout de quelque temps d'alignement, en particulier pour l'estimation de la dérive du gyroscope d'azimut.

3.3 Simulation des performances

Le programme qui permet d'évaluer les performances du filtre consiste à intégrer la matrice de covariance de l'erreur d'estimation. Pour l'étude de sensibilité, on a choisi une durée fixe d'alignement de 500 secondes et les valeurs typiques suivantes :

(1)	écart d'horizontale	1', 1σ
(2)	écart d'azimut	3°, 1σ
(3)	dérive du gyro Nord	0,025 °/h, 1σ
(4)	dérive du gyro d'azimut	0,1 °/h, 1σ
(5)	pas de calcul	5 secondes
(6)	bruit sur les observations	10^{-2} ms^{-1}, 1σ

Seules sont présentées les erreurs d'estimation sur Φ_3, E_N et E_Z, car les estimées de Ψ_1 et Ψ_2 convergent très rapidement.

On trouvera, ci-après, l'ensemble des courbes obtenues en faisant varier un des paramètres (figures 15 à 20).

En résumé, on peut dire que le filtre est sensible

(1) à la latitude du lieu d'alignement

(2) au bruit sur les observations

(3) à la durée du pas de calcul,

mais qu'il est insensible

(1) à l'écart initial d'horizontale,

(2) à l'écart initial d'azimut.

Il conviendra donc d'optimiser la programmation pour réduire la durée du pas de calcul, et d'ajuster au mieux le bruit blanc sur les observations qui représente les perturbations avion.

On choisit pour la durée de l'alignement fin 225 secondes qui correspond à une erreur finale de cap de 1,5 minute d'arc et 0,005 °/h d'erreur de compensation de dérive nord, pour un pas de 1 seconde. Dans une application opérationnelle, cette durée pourrait être définie en fonction de la latitude et doublée d'un test d'équilibre.

3.4 Algorithme d'alignement gros

L'alignement gros a pour but essentiel de dégrossir le cap, dans l'hypothèse où l'on n'a aucune information de cap initial, ceci afin de pouvoir appliquer l'hypothèse des petits angles qui est nécessaire pour pouvoir linéariser le système complet de l'alignement fin avec calibration de dérive du gyro Z.

Cet alignement gros peut de plus servir de base à un mode d'alignement rapide tolérant une certaine dégradation des performances de navigation.

Pour l'alignement gros, on choisit pendant le filtrage :

(1) de ne rien commander à la plateforme en verticale car son orientation étant inconnue, on ne peut compenser la rotation terrestre de façon utile et aussi parce que de cette façon, on élimine l'influence de la sensibilité thermique du facteur d'échelle des gyros de verticale,

(2) de compenser en azimut la rotation terrestre ce qui est en pratique nécessaire pour linéariser le système comme le montrent les équations ci-dessous.

En notation matricielle et dans le repère plateforme [p] en faisant intervenir les repères classiques calculateur [c] et géographique local [g], il vient [21] :

$$\omega_{c/i} = T_{p/g} \; \Omega_g \tag{57}$$

$$\omega_{p/i} = \Omega_{gz} + T_{p/g} \; E_g \tag{58}$$

$$\dot{\varphi}_p = \omega_{p/i} - \omega_{c/i} = T_{p/g} \; (E_g - \Omega_g) + \Omega_{gz} \tag{59}$$

Etant donné la durée très courte de l'alignement gros et les ordres de grandeur, on peut négliger la dérive gyro, alors

$$\dot{\varphi}_p = - T_{p/g} \; \Omega_g + \Omega_{gz} \tag{60}$$

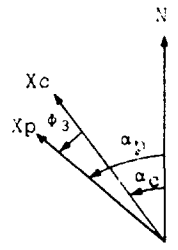

L'angle plateforme α_p étant totalement inconnu, pour simplifier on a choisi de caler [c] sur [p], c'est-à-dire

$$\alpha_c = 0 \tag{61}$$

et

$$\phi_3 = \alpha_p \tag{62}$$

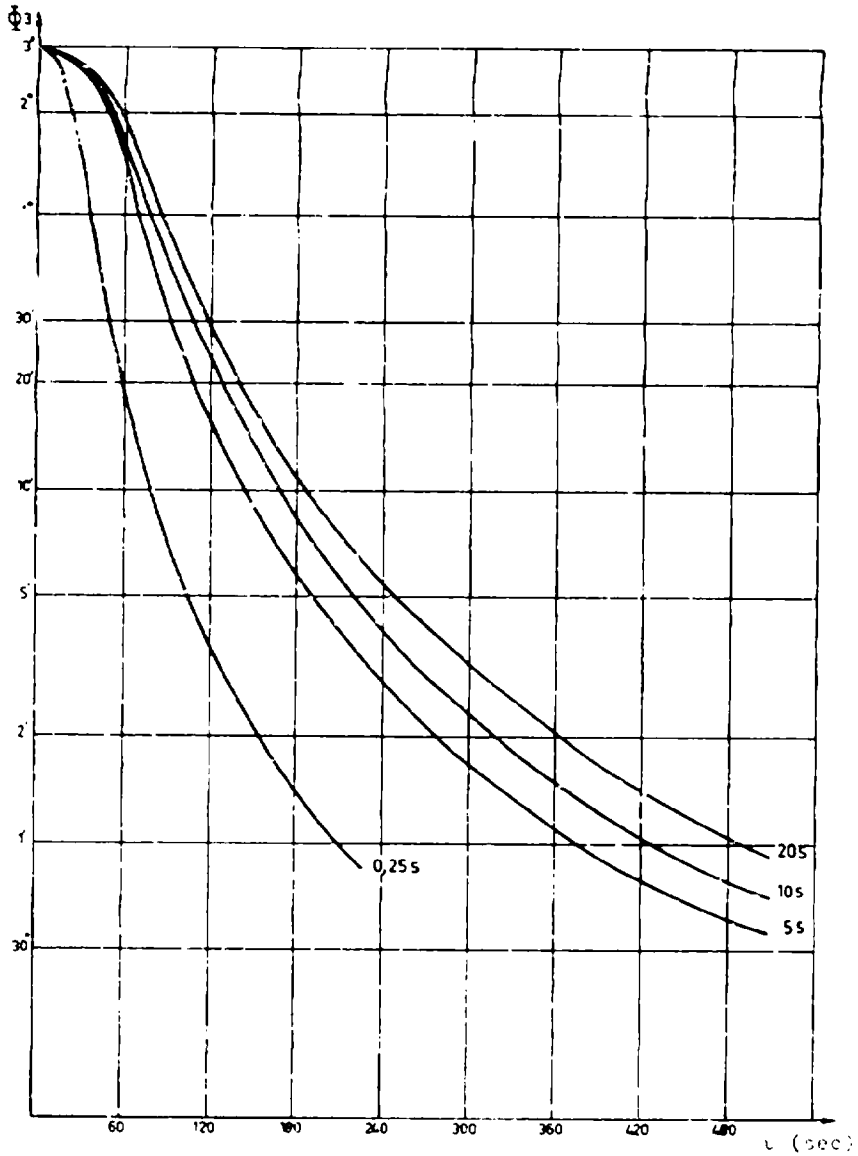

FIGURE 15 - INFLUENCE DU PAS

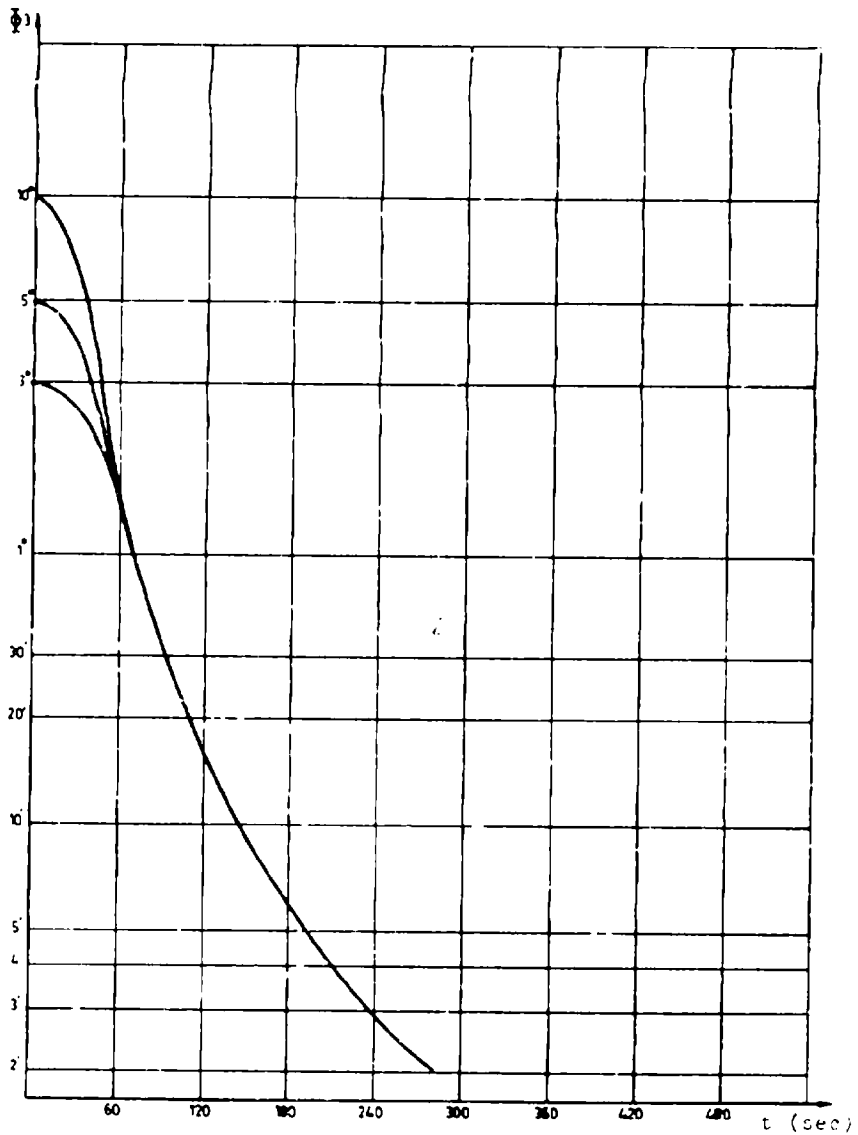

FIGURE 16 - INFLUENCE DE L'ECART INITIAL D'AZIMUT

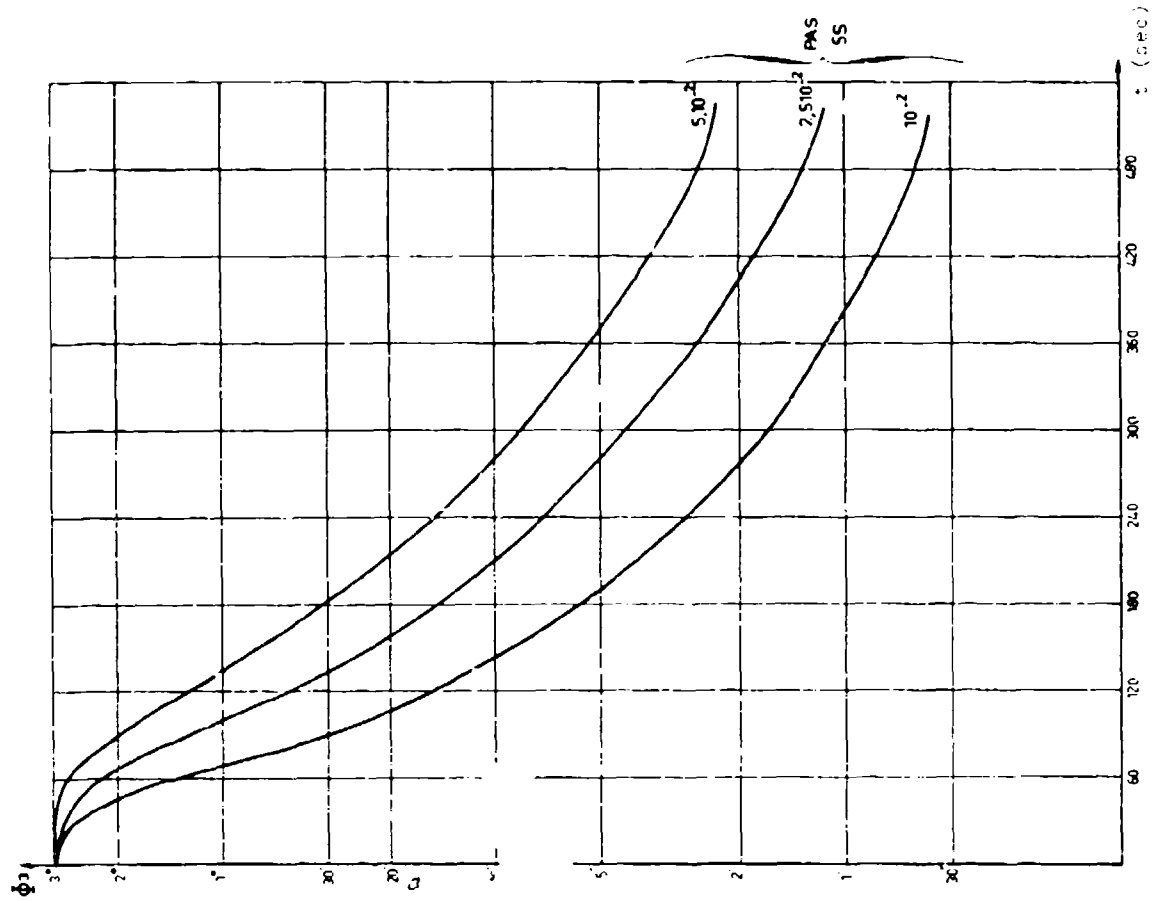
PAS
SS
5.10⁻²
2,5.10⁻²
10⁻²
t (sec)

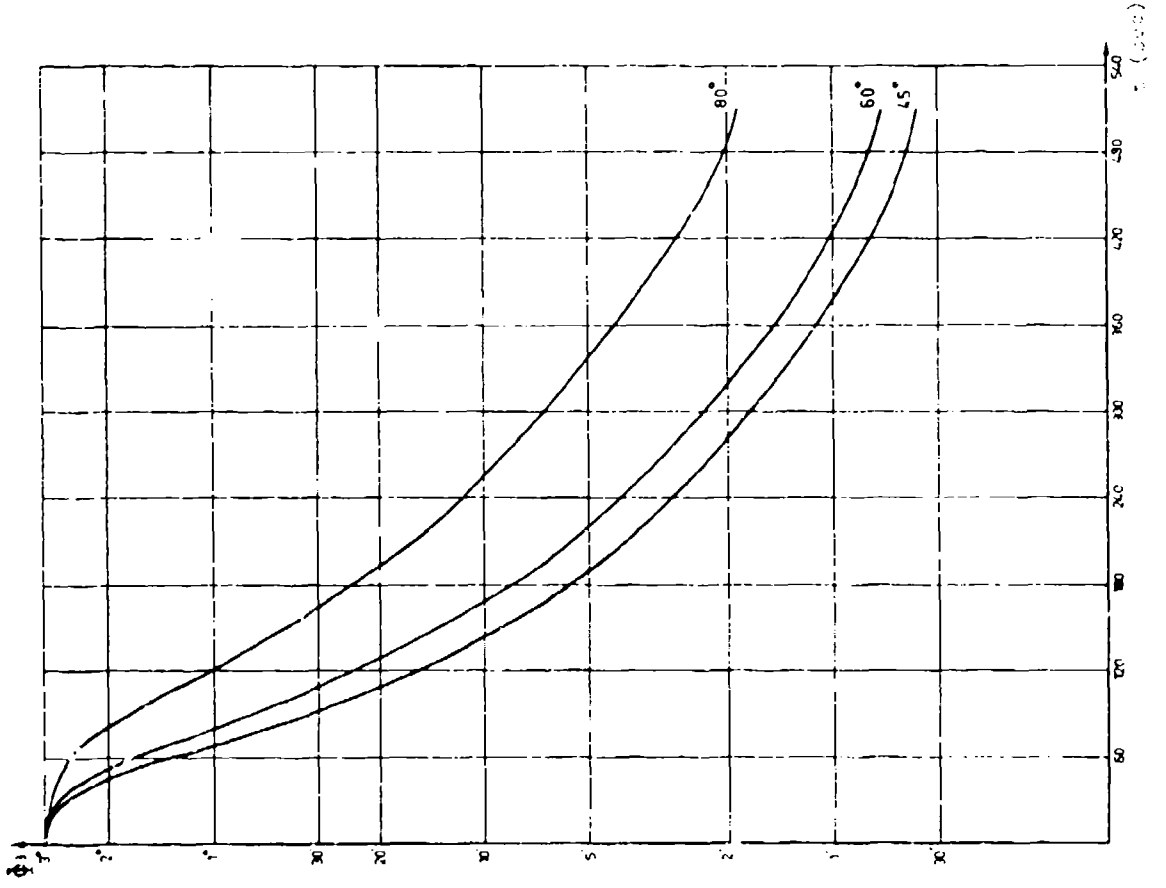
80°
60°
45°

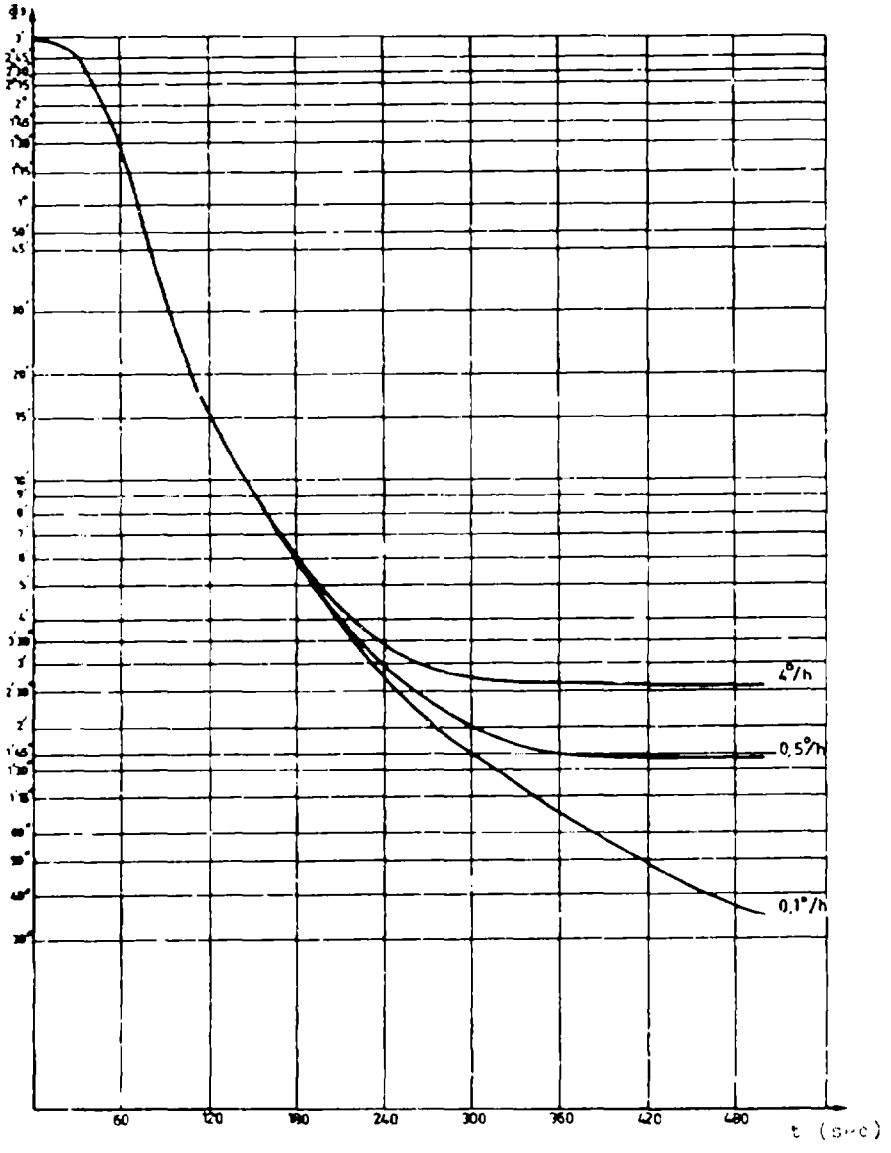

FIGURE 19 - INFLUENCE DE LA DERIVE B

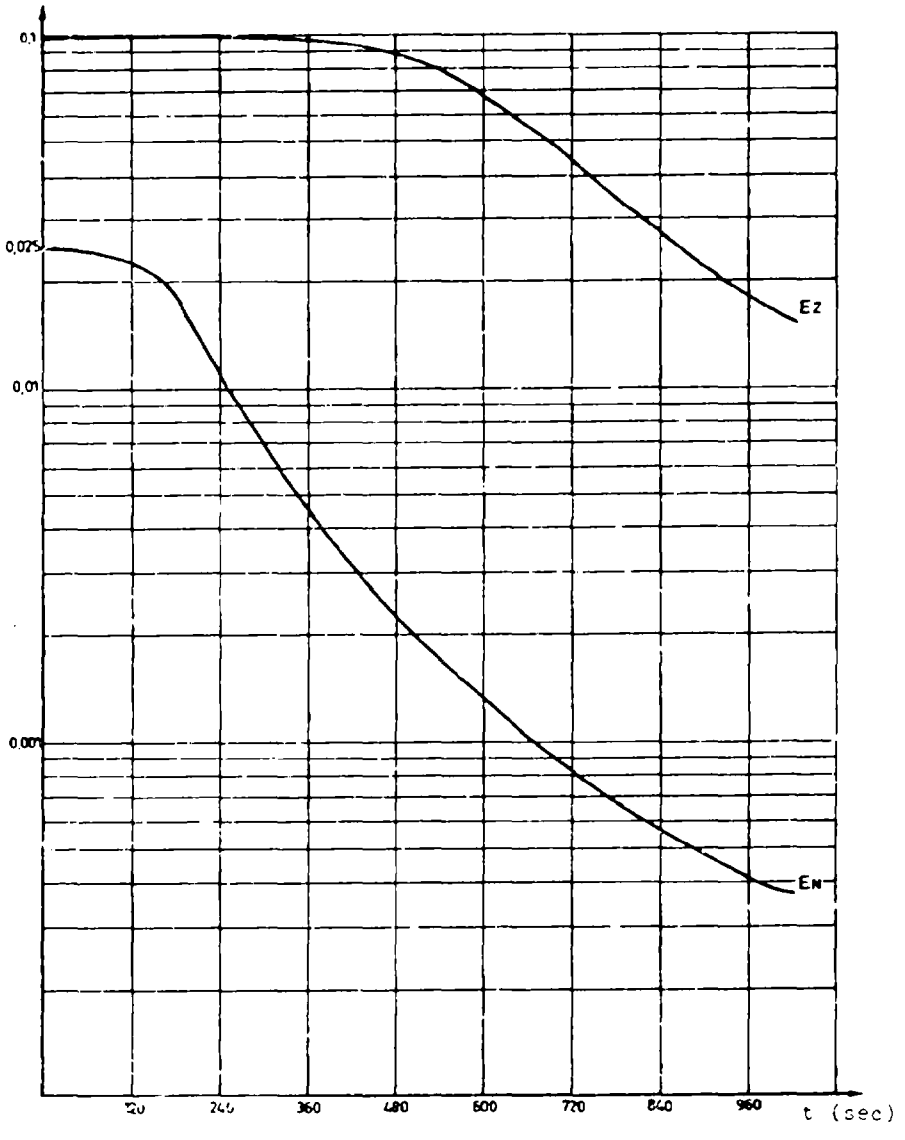

FIGURE 20 - ERREUR D'ESTIMATION DES DERIVES

La rotation qui fait passer [p] à [c] fait alors intervenir deux petits angles Ψ_1 et Ψ_2 et un angle quelconque Φ_3.

Dans ces conditions, les équations qui décrivent la dynamique de la plateforme deviennent :

$$\dot{\Psi}_1 = \Omega \sin L\, \Psi_2 - \Omega \cos L \cos \Phi_3 \quad (63)$$

$$\dot{\Psi}_2 = \Omega \sin L\, \Psi_1 + \cos L \sin \Phi_3 \quad (64)$$

$$\dot{\Phi}_3 = 0 \quad (65)$$

En posant :

$$X_5 = -\cos \Phi_3 \quad (66)$$

$$X_4 = \sin \Phi_3 \quad (67)$$

On obtient :

$$\dot{\Psi}_1 = \Omega \sin L\, \Psi_2 + \Omega \cos L\, X_5 \quad (68)$$

$$\dot{\Psi}_2 = -\Omega \sin L\, \Psi_1 + \Omega \cos L\, X_4 \quad (69)$$

$$\dot{X}_4 = 0 \quad (70)$$

$$\dot{X}_5 = 0 \quad (71)$$

L'estimation de l'angle α_p s'obtient alors par :

$$\hat{\alpha} = \text{Arc Tg} \frac{X_4}{-X_5} \quad (72)$$

L'avantage de cette approche est que le filtre a la même structure que celui de l'alignement fin, la matrice F étant :

$$F = \begin{bmatrix} 0 & \Omega \sin L & 0 & 0 & \Omega \cos L \\ -\Omega \sin L & 0 & 0 & \Omega \cos L & 0 \\ 0 & 0 & 0 & 0 & 0 \\ 0 & 0 & 0 & 0 & 0 \\ 0 & 0 & 0 & 0 & 0 \end{bmatrix} \quad (73)$$

3.5 Organisation du programme

3.5.1 Format de l'arithmétique

Le choix entre l'arithmérique en virgule fixe et l'arithmétique en virgule flottante, est dans le cas de cette expérimentation un problème très important, car le calculateur associé à la plateforme inertielle ne dispose d'aucune instruction qui permette simplement la programmation de la virgule flottante. Après une rapide étude de faisabilité, des simulations ont permis de vérifier que les calculs en virgule flottante pourraient être conduits en prenant un mot de 16 bits pour la mantisse et un mot de 16 bits pour l'exposant ce qui conduit à des précisions numériques satisfaisantes et à un pas de calcul de l'ordre de 1 seconde. Les figures 21 et 22 présentent les courbes obtenues à partir de simulations avec le DASH (voir section 4.2) dans le cas de l'algorithme d'alignement gros utilisant le flottant Univac (64 bits de mantisse) ou le flottant UTD simulé. Les sauts qui apparaissent correspondent aux perturbations aléatoires avion simulées dans le DASH conformément au modèle (20) à (22).

3.5.2 Recalage de la plateforme

A chaque fin de phase de l'alignement, on dispose de l'estimée de l'erreur d'horizontalité, et de l'estimée de α. Les taux de commande à appliquer aux gyroscopes se décomposent en deux termes :

(1) une partie pour la compensation de la rotation terrestre, ce terme restera constant jusqu'à une prochaine estimation de α,

(2) une partie pour rattraper l'horizontalité, ce terme devenant nul après la phase de recalage.

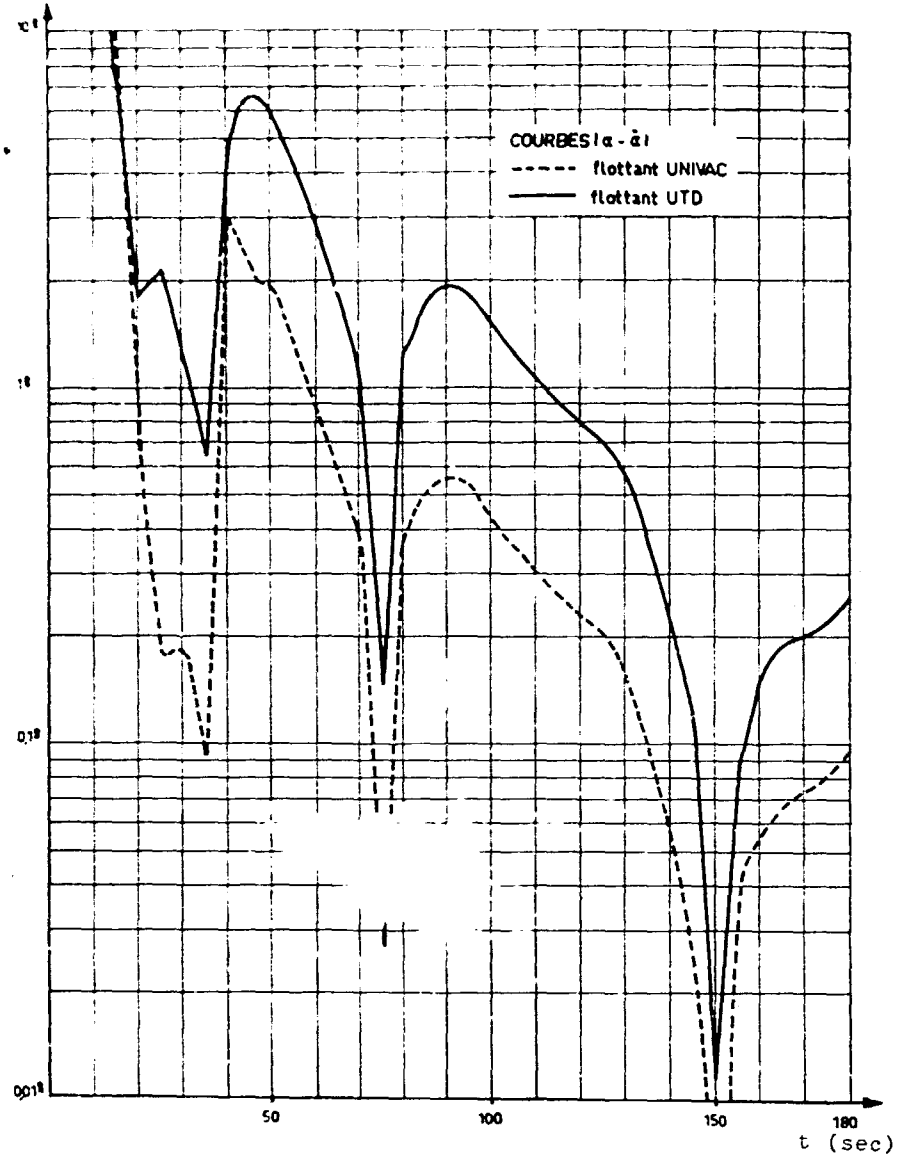

FIGURE 21 - ALIGNEMENT GROS (SIMULATION DASH)

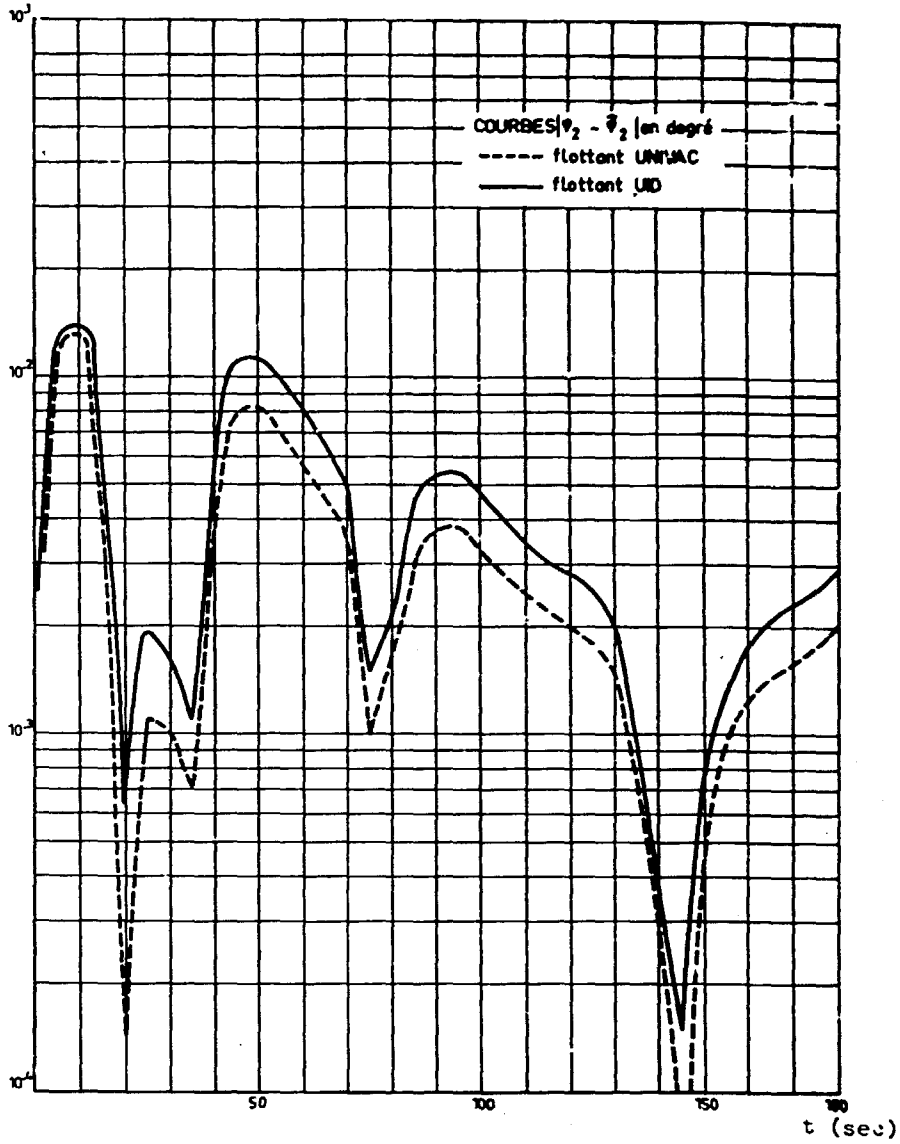

FIGURE 22 - ALIGNEMENT GROS (SIMULATION DASH)

3.5.3 Enchaînement des phases d'alignement

(1) le programme classique d'alignement de la plateforme inertielle MGC 30 utilisée pour l'expérimentation, se déroule de la façon suivante :

(a) chauffage rapide de la plateforme et calage de la plateforme sur le zéro des résolvers de chacun des axes.

Cette phase dure au minimum 136 secondes ; la phase suivante s'enchaîne si cette condition de temps est réalisée et si le chauffage rapide est terminé.

(b) calage analogique rapide.

De durée 8 secondes, cette phase consiste à asservir l'accéléromètre au zéro de son détecteur, en faisant précessionner les gyroscopes.

(c) alignement digital grossier.

Durée 190 secondes, ce premier filtre digital permet d'aborder l'alignement fin avec de bonnes conditions initiales.

(d) alignement digital fin.

Durée 672 secondes, ce filtre ne diffère du précédent que par des changements de gains.

(e) test de stabilité.

Durée 25 secondes

(f) Ready Nav.

La plateforme est alignée, le status indique alors l'estimée de la composante Nord des dérives des gyroscopes.

(2) Le programme d'alignement optimal comporte les deux premières phases (a) et (b) puis :

(c) alignement digital grossier de durée 80 secondes

(d) un recalage de la plateforme, dont la durée est inférieur à 10 secondes (ce qui correspond à 20 minutes d'arc d'inclinaison à rattraper).

(e) un alignement digital fin de durée 225 secondes

(f) un recalage de la plateforme de durée inférieure à la seconde.

Les temps comparés des deux méthodes conduisent à :

alignement classique ..... 1031 secondes = 17 minutes

alignement optimal ..... 450 secondes = 7,5 minutes

3.5.4 Caractéristiques du programme

La simplification de la programmation étant un souci constant, des programmes généraux qui permettent la manipulation des matrices ont été développés. La contrainte "temps de calcul" étant très importante dans ce problème, nous avons été amenés à optimiser les traitements, en testant par exemple, la nullité des opérandes pour n'effectuer que les opérations nécessaires.

Actuellement, la durée du pas de calcul en alignement gros et en alignement fin est de 1 seconde ; en soignant la programmation, on pourrait obtenir respectivement 0,5 seconde et 0,75 secondes, mais le coût de la programmation est non négligeable et la nécessité non encore démontrée.

Le volume mémoire utilisé pour réaliser ce filtre est de 1800 mots dont 550 mots nécessairement implantés en mémoire vive ; là encore, nous n'avons pas optimisé l'encombrement mémoire.

3.6 Résultats de l'expérimentation

La validité de l'alignement optimal programmé sur la MGC 30 a été établie par comparaison de résultats obtenus en laboratoire avec cet alignement et avec l'alignement classique de la MGC 30, le système étant chaud initialement dans les deux cas.

La qualité d'un alignement est caractérisé par celle de l'état d'équilibre de la plateforme qui en résulte. Un bon équilibre final suppose une bonne verticale, un bon cap

et une bonne compensation des dérivés gyros.

Deux types de vérifications ont été faits :

(1) un contrôle global d'équilibre

(2) un contrôle de la mesure du nord

3.6.1 Contrôle global d'équilibre

Les enregistrements présentés sur les figures 24, 25 et 26 permettent de comparer les deux méthodes. Ils représentent les sorties analogiques α_x et α_y des boucles accélérométriques en fonction du temps, après l'alignement. Ils caractérisent donc bien l'équilibre et montrent des dérives résiduelles globales de la plateforme, inférieures à 0,01 °/h dans les deux cas, pour les temps d'alignement de 1031 secondes en classique et 450 secondes en optimal.

3.6.2 Contrôle de la mesure du Nord

Les résultats du système ont été contrôlés par des mesures directes de l'erreur du Nord.

Les angles qui interviennent dans les différents calculs sont définis ci-dessous.

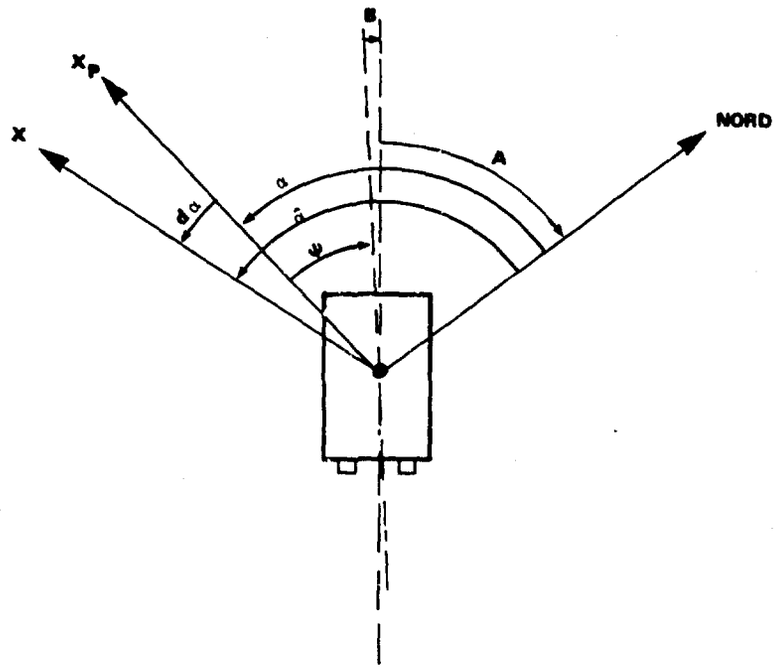

FIGURE 23 - CONTROLE DE LA MESURE DU NORD

Le boîtier plate-forme est monté sur un plateau diviseur. Son orientation A par rapport au Nord est donc lue directement ; la précision sur la connaissance du Nord est approximativement 2 minutes d'arc, mais ce qui importe est que A soit constant.

(1) Ψ angle entre l'axe du gyroscope G_X et le boîtier est mesuré avec une précision de 0,1 minute d'arc mais l'axe électrique boîtier peut différer par l'angle B de l'axe mécanique. Cet angle est constant et correspond à l'erreur de calage du résolver d'azimut.

(2) $\hat{\alpha}$, estimée de α, est donnée avec une résolution de 0,1 minute d'arc.

L'erreur $d\alpha = \hat{\alpha} - \alpha$ s'exprime par la relation

$$d\alpha = \hat{\alpha} + \Psi + B + A \qquad (74)$$

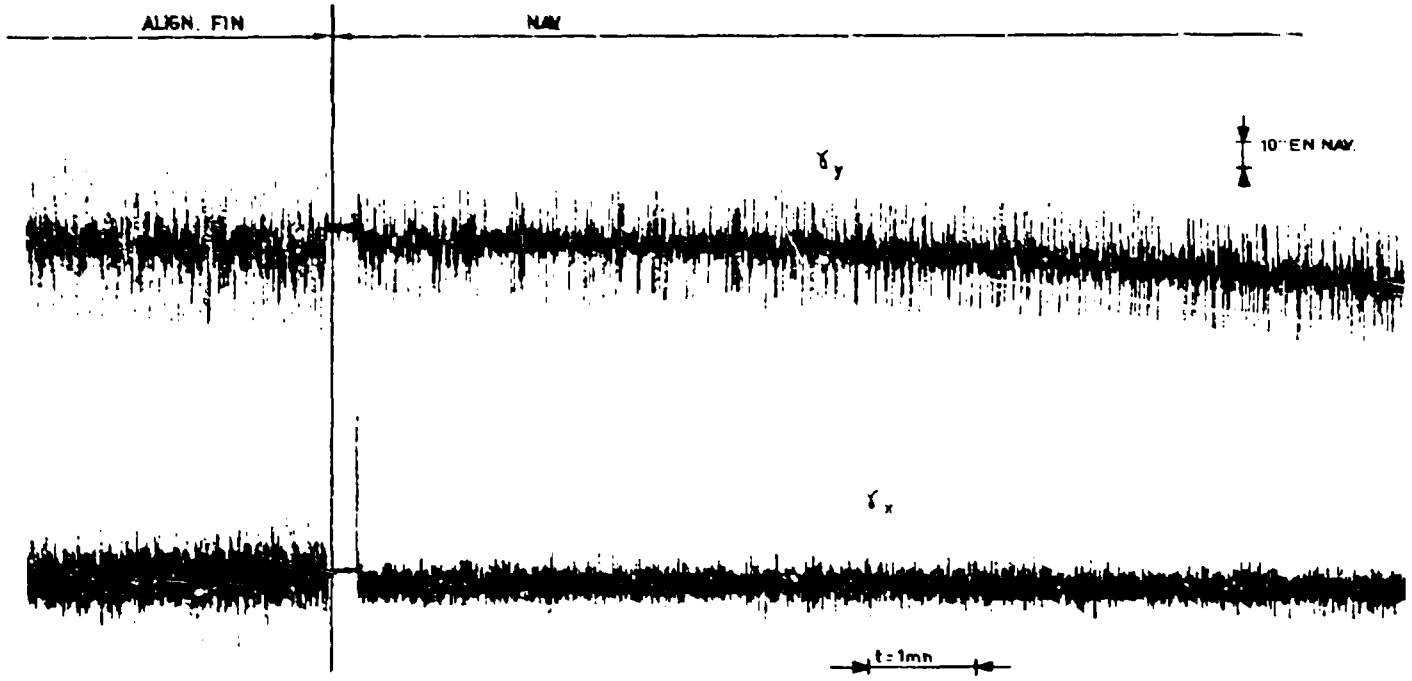

FIGURE 34 - ALIGNEMENT CLASSIQUE (OFF = SUD)

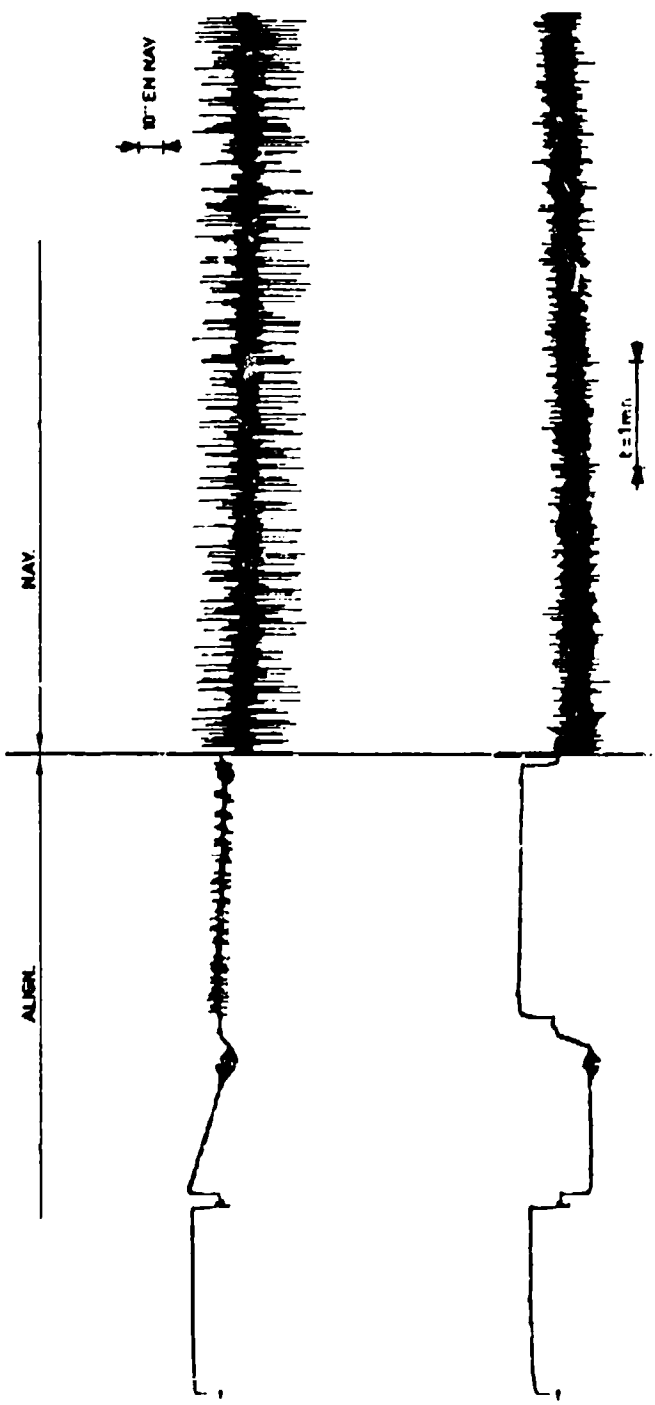

FIGURE 25 - ALIGNEMENT OPTIMAL (CAP = SUD)

Phase 1	Caging
Phase 2	Calage Analogique
Phase 3	Alignement Gros
Phase 4	Recalage Plate-Forme
Phase 5	Alignement Fin
Phase 6	Recalage Plate-Forme
Phase 7	Navigation

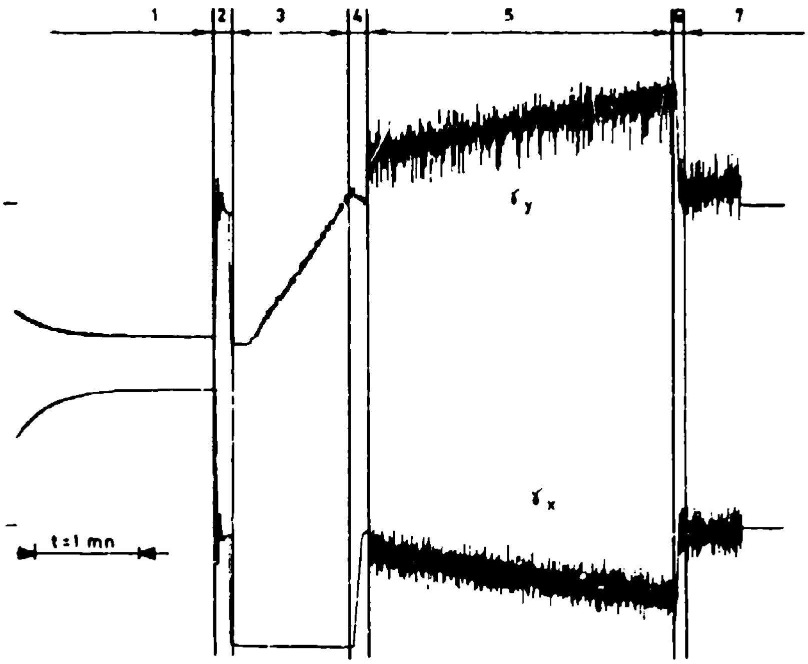

FIGURE [illegible] - ALIGNEMENT [illegible] ([illegible])

Une première série de 33 essais, a permis d'évaluer l'alignement classique, sur la connaissance de α. Les résultats sont les suivants :

$$\sigma_{\psi} = 7.8'$$

$$\sigma_{\hat{\alpha}} = 9.6'$$

$$\sigma_{d\alpha} = 6.7'$$

D'autre part, 21 essais d'alignement optimal ont donné pour résultats :

$$\sigma_{\psi} = 7.2'$$

$$\sigma_{\hat{\alpha}} = 9.7'$$

$$\sigma_{d\alpha} = 5.7'$$

Ces deux séries d'essais donnent donc des résultats comparables.

4. CONSIDERATION SUR L'INGENIERIE DES FILTRES

4.1 Méthodologie générale

Une méthode d'estimation récursive d'un paramètre à partir d'observations y_n est de la forme :

$$\hat{x}_n = f(\hat{x}_{n-1}, y_n) \qquad (75)$$

où x_n est la meilleure estimée de x compte tenu des observations $y_1, y_2, \ldots, y_n$.

La formule est dite récursive car la nouvelle estimée $\hat{x}_n$ est fonction seulement de l'observation présente y_n et de l'ancienne estimée $\hat{x}_{n-1}$, et ne fait pas intervenir explicitement les anciennes observations $y_{n-1}, y_{n-2}\ldots$ On voit immédiatement combien une telle formule est adaptée au calcul numérique en temps réel.

R.E. Kalman [3] a montré qu'il existe des formules d'estimation récursives linéaires si l'on cherche à estimer un processus gaussien-markovien x(t) à partir d'observations y dépendant linéairement de x et éventuellement bruitées par un bruit blanc. Il s'agit donc de donner une telle représentation markovienne au problème posé.

Lorsque le modèle est obtenu, il convient de simuler les performances du système optimal. Cette simulation consiste essentiellement à intégrer l'équation de Riccati du filtre optimal qui donne la covariance des erreurs d'estimation et par conséquent les performances du système optimal.

Dans la réalité cependant, le modèle mathématique n'est pas connu parfaitement. Le problème pratique important est celui de la sensibilité du filtre : quelles dégradations de performances sont entraînées par la mauvaise adaptation du filtre aux lois statistiques des paramètres traités ? Suivant les cas, les effets peuvent être faibles ou au contraire désastreux.

Enfin, la programmation du filtre peut poser certains problèmes. Le filtre optimal consiste essentiellement à intégrer l'équation de Riccati en même temps que l'équation générant la meilleure estimée $\hat{x}(t)$ de x(t).

Il se peut que le volume de calcul correspondant soit trop important et que l'on envisage une simplication des calculs par omission des termes qui semblent insignifiants ou par d'autres méthodes. Il convient dans ce cas de contrôler les dégradations de performances correspondant à ces simplifications.

Enfin, la programmation et la mise au point d'un programme qui peut faire quelques milliers d'instructions, ne sont toujours aisées. Il est nécessaire de faire appel à des méthodes de test évoluées, d'autant plus que la fiabilité recherchée est grande.

La démarche qui vient d'être décrite pour la conception d'un système de traitement optimal d'informations est résumée par l'organigramme de la figure 27. Dans la section 4.2 nous avons choisi de présenter une méthode de test et de mise au point de programmes de filtrage développée par SAGEM, renvoyant aux références pour les autres points.

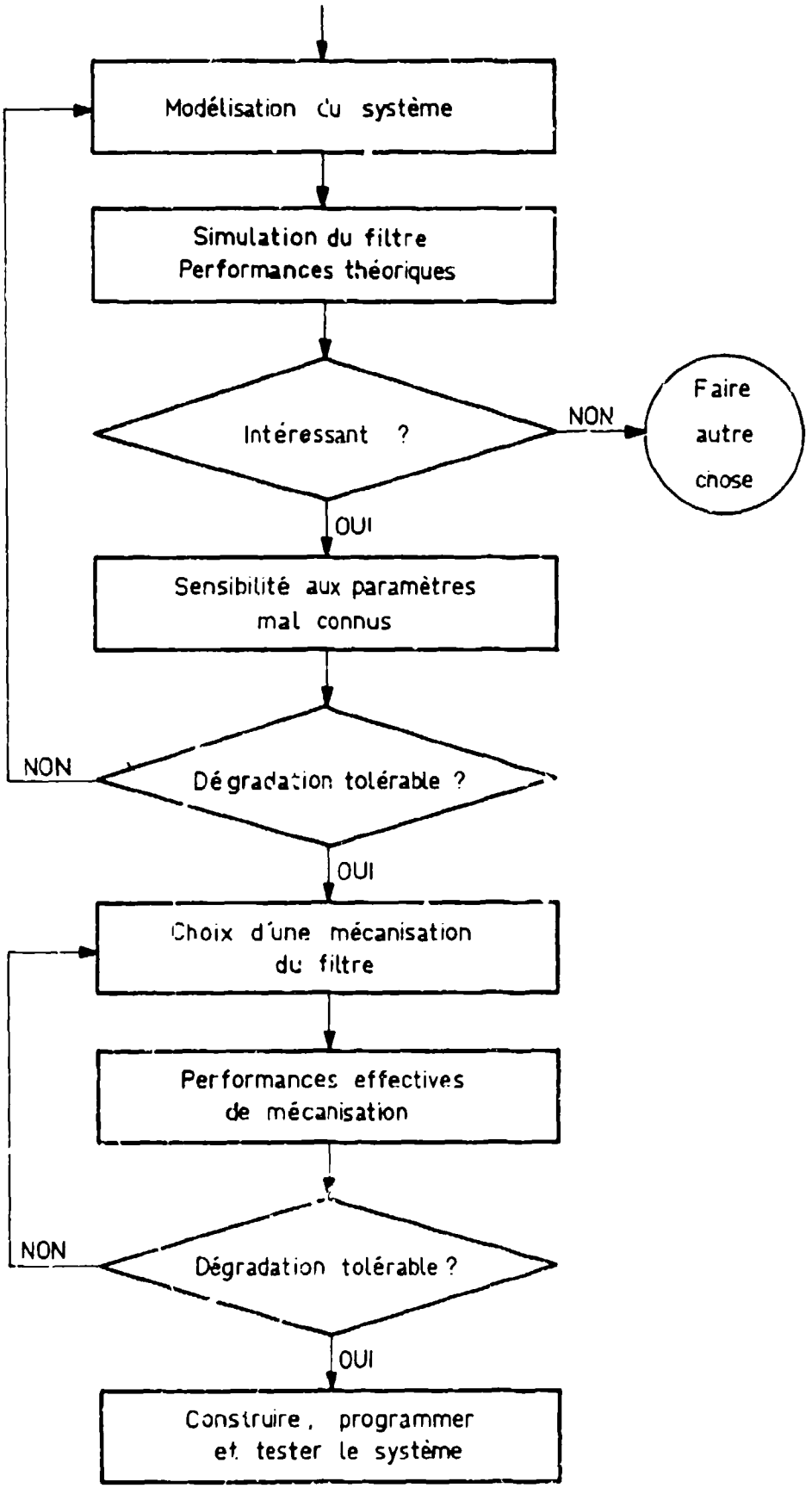
Modélisation du système
Simulation du filtre
Performances théoriques
Intéressant ?
NON
Faire
autre
chose
OUI
Sensibilité aux paramètres
mal connus
NON
Dégradation tolérable ?
OUI
Choix d'une mécanisation
du filtre
Performances effectives
de mécanisation
NON
Dégradation tolérable ?
OUI
Construire, programmer
et tester le système

4.2 Dispositif d'Aide à la Programmation des Systèmes Hybrides (DASH)

4.2.1 L'outil DASH permet de mettre au point et de contrôler le logiciel des systèmes hybrides.

En effet, le développement sur calculateur embarqué, des programmes de filtrage évolués (KALMAN), de systèmes hybrides est une opération difficile qui conduit en particulier à la simulation des performances du système envisagé, à des mises au point laborieuses, et qui pose, d'une manière générale, le problème de la qualification des programmes.

Les principales causes de ces difficultés sont :

(1) le manque de périphérique évolués,

(2) le manque de software d'aide à la programmation.

Après la période de mise au point, les essais "en vraie grandeur" apportent des informations qu'il faut analyser ; un mauvais fonctionnement peut provenir :

(1) d'erreurs de principe,

(2) d'erreurs de programmation non détectées,

(3) d'une mauvaise adaptation du filtre due :

  (a) à des erreurs de modèle

  (b) à une sensibilité trop grande

Pour résoudre ces problèmes d'étude, de mise au point et d'exploitation d'essais en vol et de leur bonne utilisation, l'expérience des systèmes hybrides a conduit la SAGEM à développer une méthodologie générale basée sur l'utilisation des ressources d'un ordinateur ; les deux grands objectifs étant de disposer (voir figure 28) :

(1) d'une simulation la plus réaliste possible pour effectuer l'étude, la mise au point du filtre et de sa programmation,

(2) d'un procédé d'enregistrement qui permette de "rejouer" un vol simulé ou réel, soit à travers le filtre programmé sur le calculateur embarqué, soit à travers le filtre théorique programmé sur ordinateur du centre de calcul.

Pour une application donnée, une fois l'étude de définition réalisée, l'utilisation pratique des outils de cette méthodologie se situe à trois niveaux :

(1) simulation sur ordinateur, qui permet :

  (a) de vérifier la validité des équations,

  (b) de démontrer les performances pour des trajectoires de vol typiques,

  (c) d'étudier la sensibilité du filtre.

(2) programmation du filtre ainsi défini sur le calculateur embarqué et mise au point en utilisant les trajectoires simulées et enregistrées sur bandes et en comparant les résultats avec ceux obtenus sur ordinateur.

(3) essais en vol avec enregistrement des sorties des senseurs et des résultats du filtre.

Si les performances ne sont pas suffisantes, les enregistrements en vol sont utilisés au centre de calcul pour contrôler les résultats et définir les modifications à réaliser.

De plus, dans le cadre d'une production en série de systèmes hybrides, cet outil peut servir à la réalisation des essais de recette au sol par contrôle des résultats obtenus sur une trajectoire type.

Le développement de cet ensemble d'aide à la programmation des systèmes hybrides comporte celui :

( ) d'un ensemble de modules de programmes sur ordinateur,

(2) d'équipement d'enregistrement compatible pour utilisation au sol et en vol.

4.2.2 De façon plus précise, le mini-ordinateur utilisé par le DASH recrée l'environnement du calculateur, par exemple simule une plateforme inertielle, un OMEGA, un Doppler, etc...

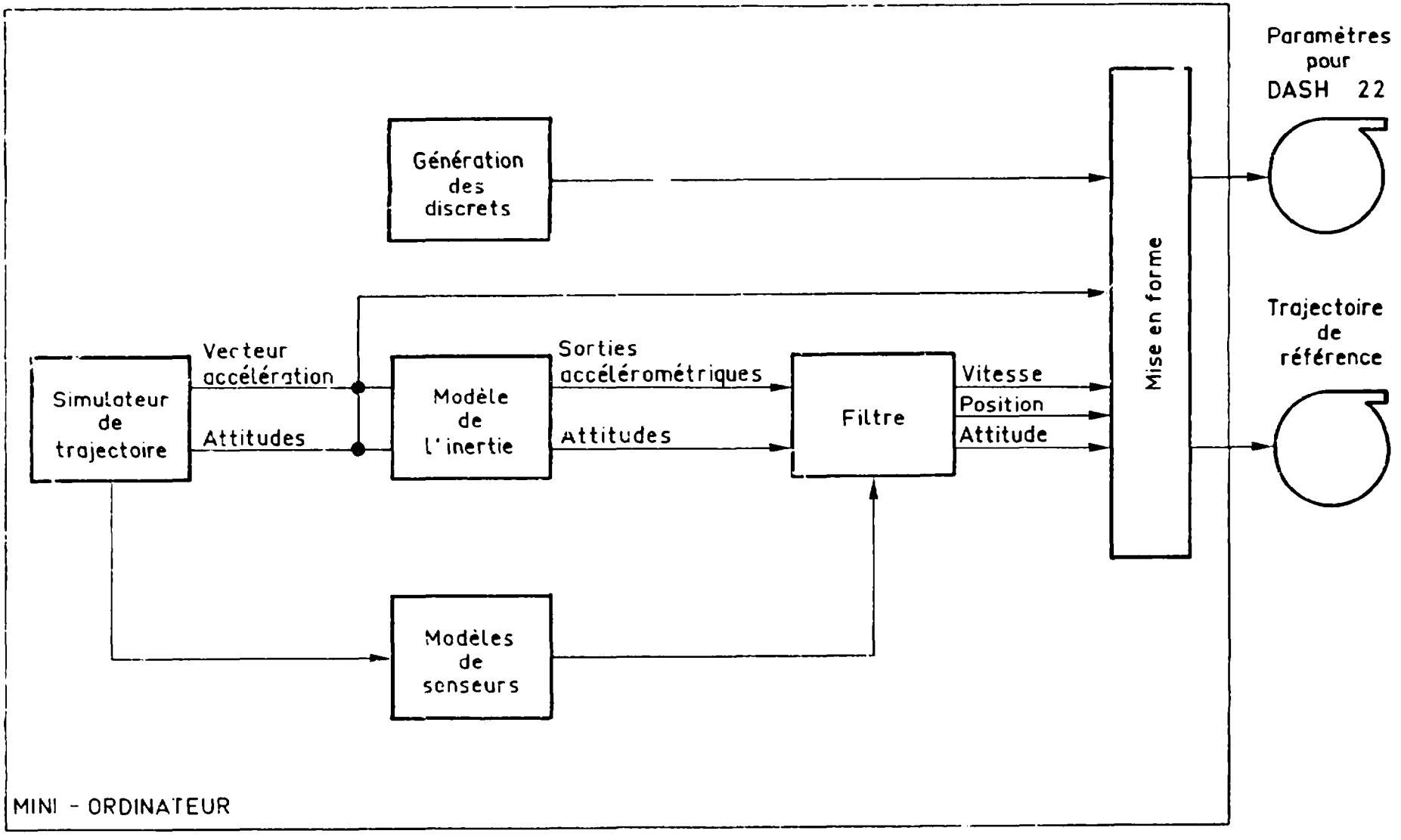
Paramètres
pour
DASH 22
Génération
des
discrets
Mise en forme
Trajectoire
de
référence
Simulateur
de
trajectoire
Vecteur
accélération
Attitudes
Modèle
de
l'inertie
Sorties
accélérométriques
Attitudes
Filtre
Vitesse
Position
Attitude
Modèles
de
senseurs
MINI - ORDINATEUR

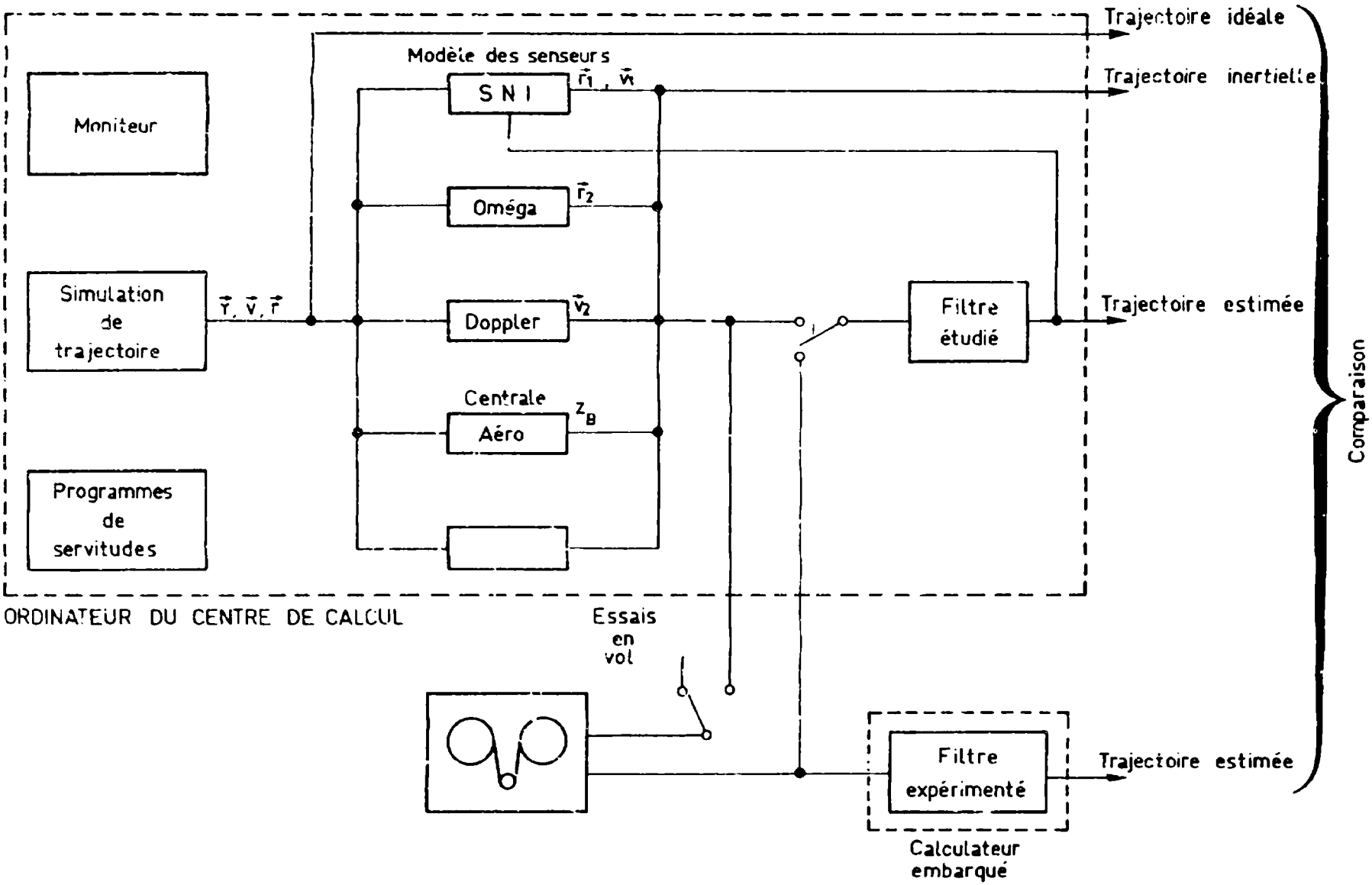

FIGURE 24 - ORGANISATION DU DISPOSITIF D'AIDE A LA PROGRAMMATION DES SYSTEMES HYBRIDES

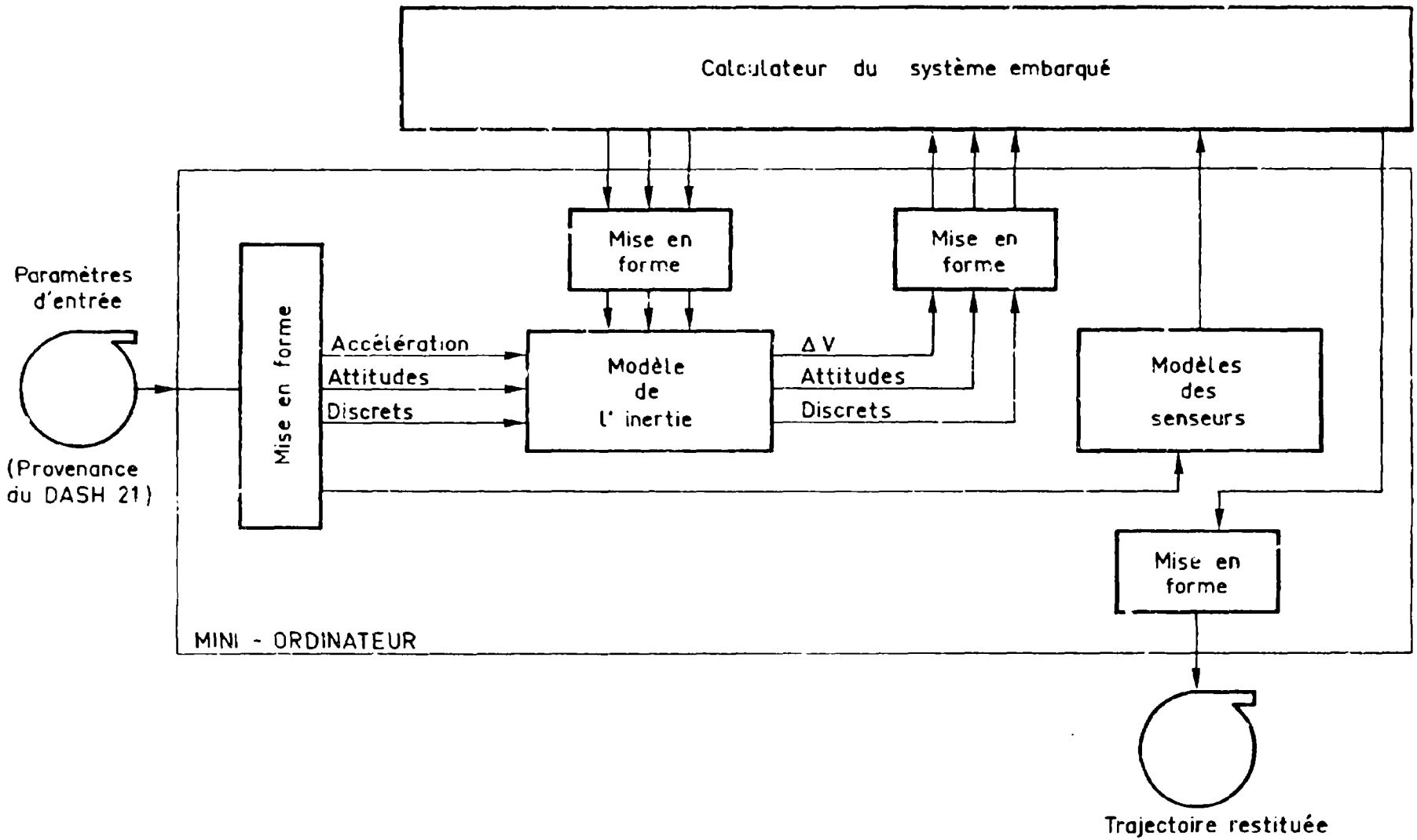
Calculateur du système embarqué
Mise en forme
Mise en forme
Paramètres d'entrée
(Provenance du DASH 21)
Mise en forme
Accélération
Attitudes
Discrets
Modèle de l' inertie
ΔV
Attitudes
Discrets
Modèles des senseurs
Mise en forme
MINI - ORDINATEUR
Trajectoire restituée

La validation du logiciel s'effectue en trois temps :

(1) élaboration d'une trajectoire de référence (DASH 21), voir figure 29.

(2) élaboration de la trajectoire restituée par le calculateur embarqué (DASH 22), voir figure 30.

(3) comparaison des trajectoires.

5. CONCLUSION

Nous avons présenté deux expérimentations concluantes et la méthodologie développée pour réaliser des filtres de navigation.

Il est clair aujourd'hui que la méthode de synthèse de filtres de Kalman est devenue "classique". La plupart des difficultés de réalisation ont été surmontées.

Restent à prévoir des améliorations ou des évolutions de technique sur au moins deux points :

(1) les méthodes d'identification des erreurs instrumentales, utilisées à ce jour sont souvent lourdes et coûteuses ; des filtres présentant certains caractères d'adaptativité seraient les bienvenus et sont en cours d'étude dans quelques centres.

(2) les méthodes d'état permettent non seulement de faire la synthèse de filtres optimaux, mais aussi de filtres numériques extrêmement simples, efficaces et bon marché; de nouveaux systèmes de navigation et de pilotage automatique utilisant ces filtres verront le jour dans un proche avenir.

REFERENCES

[1] C.E. SHANNON, W. WEAVER, The Mathematical Theory of Communications, Bell System Technical Journal, July, October 1948.

[2] Norbert WIENER, Times Series, The M.I.T Press, 1949

[3] R.E. KALMAN, A New Approach to Linear Filtering and Prediction Problems, Journal of Basic Engineering, p. 35-45, March 1960.

[4] R.E. KALMAN, R.S. BUCY, New Results in Linear Filtering and Prediction Theory, Journal of Basic Engineering, p. 95-108, March 1961.

[5] R.E. KALMAN, New Methods in Wiener Filtering Theory, Proc. of the First Symposium of Engineering Applications of Random Functions, Wiley, 1963.

[6] W.A. PORTER, L.F. KAZDA, Optimization of a Generalized Velocity Inertial System, IRE. Trans. on Aerospace and Navigational Electronics, p. 72-77 June 1961.

[7] K.J. ASTROM, Some Problems of Optimal Control in Inertial Guidance, IBM Research Paper, R.J. 229, November 15, 1962.

[8] W.A. BLUMHAGEN, Stellar Inertial Navigation Applied to Cruise Vehicles, IEEE Trans. on Aerospace and Navigational Electronics, p 235-246, September 1963.

[9] R.G. BROWN, D.T. FRIEST, Optimization of a Hybrid Inertial Solar Tracker Navigation System, IEEE International Convention Record, Vol 12, Pt. 7, 1964.

[10] R.E. BONA, C.E. HUTCHINSON, An Optimum Stellar-Inertial Navigation System, Navigation, Vol. 12, n° 2, June 1965.

[11] A. GELB, Synthesis of a Very Accurate Inertial Navigation System, IEEE Trans. on Aerospace and Navigation Electronics, p. 119-128, June 1965.

[12] P. POLACK, Exemples d'applications de procédés de navigation récursive, 16e Congrès International d'astronautique, Athènes, 1965.

[13] R.E. BONA, R.J. MAY, Optimum Reset of Ship's Inertial Navigation System, IEEE Trans. on AES, Vol. 2, n° 4, p. 409-414, July 1966.

[14] [illegible], The Impact of Statistical Estimation on Inertial Navigation, AGARD Symposium on Inertial Navigation, Oxford, September 21, 23, 1967.

[15] [illegible], Application of Kalman Filtering to Error Correction of Inertial Navigator, [illegible], 1967.

[16] [illegible], Case Study of Kalman Filtering in the [illegible] Navigation System, [illegible], University of Michigan, July 1968.

[17] H.W. SORENSON, On the Treatment of Inertial Measurement Unit Data in Optimal Linear Navigation Policies, IEEE Trans. on AES, Vol. 5, n° 3, p. 429-440, May 1969.

[18] P. FAURRE, F. GHEZ, Application du filtrage de Kalman au recalage d'un navigateur par inertie, Automatisme, Tome 14, n° 6, p. 229-234, Juin 1969.

[19] P. FAURRE, Système de Navigation à inertie optimisé, AGARD Symposium on Hybrid Navigation Systems, Delft, September 1969.

[20] P. FAURRE, Système de Navigation à inertie hybride optimisé Navigation, n° 79, p. 135-145, avril 1970.

[21] P. FAURRE, L. CAMBERLEIN, J.J. CHEVREUL, P. LLORET, C. MESSAN, Navigation inertielle optimale et filtrage statistique, Dunod 1971.

A SHIP TRACKING SYSTEM USING A KALMAN-SCHMIDT FILTER

Claude A. Darmon
Le Petit Monthélon
Acigné
35690
France

SUMMARY

This paper describes the digital processing of measurements at a high accuracy ship-tracking system. The errors affecting the azimuth measurement supplied by the measuring device of the ground-based station are found to be the most critical for the overall accuracy of the system. A Kalman-Schmidt filter is selected for an optimum estimation of the azimuth speed, following comparisons with a Kalman filter and an "averageing" filter. The estimation of the navigation parameters is described and the position and speed accuracy achieved by the system is calculated. Moreover, various effects resulting from the data processing in a computer are analyzed and optimized : for instance choice of the computation rate for the azimuth velocity, scaling of navigation parameters, etc..; finally, the programming of the data processing in a microcomputer is described and evaluated from two standpoints : memory space requirement and computation time. The results obtained confirm the efficiency of the solutions selected.

1. GENERALITIES

1.1 Purpose and Description of the Ship Tracking System (STS)

The purpose of the Ship Tracking System designed by "Laboratoire Central de Télécommunications" is to provide the pilots of large tanker-harbours with a synthetic aid to navigation in approach channels.

The data supplied to a ship pilot by the STS are (Figure 1) :-

(1) The position and speed of the ship along the channel.

(2) Its deviation from the imaginary axis of the channel, as well as its deviation speed.

With these ends in view, the STS processes the range and azimuth data provided by a radio frequency measuring device located on the shore, at, at a high altitude point in the vinicity of the harbour.

The data are processed optimally (as will be specified later on), in the computer of the ground-based station in which the measuring device is located and then, sent to the ship.

1.2. Navigation in the channel

The channel is considered as a sequence of segments smaller and smaller as the ship goes to the shore. Moreover, in the terminal area, the pilot can choose between several manoeuvers (anchoring, choice of a wharf, etc...).

In the case which is to be considered here, some specific points in the channel are taken as reference ; They are respectively 33 km, 22 km, 15 km, 12 km and 4 km far from the ground-based station.

1.3 Transmission of data between ground-based station and ship

1.3.1. Data transmitted from the ground-station computer to the display system

The data transmitted to the pilot when the ship is located between point x_i and point x_{i+1} are as follows:

(1) Manoeuver number (phase).

(2) Segment number (segment $x_i\ x_{i+1}$).

(3) e = distance from bridge center to segment $x_i\ x_{i+1}$.

(4) $\dot{e}$ = derivative of e with respect to t.

(5) L = distance from bridge center to point x_{i+1}.

(6) $\dot{L}$ = derivative of L with respect to t.

(7) Status (information on the system).

1.3.2 Data transmitted from the display system to the ground-based station computer

The above data are transmitted back to the ground-based station via the responder in order to ensure a reasonably good reliability of the transmission.

Besides, during phases where a choice is necessary, the pilot chooses his option. The instruction is then relayed to the ground-based station by pressing a specific key.

2. PRELIMINARY STUDIES

2.1 Specifications on data display rate and accuracy

The accuracy and rate of display of the navigation parameters selected are given in the table below; they result from a study carried out previously at LCT.

Displayed value	Rate	Accuracy
L	1 s	± 20 m
e	1 s	From 33 km to 12 km : ± 30 m Below 12 km : ± 10 m
$\dot{L}$	5 s	From 33 km to 12 km : ± 12,5 cm/s Below 12 km : ± 7.5 cm/s
$\dot{e}$	5 s	From 33 km to 12 km : ± 12.5 cm/s Below 12 km : ± 7.5 cm/s

2.2 Analysis of STS errors

The measuring device used by the STS provides the range and azimuth, in relation to the ground-based station, of the radio frequency responder placed on the ship bridge. The errors for which it is responsible are:

(1) Approximation errors such as systematic errors resulting from the curvature of the Earth and the parallax effect.

(2) Measurement errors resulting from radio frequency noise in the receiver. Such errors are to be found both in the range and azimuth channels.

(3) Disturbances due to non-zero accelerations on the ship.

2.2.1 Approximation errors

(1) Earth curvature effect:- The measurement carried out by the ground-based station is the straight line distance from this station to the ship responder. Assuming that there is no parallax effect, the error made at a distance of 40 km is approximately 10 cm.

(2) Parallax effect:- If we assume that the Earth is plane and if we take into account the fact that the responder is at least at 20 m above sea-level, whereas the station is at an altitude of 100 m, the error affecting the range measurement is 1.4 m over a distance of 2 km; this error decreases very rapidly as the distance increases and, in any case, can be disregarded in comparison with the other errors.

2.2.2 Measurement errors

(1) Range Tracking Loop:- The range tracking is performed by means of a mobile detection window located at the receiver output and generated by a pulse generator synchronized with that of the transmitter. The pulse frequency of the window is tuned up until it coincides exactly with the pulse sent back by the responder; The servo loop which achieves this automatic tuning is called a range tracking loop, it is demonstrated that the range tracking loop can be represented by the Fig. 2:

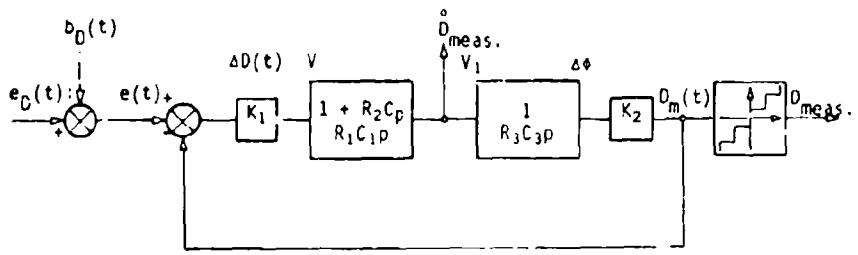

Figure 2: Range tracking loop.

The values represented are:

$e_D(t)$ = true position of the ship

$b_D(t)$ = position white noise induced by radio frequency noise

$\Delta D(t)$ = measured distance error

V = voltage passing trough the window

V_1 = control voltage of the pulse generator

$\Delta\phi$ = difference in phase between the window and the emitted pulse

D_m = distance measured (prior to quantization)

$D_{meas.}$ = quantized measured distance (2 m quantum)

The control loop compensation is chosen so that the closed loop transfer function be of the second order:

$$\frac{D_m(p)}{e_D(p)} = \frac{\omega_0^2 + 2\zeta\omega_0 p}{\omega_0^2 + 2\zeta\omega_0 p + p^2}$$

which enables it to recover the target in the case of a temporary signal loss.

In order to ensure a satisfactory operation of the overall measuring system both for acquisition and tracking, the parameters of the range-tracking loop are set in such a way as to ensure that the damping ratio $\zeta = 1$.

The value selected for ω_0 is 0.302 rad/s; for a ratio S/B = 20 dB, obtained for D = 33 km, it ensures a standard deviation σ_D of 0.55 m along the distance.

As σ_D is given by

$$\sigma_D^2 = \frac{5}{4}\omega_0 W_D$$

W_D being the energy level of the white noise $b_D(t)$, we easily derive $W_D = 1.41\ m^2/s$.

When the distances are smaller, W_D decreases, and, therefore, the lowest accuracy is to be found at 33 km. This statement will be proved later.

(2) Azimuth angle tracking loop:- The azimuth tracking loop, whose operation will not be described in detail here, can also be represented by a 2nd order transfer function, whose damping ζ is 1. The noises generated by the loop proper are negligible as compared to radio frequency noises.

The closed-loop transfer function is

$$\frac{A_m(p)}{e_A(p)} = \frac{\omega_0^2 + 2\zeta\omega_0 p}{\omega_0^2 + 2\zeta\omega_0 p + p^2}$$

$\zeta = 1$ and $\omega_0 = 2.23$ rad/s.

For various values of the distance between the ship and the ground-based station, the table hereafter gives the values of S/N_A of the angular error standard deviation σ_A, the energy level W_A of angular white noise, expressed in rad^2/s, and W'_A the corresponding energy level expressed in m^2/s.

DISTANCE km	S/B dB	σ A rad	W²A rad²/s²	W'A m²/s²
33	17.5	$0.26 \cdot 10^{-3}$	$2.43 \cdot 10^{-8}$	25.5
22	18	$0.25 \cdot 10^{-3}$	$2.24 \cdot 10^{-8}$	10.6
15	20	$0.20 \cdot 10^{-3}$	$1.43 \cdot 10^{-8}$	3.22
12	21	$0.18 \cdot 10^{-3}$	$1.15 \cdot 10^{-8}$	1.67
4	27	$0.09 \cdot 10^{-3}$	$0.29 \cdot 10^{-8}$	.047

2.2.3 Acceleration disturbances

Apart from the above errors, some disturbances affect the accuracy of the STS. Taking into account the choice which will be made for the estimator, such disturbances can be regarded as amounting to the ship accelerations.

If the ship is assumed to be moving with a constant acceleration during an estimation period -which will be shown later- the only statistical knowledge of the magnitude of the ship accelerations is sufficient

As a result of simulations carried out at LCT, it has been possible to quantify the maximum longitudinal and lateral accelerations of the ship changing its heading

(1) Lateral accelerations:- Fig. 3 shows the form of the responses obtained on the lateral speed v , for a 193,000 t, 350 m long, the "Esso Bernicia", after a 10° heading change. The ship was assumed to be equiped with an automatic pilot of the PD type with a lead of 25 s, and the rotation speed of the helm was limited to 2.5°/s.

The highest values determined for the lateral accelerations $\frac{dv}{dt}$ are

$$\left(\frac{dv}{dt}\right)_{max} = 10^{-2} \text{ m/s}^2$$

In practice, however, two phenomena have to be taken into account:

(a) At a constant speed, the maximum accelerations mentioned above are proportional to the turn. Now, most changes of heading hardly exceed 5°, as shown on Figure 4 which presents the return of the ship mentioned previously to its nominal trajectory after a 0.5 m/s step of current. (Instructions relative to the heading were fed manually during the simulation).

(b) Maximum accelerations, for a specified change of heading, are proportional to u^n, u being the longitudinal velocity of the ship and n a real number included between 1 and 2.

Considering these two phenomena, maximum values of lateral acceleration have been calculated for various positions of the ship. These values are indicated in Table 1.

(2) Longitudinal Acceleration:- When the ship sails at a constant engine rate, the variations of the longitudinal speed are very low for small angles of turn; longitudinal acceleration is then negligible in comparison to lateral accelerations. This does not apply to transient operating conditions. A reasonable value for the maximum longitudinal acceleration can be found by assuming that the ship, sailing initially at 7.5 m/s (15 knots) stops its propulsion abruptly.

The longitudinal acceleration prior to stopping the engine is

$$\theta = u_0 = \frac{F}{m} - Ku^2$$

in which

F is the thrust generated by the propellers

m the mass of the ship

K a coefficient of drag

The longitudinal acceleration after stopping the engine is

$$u_1 = - Ku^2$$

Therefore

$$u_1 = -\frac{F}{m}$$

A reasonable value for F is (cruising speed)

$$F = \frac{mg}{2000}$$

that is a deceleration of 5.10^{-13} m/s^2.

It should be pointed out that this deceleration is proportional to the square of the ship velocity.

The results obtained here have also been indicated on Table 1.

Table 1. Accelerations of the ship for several value of its distance from the ground-based station

DISTANCE km	SPEED m/s	ACCELERATIONS			
		LONGITUDINAL m/s^2	LATERAL m/s^2	RANGE CHANNEL m/s^2	AZIMUTH CHANNEL rad/s^2
33	7.5	5.10^{-3}	5.10^{-3}	5.10^{-3}	$1.50.10^{-7}$
22	7.5	5.10^{-3}	5.10^{-3}	5.10^{-3}	$2.30.10^{-7}$
15	6.5	3.10^{-3}	3.10^{-3}	3.10^{-3}	2.10^{-7}
12	6	2.10^{-3}	2.10^{-3}	2.10^{-3}	$1.65.10^{-7}$
9	2	$0,5.10^{-3}$	$0.5.10^{-3}$	$0.5.10^{-3}$	$1.25.10^{-7}$

3. DETAILED FORMULATION AND DESIGN

In order not to complicate unnecessarily the STS performance computations, we assume first that the estimation of the navigation parameters is performed continuously. Once the estimators have been chosen, their implementation in a discrete form is studied, as well as the resulting disturbances.

3.1 Selection of the variables of state

The simplest selection of the variables of state relative to the ship is the following:

x_0 = 1° Lambert coordinate of the responder

y_0 = 2° Lambert coordinate of the responder

$\dot{x}_0$ = derivative of x_0

$\dot{y}_0$ = derivative of y_0

and possibly the following derivatives of x_0 and y_0.

To reduce the task of the estimators, the number of variables of state has been brought down to 4; accelerations $\ddot{x}$ and $\ddot{y}$ have been introduced into the model whose nature is specified in section 3.2.2.

Althought the choice stated above seems to be logical a priori from a purely kinematic standpoint, the use of the azimuth (A) and distance (D) measurements provided by the measuring device may lead us to non-linear estimators since

$$A = \text{Arctg}\left(\frac{y_s - y_0}{x_s - x_0}\right) \qquad (1)$$

$$D = \sqrt{(y_s - y_0)^2 + (x_s - x_0)^2} \qquad (2)$$

Fortunately, A and D vary slowly in the particular application with which we are concerned, and, consequently, the variables of state of the system can be replaced by

$$A,\ \dot{A},\ D,\ \dot{D},$$

the azimuth and distance accelerations being regarded as disturbances.

The task which now remains for us consists in solving the following problem:

Determine the filter which provides the best estimates $\hat{A}$, $\dot{\hat{A}}$, $\hat{D}$, $\dot{\hat{D}}$ of A, $\dot{A}$, D and $\dot{D}$, based on the measurements A_m of A and D_m of D (or $\dot{D}_m$ of $\dot{D}$).

This problem will be solved by taking into account the following facts:

(1) The errors affecting A_m and D_m are completely uncorrelated.

(2) The accuracy of the measurements A_m and D_m obtained at the output of the measuring device is markedly higher than that requested in the specifications.

Thus, the initial filter is divided into:

(1) 1 filter providing the best estimate $\dot{\hat{A}}$ of $\dot{A}$

(2) 1 filter providing an estimate $\dot{\hat{D}}$ of $\dot{D}$

(3) No filters for the estimation of A and D which are estimated approximately by $\hat{A} = A_m$ and $\hat{D} = D_m$.

Besides, the filter (2) will not have to be optimal to meet the specifications, as will be demonstrated later.

3.2 Estimation of A, D, $\dot{A}$, $\dot{D}$

3.2.1 Estimation of D and A

Range and azimuth tracking loops provide D and A with much higher accuracy than required: As far as D is concerned, the error at 1 σ is 0.55 m at the worst (when the ship is 37 km away), whereas the error permitted by the specifications is up to 20 m.

As regards A, the error at 1 σ is 8.6 m at a distance of 33 km and 2.2 m at a distance of 12 km, whereas 30 m and 10 m errors, respectively, were allowed by the specifications.

Consequently, in the STS, D and A are only estimated by their respective measurements. This choice is also justified by reliability considerations, as will be shown further

3.2.2 Estimation of $\dot{D}$ and $\dot{A}$

Independance of range and azimuth channels

D and A can be estimated on two separate channels, as stated above; as a matter of fact, the ship which is being tracked can be described by the equations:

$$\frac{dA}{dt} = \dot{A} \qquad \frac{dD}{dt} = \dot{D}$$

$$\frac{d\dot{A}}{dt} = \gamma_A \qquad \frac{d\dot{D}}{dt} = \gamma_D$$

$$\gamma_A = 0 \qquad \gamma_D = 0$$

These equations are complemented by measurement equations assuming the following shape

$$A_{meas.} = A + b_A(t) \qquad D_{meas.} = D + b_D(t)$$

in which b_A and b_D are independent Gaussian white noises. Thus, the range and azimuth channels are independent of each other.

For the estimation of $\dot{A}$, the value $A_{meas.}$ is available at the computer input. An "optimum" filter has been calculated so as to extract the best estimation of $\dot{A}$. We will take up this point again later.

Estimation of $\dot{D}$

The same filter has been contemplated for the extraction of the best estimation of $\dot{D}$ based on the measurements $\dot{D}_{meas.}$; the estimation error of this filter is 6.3 cm/s at a distance of 33 km. As this error is much lower than that permitted by the specifications, a sub-optimal estimator was finally chosen.

This estimator operates directly from the output $\dot{D}_m$ of the range tracking loop and can be represented by the transfer function:

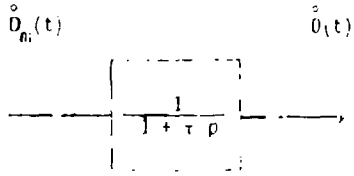

An optimisation of τ was carried out and provides

$$\tau = (\sigma_D/\sigma_{\gamma_D})^{1/2}$$

where σ_{γ_D} is the standard deviation of noise affecting D_m and σ_γ is the stanoard deviation of acceleration γ_D

The resulting estimation error of $\overset{\circ}{D}$ is

$$\epsilon_{\overset{\circ}{D}} = \sqrt{2\,\sigma_D\,\sigma_{\gamma_D}}$$

A constant gain structure was chosen for the estimator of $\overset{\circ}{D}$, with τ optimized at a distance of 33 km.

3.3 Estimation de $\overset{\circ}{A}$

The estimation of $\overset{\circ}{A}$ is the critical point of the STS. The overall accuracy of the system depends strongly on this estimation; this is the reason why it should be performed as accurately as possible.

We will consider successively the implementation of a standard Kalman filter, of a Kalman-Schmidt filter, and, finally, of an averageing filter.

3.3.1 Kalman Filter

(1) Calculation of the filter and its gains

The first solution which occurs to us as regards the processing of the data provided by the azimuth tracking loop is to feed them into a Kalman filter:

We can try to put down

$$\frac{dA}{dt} = \overset{\circ}{A} \quad , \quad \frac{d\overset{\circ}{A}}{dt} = \gamma_A \quad , \quad \gamma_A = 0$$

in the form $$\dot{x} = Fx \qquad (3)$$

with $x^T = [A, \overset{\circ}{A}]$

and the measurements $A_m(t)$ in the form: $y = Hx + v(t)$ (4)

H being [1,0] $v(t)$ being the azimuth measure noise;

$v(t)$ is the output of the azimuth loop excited by the only white noise $b_A(t)$ whose level is $W_A(t)$.

If we assume that the bandpass of the Kalman filter will be much narrower than that of the azimuth tracking loop, it is logical to regard $v(t)$ as identical with $b_A(t)$; consequently, we have

$$E(v(t)\ v(\tau)^T) = R(t)\ \delta(t-\tau) = W_A(t)\ \delta(t-\tau) \qquad (5)$$

Consequently, equations (3) and (4) assume a canonical shape and $x(t)$ is estimated by the following Kalman filter:

$$\dot{\hat{x}}(t) = F(t)\cdot\hat{x}(t) + K(t)[y(t) - H(t)\,\hat{x}(t)] \qquad (6)$$

The estimation error of the covariance matrix $P(t)$ is a solution of the equation

$$\dot{P}(t) = F(t)\,P(t) + P(t)\cdot F(t)^T - K(t)\,R(t)\,K(t)^T \qquad (7)$$

where the gain matrix $K(t)$ is defined by

$$K(t) = P(t)\,H(t)^T\,R(t)^{-1} \qquad (8)$$

The solution of equation (7) is achieved by solving the following linear equation

$$\frac{d}{dt}[P(t)^{-1}] = [P(t)^{-1}]\cdot F(t) - F(t)^T\cdot[P(t)^{-1}] + H^T(t)\cdot P(t)^{-1}\cdot H(t) \qquad (9)$$

We find that

$$P(t)^{-1} = \begin{bmatrix} \alpha + \frac{t}{R} & -\frac{t^2}{2R} + \alpha t + \beta \\ -\frac{t^2}{2R} + \alpha t + \beta & \frac{t^3}{3R} - \alpha t^2 - 2\beta t + \gamma \end{bmatrix} \qquad (10)$$

and therefore

$$P(t) \sim \begin{bmatrix} \frac{4R}{t} & \frac{6R}{t^2} \\ \frac{6R}{t^2} & \frac{12R}{t^3} \end{bmatrix} \tag{11}$$

Consequently, the gain matrix K(t) tends also towards 0 and assumes the following form

$$K(t) \sim \begin{bmatrix} \frac{4}{t} \\ \frac{6}{t^2} \end{bmatrix} \tag{12}$$

(2) Influence of accelerations on the filter

During the operation of the filter, the ships considered have a quasi-constant non-zero acceleration whose variance is σ_γ^2; as we will see, this only acceleration is sufficient to cause the Kalman filter to diverge.

The estimation error x is now given by

$$\dot{x} = (F - KH)x + Kv + \gamma \tag{13}$$

$$\gamma = \begin{bmatrix} 0 \\ \gamma_A \end{bmatrix} \tag{14}$$

as γ is deterministic, the variance of x has not changed but its average b admits the following equation

$$\dot{b}(t) = (F(t) - K(t)\,H(t))\,b(t) + \gamma(t) \tag{15}$$

Since $\bar{x}(0) = E(x(0))$, the initial condition concerning b(t) is

$$b(0) = 0 \tag{16}$$

The solution b(t) of (15) and (16) is

$$b^T = [b_1 , b_2] = \left[\gamma_A \frac{t^2}{12} , \gamma_A \frac{t}{2}\right] \tag{17}$$

If we now take into account the fact that $\sigma_\gamma^2 = E(\gamma_A^2)$, we find

$$E(b(t)\,b(t)^T) = \sigma_\gamma^2 \begin{bmatrix} \frac{t^4}{144} & \frac{t^3}{24} \\ \frac{t^3}{24} & \frac{t^2}{4} \end{bmatrix}$$

Consequently, the average quadratic deviation affecting A verifies

$$\varepsilon_A^{\circ 2}(t) = \frac{12R}{t^3} + \sigma_A^2 \frac{t^2}{4} \tag{18}$$

The error $\varepsilon_A^\circ(t)$ decreases initially like $t^{3/2}$, as a function of t; it then reaches its minimum for a time $t = t_{opt}$, then it increases again like t (see Fig. 5). The minimum value is:

$$\varepsilon_{A_{min}}^\circ = 1{,}91\, R^{1/5}\, \sigma_\gamma^{3/5} \tag{19}$$

Therefore, the Kalman filter, which is optimal in theory, is not so in practice. As will be demonstrated later, a Kalman-Schmidt filter can be calculated, is optimal in a certain way, and provides an average error $\varepsilon_A^\circ(t)$ converging towards a lower value than that of the Kalman filter considered above.

3.3.2 Kalman-Schmidt filter

(1) Mathematical formulation of the problem

Let us now introduce into the state vector the acceleration which, previously, was not modelled. It verifies $\dot{\gamma}_A = 0$. Consequently, the equation of state becomes

$$\begin{bmatrix} \dot{x}_1 \\ \dot{x}_2 \end{bmatrix} = \left[\begin{array}{cc|c} 0 & 1 & 0 \\ 0 & 0 & 1 \\ \hline 0 & 0 & 0 \end{array}\right] \begin{bmatrix} x_1 \\ x_2 \end{bmatrix} \tag{20}$$

where $x_2 = \gamma_A$ and $x_1 = [A \;\; \dot{A}]^T$

The equation of measurement will be written in the form

$$y(t) = H(t)\,x(t) + v(t) = H_1(t)\,x_1(t) + v(t) \qquad (21)$$

where $H = [1\ 0\ 0]$ and $H_1 = [1\ 0]$

(2) Kalman-Schmidt filtering

Like the standard Kalman filter, the Kalman-Schmidt filter is a Luenberger estimator which admits the equation

$$\dot{\hat{x}} = F\,\hat{x} + K[y - H\,\hat{x}] \qquad (22)$$

One tries to find the optimum K among all the K matrices of the $\begin{bmatrix} K_1 \\ \hline 0 \end{bmatrix}$ form.

If we put down $F = \left[\begin{array}{c|c} F_{11} & F_{12} \\ \hline 0 & F_{22} \end{array}\right]$, equation (22) gives

$$\dot{\hat{x}}_1 = F_{11}\,\hat{x}_1 + F_{12}\,\hat{x}_2 + K_1[y - H_1\,\hat{x}_1] \qquad (22\ a)$$

$$\dot{\hat{x}}_2 = F_{22}\,\hat{x}_2 \qquad (22\ b)$$

Based on the knowledge that $\hat{x}_2(0) = E(x_2(0))$ optimizes the filter at the moment 0, it results from equation (22 b) that $\hat{x}_2(t)$ is the average of $x_2(t)$. If, besides $E(x_2(0)) = 0$, $\hat{x}_2(0) = 0$ and therefore $\hat{x}_2(t) = 0$.

The equation (22 b) can be eliminated from the filter which is expressed as follows:

$$\dot{\hat{x}}_1 = F_{11}\,\hat{x}_1 + K_1[y - H_1\,\hat{x}_1] \qquad (23)$$

Therefore, the Kalman-Schmidt filter has become a filter of order n_1.

(3) Calculation of the optimal matrix $K_1(t)$

Let us put down $P(t) = E(x(t)x^T(t)$ and let us calculate $K_1(t)$.

As in the case of the Kalman filter, the equation of the evolution of P(t) is

$$\dot{P}(t) = [F(t) - K(t)H(t)]P(t) + P(t)[F(t) - K(t)H(t)]^T + K(t)R(t)K^T(t) \qquad (24)$$

which can also be written, by adding, then substracting $P(t)H^T(t)\,R(t)^{-1}\,H(t)\,P(t)$ in the right-side term:

$$\dot{P}(t) = F(t)\,P(t) + P(t)\,F(t)^T - P(t)\,H(t)^T\,R(t)^{-1}\,H(t)\,P(t) + \underbrace{[K(t) - P(t)\,H(t)^T\,R(t)^{-1}]\,R(t)\,[K(t) - P(t)\,H(t)^T\,R(t)^{-1}]^T}_{M(t)} \qquad (24')$$

The minimization of $tr(P(t))$ leads to that of $tr(\dot{P}(t))$ and therefore to that of $tr(M(t))$. As $tr(M(t)) \geq 0$, $tr(P(t))$ is at its lowest value if $tr(M(t)) = 0$, which is obtained by means of (8).

$$\text{Kalman filter : } K(t) = P(t)\,H(t)^T\,R(t)^{-1}$$

If, now, we impose $K(t) = \begin{bmatrix} K_1(t) \\ \hline 0 \end{bmatrix}$, the matrix M(t) can be written as follows

$$M(t) = \left[\begin{array}{c|c} M_{11}(t) & M_{12}(t) \\ \hline M_{12}(t)^T & M_{22}(t) \end{array}\right]$$

where
$$M_{11}(t) = [K_1(t) - (P(t)H(t)^T\,R(t)^{-1}{}_1]\,R(t)\,[K_1(t) - (P(t)\,H(t)^T\,R(t)^{-1}{}_1]$$
$$M_{12}(t) = -[K_1(t) - (P(t)\,H(t)^T\,R(t)^{-1}{}_1]\,R(t)\,[(P(t)\,H(t)^T\,R(t)^{-1}{}_2]^T$$
$$M_{22}(t) = [(P(t)\,H(t)^T\,R(t)^{-1}{}_2]\,R(t)\,[(P(t)\,H(t)^T\,R(t)^{-1}{}_2]^T$$

If we use $tr\,M(t) = tr\,M_{11}(t) + tr\,M_{22}(t)$, and the fact that $M_{22}(t)$ is independent of $K_1(t)$, we find the following result

$$\text{Minimum } tr(M(t)) \Rightarrow K_1(t) = (P(t)\,H(t)^T\,R(t)^{-1}{}_1$$

which we sum up as follows

$$\text{Kalman-Schmidt Filter : } \begin{array}{l} K_1(t) = (P(t)\,H(t)^T\,R(t)^{-1}{}_1 \\ K_2(t) = 0 \end{array} \qquad (25)$$

(4) Evolution of the matrix P(t)

Through the transformation of (24') by means of (25), the matrix P(t) is the solution of the differential equation

$$\dot{P}(t) = F(t)\,P(t) + P(t)\,F(t)^T - P(t)\,H(t)^T\,R(t)^{-1}\,H(t)\,P(t) + \left[\begin{array}{c|c} 0 & 0 \\ \hline 0 & (P(t)\,H(t)^T\,P(t)^{-1}\,H(t)\,P(t))_{22} \end{array}\right] \quad (26)$$

from the initial condition

$$P(0) = \left[\begin{array}{c|c} P_{11}(0) & 0 \\ \hline 0 & E(x_2(0)\,x_2(0)^T) \end{array}\right]$$

The introduction of the fourth term into the right-hand side of equation (26) corresponds simply to cancelling the fourth block of the matrix

$$P(t)\,H(t)^T\,R(t)^{-1}\,H(t)\,P(t)$$

Equation can be solved according to the same process as the evolution equation (7) of P(t) for the Kalman filter.

(5) Application of the Kalman-Schmidt filter to the filtering of azimuth data

In this phase of the study, we will not be concerned with transient operating conditions. It is demonstrated experimentally that equation (26) admits such a stable solution that p_{11}, p_{22} and p_{33} verify:

$$\varepsilon_{\dot{A}}^{\circ 2} = p_{22} = \frac{3}{8}\,\frac{p_{11}^3}{R^2} \qquad \sigma_Y^2 = p_{33} = \frac{p_{11}^5}{16\,R^4}$$

and, consequently, $\varepsilon_{\dot{A}}^{\circ}$, the speed estimation error is

$$\varepsilon_{\dot{A}}^{\circ} = 1{,}41\,R^{1/5}\,\sigma_Y^{3/5} \quad (27)$$

The steady state error is 9% smaller than that of the Kalman filter at its most accurate.

(6) Form of the filter

The calculation of $K_1(t)$ by means of formula (25) leads to the following result

$$\lim_{t\to\infty} K_1(t) = \left[\begin{array}{c} \Omega_0^2 \\ \hline \frac{1}{2}\,\Omega_0^2 \end{array}\right] \quad (28)$$

with $\Omega_0 = \sqrt{2}\,\left(\frac{\sigma_Y}{2R}\right)^{2^{1/5}}$

Under steady conditions, the tranfer function from the measurement $A_m(t)$ to the estimate $\dot{A}^{\circ}$ of the azimuth speed is

$$\frac{A(p)}{A_m(p)} = \frac{\Omega_0^2\,p}{\Omega_0^2 + \sqrt{2}\,\Omega_0 p + p^2} \quad (29)$$

The Kalman-Schmidt filter obtained has its two eigenvalues with a critical damping in the complex plane. Its block-diagram is represented on Fig. 6.

(7) Maximum error of the Kalman-Schmidt filter

The maximum speed estimation error of the filter is to be found at a distance of 33 km; based on formula (27), it amounts to

$$\varepsilon_{\dot{A}}^{\circ} = 11{,}3 \text{ cm/s}$$

3.3.3. Averageing filter

At the request of the STS project leader, a more conventional estimator of the azimuth speed $\dot{A}^{\circ}$ has been calculated and made it possible to quantify the accuracy improvement offered by the Kalman-Schmidt filter over more conventional filtering methods.

(1) Description of the averageing filter

The averageing filter operates as follows:

The measurements $A_m(t)$ supplied by the measuring equipment is averaged during consecutive time periods of fixed duration T/2, T being optimized later.

The estimate $\dot{A}$ is calculated as $(2\ T)(A_i - A_{i-1})$ where A_i is the result of the i^{th} average and A_{i-1} that of the $i-1^{th}$. Time T has been calculated in such a way as to optimize the accuracy of the estimation at a distance of 33 km. The steady state error has been calculated as follows:

(2) Steady state error

According to the superposition principle, the steady state error is

$$\varepsilon_{\dot{A}}^{\circ} = \sqrt{(\varepsilon_{\dot{A}}^{\circ})_1^2 + (\varepsilon_{\dot{A}}^{\circ})_2^2} \qquad (30)$$

where $(\varepsilon_{\dot{A}}^{\circ})_1$ is the error induced by radio frequency noise

and $(\varepsilon_{\dot{A}}^{\circ})_2$ the error resulting from the non-zero acceleration of the ship, whose standard deviation is σ_γ

Calculation of $(\varepsilon_{\dot{A}}^{\circ})_1$

As time $\frac{T}{2}$ is long as compared to the reverse of the bandpass of the azimuth tracking loop, in calculations, the coloured noise at the output of this loop can be replaced by the white noise $b_A(t)$ at the input of the loop.

The error affecting A_i is therefore the weighted integral of the white noise $b_A(t)$; consequently:

$$\varepsilon^2_{A_i} = \frac{R}{T/2}$$

Likewise, the error affecting A_{i-1} is given by

$$\varepsilon^2_{A_{i-1}} = \frac{R}{T/2}$$

and, due to the fact that the $b_A(t)$ are independent of each other, for

$$t \in [t_{i-1}, t_i] \text{ and } t \in [t_{i-2}, t_{i-1}],$$

$$(\varepsilon^2_{\dot{A}})_i = \varepsilon^2 \left(\frac{A_i - A_{i-1}}{T/2}\right) = \frac{1}{(T/2)^2} \cdot \frac{2R}{T/2} = \frac{16\ R}{T^3}$$

Calculation of $(\varepsilon_{\dot{A}}^{\circ})_2$

Let us assume that the white noise $b_A(t)$ is zero and that there is a constant acceleration $\gamma(t)$

$$\dot{A}(t_{i+1}) = \frac{\frac{2}{T}\int_{t_i}^{t_{i+1}} A_m(t)dt - \frac{2}{T}\int_{t_{i-1}}^{t_i} A_m(t)dt}{T/2} = \frac{4}{T^2}\int_{t_{i-1}}^{t_{i-1}+\frac{T}{2}} [A_m(t+\tfrac{T}{2}) - A_m(t)]dt$$

As $b_A(t) = 0$, $A_m(t) = A(t)$;

Now $$A(t+\tfrac{T}{2}) = A(t) + \frac{T}{2}\dot{A}(t) + \frac{T^2}{8}\gamma$$

Therefore $$\dot{A}(t_{i+1}) = \frac{4}{T^2}\int_{t_{i-1}}^{t_{i-1}+\frac{T}{2}} [\frac{T}{2}\dot{A}(t) + \frac{T^2}{8}\gamma]dt = \dot{A}(t_{i-1} + \tfrac{T}{4}) + \frac{T}{4}\gamma = \dot{A}(t_{i+1}) - \frac{T}{2}\gamma$$

Consequently $$(\varepsilon_{\dot{A}}^{\circ})_2^2 = E(\frac{T}{2}\gamma)^2 = \frac{T^2}{4}\sigma_\gamma^2$$

It results therefrom that the overall error is given by the formula

$$\varepsilon_{\dot{A}}^{\circ} = \sqrt{\frac{16\ R}{T^3} + \frac{T^2}{4}\sigma_\gamma^2} \qquad (31)$$

This error is at its smallest for $T = \left(\frac{96\ R}{\sigma^2_\gamma}\right)^{1/5}$ and amounts then to

$$\varepsilon^{\circ}_{\dot{A}_{min}} = 1{,}61\ R^{1/5}\ \sigma_\gamma^{3/5} \qquad (32)$$

The minimum error at a distance of 33 km amounts to 12.9 cm/s and corresponds to an integration time of 20 s (T/2 = 20 s).

Now, the specifications require that the display of $\mathring{A}$ should be up-dated every five second; therefore, we are compelled to carry out several calculations of averages in parallel for with an elementary 5 s shift, or to select a 5 s integration time; the error obtained in the latter case is:

$$\varepsilon_{\mathring{A}} = 65 \text{ cm/s}$$

3.3.4 Selection of the estimation filter of $\mathring{A}$

The accuracy performance of the three filters under consideration is, respectively:

Kalman Filter ..... (12.2 cm/s at 33 km)

Kalman-Schmidt Filter ..... (11.3 cm/s at 33 km)

Averageing Filter ..... (12.9 cm/s or 65 cm/s at 33 km)

The Kalman-Schmidt filter has been selected since it is the most accurate. As already noted, the drawbacks of the other filters are the following:

Though adequate in theory, the Kalman filter is difficult to use due to its divergence.

While the averageing filter appears to be simple a priori, it is somewhat difficult to implement if a low degree of error is to be achieved; besides, even once it has been optimized, it does not meet the specifications required (12.9 cm/s at a distance of 33 km instead of 12.5 cm/s). The estimation errors of the various filters are represented on Fig. 7, versus the distance from the ship to the station.

3.4 Estimation of the navigation parameters

3.4.1. Mathematical expression of the navigation parameters

The navigation parameters e, L, $\mathring{e}$ and $\mathring{L}$ are expressed as functions of the real values A (azimuth) and D (distance) by means of the following formulae

$$e = \frac{(x_0 - a_i)(b_i - b_{i-1}) - (y_0 - b_i)(a_i - a_{i-1})}{[(a_i - a_{i-1})^2 + (b_i - b_{i-1})^2]^{1/2}} + e_0 \tag{33}$$

$$L(x_i) = [(x_0 - a_i)^2 + (y_0 - b_i)^2]^{1/2} \tag{34}$$

$$\mathring{e} = \frac{\frac{dx_0}{dt}(b_i - b_{i-1}) - \frac{dy_0}{dt}(a_i - a_{i-1})}{[(a_i - a_{i-1})^2 + (b_i - b_{i-1})^2]^{1/2}} \tag{35}$$

$$\mathring{L}(x_i) = \frac{\frac{dx_0}{dt}(x_0 - a_i) + \frac{dy_0}{dt}(y_0 - b_i)}{[(x_0 - a_i)^2 + (y_0 - b_i)^2]^{1/2}} \tag{36}$$

where e_0 is a correcting term resulting from the position deviation between the responder and the pilot.

$\begin{bmatrix} a_i \\ b_i \end{bmatrix}$ are the Lambert coordinates (Cartesian coordinates) of the reference point x_i

and $\begin{bmatrix} x_0 \\ y_0 \end{bmatrix}$. $\begin{bmatrix} \frac{dx_0}{dt} \\ \frac{dy_0}{dt} \end{bmatrix}$ are respectively the coordinates of the ship responder and their derivatives, whose expressions as functions of A, $\mathring{A}$, D and $\mathring{D}$ are:

$$x_0 = x_s + D \sin A \tag{37}$$

$$y_0 = y_s + D \cos A \tag{38}$$

$$\frac{dx_0}{dt} = D \cos A \frac{dA}{dt} + \sin A \frac{dD}{dt} \tag{39}$$

$$\frac{dy_0}{dt} = -D \sin A \frac{dA}{dt} + \cos A \frac{dD}{dt} \tag{40}$$

where $\begin{bmatrix} x_s \\ y_s \end{bmatrix}$ are the Lambert coordinates of the ground-based station.

3.4.2. Method of estimation of navigation parameters

Estimation of e, $L(x_i)$, $\overset{\circ}{e}$, $\overset{\circ}{L}(x_i)$

The expressions of e, L, $\overset{\circ}{e}$ and $\overset{\circ}{L}$ as functions of the values of A, D, $\overset{\circ}{A}$, $\overset{\circ}{D}$ are

- linear as functions of $\overset{\circ}{A}$ and $\overset{\circ}{D}$
- non linear as functions of A and D.

Based on the fact that A and D are known with fairly good accuracy, we have chosen as the estimates of e, L, $\overset{\circ}{e}$ and $\overset{\circ}{L}$ the values $\hat{e}$, $\hat{L}(x_i)$, $\overset{\circ}{e}$, $\overset{\circ}{L}(x_i)$ provided by the formulae

$$\hat{e} = e(\hat{A},\hat{D}) \tag{41}$$

$$\hat{L}(x_i) = L(x_i, \hat{A}, \hat{D}) \tag{42}$$

$$\overset{\circ}{\hat{e}} = \overset{\circ}{e}(\hat{A}, \hat{D}, \overset{\circ}{\hat{A}}, \overset{\circ}{\hat{D}}) \tag{43}$$

$$\overset{\circ}{\hat{L}}(x_i) = \overset{\circ}{L}(x_i, \hat{A}, \hat{D}, \overset{\circ}{\hat{A}}, \overset{\circ}{\hat{D}}) \tag{44}$$

where e(.), L(.), $\overset{\circ}{e}$(.), $\overset{\circ}{L}$(.) are the functions appearing in the right-hand sides of (33), (34), (35) and (36). Due to the good accuracy of A and D, these estimate are close to the optimum.

Determination of the reference segment $(x_{i-1}\ x_i)$

The reference segment is determined iteratively since the tanker sails towards the harbour. The test permitting the incrementation of i corresponds to the tanker passing across the boundary which separates the $i+1^{th}$ area of the channel from the i^{th} area. This test is carried out simultaneously with each calculation of e and $L(x_i)$, that is to say every second.

(1) Accuracy achieved for e *and* $L(x_i)$

The accuracy achieved for e proves to be almost the same as the lowest accuracy for A (expressed in m) and D. By means of a simple calculation, we find that the error affecting L is, at the outside, equal to twice the greatest error affecting A and D. Thus, the errors ϵ_e and ϵ_L in the estimation of e and L are:

At a distance of 33 km	ϵ_e = 8.6 m	$\epsilon_L \leq$ 17.2 m
At a distance of 12 km	ϵ_e = 2.2 m	$\epsilon_L \leq$ 4.4 m

(2) Accuracy achieved for $\overset{\circ}{e}$ *and* $\overset{\circ}{L}(x_i)$

The accuracy achieved for $\overset{\circ}{e}$ and $\overset{\circ}{L}(x_i)$ estimated by means of equations (43) and (44) is almost independent of the errors affecting A and D.

A detailed calculation has revealed that the greatest possible error obtained is 0.2 cm/s.

We have also been able to demonstrate that $\overset{\circ}{e}$ and $\overset{\circ}{L}(x_i)$ are almost the optimal estimates of $\overset{\circ}{e}$ and $\overset{\circ}{L}(x_i)$ and that the error affecting $\overset{\circ}{e}$ and $\overset{\circ}{L}(x_i)$ is, at the utmost, equal to that affecting $\overset{\circ}{A}$. The degrees of accuracy achieved for $\overset{\circ}{e}$ and $\overset{\circ}{L}(x_i)$ if we estimate $\overset{\circ}{A}$ by means of a constant coefficient filter optimized for 33 km (by Kalman-Schmidt filtering) are shown on the table below:

Distance (km)	ϵ_D° (cm/s)	$D\,\epsilon_A^{\circ}$ (cm/s)	$\epsilon(\frac{de}{dt})$ (cm/s)	$\epsilon(\frac{dL}{dt})$ (cm/s)
33	8.5	12.9	12.6	12.6
22	8.3	11.3	11.1	11.1
15	5.8	6.7	6.5	6.5
12	4.7	4.5	4.5	4.7
4	2.2	1.1	1.1	2.2

Errors affecting $\frac{de}{dt}$ and $\frac{dL}{dt}$ as functions of the distance between the tanker and the ground-based station (zero lag errors)

3.5 Optimization of the STS digital processing

3.5.1 Optimization of the sampling interval for the estimation of Å

(1) Sampled Kalman-Schmidt Filter

The discrete formulation of the sampled Kalman-Schmidt filter is given below.

Suppose a sampled process in the form

$$x(k+1) = \phi(k+1, k) \cdot x(k) \tag{45}$$

where

$$x(k) = \begin{bmatrix} x_1(k) \\ x_2(k) \end{bmatrix} \quad \text{and} \quad \phi(k+1, k) = \begin{bmatrix} \phi_{11} & \phi_{12} \\ 0 & \phi_{22} \end{bmatrix}$$

Suppose the sampled measurement

$$y(k) = H(k)\, x(k) + v(k) = H_1(k)\, x_1(k) + v(k) \tag{45}$$

where $v(k)$ is a sampled white noise with the following covariance

$$E(v(k)\, v(i)^T) = R(k)\, \delta_{kl}$$

The Kalman-Schmidt filter which optimizes the estimation error affecting $x_1(k)$ is given by:

Equations of state

$$\hat{x}_1(k)^+ = \hat{x}_1(k)^- + K_1(k)\,[y(k) - H_1(k)\hat{x}_1(k)^-] \tag{47 a}$$

$$\hat{x}_1(k+1)^- = \phi_{11}\, \hat{x}_1(k)^+ \tag{47 b}$$

Equations of variance

$$P(k)^+ = P(k)^- - P(k)^- H(k)^T [R(k) + H(k)\, P(k)^- H(k)^T]_{\mathfrak{L}}^{-1} \tag{48 a}$$

where $(\cdot)_{\mathfrak{L}}$ is the operation which, from $Q = \begin{bmatrix} Q_1 & Q_2 \\ Q_3 & Q_4 \end{bmatrix}$ leads to $(Q)_{\mathfrak{L}} = \begin{bmatrix} Q_1 & Q_2 \\ Q_3 & 0 \end{bmatrix}$

$$P(k+1)^- = \phi(k+1, k)\, P(k)^+ \phi(k+1, k)^T \tag{48 b}$$

Equation of gain

$$K_1(k) = \{P(k)^- H(k)^T [R(k) + H(k)\, P(k)^- H(k)^T]^{-1}\}_1 \tag{49}$$

where $(\cdot)_1$ is the operation which, from $M = \begin{bmatrix} M_1 \\ M_2 \end{bmatrix}$ leads to $(M)_1 = M_1$

(2) Application to the estimation channel of Å

Let us call T the sampling interval of the Kalman-Schmidt filter of channel Å.

The evolution of the vector of state $x(k) = \begin{bmatrix} \dot{A}(t_k) \\ A(t_k) \\ \gamma_A(t_k) \end{bmatrix}$ is given by the formula

$$x(k) = \phi(k, k-1)\, x(k-1)$$

where

$$\phi(k, k-1) = e^{FT} = \begin{bmatrix} 1 & T & T^2/2 \\ 0 & 1 & T \\ 0 & 0 & 1 \end{bmatrix}$$

The sampled measurements selected $y(k)$ assume the following form

$$y(k) = \frac{1}{T} \int_{t_{k-1}}^{t_k} A_m(t)\, dt$$

They are the averages of the azimuth measurements in the intervals $[t_{k-1}, t_k]$

If we use $A_m(t) = H \cdot x(t) + v(t)$, where $H = [1,0,0]$ and $E(v(t)\ v(t+\tau)^T) = R\ \delta(\tau)$

we obtain

$$y(k) = H(k)\ x(\kappa) + v(k)$$

$$H(k) = H \cdot [\frac{1}{T}\int_{t_{k-1}}^{t_k} \Phi(t, t_k)dt] = [1, -\frac{T}{2}, \frac{T^2}{6}]$$

$$E(v(k)\ v(1)^T) = R(k)\ \delta_{kl} \text{ where } R(k) = \frac{R}{T}$$

The steady state accuracy of the Kalman-Schmidt filter corresponding to the above sampled equations was calculated for various sampling intervals at the most critical distance: 33 km. The average error/sampling interval curve shown on Fig. 8 offers a remarkable characteristic: *the accuracy is at its best for a non-zero value (of the order of 10 s) of the sampling interval* and is lower than that of the continuous filter only when the sampling intervals exceed 22 s.

For a 5 s sampling interval, the accuracy achieved is 11.1 cm/s.

A 5 s sampling interval is selected in view of the following requirements:-

(a) Update the estimation of $\hat{e}$ and $\hat{L}$ for each data display.

(b) Minimize the computer work load for the estimation of $\hat{A}$.

3.5.2 Sampling interval for the estimation of $\hat{D}$

The sampling interval of estimator $\hat{D}$ is not critical and, for the sake of simplicity, was chosen as 1 s.

3.5.3. Number of digits selected for each parameter

The computer used is an 8-bit computer based on an INTEL 8008 fixed point microprocessor. Consequently, the parameters should be defined either in 8 bits, or in 16 bits, or more.

It has been demonstrated that, for each of the variables D, $\hat{D}$, A, $\hat{A}$, e, L, $\hat{e}$ and $\hat{L}$, the dynamics exceed 8 bits. Consequently, these variables must be coded in 16 bits, that is to say two words.

The following table shows the values of the highest and lowest order bits for each value, together with the appropriate signs.

Value	Sign	Max. Weight	Min. Weight
D	+	32,768 m	1 m
$\hat{D}$	±	64 m/s	3.9 mm/s
A	+	π rad/s	$0.96 \cdot 10^{-4}$ rad
$\hat{A}$	±	12.27 rad/s	$7.4 \cdot 10^{-7}$ rad/s
e	±	16,384 m	1 m
L	+	32,768 m	1 m
$\hat{e}$	±	64 m/s	3.9 mm/s
$\hat{L}$	±	64 m	3.9 mm/s

In all the cases considered, the unit of lenght is 1 m and the unit of time 2^{-8} s, that is to say 3.9 ms. The only values which are not standardized are A and $\hat{A}$, which makes the computation of $\hat{x}_0$ and $\hat{y}_0$ more complex.

The values provided by the measuring device are given in the following form:

Value	Sign	Max. Weight	Min. Weight
D_m	+	65 536 m	2 m
$\dot{D}_m$	analog coded 16 bits		
A_m	+	π rad	$\frac{\pi}{2^{12}}$ rad
ΔA_m	analog coded 4 bits		

3.5.4 Influence of quantizations on the knowledge of $\hat{\dot{A}}$

$\hat{\dot{A}}(k)$ is determined by the algorithm

$$\hat{A}(k+1) = \Phi_{11}\,\hat{A}(k) + \Phi_{12}\,\hat{\dot{A}}(k) + K_1[A - \Phi_{11}\,\hat{A}(k) - \Phi'_{12}\,\hat{\dot{A}}(k)] \qquad (50)$$

$$\hat{\dot{A}}(k+1) = \Phi_{22}\,\hat{\dot{A}}(k) + K_2[A - \Phi_{11}\,\hat{A}(k) - \Phi'_{12}\,\hat{\dot{A}}(k)] \qquad (51)$$

where the parameters expressed in octal numbers are:

$\Phi_{11} = 0\ 0\ 0\ 1$ (1)

$\Phi_{12} = 0\ 5\ 0\ 0$ (T)

$\Phi'_{12} = 0\ 2\ 1\ 0$ (T/2)

$\Phi_{22} = 0\ 0\ 0\ 1$ (1)

Approximating K_1 and K_2 does not appreciably modify the filtering error; besides, no approximation is made for Φ_1

Errors resulting from the additions

Such errors are null.

Errors resulting from the truncation of A and from the multiplications

The computer calculates (50) and (51) according to the following process:

$$\Delta A = \bar{A} - \hat{A}(k) - \Phi'_{12}\,\hat{\dot{A}}(k)$$

$$\hat{A}(k+1) = \hat{A}(k) + \Phi_{12}\,\hat{\dot{A}}(k) + K_1\,\Delta A$$

$$\hat{\dot{A}}(k+1) = \hat{\dot{A}}(k) + K_2\,\Delta A$$

That is to say:

$$\Delta A = A + \varepsilon_1 - \hat{A}(k) - \Phi'_{12}\,\hat{\dot{A}}(k) - \varepsilon_2$$

$$\hat{A}(k+1) = \hat{A}(k) + \Phi_{12}\,\hat{\dot{A}}(k) + K_1\,\Delta A + \varepsilon_3$$

$$\hat{\dot{A}}(k+1) = \hat{\dot{A}}(k) + K_2\,\Delta A + \varepsilon_4$$

ε_1, ε_2, ε_3 are errors equally distributed over 0 and b where b is the lowest order bit of A and $A(A_m + \Delta A_m)$.

The average of ε_1, ε_2, ε_3 does not perturb $\hat{\dot{A}}$ in a steady state. The standard deviation of an equivalent noise ε'_1 on A is:

$$\frac{b}{\sqrt{12}}\sqrt{2} + \frac{\overline{1}}{K_1} \sim \frac{b}{2}$$

Such a noise is equivalent to a white noise on A_m, whose energy level would be

$$W_{\varepsilon'_1} = 1 \cdot \frac{b^2}{4} = 1{,}15 \cdot 10^{-8}\ \text{rad}^2/\text{s}.$$

This level is higher than the energy level of the input white noise for distances below 12 km between the ground-based station and the responder.

3.5.5 Adaptative or non-adaptative Kalman-Schmidt Filter?

The implementation of a Kalman-Schmidt filter with pre-computed variable coefficients has been contemplated during STS study.

Finally, this idea was given up for the following reasons:

- The computing workload of an adaptative filter is higher than that of a constant coefficient filter.
- On the range channel, the acquisition is achieved by the measuring system within 2 mn whereas the acquisition time is reduced to 2 s on the azimuth channel. Therefore, a short transient phase is not a necessary requirement for the azimuth Kalman-Schmidt filter; consequently, the gain parameters can be frozen at their steady state values.

However, it has been contemplated to set up later, on the STS, a gain adaptation program for the previous filter; the gains should be calculated as functions of the S/N ratio at the input of the measuring device. This S/N ratio is given indirectly by a variance computation carried out on the azimuth measurements stored in the memory every 500 ms. The principle of the filter is represented by a block-diagram on Fig. 9.

The worst-case results to be expected from such a filter are shown on Fig. 10, together with those obtained with a constant coefficient filter whose coefficients are optimized for a distance of 33 km.

It is this constant coefficient filter which will be considered from now on.

4. GENERAL ORGANIZATION OF THE DIGITAL PROCESSING

Due to its low cost and its low computing power, the computer of the STS ground-based station is quite suited to the problem under consideration.

The computer is connected with the measuring device by a 32-entry - 32-exit coupler whose functions are as follows.

- Input of data D_m, A_m, $\dot{D}_m$, return message from the responder.
- Output of the outgoing message sent to the responder.

The computer operates on three levels (see Fig. 11).

Level 0 500 ms elementary period main program synchronized with a 500 ms period interrupt sent out by the measuring device. This program is responsible for the following computations:

(1) Average of the 10 $\dot{A}_m$ data and computation of the constant coefficient Kalman-Schmidt filter (every 5 s).

(2) Iterative computation of $\dot{D}$ by the processing of $\dot{D}_m$ sampled every second.

(3) Computation of $\dot{e}$ and $L(x_1)$ every second by sampling A_m every 500 ms and D_m every second.

(4) Computation of $\dot{e}$, $L(x_1)$ every 5 second.

(5) Computation of the segment number and phase number every second based on the result of (3)

The main program is synchronized in order that the computation time of the estimates of $\dot{A}$ and $\dot{D}$ may remain constant. Computations *(1)*, *(2)*, *(3)*, *(4)*, and *(5)* are not all effected at a 500 ms rate but are repetitive every 5 second.

The time schedule of the main program is as follows:

0 Computation of cos A and sin A, of the Lambert coordinates x_0 and y_0.
Determination of segment i and phase j.
Input of A_m.

0.5 Computation of P and $L(x_1)$.
Input of A_m.
Estimation of $\dot{D}$.

1 Computation of cos A, sin A, x_0 and y_0.
Determination of i and j.
Input of A_m.

1.5 Computation of e and $L(x_1)$
Input of A_m.
Estimation of $\dot{D}$.

2 Computation of cos A, sin A
Determination of i and j
Input of A_m

2.5 Computation of e and $L(x_1)$
Input of A_m
Estimation of $\dot{D}$

3 Computation of cos A, sin A, x_0 and y_0
Determination of i and j
Input of A_m

3.5 Computation of e and $L(x_i)$
Input of A_m
Estimation of D

4 Computation of cos A, sin A, x_0, y_0
Determination of i and j
Input of A_m

4.5 Computation of e and $L(x_i)$
Input of A_m
Estimation of $\hat{A}$
Estimation of $\hat{D}$
Computation of $\hat{e}$ and $\hat{L}(x_i)$
Return to 0

The computation times of the various sub-programs are:

Computation of cos A and sin A	78 ms
Computation of x_0 and y_0	0.8 ms
Determination of segment i and phase j	32 ms
Computation of e and $L(x_i)$	73 ms
Estimation of D	5 ms
Estimation of $\hat{A}$	13 ms
Computation of $\hat{e}$ and $\hat{L}(x_i)$	40 ms

The total space requirement of the program is 4 words.

Level 1 Program over an interrupt of level 1 triggered by the measuring device every 500 ms. This program prepares and transcodes into BCD the digital message of 32 eight-bit bytes to be sent to the responder.

Level 2 Program over the interruption of level 2.

This program is initiated every 14 ms on the interruption of level 2 triggered by the measuring device; it sends out to the measuring device an eight-bit byte of the message generated previously and receives an eight-bit byte in return, which it compares with the eight-bit byte sent out and it sends forth an alarm signal if an error has been made.

88 ms are required for the running of the 1st and 2nd level programs, out of a total duration of 500 ms, which leaves 412 ms for the main program to be carried out. Now, the running of this main program necessitates 191 ms at the utmost. Therefore, the computer remains unused over 50% of its time!

The total space requirement for levels 1, 2, and 3 is 5.3 K words.

5. RELIABILITY OF THE DIGITAL PROCESSING

As shown on Fig. 11, the digital processing by the STS assumes a modular structure. Its characteristic features are:

(1) No estimation of values A and D (This way, even in the case errors occur on the estimators, parameters e, $L(x_i)$, i and j are available on the pilot's display box).

(2) Separate estimation of $\hat{A}$ and $\hat{D}$.

(3) Rusticity of estimators $\hat{A}$ and $\hat{D}$, ensuring high stability.

(4) Estimation of navigation parameters separately from that of the variables of state.

The modular structure of the programs improves considerably the reliability of their checking out and of possible on-site modifications.

CONCLUSION

This paper describes the digital processing of measurements in a high accuracy ship-tracking system. The errors affecting the azimuth measurement supplied by the measuring device of the ground-based station were found to be the most critical for the overall accuracy of the system. A Kalman-Schmidt filter was selected for an optimum estimation of the azimuth speed, following comparisons with a Kalman filter and an "averageing" filter. The estimation of the navigation parameters was described and the position and speed accuracy achieved by the system was calculated. Moreover, various effects resulting from the data processing in a computer were analyzed and optimized: f.i. choice of the computation rate for the azimuth velocity, scaling of navigation parameters, etc.; finally, the programming of the data processing in a microcomputer was described and evaluated from two standpoints: memory space requirement and computation time. The results obtained confirm the efficiency of the solutions selected.

REFERENCES

1 S. F. SCHMIDT — Application of State-Space Methods to Navigation Problems, Advan. Control Systems 3 (1966), pp. 293-340

2 A. H. JAZWINSKI — Stochastic Processes and Filtering Theory, Academic Press (1970), pp. 281-302

3 C. A. DARMON — Traitement d'informations radioélectriques pour obtenir la position et la vitesse d'un navire, Laboratoire Central de Télécommunications, Velizy, FRANCE, Rep. PL 603 256 (1973)

4 M. JULIEN, Y. LANGLOIS, Ph RICOUX — Modélisation de navires pétroliers, Laboratoire Central de Télécommunications, Velizy, FRANCE, (1973)

5 D. CLARKE, D. PATTERSON, R. WOODERSON — "Manoeuvring Trials with the 193,000 ton D.W Tanker "Esso Bernicia", The British Ship Research Association, Rep. NS 295, Naval Architecture Rep. N° 81 (1970)

5 DELATTRE, BRACHFOGEL, THIRION — "Traitement de l'information STS", Laboratoire Central de Télécommunications, Velizy, FRANCE, Rep. PL 100.412 (1974)

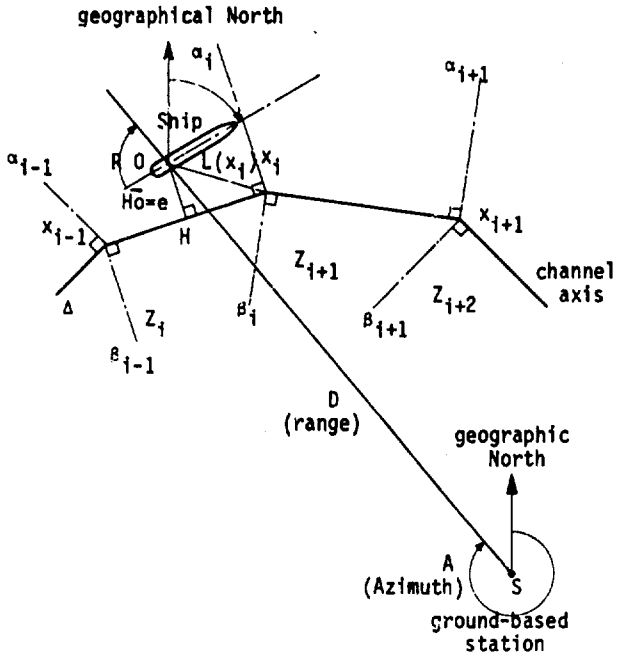

Figure 1.: Ship sailing along the channel

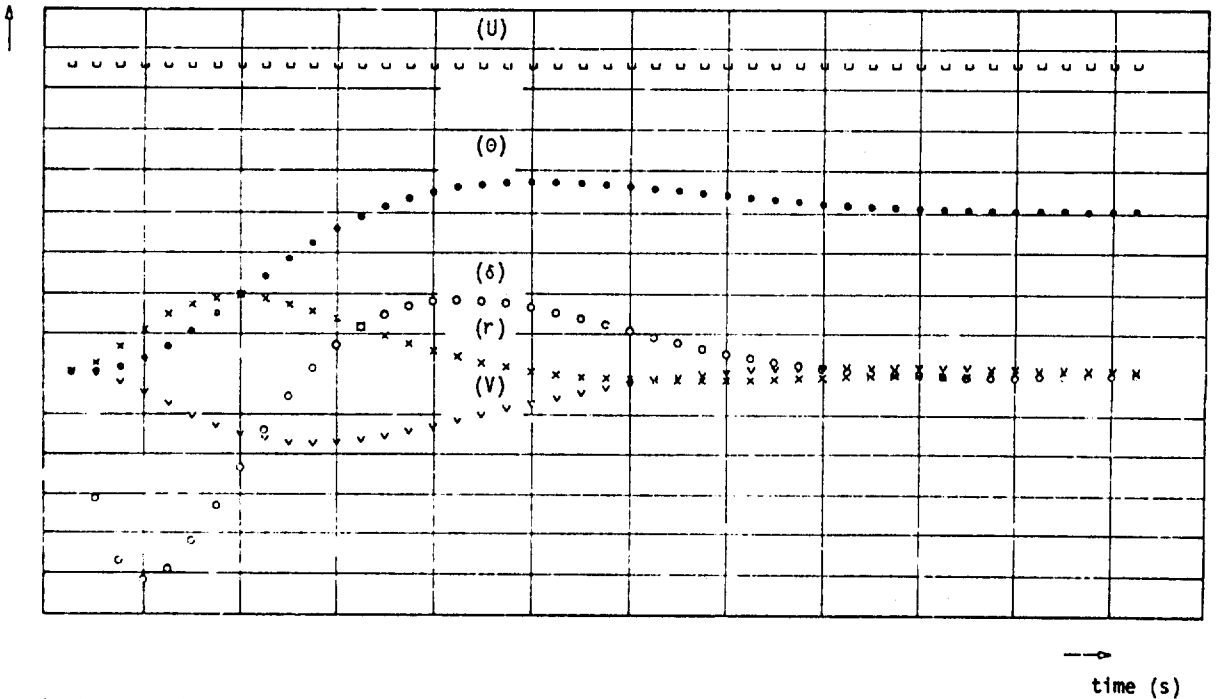

Ordinate scale:
1 division: V (v) : 0.2 m/s; ● (Θ) : 5° ; R(r) : 0.1°/s
U (u) : 1 m/s; o(δ) : 5° .

Figure 3.: 10° Heading change, speed 15 knots, of the tanker Esso-Bernicia

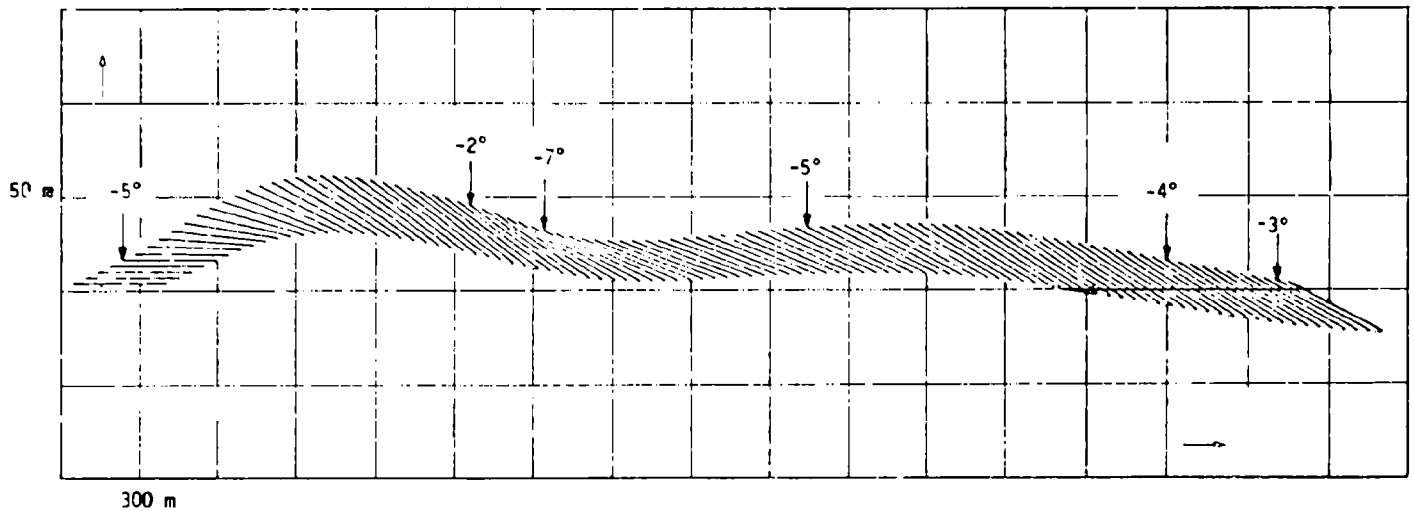

Figure 4.: Trajectory of Esso Bernicia in response to a 0.5 m/s step of current

(figure showing successives heading of the tanker and corresponding heading orders)

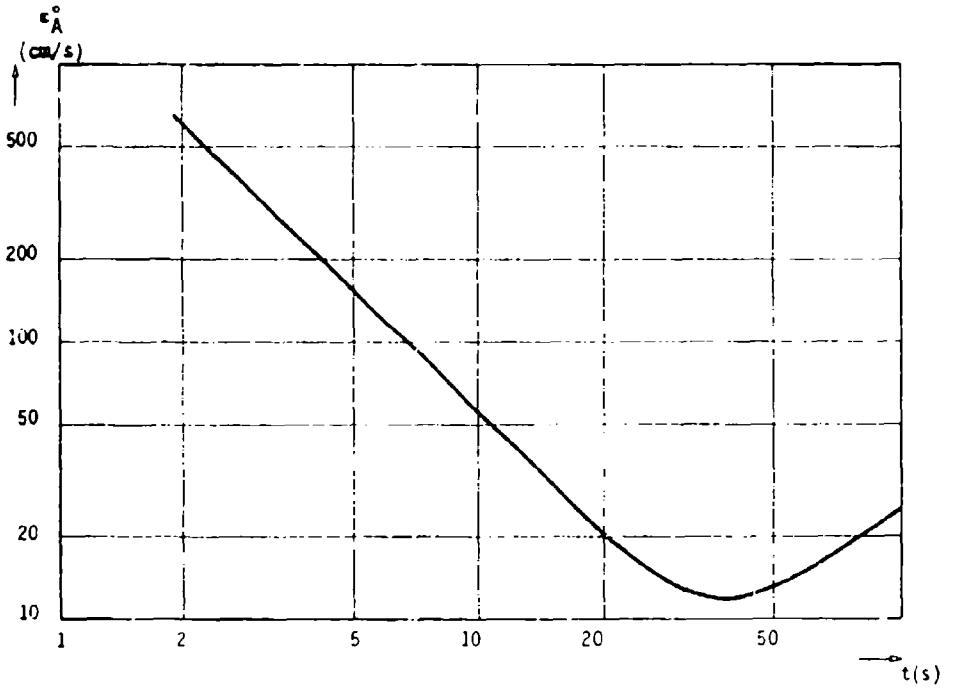

Figure 5.: Standard-deviation of the speed-error, as a function of the estimation time, for the Kalman filter (Distance: 33 km)

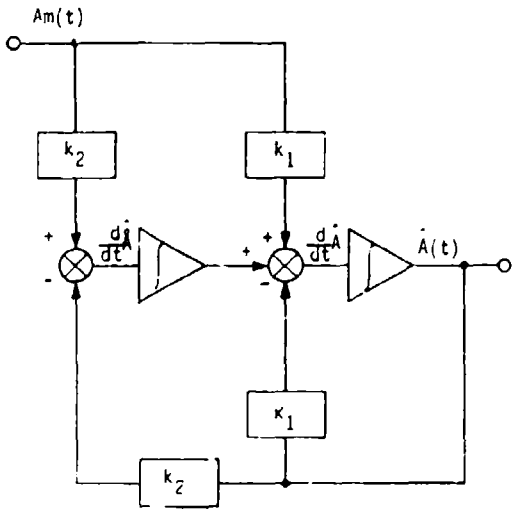

Figure 6.: Kalman-Schmidt filter

Figure 7.: Standard deviation of the speed error, as a function of the distance ship-ground-based station, for filters n° 1, 2, 3 (Kalman, Kalman-Schmidt, Averageing filter)

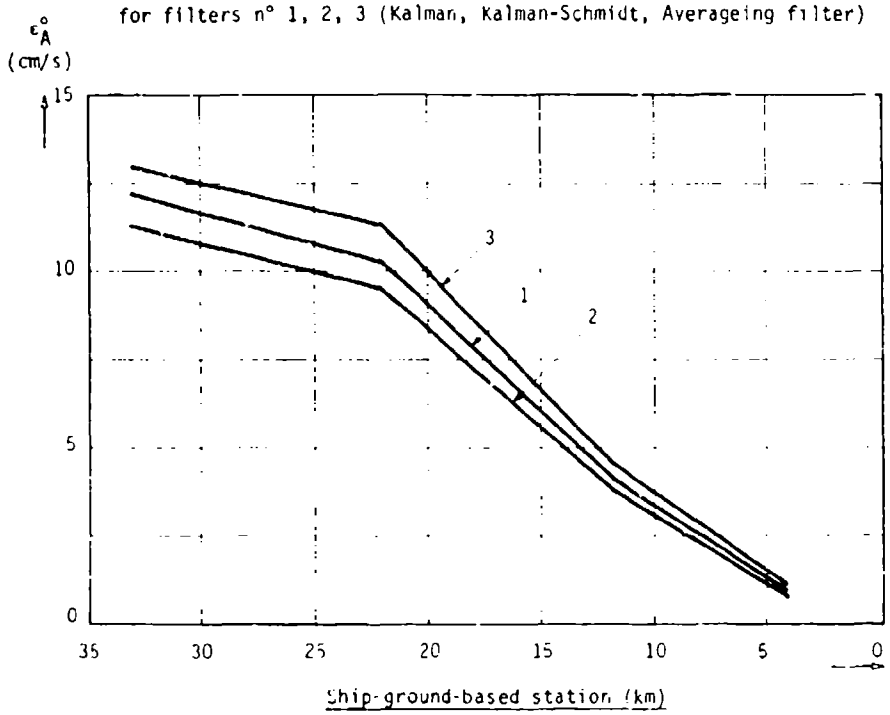

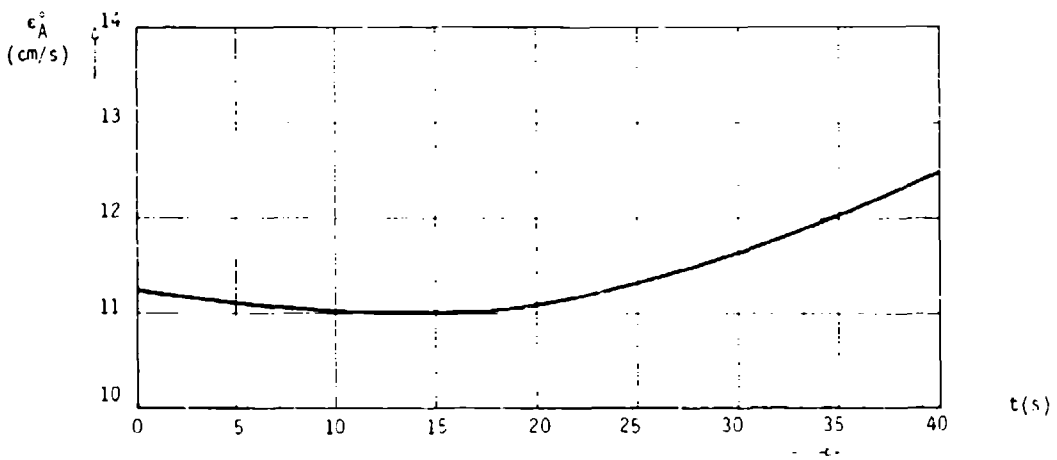

Figure 8.: Accuracy of the Kalman-Schmidt filter as a function of the sampling interval

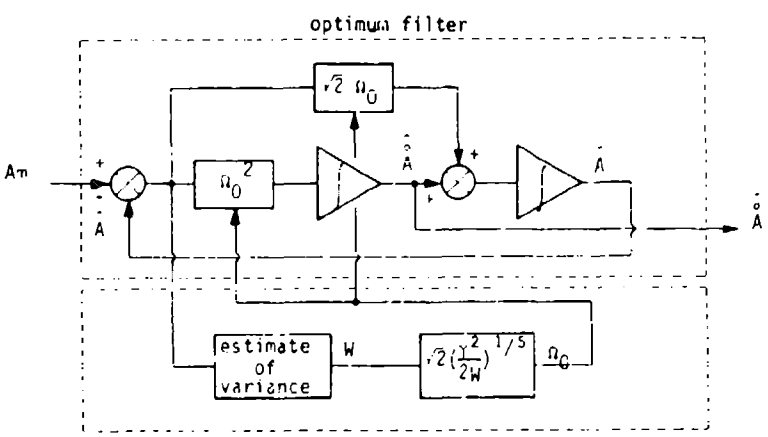

Figure 9.: Adaptive Kalman-Schmidt filter

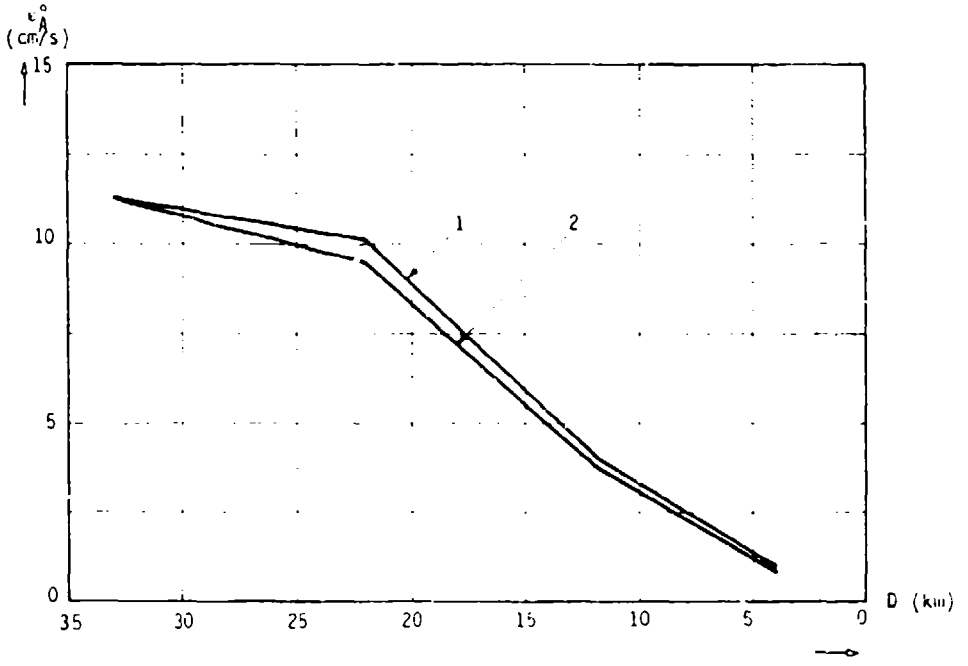

Figure 10.: Standard-deviation of the speed error as a function of the distance ship-ground based station, for the Kalman-Schmidt filter optimized at 33 km (curve n° 1), and the same one made adaptive (curve n° 2)

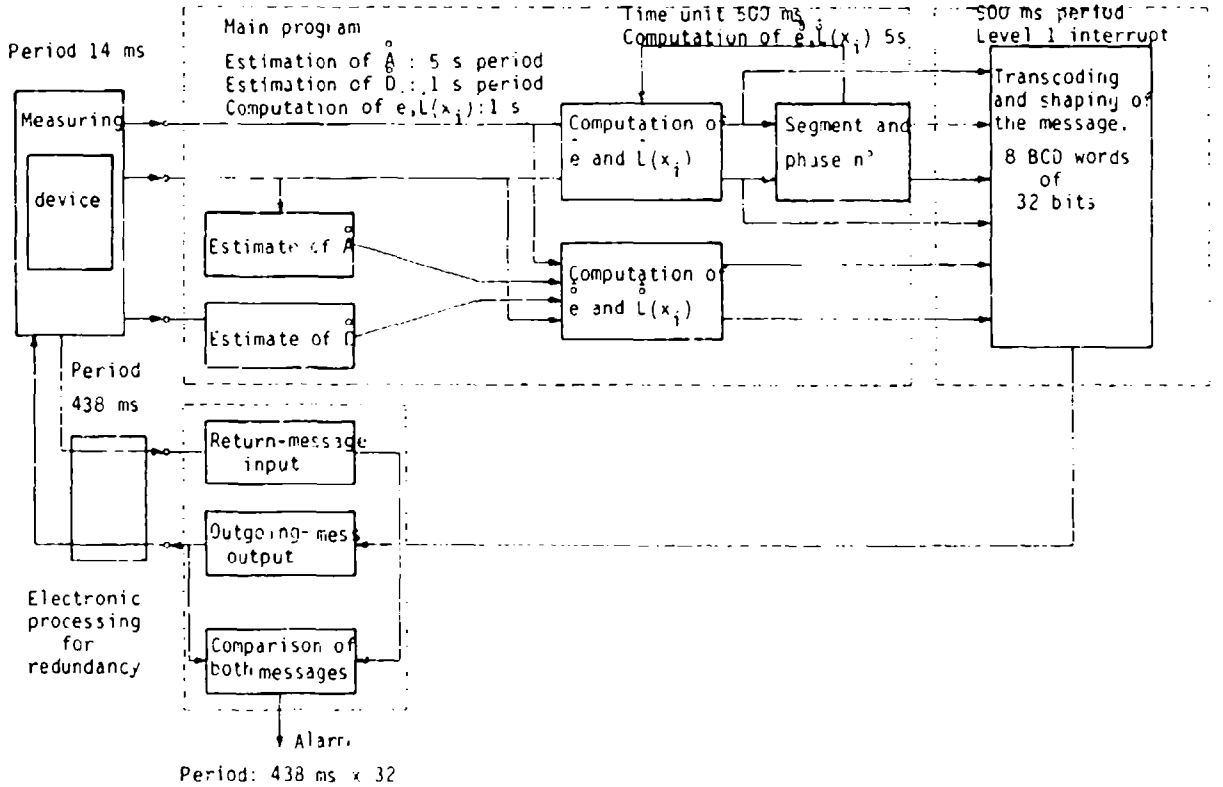

Figure 11.: Organization of STS Data Processing

DESIGN AND ANALYSIS OF LOW-ORDER FILTERS APPLIED TO THE ALIGNMENT OF INERTIAL PLATFORMS

by
Willi Kortüm
German Research Center for Aeronautics
and Astronautics (DFVLR)
Institute for Dynamics of Flight Systems
8031 Oberpfaffenhofen
Germany

SUMMARY

This lecture describes the typical steps and considerations for designing low-order efficient state estimators or Kalman filters. The design steps are demonstrated on a platform alignment problem where Kalman filtering is used rather than conventional procedures to reduce the time necessary for the required alignment accuracy. The work reported herein is based on a test series for modelling gyro-drift and accelerometer errors. The main body of the lecture concentrates on the selection of a design model for the filter (Section 2), the filter design itself (Section 3), and a complete covariance analysis (Section 4). The main goal of the filter design is to achieve a simple, i.e., low-order insensitive design.

1. INTRODUCTION

The application of modern estimation techniques (Kalman filtering) to the alignment and calibration of inertial platforms (on ground) is of great practical interest since it allows shorter alignment times and/or higher alignment accuracy. Both aspects are very desirable because they allow the time necessary for start preparations to be shortened and/or inflight navigation accuracy to be improved [1, 2]*. From the viewpoint of implementation it is desirable to keep the estimator as simple as possible while maintaining the optimal accuracy. The typical design steps for achieving simple (low-order) and efficient filters are described for the problem of fast and fine platform alignment. This problem should be understood as a case study which allows aspects of filter design which are typical and easily generalized to be described. The practical implications of the numerical results, however, depend on the special mission, and generalization must be performed with care.

To obtain reliable answers to this problem the following main tasks were carried out:

(1) A test series for setting up stochastic models for gyro-drift and accelerometer errors (at IABG-Ottobrunn).

(2) A design of an effective low-order state estimator with special attention to observability and covariance analysis (at DFVLR-Oberpfaffenhofen).

(3) Coordination of modelling, implementation of the filter and performance of experiments with the real platform (at DFVLR-Braunschweig).

The lecture concentrates on task (2); however, upgrading the results of task (1) and the comparison with the experiments of task (3) and their drawbacks on tasks (1) and (2) are also included.

Each of the following sections begins with a subsection on the general idea - applicable to a wide range of problems - followed by a discussion of its use in the problem of alignment.

2. DYNAMIC MODELS AND ERROR STATISTICS

Effective state estimation via Kalman filtering is based on a model of the dynamic system under consideration, the sensor equations as well as statistic models for the noise inputs (process and sensor noise)

$$\text{System Model:} \quad \dot{x} = F\,x + G_u\,u + G_w\,w \tag{2-1}$$

$$\text{Observations:} \quad z = H\,x + v \tag{2-2}$$

where x is the $n\times 1$ state vector, z the $m\times 1$ measurement or observation vector, u is a $n_u\times 1$ deterministic input vector (e.g., control actions) and w and v are $n_w\times 1$ and $m\times 1$ vectors termed as process and measurement noise, they are usually assumed to be white-noise terms with zero mean and spectral density matrices Q and R, respectively.

---

* Bracketed numerals refer to similarly numbered references in the List of References.

The matrices F, G, H, Q, and R are usually assumed to be precisely given and may be constant or time-varying.

In practice, however, this assumption is almost never fulfilled, i.e., usually models with sufficient precision are not available and modelling is at least partially the job of the filter designer, moreover, it usually is the toughest part of the whole problem. Once a model is established, the rest of the work is almost straightforward. The optimal (continuous) estimator or Kalman filter is then of the form, see e.g. [3]

$$\dot{\hat{x}} = F\hat{x} + G_u u + K(t)\,[z - H\hat{x}] \tag{2-3}$$

In this formulation, the state estimator, Eq. (2-2) is of the same order as the dynamic system, Eq. (2-1), whose state is to be estimated. There may be many good reasons for lowering the order of the estimator, e.g., the use of so-called "kinematic estimators", neglection of unimportant states as well as restricted observability properties. This is discussed in the following sections.

2.1 Kinematic Modelling

For modelling our dynamic system we take a viewpoint which is sometimes described as "kinematic modelling"; it leads to a suboptimal filter of reduced-order which is insensitive to several parameters [4, 5].

The procedure can briefly be described as follows: assume that the total state-vector x can be split into two portions, x_1 and x_2 of order n_1, n_2 ($n_1 + n_2 = n$), where

$$\dot{x}_1 = F_{11} x_1 + F_{12} x_2 \tag{2-4}$$

$$\dot{x}_2 = f_2 (x_1, x_2, u, w) \tag{2-5}$$

In the context of mechanical systems, Eq. (2-4) is the set of *linearized kinematic equations* which describes the dependencies of angles and angular velocity components for rotational motions. The second set of equations, Eq. (2-5), is then the *dynamic* equations of motion, which need not even be in linearized form, since they are eliminated in the following. These latter equations, e.g., the Euler equations for angular motion, describe the interrelation between angular velocity and applied moments.

The measurement equations are assumed to be available in the form

$$z_1 = H_1 x_1 + v_1 \tag{2-6}$$

$$z_2 = H_2 x_2 + v_2 \tag{2-7}$$

where the measurements z_2 should be relatively accurate to provide good information on x_2 and the $n_2 \times n_2$ matrix H_2 should be nonsingular. This means that we require relatively good information on all dynamic state components.

Solving Eq. (2-7) for x_2 and substituting in Eq. (2-4) yields the reduced-order system

$$\dot{x}_1 = F_{11} x_1 + F_{12} H_2^{-1} z_2 - F_{12} H_2^{-1} v_2 \tag{2-8}$$

where z_2 is a deterministic input and v_2 is now, in this context "process" noise. With Eq. (2-8) and (2-6) one can now design a filter of order n_1 for x_1. This filter is suboptimal since it does not make use of the information represented by Eq. (2-5). However, it does not require precise modelling of the dynamic state equations which often involve uncertainties in the parameters as well as in the noise statistics; it is, therefore, also less sensitive.

Practically, especially for navigation systems, one often goes one step further and designs filters for the so-called *excrements* defined as

$$\delta x_1 = x_1 - \hat{x}_1 \tag{2-9}$$

where

$$\dot{\bar{x}}_1 = F_{11}\,\bar{x}_1 + F_{12}H_2^{-1}\,z_2 \tag{2-10}$$

Equation (2-10) could be interpreted as the prediction equations (predicting the state x_1 without using the measurements z_1) and are sometimes called the "*navigation equations*". The equations for the increments are then

$$\Delta\dot{x}_1 = F_{11}\,\Delta x_1 - F_{12}H_2^{-1}v_2 \tag{2-11}$$

$$\Delta z_1 = z_1 - H_1\bar{x}_1 = H_1\Delta x_1 + v_1 \tag{2-12}$$

The filter for the increments, therefore, has the structure (see Figure 1)

$$\Delta\dot{\hat{x}}_1 = F_{11}\,\Delta\hat{x}_1 + K_1[\Delta z_1 - H_1\,\Delta\hat{x}_1] \tag{2-13}$$

and the state estimate itself becomes

$$\dot{\hat{x}}_1 = \bar{x}_1 + \Delta\hat{x}_1 \quad , \quad (\hat{x}_2 = H_2^{-1}z_2) \tag{2-14}$$

Remarks: These considerations are valid for the white-noise terms v_1 and v_2. If v_2 is colored noise, it appears as process noise and can be treated by extending the state vector

$$\Delta x_1' = \begin{bmatrix} \Delta x_1 \\ v_2 \end{bmatrix} \tag{2-15}$$

and

$$\dot{v}_2 = A_2\,v_2 + \xi \tag{2-16}$$

If v_1 is colored noise, we have colored measurement noise, which requires a special treatment [5]. This case is not needed for the present application.

2.2 Error Dynamics for Platform Alignment

We now apply the general considerations of Section 2.1 to our platform alignment problem: The linearized kinematic equations for the platform angles can be written as follows [2,6]

$$\begin{bmatrix} \dot{\alpha} \\ \dot{\beta} \\ \dot{\gamma} \end{bmatrix} = \begin{bmatrix} 0 & \Omega_v & -\Omega_h \\ -\Omega_v & 0 & 0 \\ \Omega_h & 0 & 0 \end{bmatrix} \begin{bmatrix} \alpha \\ \beta \\ \gamma \end{bmatrix} + \begin{bmatrix} p \\ q \\ r \end{bmatrix} \tag{2-17}$$

where α, β, and γ are the platform angles about east-west, north-south and the azimuth axes, and p, q, and r are the corresponding angular velocities. These equations could be supplemented by the three Euler dynamic equations of the type

$$\begin{bmatrix} \dot{p} \\ \dot{q} \\ \dot{r} \end{bmatrix} = f_2(p,q,r,\alpha,\beta,\gamma) + G_2 \begin{bmatrix} M_\alpha \\ M_\beta \\ M_\gamma \end{bmatrix} \tag{2-18}$$

However, using section 2.1, this is not necessary. Because of the three platform mounted gyros we have good information on the angular velocity components p,q, and r available in the form

$$z_2 = \begin{bmatrix} p - \bar{D}_e \\ q - \bar{D}_n \\ r - \bar{D}_v \end{bmatrix} \qquad (2\text{-}19)$$

where $\bar{D}_e$, $\bar{D}_n$, $\bar{D}_v$ are the total drifts of the corresponding gyros (measurement noise). Using the results of Eq. (2-11), including the fact that in the present application $\tilde{x}_1 \equiv 0$, because we measure the misalignment angles from the zero position, i.e., $\alpha \equiv \Delta\alpha$, ... one obtains as the platform error equations

$$\begin{aligned} \dot{\alpha} &= \Omega_v \beta - \Omega_h \gamma + \bar{D}_e \\ \dot{\beta} &= -\Omega_v \alpha + \bar{D}_n \\ \dot{\gamma} &= \Omega_h \alpha + \bar{D}_v \end{aligned} \qquad (2\text{-}20)$$

where the gyro drift appears now as input (process) noise to Eq. (2-20) (see Figure 2).

Information on the platform misalignment angles is available through the two platform-mounted accelerometers. (Their output is used in flight to provide information on vehicle acceleration, velocity, and position). The accelerometers are mounted in the horizontal plane so that their output is (on ground) proportional to the misalignment angles α and β

$$z_1 = \begin{bmatrix} g\,\alpha + \bar{B}_e \\ -g\,\beta + \bar{B}_n \end{bmatrix} \qquad (2\text{-}21)$$

where $\bar{B}_n$ and $\bar{B}_e$ are the total accelerometer errors (including errors of signal transmitters).

2.3 Noise Modelling

If the noise inputs in Eq. (2-20) and (2-21) would be white (known R) the design of the Kalman filter would be straightforward and, in fact, of order 3 (see conventional gyrocompassing loops). Complete noise models are, however, more complex and hardly available in the literature. We therefore agreed to set up a test series at IABG for achieving trustworthy noise models for the gyro drift of the G-200 gyro and for the accelerometer errors of the A-200 accelerometer, those instruments with which the LN-3 platform - used for the case study - is equipped. The noise models were obtained by determining the autocorrelation functions from the test, choosing simple models with known correlation functions and computing their parameters to match the measured correlation as well as possible (least-squares fit). The results are reported in [7] and are summarized in Sections 2.3.1 and 2.3.2.

2.3.1 Gyro Drift Models

The general drift model of a G-200 gyro can be described by a Gauss-Markov process of the type (Figure 3)

$$\bar{D} = D + d^r + d^c + w \qquad (2\text{-}22)$$

where

- D = bias
- d^r = random ramp
- d^c = correlated noise
- w = white noise

One therefore can write four state-equations to describe the total drift

$$\begin{aligned} \dot{D} &= 0 \\ \dot{d}^r &= c^r \\ \dot{c}^r &= 0 \\ \dot{d}^c &= -\alpha_d d^c + w^c \end{aligned} \tag{2-23}$$

where

c^r = constant slope of the ramp, $\alpha_d = 1/T_d$, T_d = correlation time constant,

w^c = white noise generating d^c.

Remark: It shall be noted that similar behavior occurs in the three channels except there is noticeable correlated noise only in the vertical channel.

If one tries to take the drift terms into account in an optimal fashion as indicated by Eq. (2-15) and (2-16), the state-vector in Eq. (2-20) has to be extended by 10 drift-states to a total size of 13 components

$$\begin{aligned}
(1)\quad \dot{\alpha} &= \Omega_V \beta - \Omega_h \gamma + D_e + d_e^r + w_e \\
(2)\quad \dot{\beta} &= -\Omega_V \alpha + D_n + d_n^r + w_n \\
(3)\quad \dot{\gamma} &= \Omega_h \alpha + D_V + d_V + d_V^r + w_V \\
(4)\quad \dot{D}_e &= 0 \\
(5)\quad \dot{D}_n &= 0 \\
(6)\quad \dot{D}_V &= 0 \\
(7)\quad \dot{d}_V &= -\alpha_V d_V + w_{d_V} \\
(8)\quad \dot{d}_e^r &= c_e^r \\
(9)\quad \dot{d}_n^r &= c_n^r \\
(10)\quad \dot{d}_V^r &= c_V^r \\
(11)\quad \dot{c}_e^r &= 0 \\
(12)\quad \dot{c}_n^r &= 0 \\
(13)\quad \dot{c}_V^r &= 0
\end{aligned} \tag{2-24}$$

The nominal set of parameters for all terms is summarized in Table 1. It should be noted that nominally, for the parameters of the spectral density matrix Q, high (pessimistic) upper bounds are taken. It is well known that in this case the filter design is on the save side and the optimal variances are not too optimistic.

2.3.2 Accelerometer Error Models

Similarly, the results of testing accelerometers of the A-200 type can be summarized as follows

$$\bar{B} = B + b^r + b^{c_1} + b^{c_2} + v \tag{2-25}$$

where

B	=	bias
b^r	=	random ramp
b^{c_1}, b^{c_2}	=	correlated-noise terms
v	=	white noise

Table 1. Nominal set of parameters for case study

Coefficients:

$\Omega_v = 5.771 \cdot 10^{-5}$ rad/s; $\Omega_h = 4.458 \cdot 10^{-5}$ rad/s; $T_v = 1/\alpha_v = 37$ min; $g = 9.814$ m/s^2

Initial Uncertainty:

rms $\alpha(0)$ = rms $\beta(0)$ = 0.2°	or	$P_\alpha(0) = P_\beta(0) = 9 \cdot 10^{-6}$ rad^2
rms $\gamma(0)$ = 5° - 6° ≅ 0.1 rad	or	$P_\gamma(0) = 10^{-2}$ rad^2
rms D_e = rms D_n = rms D_v = 0.5°/h	or	$P_{D_e}(0) = P_{D_n}(0) = P_{D_v}(0) = 0.587 \cdot 10^{-11}$ rad^2/s^2
rms $d_v \leq$ 0.15 °/h	or	$P_{d_v}(0) = 2 \cdot 10^{-13}$ rad^2/s^2
rms $d_e^r(0)$ = rms $d_n^r(0)$ = rms $d_v^r(0)$ = 0	or	$P_{d_e^r}(0) = P_{d_n^r}(0) = P_{d_v^r}(0) = 0$
rms c_e^r = rms c_n^r = rms $c_v^r = 5 \cdot 10^{-4}$ °/h^2	or	$P_{c_e^r}(0) = P_{c_n^r}(0) = P_{c_v^r}(0) = 0.5 \cdot 10^{-24}$ rad^2/s^4
rms B_e = rms $B_n = 6 \cdot 10^{-5}$ g	or	$P_{B_e}(0) = P_{B_n}(0) = 3.5 \cdot 10^{-7}$ m/s^2

Spectral Densities:

Q : $q_e = q_n = 0.56 \cdot 10^{-14}$ 1/s ; $q_v = 1.69 \cdot 10^{-14}$ 1/s ; $q_{d_v} = 1.06 \cdot 10^{-18}$ 1/s

R : $r_e = r_n = 0.5 \cdot 10^{-4}$ m^2/s^2

For each accelerometer, the total error can be expressed by five state equations

$$\begin{aligned} \dot{B} &= 0 \\ \dot{b}^r &= c^b \\ \dot{c}^b &= 0 \\ \dot{b}^{c_1} &= -\alpha_1 b^{c_1} + w^{b_1} \\ \dot{b}^{c_2} &= -\alpha_2 b^{c_2} + w^{b_2} \end{aligned} \qquad (2\text{-}26)$$

Also, to take this noise into account in an optimal fashion, one has to extend the state vector of Eq. (2-24) by 10 more state components for $\bar{B}_n$ and $\bar{B}_e$ and arrives at a total state vector with 23 components.

Note: The level of the white noise does not only contain the accelerometer-instrument error, but also the signal-transmission error, which in this case is dominant [6]. The significant values are again given in Table 1.

2.4 Selection of a Design Model

The goal of the state-estimator design, in the present case, is to provide indications of the physically interesting values, i.e., the misalignment angles α, β and γ. Their estimates, $\hat{\alpha}$, $\hat{\beta}$ and $\hat{\gamma}$ should be as close as possible to the exact values, keeping also in mind the effort for implementation. In this context, the extra states are to be considered as auxiliary quantities, which theoretically need also to be estimated to provide optimal values for the angles, but are not of prime interest in themselves. Thus,

in theory, the optimal filter is of order 23, equal to the order of the total process (see Eq. (2-1,3) and (2-3)).

However, this would not be economic, mainly because:

(1) Some of the terms may be taken into account, whose influence on the system behavior is not significant.

(2) Some terms may be not observable and there may be, therefore, an estimator of lower order yielding the same accuracy as the full-order Kalman filter.

We consider first terms of the first kind and suggest that they be neglected for the estimator design. This procedure will ultimately be justified by analyzing the resulting filter on the full scale model, (Section 4.2).

2.4.1 Negligible Drift Components

We have already noticed that there were no noteworthy correlated drift components in the horizontal axes.

Secondly, the random ramp components - theoretically growing unbounded - are of minor influence during alignment times of interest in the range of 3 to 15 minutes. For these timespans their rms values are one to two orders of magnitude smaller as, e.g., the bias terms. Therefore all random ramps are neglected in the design.

2.4.2 Negligible Sensor Errors

It follows from the parameters of the test results that, as in Section 2.4.1, the random ramps are very small, which in this case is also true for the correlated-noise terms as compared, e.g., to the bias; they can therefore be neglected without hesitation.

The relation of the level of the bias to the level of the white noise depends on the quality of the signal which can be tapped at the platform. For the noise level in the nominal case (Table 1), the bias terms B_e and B_n seem to be negligible. However, for the north-south accelerometer at the analog navigation computer of the LN-3 platform a signal of higher quality could be tapped (leading to a lower value of r_e)

$$\text{rms } v_e \approx 7 \times 10^{-5} \text{ g or } r_e \approx 0.5 \times 10^{-6} \text{ m}^2/\text{s}^3 \qquad (2\text{-}27)$$

In this case the bias (maximum 6×10^{-5} g) is not negligible any more. Therefore depending on the situation, we may or may not neglect the accelerometer bias, especially B_e.

In conclusion, we arrive at the following design model:

Process:

$$\begin{aligned}
&(1)\quad \dot{\alpha} = \Omega_v \beta - \Omega_h \gamma + D_e + w_e \\
&(2)\quad \dot{\beta} = -\Omega_v \alpha + D_n + w_n \\
&(3)\quad \dot{\gamma} = \Omega_h \alpha + D_v + d_v + w_v \\
&(4)\quad \dot{D}_e = 0 \\
&(5)\quad \dot{D}_n = 0 \\
&(6)\quad \dot{D}_v = 0 \\
&(7)\quad \dot{d}_v = -\tau_v d_v + w_{d_v}
\end{aligned} \qquad (2\text{-}28)$$

Measurements:

$$\begin{aligned}
z_e &= g\alpha + B_e + v_e \\
z_n &= -g\beta + B_n + v_n
\end{aligned} \qquad (2\text{-}29)$$

Measurement Bias:

$$\text{(8)}\quad \dot{B}_e = 0 \qquad \text{(9)}\quad \dot{B}_n = 0 \tag{2-30}$$

3. FILTER DESIGN AND REDUCTION OF ORDER

After all of these preparatory considerations, we now enter the actual filter design. The most important requirement, expressing the filter's ability to reduce the estimation error as compared with the unfiltered process (see Eq. (2-28) and (2-30)) is the observability of this process under the observations (see Eq. (2-29)) [1,5]. The problem of observability can partially be treated by deterministic means, i.e., it is a structural property expressed by the matrices F and H. However, this does not answer the question of how 'well' certain quantities can be determined. The latter can only be answered by stochastic means. We shall handle both problems which both give rise to order-reduction in this section.

3.1 Consequences of Restricted Observability

In most cases of filter application, one is faced with the fact that a given process is not completely observable, especially if - as is the case here - noise models are added to the physical quantities. The best insight in the consequences for the filter design is obtained then by transforming the original system, Eq. (2-1) and (2-2), to (observable) canonical form [5] via the linear transformation

$$y = T_o\, x \;;\quad T_o = \begin{bmatrix} I_q & \vdots & L \\ \cdots & \vdots & \cdots \\ 0 & \vdots & I_{n-q} \end{bmatrix} \tag{3-1}$$

This brings Eq. (2.1) and (2-2) into the form

$$\dot{y}_1 = A_{11}\, y_1 + B_1\, w \tag{3-2}$$

$$\dot{y}_2 = A_{21}\, y_1 + A_{22}\, y_2 + B_2\, w$$

$$z = C_1\, y_1 + v \tag{3-3}$$

Here y_1 is observable (q terms) and y_2 is the unobservable part (n-q terms). Note that the nonobservable part of the state vector remains unchanged by the linear transformation $y_2 = x_2$ (possibly after reordering), whereas the observable quantities y_1 are linear combinations of the original states x_1 and the unobservable states x_2

$$y_1 = x_1 + L\, x_2 \tag{3-4}$$

Formal application of the filter equations (Eq. (2-3)) to Eq. (3-2) and (3-3) yields (see Figure 4)

$$\dot{\hat{y}}_1 = A_{11}\, \hat{y}_1 + K_1[z - C_1\, \hat{y}_1] \tag{3-5}$$

$$\dot{\hat{y}}_2 = A_{21}\, \hat{y}_1 + A_{22}\, \hat{y}_2 + K_2[z - C_1\, \hat{y}_1]$$

If we denote the covariance matrix of the transformed system by Π

$$\Pi = E\{(y-\hat{y})(y-\hat{y})^T\} = \begin{bmatrix} \Pi_{11} & \Pi_{12} \\ \Pi_{12}^T & \Pi_{22} \end{bmatrix} \tag{3-6}$$

we can formulate the properties [5]:

(1) The problem of estimating the qx1 vector y_1 can be treated separately as neither y_2 nor Π_{12} or Π_{22} are needed, and

$$K_1 = \Pi_{11} C_1^T R^{-1} \tag{3-7}$$

The filter for $\hat{y}_1$ is of order q.

(2) The estimation problem for $y_2 = x_2$ depends on y_1 and Π_{11}. Thus, this may influence the accuracy of $\hat{x}_1$ via $\hat{x}_1 = \hat{y}_1 - L\hat{x}_2$. Very often it is, however, sufficient to let $\hat{x}_1 \approx \hat{y}_1$ and abandon the estimation of x_2.

(3) It is questionable whether the overall filter, Eq. (3-5), is stable. In fact, it is not stable if A_{22} is not stable from the outset [5]. If A_{22} is stable, the system is called "detectable" and the resulting filter is stable.

At DFVLR we have developed a computer program, which transforms a general given system of the type of Eq. (2-1) and (2-2) into the canonical form of Eq. (3-2) and (3-3); it provides the number of observable states and their dependencies on the unobservable states, i.e., the matrix L in Eq. (3-4).

In the present case, it is also possible to decide on observability analytically; this allows an independent check on the numerical results and more clearly provides the dependencies on the general parameters. The idea is to use the measurement equations and their time derivatives inserted in the differential equations and then to solve for the states if possible. Usually, the more differentiations that are needed for a state, the poorer are its estimates. However, precise quantitative answers are obtained only from a covariance analysis.

3.2 Observability Analysis

3.2.1 Observability of the Drift ($B_e \equiv B_n \equiv 0$)

It can be shown that the observable quantities are

$$y_1^T = [\alpha, \beta, \bar{\gamma}, D_n, D_v, d_v] \tag{3-8}$$

with

$$\bar{\gamma} = \gamma - \frac{D_e}{\Omega_h}$$

The observable subsystem is

$$\begin{aligned}
(1)\quad \dot{\alpha} &= \Omega_v \beta - \Omega_h \bar{\gamma} + w_e \\
(2)\quad \dot{\beta} &= -\Omega_v \alpha + D_n + w_n \\
(3)\quad \dot{\bar{\gamma}} &= \Omega_h \alpha + D_v + d_v + w_v \\
(4)\quad \dot{D}_n &= 0 \\
(5)\quad \dot{D}_v &= 0 \\
(6)\quad \dot{d}_v &= -\alpha_v d_v + w_{d_v}
\end{aligned} \tag{3-9}$$

with

$$\begin{aligned}
z_e &= \beta + v_e \\
z_n &= -\alpha + v_n
\end{aligned} \tag{3-10}$$

It is easily seen that all quantities in Eq. (3-9) are observable; however, the estimate of the azimuth angle γ, using $\bar{\gamma}$, is contaminated by an unobservable bias of the size D_e/Ω_h.

3.2.2 Observability of the Accelerometer Bias

If the accelerometer biases B_e and B_n are not negligible, estimation of them could be considered to reduce their influence on the accuracy of the misalignment angles. Thus, it needs to be investigated whether these quantities are observable.

It can shown, however, that the observable subsystem remains of order 6 as in Eq. (3-9). That is, the two additional states, B_e and B_n, Eq. (2-29) and (2-30), are not observable. In fact the observable states are now

$$
\begin{aligned}
(1)\quad \bar{\alpha} &= \alpha + \frac{B_e}{g} \\
(2)\quad \bar{\beta} &= \beta - \frac{B_n}{g} \\
(3)\quad \bar{\gamma} &= \gamma - \frac{D_e}{\Omega_h} - \frac{\Omega_v}{\Omega_h}\frac{B_n}{g} \\
(4)\quad \bar{D}_n &= D_n + \Omega_v \frac{B_e}{g} \\
(5)\quad \bar{D}_v &= D_v - \Omega_h \frac{B_e}{g} \\
(6)\quad \bar{d}_v &= d_v
\end{aligned}
\tag{3-11}
$$

Unobservable are D_e, B_e and B_n, which means that an estimator of order 6 is most likely to provide the same estimation accuracy as would an estimator of order 9.

3.3 Proposed Low-Order Filter

The structural considerations of the previous subsections are still somewhat abstract since they do not allow the question of how good the estimates may be to be answered. Quantitative statements of this kind are reserved for the optimal filter and its accompanying covariance equation of the Riccati type. We therefore computed a variety of optimal covariances to develop a nominal filter of minimal order.

In order to confirm the statements of Section 3.2 we ran the full size filter for all nine states of Eq. (2-28) and (2-29). In addition, this filter has the advantage of setting the standard for comparison with all other filters because it provides the minimum possible variances for all states.

The results can be summarized as follows:

(1) The variances of the unobservable states D_e, B_e and B_n remain constant as expected. Thus, it does not pay to keep these states in the filter.

(2) The variances of the misalignment angles about the horizontal axes decrease very rapidly to small values (see Figure 5). This behavior is due to the fact that direct information for α and β is available through the accelerometers. The stationary variances are predominantly determined by the level of the (white) accelerometer noise; only in α does the variance continue to decrease slightly due to the improvement in the drift estimates ($\hat{D}_n$).

(3) The azimuth estimate γ has to be determined through the dynamic equations (no direct measurement) and therefore does not decrease as rapidly. It reaches its stationary value after about 30 or 40 minutes (Figure 6).

(4) The estimation of D_n behaves, qualitatively, similarly to γ. Its variance decreases to small values after a few minutes (Figure 7). Theoretically, D_n can be estimated exactly (no process noise); however, the stationary filter would not be stable [5].

(5) The estimate of d_v improves still more slowly (in agreement with the necessity of taking higher derivatives of the measurements as explained in Section 3.2), and the improvement in D_v is almost not recognizable within the interesting observation interval (3 to 20 minutes) (Figure 8).

As a result, it seems worthless to keep the state D_v in the filter - it is very weakly observable within the time-interval of interest. The resulting filter is then of order 5 and has the form

$$\begin{aligned}
\dot{\hat{\alpha}} &= \Omega_v \hat{\beta} - \Omega_h \hat{\gamma} + K_{11}(t)[z_e - g\hat{\alpha}] + K_{12}(t)[z_n + g\hat{\beta}] \\
\dot{\hat{\beta}} &= -\Omega_v \hat{\alpha} + \hat{D}_n + K_{21}(t)[\quad " \quad] + K_{22}(t)[\quad " \quad] \\
\dot{\hat{\gamma}} &= \Omega_h \hat{\alpha} + \hat{d}_v + K_{31}(t)[\quad " \quad] + K_{32}(t)[\quad " \quad] \\
\dot{\hat{D}}_n &= 0 + K_{41}(t)[\quad " \quad] + K_{42}(t)[\quad " \quad] \\
\dot{\hat{d}}_v &= -a_v \hat{d}_v + K_{51}(t)[\quad " \quad] + K_{52}(t)[\quad " \quad]
\end{aligned} \tag{3-12}$$

The following simplifications may be considered:

(1) Depending on the observation interval, the consequences of leaving off the states d_v and finally D_n may be investigated (Section 4.2).

(2) Some of the gains can be approximated by constant or piecewise-constant gains.

(3) Moreover, the continuous filter may be - for ease of implementation - approximated by a discrete filter [6].

In any event, the continuous filter, as discussed above, sets the standards for comparison.

4. ANALYSIS OF THE PROPOSED FILTER

As we have seen in the foregoing discussions, there are a variety of reasons why the model used in the filter differs from the real model. Some of these are:

(1) Insufficiencies in the model itself resulting from varying and unknown parameters.

(2) Neglecting quantities which do not seem to have significant influences.

(3) Neglecting unobservable or weakly observable states.

(4) Approximate gains for implementation.

In all of these cases the accompanying optimal covariance matrix is suspicious because it is based on the simplified model (selfdiagnostic) [3]. A remedy to this situation is a complete covariance analysis of the filter design on the real system model and the applied gains. Such a covariance analysis can be performed as long as the exact system can be linearized, which is certainly true for fine alignment. To get answers of any statistical value from simulation, many expensive simulations and evaluations would have to be performed.

In any event, a final experimental verification is always appropriate [6].

4.1 A General Program for Filter Covariance Analysis

The aforementioned covariance analysis can be performed as follows:

(1) Let the design model for the filter be

$$\dot{x}_1 = F_{11}^{*} x_1 + G_1^{*} w_1 \tag{4-1}$$

$$z^{*} = H_1^{*} x_1 + v \tag{4-2}$$

where for w_1 and v spectral density matrices Q_1^{*} and R^{*} are assumed, leading to an optimal filter for the nominal values of the form

$$\dot{\hat{x}}_1 = F_{11}^* \hat{x}_1 + K_1^* (z^* - H_1^* \hat{x}_1) \tag{4-3}$$

(2) The actual system, however, is assumed to be described by

$$\dot{x}_1 = F_{11} x_1 + F_{12} x_2 + G_1 w_1 \tag{4-4}$$

$$\dot{x}_2 = F_{21} x_1 + F_{22} x_2 + G_2 w_2 \tag{4-5}$$

$$z = H_1 x_1 + H_2 x_2 + v \tag{4-6}$$

where w_1, w_2 and v actually have spectral densities Q_1, Q_2 and R respectively.

(3) The deviations of the design parameters from the system parameters are defined as

$$\Delta F_{11} = F_{11} - F_{11}^* \tag{4-7}$$

$$\Delta H_1 = H_1 - H_1^* \tag{4-8}$$

(4) Finally, the covariance of the estimation error, $\tilde{x}_1 = x_1 - \hat{x}_1$, resulting from using the filter Eq. (4-3) at the process Eq. (4-4) through (4-6) is to be computed from the following set of equations

$$\dot{X} = F X + X F^T + G Q G^T \tag{4-9}$$

$$\begin{aligned} \dot{U} = {} & F U + U(F_{11}^* - K_1^* H_1^*)^T \\ & + X[\Delta F_{11} - K_1^* \Delta H_1 \,\vdots\, F_{12} - K_1^* H_2]^T \\ & + \left[\begin{array}{c|ccc} G_1 & Q_1 & & G_1^T \\ \hline & 0 & & \end{array}\right] \end{aligned} \tag{4-10}$$

$$\begin{aligned} \dot{S}_1 = {} & (F_{11}^* - K_1^* H_1) S_1 + S_1 (F_{11}^* - K_1^* H_1^*)^T + \\ & + [\Delta F_{11} - K_1^* \Delta H_1 \,\vdots\, F_{12} - K_1^* H_2] U + \\ & + U^T [\Delta F_{11} - K_1^* \Delta H_1 \,\vdots\, F_{12} - K_1^* H_2]^T + \\ & + G_1 Q G_1^T + K_1^* R K_1^{*T} \end{aligned} \tag{4-11}$$

where

$$S_1 = E\{\tilde{x}_1 \tilde{x}_1^T\}, \qquad U = E\{x \tilde{x}_1^T\}, \qquad X = E\{x x^T\}$$

and

$$F = \begin{bmatrix} F_{11} & F_{12} \\ F_{21} & F_{22} \end{bmatrix}, \qquad G = \begin{bmatrix} G_1 & 0 \\ 0 & G_2 \end{bmatrix}, \qquad Q = \begin{bmatrix} Q_1 & 0 \\ 0 & Q_2 \end{bmatrix}$$

Remarks:

(1) The filter gains used in Eq. (4-3) do not need to result from an optimal filter design for Eq. (4-1) and (4-2); in fact, they can be any gains (time-varying or constant), used in the actual filter.

Remarks (Cont.):

(2) Note that Eq. (4-9) through (4-11) are coupled in one direction, i.e., X. The covariance of the process without filtering, from Eq. (4-9) is used to obtain U via Eq. (4-10) and finally U is needed in Eq. (4-11) to compute the error covariance of the estimate $\hat{x}_1$.

(3) Note also, that for exact system order and parameters ($\Delta F_{11} = 0$, $\Delta H_1 = 0$) only Eq. (4-11) is needed and reduces to

$$\dot{S} = (F - K^* H)\, S + S(F - K^* H)^T + G\, Q\, G^T + K^*\, R\, K^{*T} \qquad (4\text{-}12)$$

i.e., a set of linear equations for given K^*. Furthermore, Eq. (4-12) is identical to the Riccati equation for $K^* = PH^T R^{-1}$, i.e., for optimal gains.

The general approach presented in this section is used in the following for two purposes: first, for verification of the filter reductions by choosing the design model of Section 2.4 and the observability consequences of Section 3.3; and second, investigating the filter sensitivity on parameter changes.

4.2 Filter Reduction via Covariance Analysis

To verify the previously mentioned reductions of order and to investigate possible further reductions, an extensive covariance analysis was performed: first, with reference to the design model of order 7 and nominal parameters; second, the resulting filter was analyzed on the full-size model of order 15.

The following cases were considered:

(1) A seventh-order filter for α, β, γ, D_e, D_n, D_v, d_v

(2) A sixth-order filter for α, β, γ, D_n, D_v, d_v

(3) A fifth-order filter for α, β, γ, D_n, D_v (or d_v)

(4) A fourth-order filter for α, β, γ, D_n

(5) A third-order filter for α, β, γ

The analysis was performed on the design model and considers in each case the influence of all neglected quantities. The results are summarized in Table 2 and in the following:

(1) The seventh-order filter provides the bounds for the reachable accuracy and serves as the reference for evaluation.

(2) It is very interesting to note that the following filters of order 6 to 4 provide the same accuracy as the seventh-order one in the remaining states. (However, their selfdiagnostic is too optimistic, as expected.) For that reason, it is - at least for the short estimation interval of 3 minutes - most efficient to implement only a filter of fourth-order. If longer duration for fine alignment is allowed, or if larger values of the (observable) drift components have to be considered, a sixth-order filter can provide improved estimates on D_n, D_v, and d_v, and reduce their undesirable influence on the estimates of α and β. However, a noticeable effect during an interval of 10 minutes occurs only in estimating D_n and its influence on β (see Table 2). The quantities D_v and especially d_v can only be estimated if a very long observation time were allowed.

(3) A further reduction to a filter of third-order seems not to be appropriate in comparison with the results for the fourth-order filter: the accuracy of the estimate of β deteriorates significantly (see Table 2).

As a result, a fourth-order filter seems to be the best compromise between estimation accuracy and expenditure for implementation.

In order to verify that all neglected quantities are really negligible, we analyzed the proposed fourth-order filter on the full-size model, taking into account all drift components, i.e., Eq. (2.24), as well as the accelerometer bias terms, Eq. (2-30).

The results prove the validity of the preceding reductions:

(1) Within an estimation period of at least up to 15 minutes the random ramps are negligible. Their inclusion would not in any respect improve the estimates.

(2) The unobservable bias terms B_c, B_e, and B_n do contribute to the estimation error. However, their inclusion in the filter would not bring any advantage because of the filter's inability to reduce their uncertainties.

Table 2. Error variances after 3 and 10 minutes of operation - nominal data.

Estimation Error After 3 minutes	Initial Variances (Nominal)	Seventh-Order Filter	Sixth-Order Filter	Analysis of Sixth-Order Filter	Fifth-Order Filter	Analysis of Fifth-Order Filter	Fourth-Order Filter	Analysis of Fourth-Order Filter	Third-Order Filter	Analysis of Third-Order Filter
σ_α^2 [rad^2]	$0.9\cdot10^{-5}$	$0.111\cdot10^{-7}$	$0.110\cdot10^{-7}$	$0.112\cdot10^{-7}$	$0.110\cdot10^{-7}$	$0.112\cdot10^{-7}$	$0.110\cdot10^{-7}$	$0.112\cdot10^{-7}$	$0.110\cdot10^{-7}$	$0.112\cdot10^{-7}$
σ_β^2 [rad^2]	$0.9\cdot10^{-5}$	$0.101\cdot10^{-7}$	$0.101\cdot10^{-7}$	$0.101\cdot10^{-7}$	$0.101\cdot10^{-7}$	$0.102\cdot10^{-7}$	$0.101\cdot10^{-7}$	$0.102\cdot10^{-7}$	$0.288\cdot10^{-8}$	$0.502\cdot10^{-7}$
σ_γ^2 [rad^2]	$0.1\cdot10^{-1}$	$0.318\cdot10^{-2}$	$0.509\cdot10^{-3}$	$0.318\cdot10^{-2}$	$0.509\cdot10^{-3}$	$0.318\cdot10^{-2}$	$0.509\cdot10^{-3}$	$0.318\cdot10^{-2}$	$0.509\cdot10^{-3}$	$0.318\cdot10^{-2}$
$\sigma_{D_e}^2$ [rad^2/s^2]	$0.587\cdot10^{-11}$	$0.587\cdot10^{-11}$	-	-	-	-	-	-	-	-
$\sigma_{D_n}^2$ [rad^2/s^2]	$0.587\cdot10^{-11}$	$0.903\cdot10^{-12}$	$0.903\cdot10^{-12}$	$0.904\cdot10^{-12}$	$0.903\cdot10^{-12}$	$0.904\cdot10^{-12}$	$0.903\cdot10^{-12}$	$0.904\cdot10^{-12}$	-	-
$\sigma_{D_v}^2$ [rad^2/s^2]	$0.587\cdot10^{-11}$	$0.587\cdot10^{-11}$	$0.587\cdot10^{-11}$	$0.587\cdot10^{-12}$	$0.587\cdot10^{-11}$	$0.587\cdot10^{-11}$	-	-	-	-
$\sigma_{d_v}^2$ [rad^2/s^2]	$0.2\cdot10^{-12}$	$0.170\cdot10^{-12}$	$0.170\cdot10^{-12}$	$0.170\cdot10^{-12}$	-	-	-	-	-	-
After 10 minutes				As above						
		$0.364\cdot10^{-8}$			$0.364\cdot10^{-8}$	$0.347\cdot10^{-8}$	$0.345\cdot10^{-8}$	$0.347\cdot10^{-8}$	$0.345\cdot10^{-8}$	$0.334\cdot10^{-8}$
		$0.344\cdot10^{-8}$			$0.344\cdot10^{-8}$	$0.345\cdot10^{-8}$	$0.344\cdot10^{-8}$	$0.345\cdot10^{-8}$	$0.867\cdot10^{-9}$	$0.526\cdot10^{-6}$
		$0.229\cdot10^{-2}$			$0.150\cdot10^{-4}$	$0.269\cdot10^{-2}$	$0.145\cdot10^{-4}$	$0.296\cdot10^{-2}$	$0.115\cdot10^{-4}$	$0.296\cdot10^{-2}$
As above		$0.587\cdot10^{-11}$			-	-	-	-	-	-
		$0.287\cdot10^{-13}$			$0.287\cdot10^{-13}$	$0.287\cdot10^{-13}$	$0.287\cdot10^{-13}$	$0.287\cdot10^{-13}$	-	-
		$0.586\cdot10^{-11}$			$0.586\cdot10^{-11}$	$0.586\cdot10^{-11}$	-	-	-	-
		$0.117\cdot10^{-11}$			-	-	-	-	-	-

The difference between the previous seventh-order analysis and the present one is due only to the accelerometer bias terms. The error variances of α and β are higher by exactly these sensor biases (0.36×10^{-8} rad^2). The influence is still modest: about 30% after 3 minutes and a factor of 2 after 10 minutes in the α and β variances; no change at all in γ.

The situation, however, changes significantly if the noise level of the accelerometer is lower, as we shall see.

4.3 Analysis of the Proposed Filter Under Parameter Uncertainties

To localize the sensitivity of the filter with respect to parameter uncertainties, only some of the parameters were changed in each of the following cases.

4.3.1 Variation of the Drift Time Constant

The nominal value of the drift time constant is $T_v^* = 37$ minutes; the variation about this value can be as big as ±20 minutes [7]. Of most significance could be the variation to lower values, since for higher values the drift d_v approaches a bias. It was, therefore, investigated how a filter (designed for $T_v^* = 37$ minutes) behaves if actually $T_v = 17$ minutes.

As expected, the result was as follows: the analysis of the seventh-order filter on the seventh-order process yielded a slight change only in the estimate of d_v; all other errors remained unchanged in the relevant figures; this was also the case for the low-order filters down to order 4. The reason for this behavior is due to the fact that the time constant of the drift is still relatively large with respect to the observation time and, moreover, the effect of d_v on the physical quantities is modest.

4.3.2 Variation of the Drift Noise Level

Because upper bounds were assumed for the drifts in the previous considerations, the results obtained are on the pessimistic side, i.e. if the actual drift level is lower, the filter may allow better accuracy as indicated so far. Especially, if the spectral densities (Q-matrix) are nominally set fairly high. Thus, we investigated two cases:

Case 1: Lowering the spectral density parameters by a factor of 4, but keeping the initial variances of the drift to their nominal values. This corresponds to an uncalibrated platform with rather big bias terms (0.5 °/h).

Case 2: Lowering in addition the bias D_e to 0.04 °/h, corresponding to a calibrated platform. This value could also be achieved for a noncalibrated platform by the following procedure: Turn the whole platform so that the east-west gyro becomes a north-south gyro, i.e., $D_e = D_n'$; estimate the north-south's gyro drift D_n', i.e. $\hat{D}_n' = D_e$ for some minutes and turn the platform to its normal attitude.

The results are summarized in Table 3: there is no significant change in the accuracy of α and β as compared with the nominal case. This is not surprising since their error mainly depends on the accuracy of the accelerometer. The azimuth estimate is improved slightly in Case 1. The size of the spectral density Q is already such that its influence on the state estimates is modest. This was confirmed by letting $Q = 0$ and still having about the same results. Significant changes in the azimuth estimate are, however, recorded in Case 2, where the azimuth error variance is improved after 3 minutes by one order of magnitude and after 10 minutes by two orders of magnitude as compared to the nominal. This result is caused by the fact that the unobservable drift D_e which rests upon $\hat{\gamma}$ is much lower.

4.3.3 Variation of the Accelerometer Noise Level

Last, but not least, the influence of the accelerometer noise level on the filter accuracy was investigated. This is of special interest, since it is expected that the dependency is very significant and accelerometer signals of different quality are available, Eq. (2-27).

The results were computed with the low values in the drift as previously described and can be summarized as follows (see Table 4):

The strongest influence to be recorded is on the accuracy of estimating α and β; in fact, the optimal filter's variances are direct proportional to R (see Table 4). The influence on the accuracy of the azimuth estimate is not as big.

It is very interesting to note that the filter designed with the incorrect values (R^*) and analyzed with the correct values (R) does not deteriorate significantly. That is, even if the design values for the noise are set wrongly (at R^*) and the real values are higher (at R) the filter is still able to provide almost optimal estimates (see Table 4).

Also, an accelerometer bias of $6 \cdot 10^{-5}$ g may no longer be negligible. Therefore we added this bias to the error budget for Case 1, leading considerably higher error variances for α and β (see Table 4). Especially with respect to α, it does not pay to search for improved signals in v_e (white noise) as long as we have to deal with the above-mentioned bias. In this case, the bias determines the level of the error in $\hat{\alpha}$.

Table 3 Error variances for variation of drift noise level

	Initial Variances	Case 1 After 3 min	Case 1 After 10 min	Case 2 After 3 min	Case 2 After 10 min
σ_α^2 [rad^2]	$0.9 \cdot 10^{-5}$	$0.112 \cdot 10^{-7}$	$0.347 \cdot 10^{-8}$	$0.111 \cdot 10^{-7}$	$0.347 \cdot 10^{-8}$
σ_β^2 [rad^2]	$0.9 \cdot 10^{-5}$	$0.102 \cdot 10^{-7}$	$0.345 \cdot 10^{-8}$	$0.102 \cdot 10^{-7}$	$0.345 \cdot 10^{-8}$
σ_γ^2 [rad^2]	$0.1 \cdot 10^{-1}$	$0.259 \cdot 10^{-2}$	$0.229 \cdot 10^{-2}$	$0.528 \cdot 10^{-3}$	$0.339 \cdot 10^{-4}$

Case 1: $q_e = q_n = 0.14 \cdot 10^{-14}$ 1/s ; $q_v = 0.42 \cdot 10^{-14}$ 1/s ; elsewhere nominal

Case 2: q_e, q_n, q_v as Case 1; $P_{D_e}(o) = 3.76 \cdot 10^{-14}$ rad^2/s^2 ; elsewhere nominal

Table 4 Error variances for variation of accelerometer noise level ($P_{D_e} = 3.76 \cdot 10^{-14}$ rad^2/s^2).

3 min of operation	Initial Variances	Case 1	Case 2	Case 3	Case 4	Case 5
σ_1^2 [rad^2]	$0.9 \cdot 10^{-5}$	$0.572 \cdot 10^{-10}$	$0.580 \cdot 10^{-10}$	$0.369 \cdot 10^{-8}$	$0.116 \cdot 10^{-9}$	$0.114 \cdot 10^{-9}$
σ_2^2 [rad^2]	$0.9 \cdot 10^{-5}$	$0.536 \cdot 10^{-8}$	$0.541 \cdot 10^{-8}$	$0.905 \cdot 10^{-8}$	$0.105 \cdot 10^{-7}$	$0.101 \cdot 10^{-7}$
σ_3^2 [rad^2]	$0.1 \cdot 10^{-1}$	$0.269 \cdot 10^{-5}$	$0.217 \cdot 10^{-4}$	$0.217 \cdot 10^{-4}$	$0.244 \cdot 10^{-4}$	$0.538 \cdot 10^{-5}$

Case 1: Reduced R^* : $r_e = 0.25 \cdot 10^{-6}$ m^2/s^3 ; $r_n = 0.25 \cdot 10^{-4}$ m^2/s^3 ;

Case 2: Analysis of fourth-order filter (Case 1) on seventh-order design model ;

Case 3: Analysis of fourth-order filter (Case 1) on 15th-order full model ;

Case 4: Analysis of fourth-order filter (Case 1) on design model with $R = 2 \cdot R^*$;

Case 5: Optimal fourth-order filter designed with $R = 2 \cdot R^*$.

5. RESUMÉ, EXPERIMENTAL VERIFICATION, AND FUTURE INVESTIGATIONS

5.1 Resumé

This presentation demonstrates the steps to be taken to design low-order efficient state estimators for the problem of fast and fine alignment of inertial platforms. The characteristic features of this study can be summarized as follows:

(1) The investigation is based on a thorough modelling of gyro drift and accelerometer noise. The stochastic models are determined through evaluating extensive series of tests.

(2) The overall system dynamics is formulated within the framework of kinematic modelling leading to a reduced-order filter, which is insensitive with respect to certain parameters.

(3) For the relatively short-term operation, in the present problem only some of the identified components of the noise models have significant influence.

(4) An observability study in connection with an investigation of the filter's own covariance behavior proves to be a source of further reductions.

(5) Finally, a complete covariance analysis is performed to check whether the suggested simplifications are allowed and to investigate the filter's reaction to certain parameter variations.

From the numerical results we can draw the following conclusions:

(1) It is sufficient to implement a fourth-order filter for α, β, γ, and D_n, since additional components are either not observable (D_e, B_e, and B_n) or their error variance is not significantly reduced within the observation time in the range of 3 - 10 minutes (D_v and d_v).

(2) The influence of the gyro-drift parameters show that the resulting filter is rather insensitive with respect to the variation of these values.

(3) The estimation accuracy depends largely on the size of the accelerometer noise level. However, it is surprising that a filter designed with incorrect values for this noise does not deteriorate significantly when compared to the optimal filter.

(4) Typical error reductions in the alignment angles are almost two orders of magnitude in α, β and γ within 3 minutes of operation. It has to be taken into account that α, β are already much better known at the beginning of the fine-alignment.

5.2 Experimental Verification

To verify the theoretical considerations the following test configuration was set up at the DFVLR laboratories in Braunschweig:

An LN3-platform was opened to read the outputs of the two horizontal accelerometers. These signals were fed into the Kalman filter; the filter was approximated by its discrete pendant, which was programmed on an EAI Pacer 100 process computer. Due to the estimates provided by the filter, torquer signals were applied to align the platform to its nominal attitude. To read out the exact misalignment angles for comparison with those indicated by the filter, the platform was opened and a mirror was attached whose position can be recorded with the help of a collimator.

The first encouraging results of the experimental verification are available [6]. Details will be shown in the oral presentation.

5.3 Future Investigations

Future investigations will include the influence of prefiltering of sensor data, the incorporation of temperature models for the noise terms as well as tests of the complete system within the vehicle.

LIST OF REFERENCES

1. Leondes, C.T., ed., Theory and Application of Kalman Filtering, AGARDograph No. 139, AGARD, Neuilly-Sur-Seine, France, Feb. 1970

2. Winter, H., The Modelling Error Sensitivity of Digital Filters for the Alignment of Inertial Platforms, AGARD-CCP-116, 1972

3. Gelb, A., ed., Applied Optimal Estimation, The MIT-Press, 1974

4. Hofmann, W., and Kortüm, W., Design of Optimal and Suboptimal State-Estimators under Regularity Defects,
Deutsche Luft- und Raumfahrt, Forschungsbericht 74-13, 1974

5. Stieler, B., Schnelle Feinausrichtung von Trägheitsplattformen mit Hilfe eines Kalman-Filters -- erste Versuchsergebnisse,
DFVLR-Braunschweig, IB 153-74/26, 1974

6. --, Untersuchung des Fehlerverhaltens an G-200 Kreiseln und A-200 Beschleunigungsmessern -- Meßergebnisse der Phase A, IABG-Ottobrunn, IABG Bericht Nr. 1/74, 1974

ACKNOWLEDGEMENTS

The author wishes to express his thanks to his colleague Mr. Richter, who has done an excellent job on setting up the necessary programs. He would also like to thank Dr. Handrich (IABG) and Dr. Stieler (DFVLR) for making their test results available to him, as well as Dr. Winter (DFVLR) for the fruitful cooperation in the initial phase of this study.

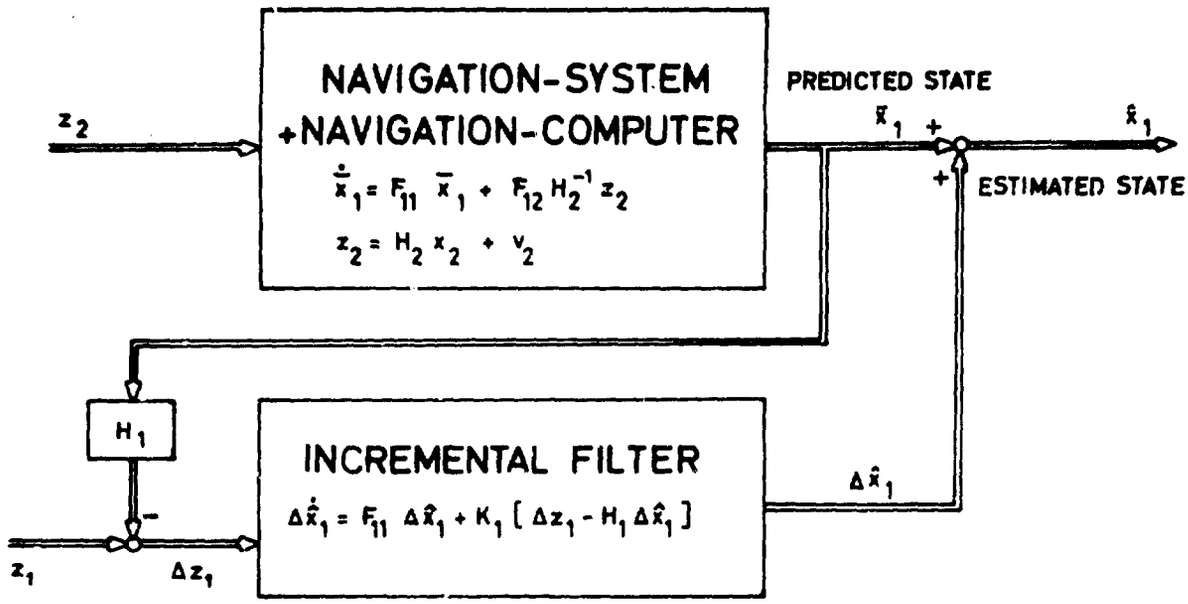

Figure 1. Incremental filter - kinematic modelling.

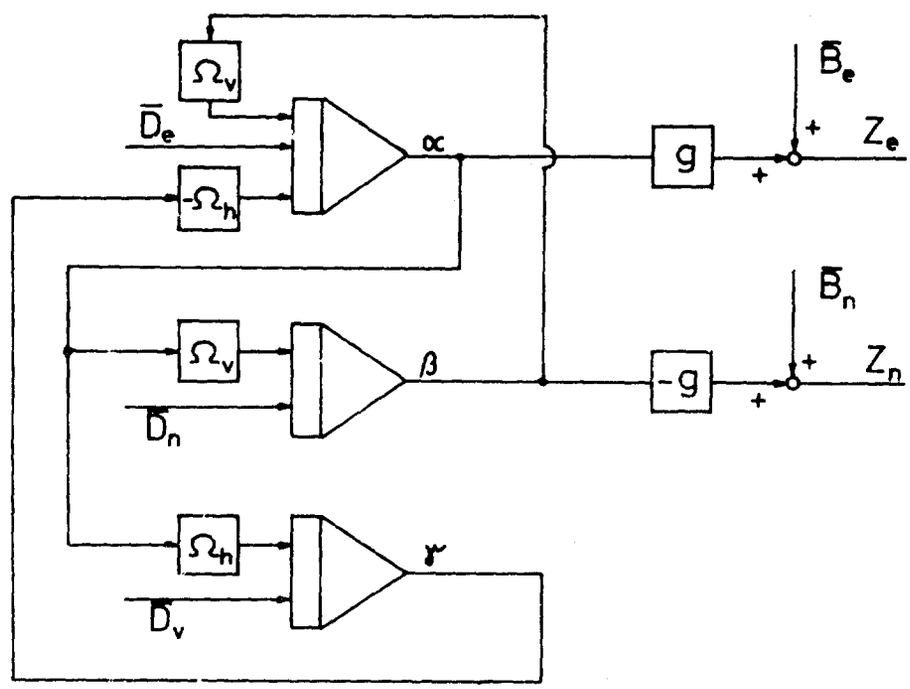

Figure 2. Platform error dynamics and measurement modelling.

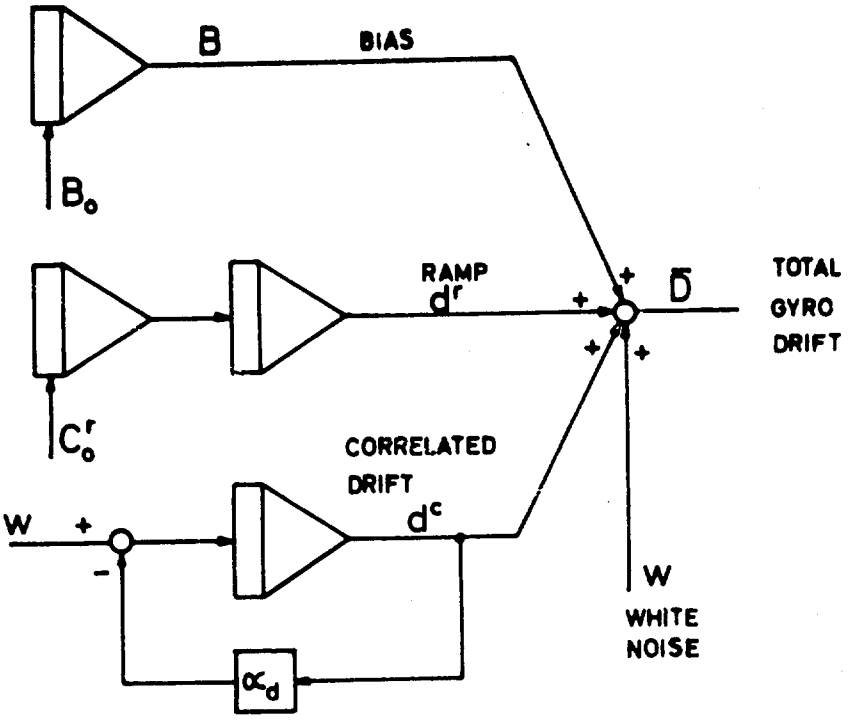

Figure 3. State model for gyro drift.

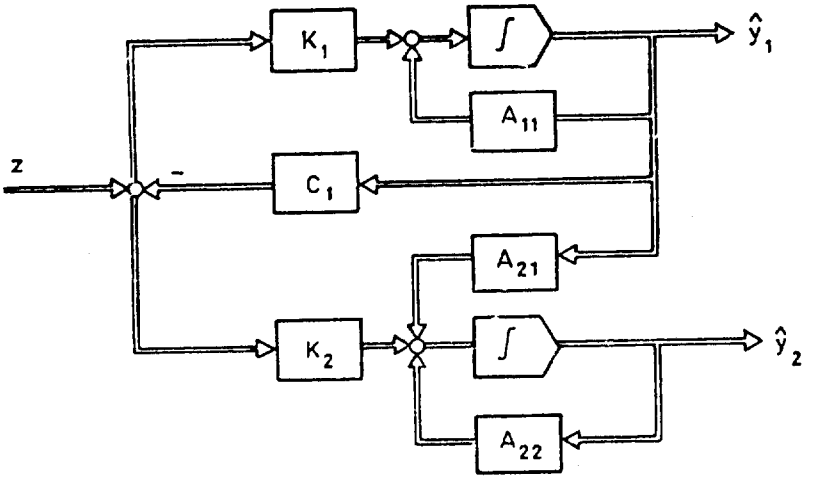

Figure 4. Filter structure for partially observable systems.

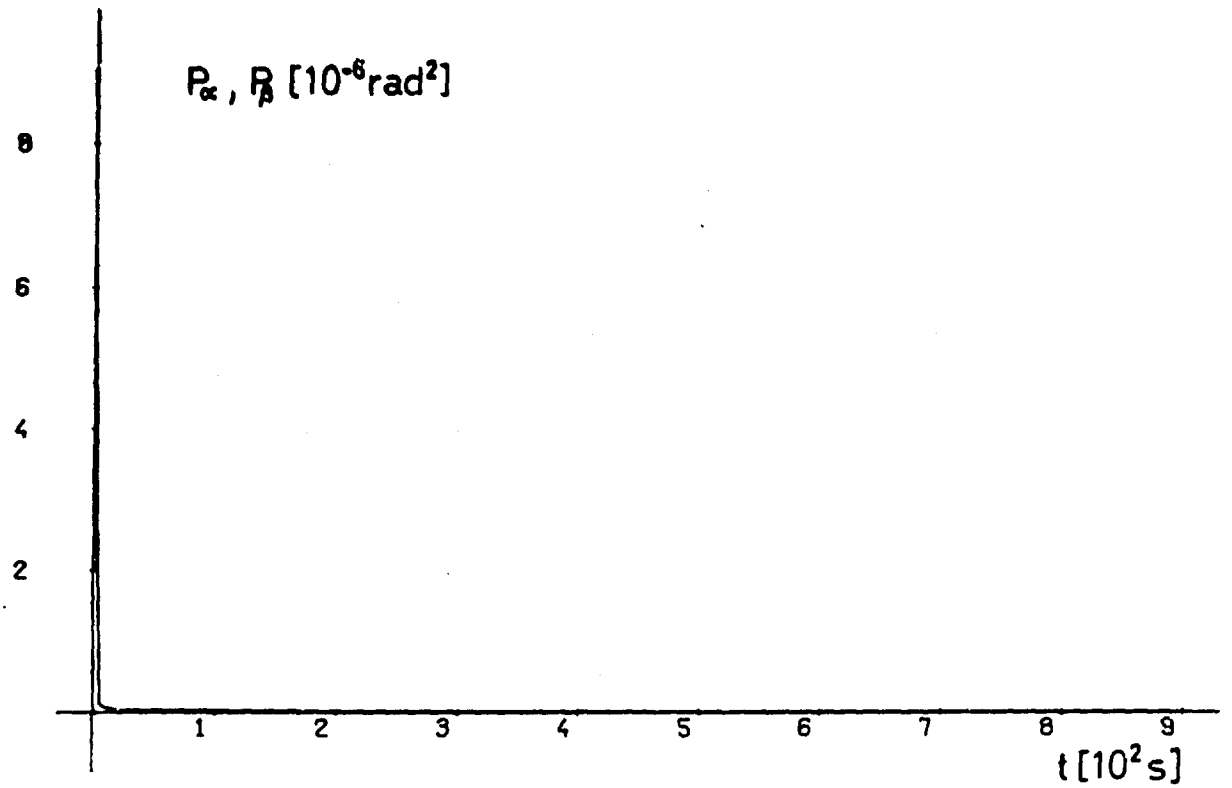

Figure 5. Optimal error variances for misalignment angles α and β - nominal data.

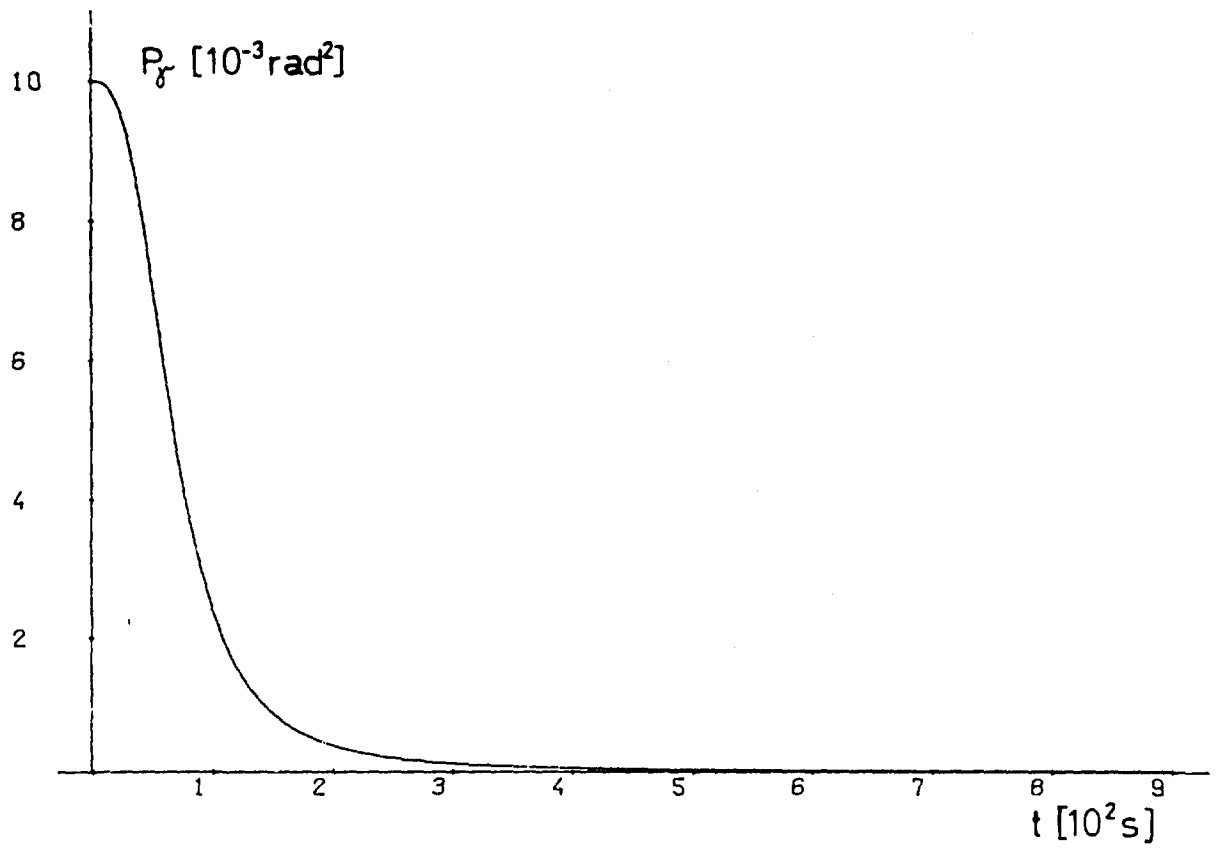

Figure 6. Optimal error variance for azimuth angle γ - nominal data.

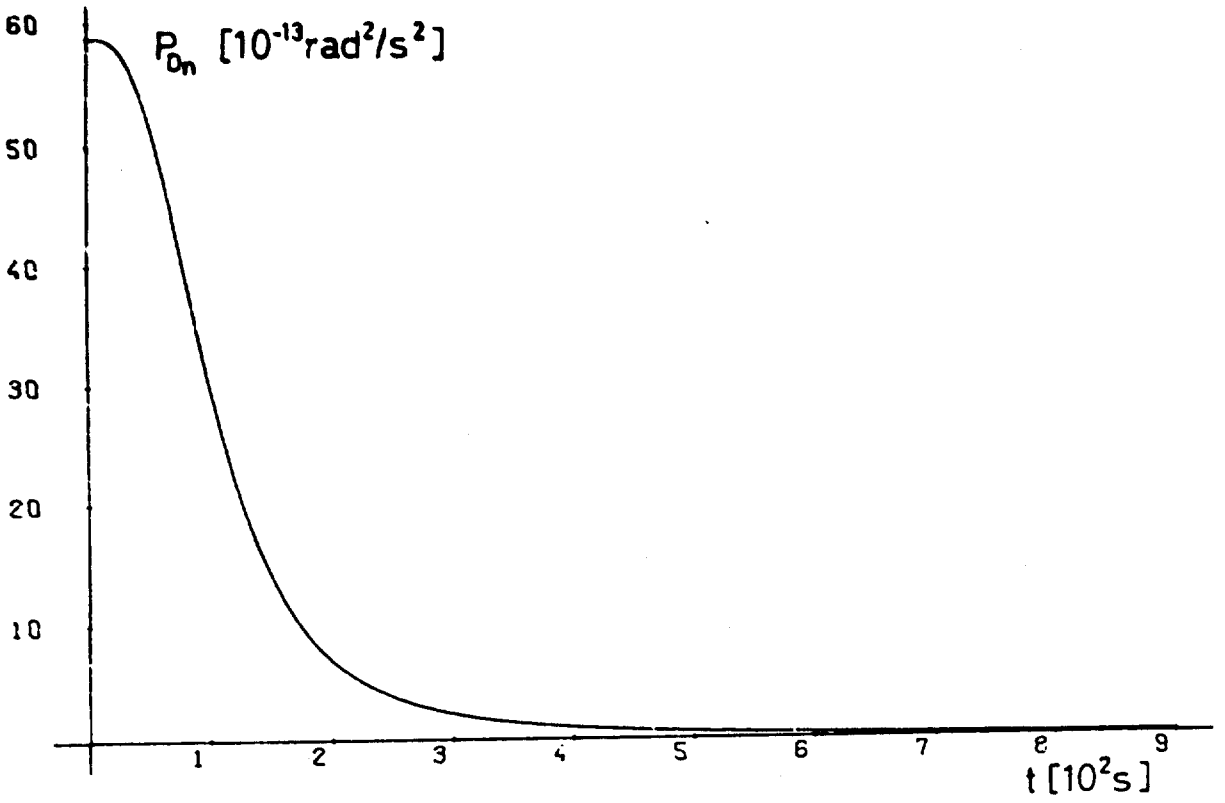

Figure 7. Optimal variance for drift D_n - nominal data.

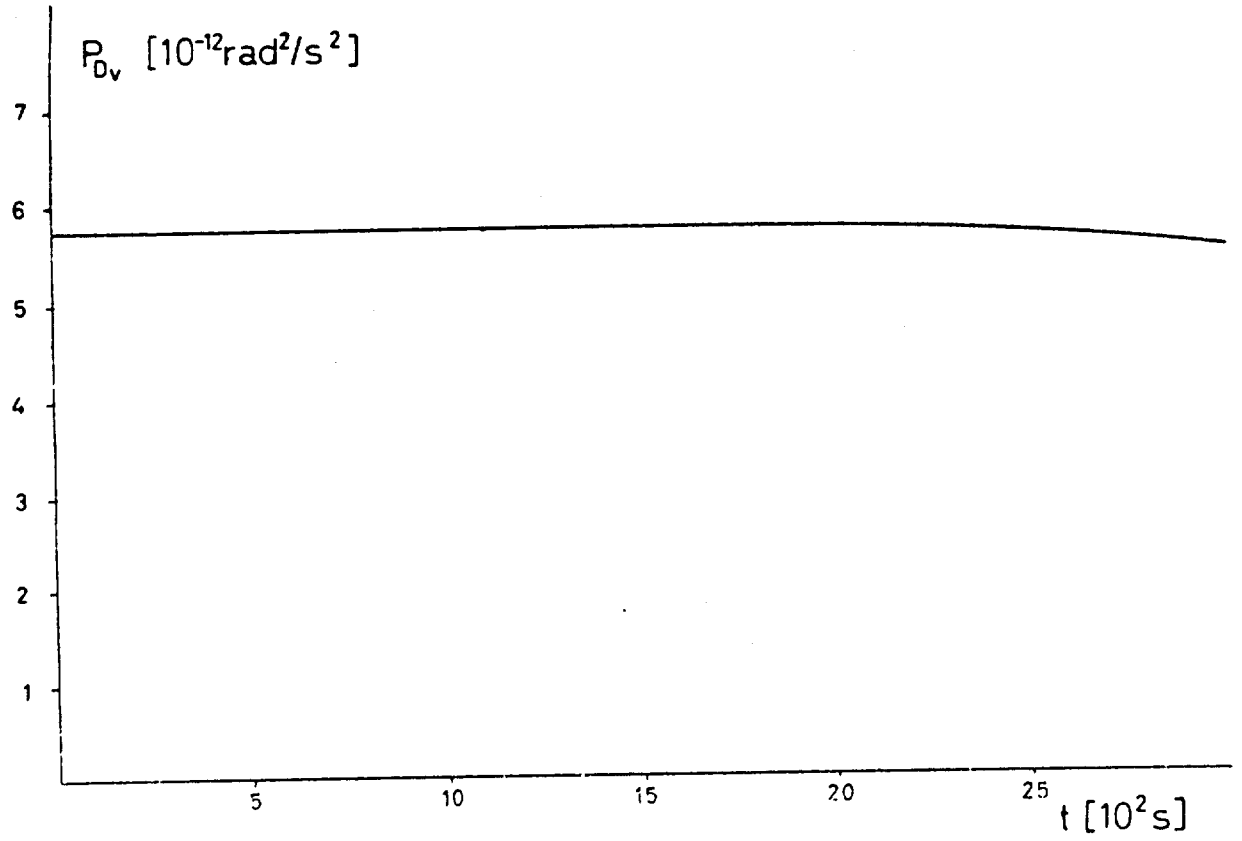

Figure 8. Optimal error variance for drift D_v - nominal data.

KALMAN FILTER BIBLIOGRAPHY

1. Toda, N.F., Schlee, F.H., Obscharsky, P., "Region of Kalman Filter Convergence for Several Autonomous Navigation Modes", A.I.A.A. Journal, Vol. 7, No. 4, April 1969, p. 622-7.

2. Faurre, P., Ghez, F., "Application of Kalman Filtering to Adjustment of Inertial Navigator", Automatisme, Vol. 14, No. 6, June 1969, p. 229-34.

3. Hafner, D.J., Brown, J.L., Doffing, C.G., "Fail-Operational Landing Commands Using Kalman Filtering", IEEE National Aerospace Electronics Conference, 21st Proceedings (Dayton Sec), May 19-21, 1969, p. 343-8.

4. Ackerson, G.A., Fu, K.S., "On State Estimation in Switching Environments", IEEE Trans. Automat. Contr., Vol. AC-15, No. 1, Feb. 1970, p. 10-17.

5. Johnson, D.J., "Application of a Colored Noise Kalman Filter to a Radio - Guide D Ascent Mission", Journal of Spacecraft and Rockets, Vol. 7, No. 3, March 1970, p. 277-81.

6. Mehra, R.K., "On the Identification of Variances and Adaptive Kalman Filtering", Joint Automat. Cpntr. Conference 10th, Preparation Technical Paper, Boulder, Colorado, August 5, 1969, No. 7, p. 494-505.

7. Kaufman, H., "Aircraft Parameter Identification Using Kalman Filtering", Proceedings National Electronics Conference, Vol. 25, Dec. 8-10, 1969, Chicago, Illinois, NEC Paper 26-B, p. 85-9.

8. Sidar, M., "Self-Optimizing Filter for Hybrid Inertial Navigation Systems", Proceedings 12th Israel Annual Conference on Aviation and Astronaut, Tel Aviv and Haifa, Israel, March 4-5, 1970, p. 57-64.

9. Swik, R., Schmidt, G., "Optimal Correction of Stochastic Errors of an Inertial Navigation System - Simulation Studies", Agard Conf. Proceedings No. 54 Guidance and Control Panel 9th Meeting, Delft, Netherlands, Sept. 22-26, 1969, 10 p.

10. Hutchinson, C.E., D'Appolito, J.A., "Design of Low Sensitivity Kalman Filters for Hybrid Navigation Systems", Agard Conf. Proceedings No. 54 Guidance and Control Panel 9th Meeting, Delft, Netherlands, Sept. 22-26, 1969, 5 p.

11. Halamandaris, H., Ozdes, D., "Kalman Filter Augmented Marine Navigation System" Agardograph 139, Theory and Applications of Kalman Filtering, Feb. 1970, p. 513-37.

12. Kouba, J.T. "Application of Kalman Filtering for the Alignment of Carrier Aircraft Inertial Navigation Systems", Agardograph 139, Theory and Applications of Kalman Filtering, Feb. 1970, 1970, p. 405-21.

13. Battin, R.H., Levine, G.M., "Application of Kalman Filtering Techniques to the Apollo Program", Agardograph 139, Theory and Applications of Kalman Filtering, Feb. 1970, p. 335-61.

14. Bellantoni, J.F., "Some Applications of Kalman Filtering in Space Guidance", Agardograph 139, Theory and Applications of Kalman Filtering, Feb. 1970, p. 363-404.

15. Buis, G.R., Tanger, J.A., "Use of 'P' Pattern Search 'P' for the Determination of the Kalman Filter Constants for a Tracking Data Processor for Powered F Light Lunar Navigation" Digest Rec. of ACM/SIAM/IEEE, Joint Conf. on Math. Comput Aids to Design, Anaheim, California, Oct. 27-31, 1969, p. 429.

16. Stubberud, A.R., Wismer D.A., "Suboptimal Kalman Filter Techniques" Agardograph 139, Theory and Applications of Kalman Filtering, Feb. 1970, p. 105-17.

17. Schmidt, W., Kanarachos, "Improvement of the Accuracy of Automatic Landing Systems by use of Kalman-Filtering - Techniques and Incorporation of Inertial Data" Agard Conf. Proceedings No. 54 Guidance and Control Panel 9th Meeting, Delft, Netherlands, Sept. 22-26, 1969, 17 p.

18. Wells, C.H., "Optimum Estimation of Carbon and Temperature in a Simulated Bof", ASME, 11th Joint Automat. Contr. Conference American Automat. Contr. Council, Atlanta, Georgia, Preparation Paper 1-B, June 22-26, 1970, p. 7-18.

19. Mehra, R.K., "On-Line Identification of Linear Dynamic Systems with Applications to Kalman Filtering", ASME, 11th Joint Automat. Contr. Conf. American Automat. Contr. Council, Atlanta, Georgia, Preparation Paper 16-C, June 22-26, 1970, p. 373-82.

20. Singer, R.A., Behnke, K.W., "Reducing the Computational Requirements of Aircraft Tracking", Proceedings 3rd Hawaii Int. Conf. on Syst. Sci., Honolulu, Hawaii, Pt. 1, Jan. 14-16, 1970, p. 320-3.

21. Tait, G.R., Belanger, P.R., "Comparison of Some Parameter Identification Schemes Using First and Second Order Extended Kal[illegible] Bucy Filter and Sensitivity Functions", 2nd Prague IFAC Symp., Czechoslovakia, (Identifi[illegible]n Process Parameter Estimation), Pt. 2 Prepr. 10.3, June 15-20, 1970.

22. Sahinkaya, Y., Sridhar, R., "Minimum Energy Control of a Class of Electrically Driven Vehicles", ASME, 11th Joint Automat. Contr. Conf, Amer. Automat. Contr. Council, Atlanta, Georgia, Prepr. Paper 6-D, June 22-26, 1970, p. 169-74.

23. Farooq, M., Mahalanabis, A.K., "Note on the Maximum Likelihood State Estimation of Linear Discrete Systems with Multiple Time Delays", IEEE Trans. Automat. Contr., Vol. AC-16, No. 1, Feb. 1971, p. 104-5.

24. Mehra, R.K., "Identification of Stochastic Linear Dynamic System Using Kalman Filter Representation", AIAA Journal, Vol. 9, No. 1, Jan. 1971, p. 28-31.

25. Covington, W.O., Jr., "Attitude Determination of a Spin-Stabilized Lunar Satellite", Journal of Spacecrafts and Rockets, Vol. 8, No. 10, Oct. 1971, p. 1088-90.

26. Meditch, J.S., "Least - Squares Filtering and Smoothing for Linear Distributed Parameter Systems", Automatica, Vol. 7, No. 3, May 1971, p. 315-22.

27. Dressler, R.M., Tabak, D., "Satellite Tracking by Combined Optimal Estimation and Control Techniques", IEEE Trans. Autom. Control., Vol. AC-16, No. 6, Dec. 1971, p. 833-40.

28. Coggan, G.C., Wilson, J.A., "On-Line State Estimation with a Small Computer", Comput. Journal, Vol. 14, No. 1, Feb. 1971, p. 61-4.

29. Buxbaum, P.J., "Decoupled Tracking of Reentering Ballistic Missiles", Joint Autom. Control Conf., 12th, Aug. 11-13, 1971, Paper No. 3-A5, p. 132.

30. Webber, R.F., Hendricks, T.C., "Efficient Computation of Large Scale Sensitivity of Kalman Filters to Measure Noise Statistics", Joint Autom. Control. Conf., 12th, Paper No. 3-A2, Aug. 11-13, 1971, p. 127-8.

31. Young, P.C., "Comments on 'P' On-Line Identification of Linear Dynamic Systems with Applications to Kalman Filtering 'P'", IEEE Trans. Autom. Control Vol.AC-17, No. 2, April 1972, p. 269-71.

32. Sage, A.P., Wakefield, C.D., "Maximum Likelihood Identification of Time Varying and Random System Parameters", Int. Journal Control, Vol. 16, No. 1, Jul. 1972, p. 81-100.

33. Khutorovskii, Z.N., "Effective Memory of a Discrete Kalman Filter", Autom. Remote Control, Vol. 333, No. 2, Pt. 1, Feb. 1972, p. 228-233.

34. Park, S.K., Lainiotis, D.G., "Monte Carlo Study of the Optimal Non-Linear Estimator: Linear Systems with Non-Gaussian Initial States", Int. Journal Control, Vol. 16, No. 6, Dec. 1972, p. 1029-1040.

35. Szeto, Michael W., Gazis, Denos C., "Application of Kalman Filtering to the Surveillance and Control of Traffic Systems", Transp. Sci., Vol. 6, No. 4, Nov. 1972, p. 419-439.

36. Farrington, F.D., Goodson, R.E., "Simulated Flight Tests of a Digitally Autopiloted Stol-Craft on a Curved Approach with Scanning Microwave Guidance", J. Dyn. Syst. Meas. Control., Trans. ASME, Vol. 95, Ser. G, No. 1, March 1973, p. 55-63.

37. Porebski, W., "Kalman Inverse Filter with Discrete Time Observations", Bull. Acad. Pol Sci., Ser. Sci. Tech., Vol. 20, No. 1, 1972, p. 73-77.

38. Krogmann, U.W.E., "Kalman Filter, Fundamental Consideration and Application Possibilities in Inertial Navigation Systems, Z. Flugwiss, Vol. 20, No. 4, April 1972, p. 155-161.

39. Hutchinson, C.E., D'Appolito, J.A., Bongiovanni, P.L., "Minimax Design of Kalman-Like Filters in the Presence of Large-Parameter Uncertainties", AIAA Journal, Vol. 11, No. 5, May 1973, p. 694-699.

40. Park, Gerald L., Schlueter, Robert A., Needler, Marvin A., "State Estimation of a Simulated Turbine Generator", IEEE Trans. Power Appar. Systems, Vol. PAS-92, No. 1, Jan.-Feb. 1973, p. 98-103.

41. Krut'Ko, P.D., "Adaptive Algorithms for Observation of Dynamic Systems", Eng. Cybern., Vol. 9, No. 6, Nov.-Dec. 1971, p. 1133-1137.

42. Monzingo, Robert A., "Nonrecursive Algebraic Solution for the Discrete Smoothed Error Covariance Matrix", IEEE Trans. Autom. Control, Vol. AC-18, No. 2, April 1973, p. 175.

43. Son, Le Hung, Anderson, B.D.O., "Design of Kalman Filters Using Signal-Model Output Statistics", Proc. Inst. Electr. Eng. (London), Vol. 120, No. 2, Feb. 1973, p. 312-318.

44. Carlson, Neal A., "Fast Triangular Formulation of the Square Root Filter", AIAA Journal, Vol. 11, No. 9, Sept. 1973, p. 1259-1265.

45. Moore, John B., Hetrakul, Priti, "Optimal Demodulation of Pam Signals", IEEE Trans. INF Theory, Vol. IT-19, No. 2, Mar. 1973, p. 188-196.

46. Ishitani, Hisashi, Tamaki, Yasuko, "On the Application of a Kalman Filtering Technique to On-Line Orbit Estimation of a Launching Vehicle", Bull. Inst. Space Aeronaut Sci., Univ. of Tokyo, Vol. 8, No. 2 (A), April 1972, p. 264-292.

47. Hino, Mikio, "Prediction of Hydrolo_ic System by Kalman Filtering", Proc. Jap. Soc. Civ. Eng., No. 221, Jan. 1974, p. 39-47.

48. Carew, Burian, Beianger, Pierre R., "Identification of Optimum Filter Steady-State Gain for Systems with Unknown Noise Covariances", IEEE Trans. Autom. Control., Vol. AC-18, No. 6, Dec. 1973, p. 582-587.

49. Godard, D., "Channel Equalization Using a Kalman Filter for Fast Data Transmission", IBM Journal Res. Dev., Vol. 18, No. 3, May 1974, p. 267-273.

50. Revkin, S.S., Tyumeneva, G.V., "Use of the Kalman Filter in a Vertical Gyro Correction Circuit", Izv Akad Nauk (SSSR), Mekh Tverd Tela, No. 2, Mar-April, 1974, p. 30-35.

51. Hino, Mikio, Mori, Yoshikazu, Yoshikawa, Shinjiro, "Prediction of Atmospheric Pollution by Kalman Filter", Proc. Jap. Soc. Civ. Eng., No. 224, April 1974, p. 79-90.

52. Brammer, Robert F., "Real-Time Shipboard Orbit Determination Using Kalman Filtering Techniques", IEEE Trans. Aerosp. Electron. Systems, Vol. AES-10, No. 4, July 1974, p. 492-4.

53. Baird, Charles, A., Jr., "Kalman-Type Processing for Adaptive Antenna Arrays", IEEE Int. Conf. on Commun., Conf. Rec. Paper, Minneapolis, Minn., June 17-19 1974, Paper 10G, 4 p., published by IEEE, Vol. 10.

54. Sandberg, Herbert J., Dushman, Allan, "System Design and Analysis of FSGM/SINS navigation Systems", Inst. of Navig., Natl. Mar. Meet, Proc. U.S. Merchant Mar. Acad, Kings Point, N.Y., Oct. 23-24, 1973, p. 111-121.

55. Karpeta, C., Stirsky, P., Volf, K., Roubal, S., "Simulation Studies of the Optimal Direct Digital Control of the A-1 Reactor", Nucl. Power Plant Control and Instrum. Symp. Proc. Prague, Czech., Jan. 22-26, 1973, p. 289-302.

56. Szeto, Michael W., "Estimation of the Volatility of Securities in the Stock Market by Kalman Filtering Techniques", Journal Autom. Control Conf. of the AM Autom Control Council, 14th Annual, Prepr. Ohio State Univ. Columbus, June 20-22, 1973, Paper 12.

57. Yang, S.C., Garrard, W.L., "Low Sensitivity, Modern Approach to the Longitudinal Control of Automated Transit Vehicles", ASME Paper No. 74-AUT-N, 1974, 11 p.

58. Soliman, M.A., Ray W.H., Szekely, J., "Applications of Non-Linear Filtering to the Stainless-Steel Decarbonization Process", Int. Journal of Control, Vol 20, No. 4, Oct. 1974, p. 641-653.

59. Sodbole, S.S., "Kalman Filtering with no a priori information about Noise - White Noise Case: Identification of Covariances", IEEE Trans. Autom. Control. Vol. AC-19, No. 5, Oct. 1974, p. 561-563.

60. Srinivasan, K., Robichaud, Yvan, "Dynamic Estimator for Complex Bus Voltage Determination", IEEE Trans. Power Appar. Syst., Vol. PAS-93, No. 5, Sept-Oct. 1974, p. 1581-1588.

This bibliography was prepared by

Technical Information Service

National Research Council of Canada